New Perspectives on Wave Energy Converter Control

Alexandra Anne Elizabeth Price

A thesis submitted for the degree of Doctor of Philosophy.

The University of Edinburgh.

March 2009

Abstract

This work examines some of the fundamental problems behind the control of wave energy converters (WECs). Several new perspectives are presented to aid the understanding of the problem and the interpretation of the literature. The first of these is a group of methods for classifying control of WECs. One way to classify control is to consider the stage of power transfer from the wave to the final energy carrier. Consideration of power transfer can also be used to classify WECs into families. This approach makes it possible to classify all WECs, including those that had previously eluded classification. It also relates the equations of motion of different classes of WECs to a generalised equation of motion. This in turn clarifies why some types of control are suited to some WECs, but not others. These classification systems are used to demarcate the boundary for the theoretical work that follows. The theory applies to WECs with governing equations of motion that are linear, and to control systems that are linear, aim to maximise power, and which regulate the PTO stage of power flow.

Another important perspective is the new wet and dry oscillator paradigm, which is used to differentiate between frequency domain modelling and a commonly used technique, monochromatic modelling. This distinction is necessary background for many of the new ideas discussed. It is used to resolve an ongoing debate in wave energy research: whether frequency domain modelling can be applied to cases that are not monochromatic. It is the key to an extension to the theory of capture width, a widely used performance indicator. This distinction is also the rationale behind an improved method of presenting frequency domain results: the frequency responses due to both monochromatic and polychromatic forcing are represented on the same graph. These responses are different because the optimal control problem is acausal, a topic that is also discussed in depth. This visual tool is used to investigate and confirm various ideas about the control of WECs, and to demonstrate how the newly redefined capture width encapsulates the essential control problem of WECs. The optimal control problem is said to be acausal because information about the future is required to achieve optimal control. Another vantage point offered is that of the duration of the prediction interval required for optimal control. This is given by a new parameter emerging from this work, which has been termed the premonition time. The premonition time depends on the amount of knowledge required, which is determined by the geometry of the WEC, and the amount of information available, which is largely determined by the bandwidth of the sea state.

The new perspectives introduced are the various systems of classification, the wet and dry oscillator paradigm, the presentation of monochromatic and polychromatic results on the same axes, premonition time, and the revised theory on capture width. These are all used to discuss the interrelationship between WEC geometry, the control strategy and the sea-state. The opportunities for, and limitations of, the use of intelligent control techniques such as artificial neural networks are discussed. The potential contribution of various control strategies and associated design principles is explored. This discussion culminates in a series of recommendations for control strategies that are suited to each class of WEC, and for the areas of research that have the potential to bring about the greatest reductions in the cost of harnessing energy from sea waves.

Declaration of originality

I hereby declare that the research recorded in this thesis and the thesis itself was composed and originated entirely by myself in the School of Engineering at The University of Edinburgh, unless otherwise stated. This work has not been submitted for any other degree or professional qualification.

Alexandra Price

Acknowledgements

I would like to thank my supervisor Robin Wallace for making this work possible, and everyone in the Institute for Energy Systems for their support and team spirit. The final version of this thesis benefited from many proof-readers, including David Forehand, Ben Child, Audrey Mukora, Eoghan Maquire, Remy Pascal, Sarah Caraher, Alasdair McDonald, Mark Shannon, and in particular, Robin Wallace and Grégory Payne. I would like to thank those who have mentored me at various stages of this degree, namely Alan Murray, Grégory Payne, Jamie Taylor, Chris Dent, David Forehand, Jørgen Hals from the Norwegian University of Science and Technology and Aurélien Babarit from Ecole Centrale de Nantes. Chris Dent also made a significant contribution the novel ideas in a joint paper submitted to a journal. This paper, "On the capture width of wave energy converters", which is bound into the back of this thesis, contributed to the material in Chapter 5 and forms the foundation for the most important results presented in this thesis. Finally I'd like to thank Mark Shannon for non-technical support.

The PhD studentship was funded by SuperGen Marine (Phase 1). The secondment to Ecole Centrale de Nantes was hosted by Alain Clément and was funded by the Royal Society of Edinburgh's Lessels Award, the University of Edinburgh, and the Carnegie Trust.

Contents

List of figures

List of tables

Chapter 1

Introduction

1.1 The importance of wave energy converter control

The present moment is an incredibly exciting time to be working on wave energy research. There is an intense interest and optimism in the idea of developing this fledgeling technology into a major player in the energy industry. This rapidly accelerating enthusiasm can be seen in many forms. These include substantial academic research funding, increased attendance of wave energy conferences, political support in many countries including Portugal, Canada, New Zealand and Japan, statements of support from the British government, financial support mechanisms such as the Carbon Trust Marine Energy Accelerator [1], the Marine Renewables Deployment Fund [2] and the Renewable Obligations Certificates [3], and the development of test sites such as the Maritime Pilot Zone in Portugal, the Billia Croo test site at the European Marine Energy Centre in Scotland, and the Wave Hub in England. With these support mechanisms, the development of wave energy technologies has moved out of university test tanks and into commercial development. The last decade has seen the emergence of several small wave device developers, many of which have performed sea-trails of full-scale prototypes. The private investment in these start-up companies is a sign that there is optimism about the economic viability of the technology, while the first commercial wave farm at Aguçaduora in Portugal [4] is a first step in gaining vital operational experience.

The work presented here concerns the control of wave energy converters (WECs). It is first necessary to place the development of WECs in the context of the present political and commercial enthusiasm for wave energy. Then the importance of control to the development of the wave energy industry will be discussed.

1.1.1 The potential benefits of wave energy

Energy capture from ocean waves has the potential to make a significant contribution to future energy supply. Although this new technology is not currently economically competitive with other energy technologies, there is potential for it to be competitive once the technology is mature. The high energy density of the resource compared to other sources of renewable energy is one of the reasons why wave energy has the potential to be economically viable [5]. The annual wave resource is large, so there is a potential for the mature technology to contribute a large percentage of the energy mix [6]. The life-cycle carbon costs are low [7], there is minimal

environmental pollution, and visual intrusion is not a problem. While there will be competition for space with the shipping and fishing industries, there is no indication that these industries will suffer economically if large wave farms are installed.

There is considerable political support for wave energy not only for its potential contributions to energy security and de-carbonising of the energy supply, but also because of the potential boost to the economy. There are many device developers in Britain, and the British economy would benefit from being at the centre of a global wave energy industry.

1.1.2 Requirements for wave energy to be an important future energy source

To make a contribution to security of supply and the de-carbonisation of energy, the cost of wave generated electricity needs to be reduced, and a large installed capacity is required. Cost of energy is highly correlated to the installed capacity. Studying the trends of other energy technologies, it can be seen that cost of energy reduces down a cost curve, with a negative gradient that gradually becomes less steep with more installed capacity. There has not been enough operational experience with wave farms to model the cost curve for the technology and to project the final cost of the mature technology [8]. While large installed capacity will inevitably lead to cost reductions, technological improvements that result in cost reductions will stimulate interest and investment in the technology and will lead to faster installation of generating plant.

In order for wave energy conversion to make a large contribution to Britain's conflicting energy aspirations, it is crucial to reduce the cost of the energy produced. The cost of energy is influenced by factors such as the primary energy capture, capacity factor, availability, operating costs, plant life, plant manufacturing costs, cost of capital, and research and development costs. Increased installed capacity will give vital operational experience, with which it should be possible to optimise the capacity factor, increase availability, reduce operating costs, and extend plant life. Increased installed capacity will also reduce the cost of energy via mass production and commercial competition.

There is also an opportunity for a contribution to cost reductions due to research in these areas. Two areas where wave energy research can make the biggest contribution is in increasing power production and limiting destructive forces and motions, thereby increasing availability and plant life. These goals can be tackled from two directions: from the design of the WEC or from the point of view of control.

1.1.3 The benefits of control

This research focusses on the control of WECs, but the results also have implications for the design of WECs. Both control and design of WECs require a knowledge of the interaction between the WEC's geometry, the control scheme, and the sea state. An understanding of their

interaction is crucial for designing a WEC, for adapting a WEC to a particular location, or for scaling up a design.

Once a WEC has been designed and constructed, the control system is the only way of having any effect on performance. The design process results in optimised performance for a given *design sea state*, so performance is not optimised at other sea states. Using control, it is possible to lessen the extent to which a device is dependent on a particular sea state. Furthermore, control is potentially cheap to implement, could significantly improve energy production or stress limitation, and could be fitted retrospectively. Improvements from control schemes can also stimulate improvements in design. For instance, a control scheme that reduces mechanical stresses has immediate benefits of improved availability and reduced operating costs, but could also lead to reduced manufacturing costs for the next generation of technology.

1.2 Research context

The focus of the research leading to the production of this thesis has shifted several times as the research question evolved. This work was conducted as part of work package 9 of the SuperGen Marine (Phase 1) consortium [9]. Several of the areas of work in this thesis give answers to the some of the original research questions presented in the SuperGen Marine proposal. The exploration of other proposed tasks uncovered yet more pressing questions, and the main results presented in this thesis are in response to these newly uncovered questions.

1.2.1 Supergen Marine tasks

The tasks set out in the SuperGen Marine (Phase 1) work package, that provided the original direction for this research, were:

1. Examination and categorisation by function and means the different forms of WEC and control systems
2. Modelling selected marine devices in 1, 2, and 3D motion and understanding their behaviour in linear and non-linear conditions
3. Identification of the control means and strategies of single and multi-point WECs and determination of their amenability to self-learning or adaptive control aimed at improvement of energy capture
4. Development of generic evolutionary computing models on a range of marine energy converters and studying their effectiveness for real-time control
5. Examination of the applicability of differing control strategies to a range of WECs over a range of sea states

1.2.2 Work on Supergen Marine tasks

The classification of WECs in § 2.2 on page 10 and their control systems in § 4.3 on page 124 addresses the first research task. The second task was explored by Andy McCabe, another member of the consortium, who developed a linear time domain simulation of a WEC moving with one degree of freedom in directional waves (2D) [10]. McCabe's approach is different to the work presented in this thesis, which uses standard mathematical linear models, and does not attempt to simulate the operation of a WEC. The third task has been partially addressed in Chapter 4, which identifies control means and strategies, many of which are already used in industry, and highlights which of these have the most potential for increasing energy production. The third task also suggests the assessment of the amenability to self-learning or adaptive control. If this question is reframed as the assessment of the amenability to control requiring near-future predictions, then this task is covered in § 5.4 on page 228. The last task is the focus of Chapter 5.

The fourth Supergen Marine task was the original focus of this research. The use of neural networks for real-time control of WECs was explored. The first research area explored was the use of neural networks for system identification. The idea explored was a black-box dynamic model that could be used to explore control strategies. Strategies chosen off-line would then be converted to a set of heuristic rules for on-line modelling. This concept was described in [11]. After publication it was discovered that the idea being described was a standard technique called model predictive control [12], which is offered as a Simulink® block in Matlab® 's neural network toolbox. This technique is suitable when a neural network can predict the forward dynamics of the plant better than a dynamic equation, and when this dynamic model can be used to predict near future response.

The research question that was stimulated by this work was whether neural networks could model the response of a WEC better than a non-linear dynamic model, and whether an accurate model of a WEC could be used to predict future response for the time horizon required for improved control. There is evidence that WEC developers have accurate dynamic non-linear models of their devices [13, 14], and it is well-known that neural networks do not perform well compared to dynamic models [15]. However, no matter how accurate the a dynamic model, it cannot be used to predict future response for the required time horizon (§ 5.4 on page 228)- information about future waves is required, and this information cannot be deduced from locally gathered data.

The second research area studied was the effectiveness of evolutionary models for real time control (the fourth task) was the use of neural networks for predicting near future values of wave excitation force. This work was carried out on secondment to Ecole Central de Nantes (ECN). The visit was hosted and supervised by Alain Clément and the work was carried out in collaboration with Aurélian Babarit. The outcomes of this research were described in [16].

1.2.3 Secondment to Ecole Centrale de Nantes

The work carried out over the eight month secondment and for several months afterwards focussed on the use of neural networks as a non-linear regression method to predict the time until the next significant events in future excitation force. ECN were interested in the time until the next peak or trough in excitation force, as this was information that could be used with in-house code to calculate the best time to unlatch a latched WEC [17]. ECN are developing a WEC that has a latching control strategy as part of its integral design [18].

Fortran code developed by Barbarit was used to generate time series of wave excitation data. Babarit's code generated Pierson Moskowitz (PM) spectra [19] of a specified peak frequency and pseudo-random phase, and multiplied these by the excitation coefficients calculated for a simple geometry. An inverse discrete Fourier transform was then used to synthesise a time series of excitation force. The work carried out during the secondment to ECN involved using Matlab® to run Babarit's code, which generated time series using PM spectra with a wide range of peak frequencies. Pairs of past and future data were extracted, and training information was calculated. The training data was used to develop neural network predictors, and the results were compared to a simple sinusoidal extrapolation method. This procedure was repeated using noisy sinusoidal data. The results were not surprising. Simple sinusoidal extrapolation was marginally better than neural networks when used with the noisy sinusoidal data. Neural networks were marginally better than sinusoidal extrapolation when used with the filtered PM spectrum data. Regardless of technique, the accuracy for the noisy sinusoidal data was far better than for the spectral data. The first peak or trough could be predicted with higher accuracy than the second peak or trough.

The research question stimulated by this work the dependency of the prediction accuracy of the neural network and sinusoidal extrapolation methods on how far into the future an event occurred. The development of the theory in Chapter 5 was in response to this question. It was realised that the time horizon for which sinusoidal extrapolation is likely to give a more accurate prediction than neural networks is inversely related to the bandwidth of the function (in this case the excitation force). The bandwidth of a PM spectrum depends upon its spectral peak and thus the training data was not suitable for studying the relative accuracy of predictions given by neural networks and sinusoidal extrapolation, as a function of time from the present moment.

At this point the focus of the work changed from the use of neural networks for prediction, to the theoretical study of the interaction of the knowledge required for optimal control, and the knowledge available from locally gathered data. The thesis presented here is based on the new focal point. The previous work on neural networks is not reported on, but the conference papers are included in Appendix C at the end of the thesis.

1.3 The research question

The focus of the work presented here is centred around the research challenge posed by Stephen Salter in [20]:

> "*The initial research requirement is to establish the extent to which forecasts can improve power conversion.*"

Accordingly, the thesis presented here is that it is possible to establish the extent to which forecasts can improve power conversion. In order to have a comprehensive view of how forecasts could improve power conversion, it is necessary to study the interaction between the sea state, the geometry of the WEC, and the particular control scheme used. The extreme cases of each of these parameters must be analysed. It is important to not only examine sea states that are sinusoidal or a single-peaked PM spectrum, but also to ensure the thesis is applied to sea states with broad bandwidths and multiple peaks. Likewise, it is important to consider how the size of a WEC and the type of control scheme influences the research question.

1.4 Key new results

This thesis presents for the first time (new terminology indicated with italics):

- A classification system that considers all WECs (Chapter 2).
- A classification of WEC control, including the distinction between *PTO control* and *geometry control*, and the identification of *acausal sub-optimal control* (Chapter 4).
- Theory showing that a linear PTO force composed of a mass, damper and spring is different from one composed of a spring and damper: the *optimum mass-damper-spring scheme* is defined, and is shown to give broader bandwidths of performance and displacement than the better known *damper-spring scheme* (Chapter 4).
- A clarification of capture width theory that shows the relationship between the *monochromatic and polychromatic capture widths*, and describes the influence of the sea-state using the *spectral power fraction* parameter (Chapter 5).
- Case-studies that demonstrate that the linear unrestrained performance of a large WEC has a broader bandwidth than that of a smaller WEC (Chapter 4).
- Case-studies that demonstrate why the capture width for a sinusoidal sea of a given period is greater than that for a spectral sea of the corresponding energy period (Chapter 5).
- The concepts of *wet and dry oscillators*, which are used to understand commonly used models (Chapter 3), and to add clarity to wave energy literature (Chapter 6).

- The distinction between monochromatic and polychromatic behaviour, which provides a useful lens for re-examining literature: this identified the misinterpretation of a crucial experimental result; it was previously thought that the use of forecasts to improve power capture had been experimentally verified (Chapter 6).
- Theory demonstrating how performance could be improved without forecasts: e.g. geometry control, the PTO impedance configuration, or the choice of *operating frequency*, which is not necessarily the peak frequency of the wave spectrum (Chapter 5).
- Parameters that indicate the potential improvement in power capture, assuming linear unrestrained behaviour, if it were possible to upgrade to optimal control (Chapter 5).
- The *premonition time*, which is the shortfall between the required prediction horizon, or *memory duration*, and the realisable prediction horizon, or *coherence time* (Chapter 5).
- A discussion of whether performance enhancements using forecasts would be significant, and whether the required forecasts would be possible, taking into account displacement restraints and the interaction between WEC geometry and sea-state (Chapters 5 and 6).
- The distinction between locally and remotely gathered data, and evidence that locally gathered data and intelligent techniques such as neural networks are not suited to the task of providing forecasts for optimal PTO control (Chapter 6).

1.5 Chapter breakdown

Chapter 2 begins with a classification of WECs according to the flow of power from the wave to the final energy carrier. This classification is inherently meaningful because it can be related to the research question. The extent to which forecasts can improve power capture depends on the intrinsic impedance of the WEC, the value of which is determined by the first category in the power flow classification. The usefulness of forecasts also depends on the PTO impedance, which is determined in the second category of the power flow classification. In later chapters, the interaction between the sea state, geometry and control is described using a frequency domain model. The second half of Chapter 2 reviews the principles and pitfalls of frequency domain modelling. Applications to measurement of sea waves, generation of waves in experimental facilities, and presentation of experimental results are discussed.

Chapter 3 reviews well-known and widely used theory on the sea state and dynamic motion of a WEC. Modelling assumptions and common sources of ambiguity are highlighted. A literature review indicated that the frequency response was interpreted in two different ways: sometimes as the response to excitation at a single frequency, and sometimes as the components of response to excitation containing many frequencies. To reconcile and compare these two viewpoints, § 3.8 on page 111 introduces the wet and dry oscillator models.

the improvement due to control using future predictions is marginal compared to the improved configuration highlighted by this research.

Chapter 4 reviews well-known theory on linear optimal control of WECs. An extension to the qualitative classification in Chapter 2 highlights the difference between types of control previously treated on equal terms: in particular, *geometry control*, *PTO control* and *power regulation*. The requirement for forecasts and the proximity to the ideal condition are introduced as classification categories, and this identifies a new category of PTO control: *acausal sub-optimal control*, which describes the behaviour that would be expected if accurate forecasts were available for only a short time into the future. A further classification category is the configuration of of PTO settings; formulae for the PTO impedance of four configurations are given. The performance of control schemes that do not require forecasts is plotted alongside performance of the scheme that does require forecasts. Control schemes that were previously considered equivalent are shown to be different when considering the performance across all frequencies. Reactive control using mass, damping, and spring coefficients is shown to be superior to other types of reactive control. The performance improvements given by changing from the widely researched damping-spring scheme to the mass-damping-spring scheme is significantly greater than the improvement due to upgrading from the mass-damping-spring scheme to control requiring forecasts.

Chapter 5 focusses on the interaction between the sea state and the net impedance due to the combined effects of geometry and control. The sea state is described with two newly introduced parameters: the spectral power fraction, and the coherence time. A fresh interpretation of capture width theory demonstrates how the control schemes defined in Chapter 4 interact with the spectral power fraction of the sea state. This work highlights the advantages of geometry control, and suggests a new way of calculating the operating frequency for use with PTO control. The forecast benefit parameter is used to quantify the potential benefits of optimal control for linear unrestrained behaviour. A new theory about premonition time is introduced. The duration of the time horizon for which future knowledge is required, is shown to depend on the geometry. The duration of time for which this knowledge can be predicted with acceptable accuracy from locally collected data, is shown to depend on primarily on the sea state. The premonition time and the parameters indicating the performance enhancement potential of forecasts are used to assess the usefulness of forecasts, taking into account the requirement for displacement restraints.

Chapter 6 brings together various points raised in the thesis. The wet and dry oscillator concepts introduced in Chapter 3, and the classification of PTO control in Chapter 4 are extended and applied to the literature. Work in Chapter 4 suggested that larger WECs can capture more power in broad bandwidth seas. The importance of the debate about the ideal size of a WEC is discussed, and the new results are discussed in the context of real operating conditions.

Chapter 7 summarises the work presented in this thesis. Much of the research has developed

useful tools, challenged assumptions about which types of control were best, or pointed at intriguing opportunities. These results are best described as a shift in perspective. Opportunities presented by this shift in perspective are gathered together as recommendations for further industrial and academic research.

Reader's guide

Chapters 2 and 3 are intended as an accessible introduction to the field of study, because many existing texts are either not immediately accessible, or simplify the problem by considering only sinusoidal waves. The intention of these chapters is to encourage the research community to interpret the simpler theory in the correct context, and to clarify issues that are often missed when first studying wave energy.

Despite the elementary beginnings of the material in Chapter 3, it may nevertheless be of interest to researchers who have an in depth knowledge of wave energy. The discussion of time domain modelling in § 3.2 - 3.4 on pages 69 - 91 and in § 3.6 - 3.7 on pages 103 - 106 is intended to be accessible to those with previous experience of frequency domain modelling of WECs. In § 3.8 on page 111 there is a useful framework for discussing how the concepts of time and frequency domain interact with models suitable only for sinusoidal behaviour.

Chapters 4 and 6 should be of interest to researchers familiar with frequency domain modelling of WECs. However, the classification method in Chapter 2 and the concepts presented in § 3.8 provide essential background material to Chapter 4. Chapter 5 is intended for the expert reader, and builds on essential concepts introduced in Chapter 4.

Chapter 2

Background

2.1 The scope and context of this chapter

In this thesis the performance and control of wave energy converters (WECs) is explored. The principal approach, as outlined in Chapter 3, is to model WECs as linear systems. This present chapter provides the background and context to this approach. A new classification system is introduced, and this is used to compare and contrast well known types of WEC. This is important as some of the topics discussed apply to all types of WEC, while others only apply to those that behave in a linear fashion some of the time. The new classification system examines the process of power transfer from the wave to electricity. The stages of power transfer can also be used to classify different families of control methods. This chapter uses a case study of a leading commercial WEC to demonstrate how the different families of control interact.

WECs do not, in general, exhibit linear behaviour. A linear model of a WEC is only capable of representing a limited sub-set of its behaviour. Nevertheless, a linear model is useful, as it allows the use of a powerful tool: frequency domain analysis. The use of the frequency domain for modelling WECs is not universally understood, as discussed in Chapter 6. It is therefore necessary that some fundamental principles of frequency domain modelling are laid down in this chapter. The background to the Fourier transform and linear systems theory is presented. The difference between the frequency response and another commonly used modelling and experimental technique, the monochromatic approach, is highlighted. The various uses of Fourier analysis in the field of wave energy engineering, including the characterisation of sea waves, theoretical modelling, and experimental work are contrasted.

2.2 Classification of wave energy converters

Since the oil crisis in the 1970s [21], many concepts for wave energy converters (WECs) have been designed, patented, tested and developed commercially [22]. These designs are very different in appearance and it is useful to have some method of comparing them to one another. The diversity in concepts of WEC has been matched by the diversity in methods for classifying WECs. These methods are now briefly described.

2.2.1 Review of existing systems for classifying wave energy converters

Classification according to location (*shoreline*, *near shore* or *offshore*) [23] was, and still is [24], a widely used system. A form of classification that has been around for a long time is the *generation* of development [24]. The descriptions *first*, *second* and *third generation* were used to indicate concepts that had been tested, concepts under development that were due to be tested in the foreseeable future, and concepts that required technology not available at the time. The first, second and third generations roughly coincided with the location classifications shoreline, near shore and offshore. This is probably because shoreline and nearshore installations were seen as easy to build with limited budgets and technology development. Moving further offshore to exploit the better wave climate was seen as the next logical progression. Despite the general overlap of the classification by location and by generation, they are not equivalent. For example, Japan built a demonstration near shore device called the Kaimei in the 70s [25]. Classification by generation is a subjective view of the state of development. It results in different classifications of the same device, such as [26] which classes Salter's duck as a first generation device.

A major disadvantage of classification by location or generation is that they are not useful for comparing operating principles of WECs. They do not give any information about the equation of motion and hence efficiency of a WEC concept. Classification according to mode of motion or functional decomposition can be used to compare groups of WECs, as these systems are based on information that can be related to the equation of motion. Classification according to sub-system or operational principles gives specific information about the type of machinery required, and hence the types of engineering challenges that a given WEC concept will encounter.

Classification according to mode of motion [27, 28] groups WECs that move in similar directions. The modes of motion are the six degrees of freedom named according to the ship-keeping convention (see Fig. 2.3 on page 16). In § 2.3.6 the relationship between the modes of motion and the upper limit in a measure of efficiency (capture width) is discussed.

The oldest form of WEC classification is French's functional decomposition [29], and many of the concepts and terms introduced are still in use today. This method regards various solutions to each functional requirement in isolation from the requirements or outputs of adjacent sub-systems. French considered four main functional categories [29]:

- Working surface (a rigid solid, flexible solid or gas),
- Means of reaction (fixed, such as to the seabed or shoreline; balancing; inertial),
- Configuration (terminator; attenuator; point-absorber),
- Means of power extraction (pneumatic; oil hydraulic; water hydraulic; direct electrical).

Clément [30] classifies WECs according to their operating principles and location. The main operating principles are:

- Oscillating water columns,
- Wave activated bodies,
- Overtopping devices,
- Unclassifiable (for example the Clam flexible bag device).

A report written for the International Energy Agency takes a similar approach [31], and notes that floating OWCs (the Backward Bent Duct Buoy) and floating overtopping devices (the Wave Dragon) can belong to two of these classes.

Salter et al [32] suggested a system of classification according to sub-system. The sub-systems considered were:

- A slow primary displacement element (float; flap; water column).
- Means of reaction (fixed; water column inertia; device mass inertia; balancing).
- A connecting linkage which transmits the required forces while avoiding forces which would be damaging for the structure.
- Power conditioning: velocity increase and direction rectification.
- Generation: a fast moving unidirectional rotating part, driving an electrical machine.
- Transmission: cables, transformers and switch gear for transmitting power to shore.

In fact Salter's classification fits the description of functional decomposition more closely than French's. French's list of functional categories contains configuration, which unlike the other categories that perform specific functional tasks, is an attribute rather than a function. All of Salter's sub-systems do however describe a necessary functional task, and do so in a more complete manner. These tasks all concern the transfer of energy.

2.2.2 Rationale for a new classification system

Given that there are so many existing methods of classifying and describing WECs, there had to be a good reason to introduce a new method. The motivation for finding a new classification method was that some of the existing methods (location, generation of technology or configuration) did not give sufficient information, while the more descriptive methods of classification (functional decomposition, sub-system or operating principle) were not able to classify all types of WEC.

Using the present method of classification, which is an extension of the functional decomposition [33] and sub-system methods [32], it is possible to classify all types of WECs. Furthermore, this method allows all WECs to be compared with each other on an equal basis. Previous classification methods described oscillating bodies and oscillating water columns (OWCs) as different operating principles [30, 31], or made exceptions for certain types of WEC [30], most notably overtopping devices [32]. Existing classification methods either did not consider direct drive systems [32] (see § 2.2.1) or did not provide the tools for a direct comparison between direct drive and other types of power conversion chain [34, 35]. The new system of classification presented here emphasises the operating principles that all WECs have in common. It allows comparison of oscillating bodies, OWCs and overtopping devices. It allows comparison between direct drive and other types of power conversion chain, which highlights their relative merits.

Classification of WECs according to the flow of power clarifies the impact of the design on the equation of motion, and explains how the design of a WEC and the control procedures interact. This classification system can also be used to classify different types of WEC control.

2.2.3 Classification according to power flow

In the new classification system suggested here, the various stages required to convert the power in the wave to the final useful energy carrier, are considered. This power transfer is broken up into three stages, as shown in Fig. 2.1:

- Stage one: is the flow of power between the wave (0) and the primary interface (1), giving the intercepted power.
- Stage two: is the flow of power between the primary interface and the PTO (2), giving the captured power .
- Stage three: is the flow of power between the PTO and the final stage of power conversion (3), giving the delivered power.

Each power transfer stage can be described by a number of attributes. A WEC can be classified by choosing from a number of possibilities to describe a given attribute. The attributes of each power transfer stage are described in the sections that follow. A summary is given in Table 2.1.

During these three stages of power transfer, the WEC must also perform the power conditioning tasks described by Salter et al [32], namely:

- Gearing: conversion of wave induced motion, characterised by low velocities and high forces, to motion with high velocities and low forces, as is required for electricity generation

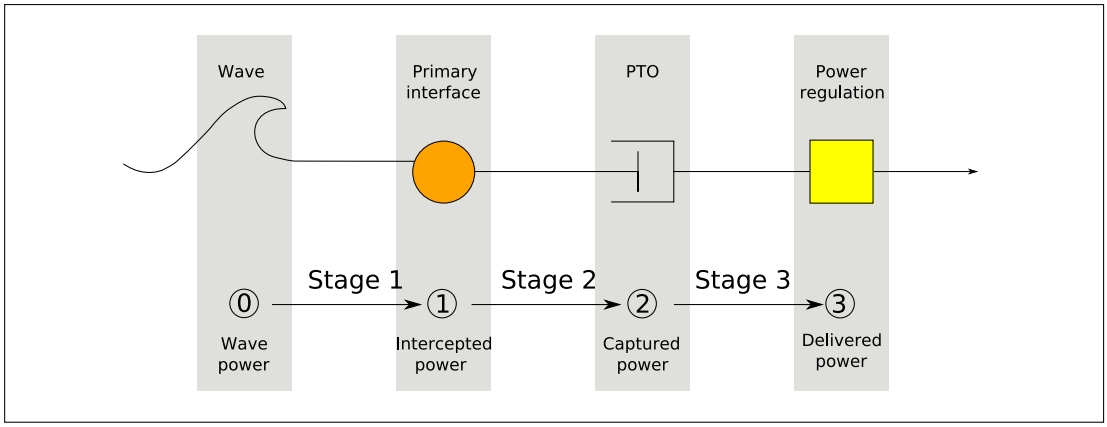

Figure 2.1: ***Power transfer in a generic WEC:*** *Power flows from the wave (0), to the primary interface (1), to the power take off (2) and finally to the delivered energy carrier (3).*

- Rectification: conversion of bi-directional motion into uni-directional motion.
- Limitation: restraints on forces that exceed design limits.
- Storage: conversion of a random or cyclical flow of power into a smoother power output.

The power conditioning functions of gearing, rectification and limitation may take place in any or all of the stages of power flow. Power conditioning can be considered an attribute of each of the power transfer stages, as shown in Table 2.1. It is also possible for no power conditioning to take place at a given stage, and so *none* is an option. Examples of typical distributions of power conditioning functions are given in § 2.2.7. Storage may only take place in the third stage of power transfer: the power regulation stage.

2.2.4 Intercepted power

Type of primary interface

The first step in wave power conversion is to transfer the power carried by the wave to something that is not the wave. This *something* is the primary interface. In the classification system described here, the three types of primary interface are:

- An oscillating solid,
- A pulsating solid,
- A pulsating liquid.

The orientation of the interface and its modes of motion can also be used as classification criteria.

An oscillating solid is a solid body, of fixed volume, which is caused to oscillate. It may be semi-submerged or fully submerged. The Pelamis (Table 2.2 on page 27) is an example of a WEC with a primary interface that is an oscillating solid. As an alternative to inducing an oscillation in a body's position, the power in the wave could be used to induce an oscillation in a body's volume. This is known as pulsation. This body may be a solid, or a volume of fluid whose motion is different to that of the wave. The Archimedes Wave Swing (AWS) is an example of a WEC with a primary interface that is a pulsating solid (Table 2.2).

There are two well known types of pulsating fluid WECs; oscillating water columns (OWCs) and overtopping devices. In an OWC, the primary interface is a vertical column of water enclosed within a solid cassion. The oscillation of the water column is coupled to the oscillation of the enclosed column of air above it. In an overtopping device, the primary interface is a column of water moving on a solid guide. In the Wavedragon (Table 2.2), this column of water oscillates diagonally up a ramp.

There are several WECs that have a secondary interface as well as a primary interface. Examples are given in § 2.2.9 on page 25.

Modes of motion

Classification by mode of motion is an established method of classification. It has been included in the classification system described here, because the modes of motion of the primary

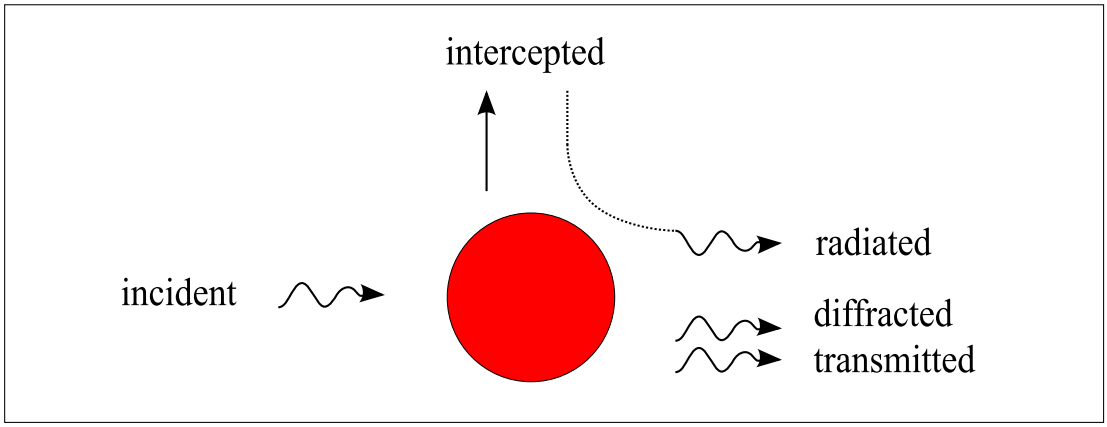

Figure 2.2: ***Intercepted power: power flow from wave to primary interface:*** *Incident power arrives in the form of a water wave. This power leaves the system as water waves associated with diffracted, transmitted and radiated power. Some of the incident power is intercepted by the primary interface. If there is no PTO, this is all returned in the form of a radiated wave.*

interface play an important role in determining how much power can be captured (§ 2.3.6). Each individual interface may move with six degrees of freedom: three rotational (pitch, roll, yaw) and three translational (heave, surge, sway). The conventional notation [36] associated with ships is used (see Fig. 2.3). Here degrees of freedom are described with reference to Cartesian axes parallel to the equilibrium water surface and the direction of wave propagation. The degrees of freedom according to these axes are known as the modes of motion.

Orientation

Orientation is yet another well established classification criterion. Like mode of motion, orientation determines the upper limit of power capture. The orientation of a WEC describes the position of the primary interface relative to the principal wave direction. The three most common descriptions of orientation are:

- Terminator: (beam sea) the waves impact the largest cross-section of the WEC.
- Attenuator: (head sea) the waves impact the smallest cross-section of the WEC.
- Point-absorber: the WEC is small compared to the waves.

The term point-absorber usually describes an axi-symmetric non-directional WEC, but is also used to describe small asymmetric WECs. The terms attenuator and terminator describe WECs that span several wavelengths. A terminator lies along the wave front, whereas an attenuator lies across the wave front. It is possible to have a large WEC that is asymmetric and thus non-directional, for example the Clam, which acts as both an attenuator and a terminator to waves from all directions. This would be classified as omnidirectional by Mei, who considered point absorbers a sub-set of the omni-directional category [37].

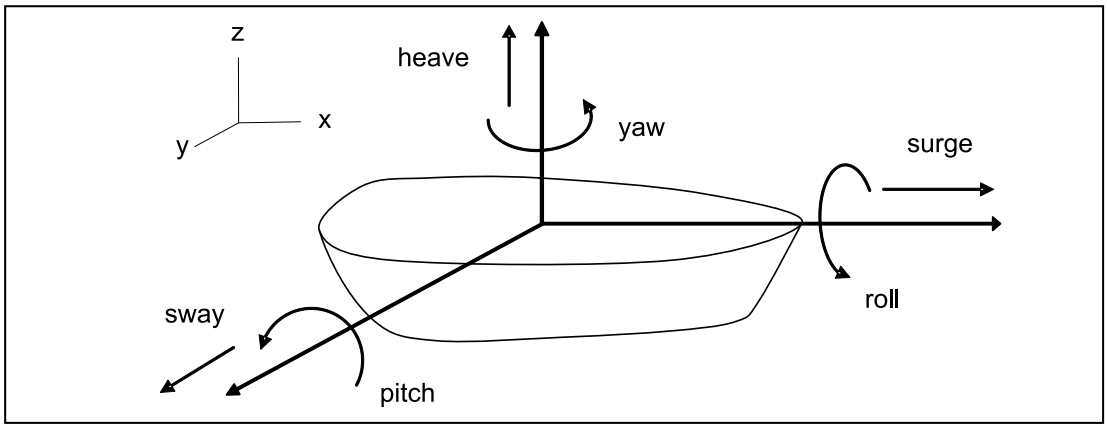

Figure 2.3: ***Naming conventions of the six modes of motion:*** *after Newman [36].*

Location

As described in § 2.2.1, describing the location of a WEC as shoreline, near shore or offshore is an established method of classification. It is useful to include it in the present classification system as it gives an indication of the engineering operational challenges, and also of the magnitude and direction of the exciting forces. For this reason the location has been listed as an attribute of the first stage of energy capture. In some WECs the first stage of power transfer is located offshore or near shore, while the third stage is located at the shoreline in the form of a reservoir of seawater and a low-head hydro plant. As the location of the third stage does not affect the exciting forces on the primary interface, location has not been included as an attribute of the delivered power.

2.2.5 Captured power

The primary interface determines how much of the power in the waves is modified into a more *readily captured* form. The second stage determines how much of this intercepted power is retained by the WEC (captured power in Fig. 2.4) and how much is returned back to the sea (radiated power in Fig. 2.4). When there is no PTO, all the intercepted power is returned to the sea. This can be seen in Fig. 2.2: the combined intercepted, diffracted and transmitted powers equal the incident power. Assuming that there is no source of damping (losses or PTO) other than radiation, the intercepted power equals the radiated power. All the power in the incident wave remains in the sea in the form of radiated, diffracted and transmitted waves. However, when there is PTO damping, as in Fig. 2.4, some of the intercepted power becomes the captured

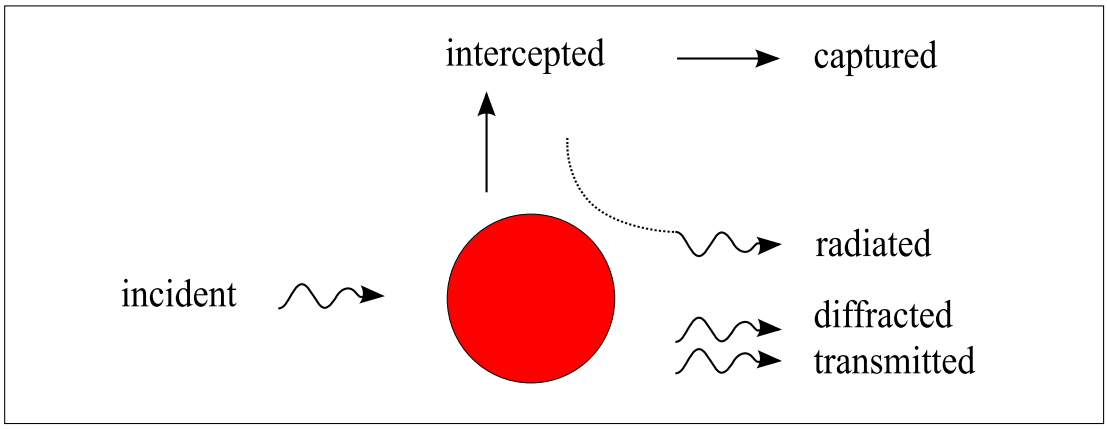

Figure 2.4: ***Captured power: power flow from wave to PTO:*** *Incident power arrives in the form of a water wave. This energy leaves the system as water waves associated with diffracted, transmitted and radiated power. Some of the incident power is intercepted by the primary interface. If there is a PTO force, some of this is returned in the form of a radiated wave, and some of this is captured by the PTO system.*

power, and some of it is returned to the sea as radiated waves.

Intermediate energy carrier

The PTO captures a portion of the intercepted power. This captured power may be transferred to the next stage by any suitable intermediate energy carrier. Energy carriers that are currently in common use are electricity and hydraulic flow. Other energy carriers are possible, and this is indicated by an ellipsis (...) in Table 2.1.

Means of reaction

The second stage captures power by opposing the relative motion of the primary interface and a reference point. This reference point may be classified as:

- Fixed: static or dynamic coupling to ground (the sea bed).
- Referenced: to a neighbouring body (either horizontally or vertically adjacent) that experiences a different exciting force.
- Inertial: a body with a motion coupled to that of the primary interface, which is positioned so that it does not experience a wave exciting force (either a solid or a water column).

This definition of means of reaction is useful because the means of reaction has an important impact on the types of terms found in the governing equation (§ 2.3.6), and because the different categories correspond to types of moorings. Moorings are broadly classified into three groups, according to their opposition to motion in the direction of the PTO force:

- Rigid: a solid connection to ground (the sea bed), for example a cassion with a foundation on the seabed, a fixed tower mooring, or an articulated loading column [38].
- Tight: an elastic but stiff connection to ground, for example taut spread mooring.
- Slack: station-keeping, negligible opposition to displacement in the direction of PTO, highly non-linear spring to oppose non-linear second-order forces, for example multi-catenary mooring.

Rigid mooring is required when the means of reaction is a static coupling to ground. Tight mooring is required when the means of reaction is a dynamic coupling to ground. Slack mooring is required when the means of reaction is either referenced or inertial.

The correspondence between these types of moorings and the means of reaction may be examined by considering various ways of applying these each of these types of mooring to means of reaction other than those indicated above. When modelling tight mooring as a way

of applying a fixed point of reference, the forces provided by the mooring (principally spring) are in series with the PTO force. It does not make sense to model the forces provided by tight mooring as being in parallel with the PTO force because this would be equivalent to the PTO force reacting against (a static coupling to) the sea bed, with displacements (and thus power production) highly constrained by the mooring force. Application of tight mooring to WECs with referenced or inertial reactions would essentially change the point of reactions: for instance, applying a tight mooring to the lower buoy of a WEC with PTO relative to this vertically adjacent submerged body would result in a reaction point to ground via a dynamic coupling.

Note that here the emphasis is on the opposition to motion in the direction of the PTO force. The standard definition considers the opposition to motion in all degrees of freedom. Thus catenary mooring, which provides little opposition to heave, but a substantial opposition to surge (or drift forces) could be considered slack mooring if the referenced or inertial PTO was in heave. If however the PTO was in surge, then this type of mooring might hinder the high surge displacements that are required for efficient energy capture.

The uses of the reaction means to identify the type of mooring is introduced here for the first time. The most rigorous study to date is a conference paper by Harris et al [38]. It relates the choice of moorings to the classification categories of configuration and location. The configuration is important because axi-symmetrical devices (typically point absorbers) are non-directional, so are suitable for spread mooring, whereas asymmetrical devices such as terminators and attenuators are highly directional and require single point mooring to allow them to align to the principal wave direction. In [38] the onshore category of WECs is associated with cassions built into the bedrock, the near-shore category with built-in cassions or fixed tower moorings for providing fixed static coupling to ground, while the offshore category of WECs is associated with slack mooring. The association in this thesis is between moorings and point of reaction, rather than between moorings and location, as in [38]. For shoreline devices a fixed static coupling to the ground is the only option, and for offshore (deep water) devices, reacting against the ground is not possible, so referenced or inertial reaction points are necessary. However, in near-shore (shallow water) conditions, it is not inevitable that the point of reaction is a fixed rigid connection to the sea bed. Referenced or inertial reaction points, as well as a fixed dynamic connection to the sea bed, are also possible. While it could be argued that the definition of near-shore assumes a fixed rigid reference point, this neglects the fact that most of the WECs under development which have referenced [4] or inertial [18] means of reactions, are designed for testing in, and are suitable for operation in, sites that can be described as near-shore in terms of water depth. It is therefore more exact to associate types of moorings with reaction point, rather than location.

Other studies [39, 40] relate the type of moorings to a classification system that recognises two broad categories of WECs: *motion independent* and *motion dependent*. In [39] this

classification was described as filling the gap in [38]. The association between mooring and point of reaction given in this thesis has the same motivation, and improves on, the classification given in [39]. The classification in [39] is less rigorous as it does not pinpoint the behaviours that relate to mooring. For instance, the category *motion dependant* could be interpreted as described all types of wave activated body, including those with a fixed point of reaction. A fixed reaction leads to different mooring requirements to inertial and referenced reactions. The classification in [39] also does not compare like for like: the category *motion dependant* describes the primary absorber (which moves), while the category *motion independant* describes the point of reaction (which is fixed). The use of this categorisation makes the understanding of the mooring requirements less clear than in [38]. For instance, its use could lead to a model of a heaving buoy WEC with PTO referenced to ground, where the buoy's motion is impeded by catenary mooring [40]. In such a model, the treatment of the mooring and PTO systems are not consistent. The structure that provided the PTO's reference to ground would also provide a rigid mooring, so a caternary mooring would not be necessary. A catenary mooring might be suitable for a WEC with referenced or inertial reaction, in which case the governing equation would have a different form (§ 2.3.6), and the relationship between the mooring and PTO forces would be more complicated.

2.2.6 Delivered power

The captured power is usually not in a form convenient for transmission or consumption. It may require a change of energy carrier, or it may require conditioning (gearing, rectification, storage, limitation as described in § 2.2.3) so that it fits the standards of the form of the delivered power. These two options are described in more detail in § 2.2.7, which describes the difference between direct drive and buffered systems. The tasks performed in this final stage, whether a change of energy carrier, conditioning, or both, are collectively referred to as power regulation.

Final energy carrier

It is assumed that power leaves the WEC in the form of grid-connected electricity, as this is presently the goal of the major device developers; however the principles described here apply to other forms of energy carriers. Storable energy carriers such as hydrogen could be treated as the delivered product with an inbuilt element of storage, or they can be considered as a storage step in the power delivery stage of the power conversion chain, prior to the final step which would be conversion to electrical or motive power. Other forms of energy carriers are chemical products that are directly useful commodities, including potable water. These are indirect forms of energy carrier; they represent the savings in conventional power that would have otherwise been required to create the chemical products.

Power transfer stage	Attributes	Options
Intercepted power	type of primary/secondary interface	oscillator / pulsating solid / pulsating fluid
	modes of motion	heave, sway, surge, pitch, yaw, roll
	orientation	point absorber / terminator, attenuator
	location	shoreline / near shore, offshore
	power conditioning	none / gearing, rectification, storage, limitation
Captured power	means of reaction	fixed / balancing / inertia
	energy carrier	electricity / fluid flow ...
	power conditioning	none / gearing, rectification, storage, limitation
Delivered power	energy carrier	electricity / chemical ...
	power conditioning	none / gearing, rectification, storage, limitation

Table 2.1: ***Classification according to power flow:*** *Options separated by commas are independent and any number may be selected; options separated by forward slashes are mutually exclusive and one must be selected. The ellipsis (...) indicates that other suitable options are possible.*

2.2.7 Direct drive and buffered power conversion chains

In a WEC, the power conditioning functions of gearing, rectification, storage and limitation (§ 2.2.3) may take place in any or all of the three stages of power flow. Two common configurations, direct drive and buffered drive (Fig. 2.5) are discussed here to demonstrate the effect of the position of the power conditioning functions within the power conversion chain. Although there is no formal definition of direct drive WECs, the definition considered here is simply that the PTO (stage two) is undertaken by an electrical generator. In direct drive systems, the power conditioning is typically concentrated in the final stage of power transfer. Linear generators are an example of the PTO mechanism for a direct drive system. Buffered drive systems describe WECs where the primary energy capture is not in electrical form. The power conditioning tasks take place before electricity generation. Hydraulic transmission is an example of the PTO mechanism for a buffered drive system.

In Fig. 2.1 (page 14) the power regulation (stage three) is shown in yellow. In Fig. 2.5, the generator is located at stage three in the buffered drive and stage two in the direct drive system. Power regulation is once again highlighted in yellow to show that the different plant at stage

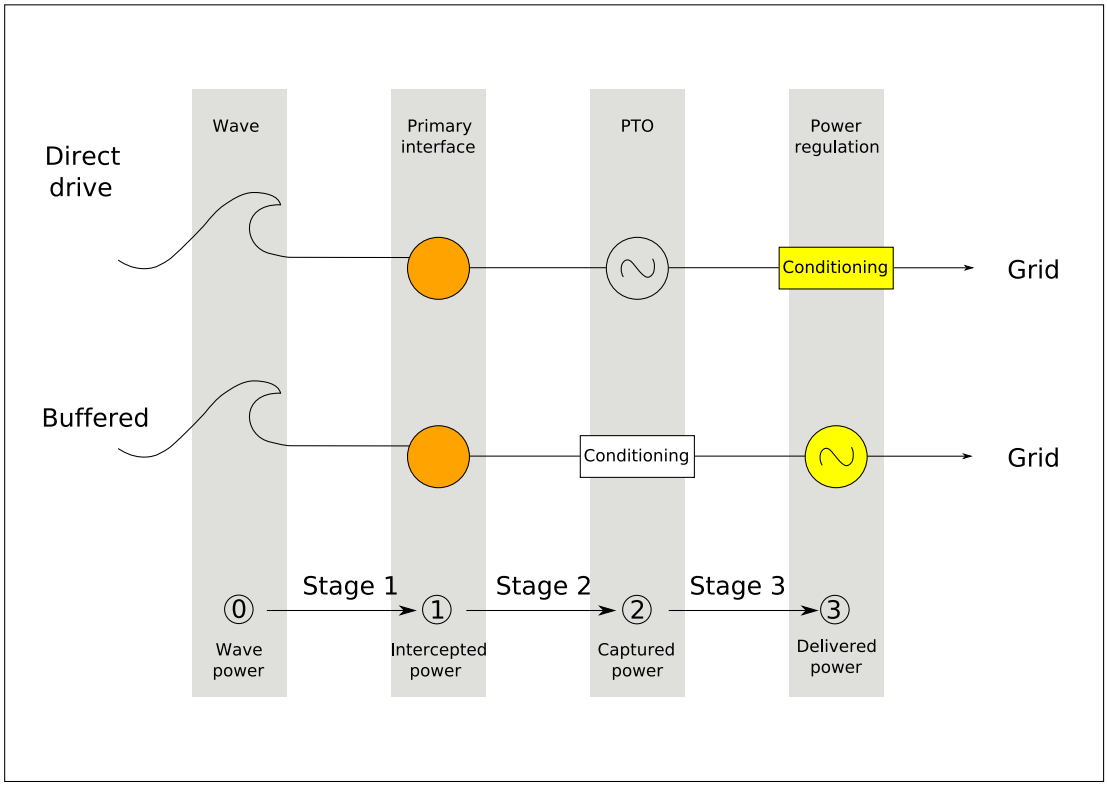

Figure 2.5: ***Direct and buffered drive WEC power conversion chains:*** *Power flows from the wave (0), to the primary interface (1), to the power take off (2) to the delivered energy carrier (3).*

three, the generator for buffered drive and the power conditioning for direct drive, perform the same roles.

In a direct drive system, power is captured directly by the generator in the second stage of power flow. The third stage conditions the electricity to be suitable for the grid. A power electronic converter is required to transfer the low frequency power to DC and then back into AC at grid frequency. If power smoothing (storage) is required, then it is included in this stage. If power smoothing is performed after the outputs of a large number if WECs have been summed, then storage will still be required for power smoothing, but the total storage capacity required will be less than if smoothing is performed before the outputs are summed. Anything that is done to the electricity up to the point of grid connection, whether this is on-board the WEC or onshore, is included as a power conditioning task in stage three.

In a buffered system, the power is captured in the second stage and is transferred to a medium that is easy to store. At present the preferred medium is pressurised fluid. Storage of hydraulic oil in paired high and low pressure accumulators is favoured by many device developers, while others are considering pumping water to onshore reservoirs (see Table 2.2 on page 27). The third stage is the power flow from the short-term energy storage to the generator. This storage acts as a buffer between the PTO stage and the generator in the power regulation stage.

This comparison of direct and buffered drive systems highlights an advantage of this new classification system: it allows the direct comparison of like for like. In Fig. 2.5 it is clear that to compare direct drive and hydraulic PTO, all three stages of the power conversion chain must be considered. Without the reminder that the generators in Fig. 2.5 are performing different tasks (PTO in the case of direct drive, and power regulation in the case buffered drive), it is tempting to compare the systems up to the point of the generator. Comparing stages one to three of a buffered drive system with stages one and two of a direct drive system is not comparing like for like. Such a comparison would overestimate the complete power conversion chain efficiency of a direct drive system, as well as underestimating its costs, mass and reliability. For example, [41] notes that direct drive compares favourably to hydraulic transmission, but does not include a full power electronic converter in the comparison. Furthermore, using sinusoidal excitation underestimates the power fluctuation in a system with no storage; in order to truly compare like for like, storage (batteries or capacitors) must be included in the power regulation stage of the direct drive system.

Classification methods that focus on the type of electricity generating mechanism are also prone to compare the PTO stage of direct drive systems to the combined PTO and power regulation stages of buffered systems. Nielsen [34] compares the efficiencies of direct drive generators (the PTO stage), air turbines for OWCs (the PTO stage), hydraulic transmission (the combined PTO stage and power regulation stage), and water turbines used by overtopping devices (it is not clear whether the combination of the PTO and power regulation stages, or only the power regulation stage, is considered). This comparison gives the impression that, for the same cost, a direct

drive system is far more efficient than the other drive trains considered. Khan et al [35] classify WECs according to the mechansim driving the electrical generator. This could be the motion of the waves (relative motion - either geared or direct drive), an air turbine (OWC), a hydraulic motor, or a water-turbine (in over-topping devices). Once again, the electrical generators are all assumed to perform the same function, making it difficult to compare direct drive with buffered drive systems. There is however an excellent diagram in this paper (Fig. 13.27 of [35]) which does compare the entire power conversion chains of direct drive and buffered systems.

Direct and buffered drive systems can only be fairly compared if all three stages of power transfer are considered. From this vantage point is it clear that a comparison of the methods should include the power conditioning methods. A comparison of (the costs and reliabilities of) gearing and storage in direct drive versus buffered systems is as important as the comparison of the respective generating machinery.

2.2.8 Classification of the power conversion chain

The secondary interface

There are several WECs that have a couple of steps in the power interception (first) stage. In an OWC, the primary interface is the pulsating volume of water. The water free surface transmits power to the enclosed volume of air above it. The volume of air is thus the secondary interface. The AquaBoUY primary interface is a pulsating column of water within an *acceleration tube*. This causes the coupled motion of the secondary interface, an oscillating solid in the form of a neutrally buoyant float within the acceleration tube. In the Clam WEC the primary interface is a pulsating solid, in the form of a solid flap which compresses a flexible bag. This pulsating solid is coupled to a pulsating fluid; the air which is caused to flow between the bag and a central reservoir shared by flexible bag modules. In the AWS, the PTO is configured to oppose the relative motion between the extremities of its pulsating volume. The body of the AWS is considered a pulsating solid for the purposes of its interaction with the water, and an oscillating solid for the purposes of its interaction with the PTO. Although there are not two distinct interfaces, there are two distinct behaviours. In all cases the secondary part of the primary interface exists even when no PTO force is applied. Its purpose is not to apply an opposing force to the primary interface, and hence it does not form part of the PTO stage. Its purpose is transmission, which can include gearing. In all cases, both the primary and secondary interfaces are part of stage one, the power interception process.

Classification rules for the PTO stage

The classification of several other concepts is summarised in Table 2.2 on page 27. Here only the attributes related to the form of the power, and the power conditioning functions (as described in § 2.2.3 on page 13) are listed. In the power interception stage, the form of the power

is described by the primary (and, if applicable, secondary) interface. In the power capture and delivery stages, the form of the power is described by the energy carrier. Classing components of a WEC's power conversion chain as either stage one (primary interface) or stage two (PTO) is not intuitive. Hence the following rules have been consistently applied:

- All parts of the power conversion chain that occur before the application of an external (driving or opposing) force are classified as stage one.
- The step where a PTO force is applied is stage two.
- Any further modifications to the power flow are stage three.

2.2.9 Power conversion chains for selected WECs

To demonstrate this new classification system, the complete power conversion chains for selected WEC concepts are now described. Full classifications (as shown in Table 2.1) for two well known concepts are given in Tables 2.3 and 2.4.

Oscillating water columns

An OWC can be compared to a wave activated body (such as a buoy) by considering the three stages of power flow. In the first stage, the energy in the wave is diverted into a different form: an oscillating solid in the case of a buoy, and a pulsating volume in the case of an OWC. If there is no PTO force, then all the energy is returned to the sea in the form of radiated waves, turbulence, or heat. When a PTO force is applied, this retards the primary absorber. Less energy is returned to the sea, so it is clear that the prime absorber is slowed down: the buoy will not reach the same amplitude of displacement as when there was no PTO. Likewise the OWC will not reach the same peaks of volume. If high levels of damping are chosen, then the displacement of the buoy, or the pulsation of the water column, will be retarded considerably. In a buoy this is achieved by the choice of damping coefficient, in an OWC by the turbine torque, via the choice of generator field current.

The PTO stage occurs at the point of application of the PTO force, which opposes the motion of the primary absorber. For this reason the first mechanism resisting a buoy's motion, often a hydraulic damper, is the PTO (second) stage, while in an OWC the turbine is the PTO stage. In an OWC the water and air columns are coupled: neglecting compressibility, they move together. The PTO force applied to the secondary interface, the air column, is transmitted back to the primary interface, the water column. The Wells turbine, shaft, and electrical generator are also coupled (neglecting torsion), as it is the generator that supplies the opposing force.

In both a wave activated body and an OWC, the transformations to the power flow that occur in the power regulation (third) stage do not directly effect the primary absorber. Power regulation

consists of a series of power transformations, including storage. Power could be stored by a pressure accumulator or flywheel before electrical conversion, or with capacitors or chemical storage after electrical conversion. In a wave activated body, storage can take place before or after electrical conversion, as described in § 2.2.7 on direct and buffered drives. In an OWC, storage can only take place after electrical conversion, as the power is already in electrical form after the PTO stage.

Overtopping devices

In the same way that an analogy may be drawn between OWCs and wave activated bodies, overtopping devices can be compared to other types of WEC. Like an OWC, the primary absorber of an overtopping device is a pulsating volume of water. In an OWC the volume moves vertically and is completely surrounded by a solid cassion. The air-water interface is coupled because the air is contained by the cassion, and the PTO force applied to the air column is transmitted back to the water column. In an overtopping device, the water volume moves diagonally, and the water-air free surface is not coupled in the same manner: the PTO force is applied directly to the water column.

To determine the location of the PTO stage in an overtopping device, it is necessary to consider the unimpeded and impeded behaviour of the primary absorber. Unimpeded flow, with all the energy returned to the sea, occurs when the maximum height of the water column has not reached the top of the overtopping ramp. The volume of water pulsating along the ramp is the primary absorber. If it were possible to lower the freeboard by mechanically dropping a panel at the top of the ramp, then any water that would previously have passed this point would now overtop into the reservoir. As some of the water volume is transfered to the reserviour, so there is less on the ramp: primary absorber has been impeded.

The oscillating volume of water on the ramp is modified in a highly non-linear fashion: it has been partially rectified. This is analogous to applying a non-linear damping law that only resists motion in one direction, is only applied once a limiting value of velocity is reached, and thereafter maintains the velocity at that limit. An analogy can be drawn to the choice of damping coefficient in a wave activated body by imagining an overtopping device with a series of panels at different heights that could be opened or shut, such as a version of the Slot-Cone device [42] that could mechanically control the openings to the lower reservoirs. Opening the lower panels on an overtopping device is analogous to using a high damping coefficient to resist the motion of a wave activated body: the volume of the water on the ramp will be greatly impeded. In a floating overtopping device such as the wave dragon, the freeboard can be adjusted using air ballast, and this effectively determines the level of damping of the water column.

WEC concept	Examples	Stage 1	Stage 2	Stage 3
Oscillator with hydraulic transmission	Pelamis, Duck	oscillating solid	hydraulic transmission - pulsating fluid: rectification, gearing, storage	fluid machine
	CETO, Oyster	oscillating solid	pressurised seawater: rectification, gearing, storage	high head hydro turbine
Oscillator with rotational transmission	Manchester bobber	oscillating solid	rotating shaft: gearing, storage (flywheel), $\frac{1}{2}$ rectification	generator
Solid pulsator with hydraulic transmission	AWS 2008	pulsating solid - oscillating solid	hydraulic transmission: gearing, storage, rectification	fluid machine
Solid pulsator with direct drive	AWS 2004	pulsating solid - oscillating solid	direct drive generator	power conditioning: gearing, smoothing
	Clam	pulsating solid - pulsating air	water turbine directly driven	power conditioning: gearing, smoothing
OWC	Limpet; Azores OWC	pulsating water - pulsating air	oscillating air column: gearing	air turbine: rectification
Overtopping device	Wave dragon	pulsating water	overtopping volume of seawater: gearing,$\frac{1}{2}$ rectification, storage	low head hydro turbine
OWC activated oscillator	AquaBoUY	pulsating water - oscillating solid	hydraulic transmission - pulsating fluid : gearing, rectification	water turbine

Table 2.2: ***Power conversion chains for selected WECs.***

Power transfer stage	Attributes	Options
Intercepted power	type of primary interface	oscillator
	modes of motion	heave, sway
	orientation	attenuator
	location	near shore, offshore
	power conditioning	limitation
Captured power	means of reaction	balancing
	energy carrier	fluid flow
	power conditioning	rectification, limitation
Delivered power	energy carrier	electricity
	power conditioning	gearing, storage, limitation

Table 2.3: ***Classification of Pelamis according to power flow.***

Power conditioning in direct and buffered drive systems

Two well known WECs under commercial development, Pelamis and Achimedes Waveswing (AWS), are described here. The summarised classification in Table 2.2 is extended in Tables 2.3 and 2.4. The older version of the AWS [43] is described, as it has a linear generator, which makes it direct drive. The classification shows the distribution of the power conditioning functions. The power conditioning in the Pelamis is typical of a buffered drive system, while the power conditioning in the AWS with a linear generator is typical of a direct drive system.

In the Pelamis, the power conditioning function of limitation is carried out at all three stages. In the first stage, the power in large waves is not translated into motion. Large waves cause submergence of the device. Another way of viewing this is to say that the relationship between excitation and response becomes non-linear for high wave elevations. In fact, this is the case for all WECs, so it is not clear whether it is necessary to specify limitation as a function of the primary absorber. In the power capture stage, forces can be limited through the choice of the PTO impedance. The PTO mechanism is a hydraulic pump that works with both low and high pressures. The PTO mechanism thus performs the power conditioning function of rectification. In the power regulation stage, the high and low pressures are stored in accumulators, which feed a high speed hydraulic rotary machine. This process does the job of storage and gearing. In the regulation stage the limitation is in the form of a heat dump; excess power is dissipated in a resistive water heater.

In the AWS with a direct drive PTO, all the power conditioning functions occur in the

Power transfer stage	Attributes	Options
Intercepted power	primary/secondary interface	pulsating solid / oscillating solid
	modes of motion	heave
	orientation	point absorber
	location	near shore, offshore
	power conditioning	limitation
Captured power	means of reaction	fixed
	energy carrier	electricity
	power conditioning	limitation
Delivered power	energy carrier	electricity / chemical ...
	power conditioning	gearing, rectification, storage, limitation

Table 2.4: ***Classification of the AWS according to power flow.***

power regulation stage. The power electronics converter changes the AC electricity to DC (rectification), and then back to AC of the correct frequency (gearing). If a steady power level is required then storage can be included. Limitation can occur at all three stages. The relationship between excitation and response becomes more non-linear for higher waves. The choice of PTO damping (applied via the field current) limits the amount of power captured. It is possible to include a heat dump in the power electronics converter, so limitation can also take place in the regulation stage.

Comparison to an existing method of defining the power conversion chain

In [35] the break-down of the power conversion chain appears similar to the method proposed here. In Fig. 13.11 of [35] the power conversion chain is also split into a primary interface (front-end conversion), a PTO system (intermediate conversion) and a power regulation (final conversion) stage. Closer inspection shows that criteria different to those described above (§ 2.2.8) have been used, leading to a different way of classifying the power conversion chain:

- For systems with air-turbines, [35] classifies the air flow and air turbine as part of the PTO system, whereas the new classification (§ 2.2.3) considers the air flow as the primary interface, and the air turbine and generator as the PTO stage.
- For overtopping systems, [35] classifies the water flow and water turbine as the PTO

system, whereas the new classification (§ 2.2.3) considers the water turbine and the water flowing past as part of the power regulation stage.

- For systems with hydraulic transmission, [35] classifies the relative body motion, hydraulic pump, and hydraulic motor as the PTO system, whereas the new classification (§ 2.2.3) considers the relative body motion as the primary interface, the hydraulic pump as the PTO stage, and the hydraulic motor as the power regulation stage.

- For systems with mechanical transmission, [35] classifies the relative motion, the mechanical transmission (for example rotating shaft), and the gears as the PTO stage. The electrical generator is classified as part of the final conversion (power regulation) stage, along with the power converter. However, in the new classification (§ 2.2.3), relative motion is classified as the primary part of the primary interface, the rotating shaft and gears as a secondary part to the primary interface, the electrical generator as the PTO, and the power converter as the power regulation.

- For direct drive systems, [35] classifies the relative motion as the PTO stage. The direct drive generator is classified as part of the final conversion stage, along with the power converter. However, in the new classification (§ 2.2.3), the relative motion is classified as the primary interface, the direct drive generator as the PTO, and the power converter as the power regulation.

The proposed method of defining the power conversion chain (§ 2.2.8) is better because the elements classified as the PTO stage perform the same task: opposing the relative motion of the primary interface. This results in a classification system that is compatible with the governing equation of motion and underlying physical processes, such as the generation of radiated waves. A classification that identifies components that perform the same task is useful. It allows a fair comparison of the relative merits of different WECs or subcomponents. Furthermore, it provides a link between the theory and the classification. It explains why the PTO force and velocity in an oscillating body are analogous to the pressure and flow rate in an OWC. It also explains why these are not analogous to the head and velocity of the fluid flow through an overtopping device's water turbine, which instead can be compared to the pressure and flow in a hydraulic motor (the power regulation stage).

Lastly, this method of classification is useful for understanding the types of control problems and solutions associated with each stage of the power conversion chain (§ 2.3.1). In [35], the direct drive generator driven by the relative motion between it and the primary interface, is compared to the electrical generator driven by a hydraulic motor. Impedance matching as described in Chapter 4, is a technique that is suitable for the direct drive generator, but not for the generator driven by the hydraulic motor.

2.3 Definition of control

Another advantage of classification according to the chain of power flow is that it lends itself to classification of the control problem. A good understanding of the difference between control performed at each of the three stages of power transfer aids communication by limiting ambiguity. It also provides a tool for understanding the interaction between the three stages of control and thus can focus research and development priorities.

The term *control* can be used to describe the regulation of power flow in any of the three stages in the power conversion chain. This section describes the type of control at each stage and defines the interpretation of control in the literature and in this research.

2.3.1 Classification of control by power flow

Stage 1: Geometry control

Geometry control is a new term introduced here for the first time. It is defined as anything that alters a WEC's geometry dependent hydrodynamic parameters (the radiation impedance or excitation coefficient), or its dynamic parameters (terms in the intrinsic impedance other than the radiation impedance), during operation (terms described in Chapter 3). It can be used to change amount of incident energy, via the directionality; the upper limit of monochromatic capture width, via modes of motion; or the proximity of the achievable monochromatic capture width to this upper limit, via the intrinsic impedance. Examples of geometry control include:

- Aligning a directional device with respect to the principal wave direction, which changes the excitation coefficient.
- Altering mechanical mass or spring coefficients (often referred to as 'slow tuning'), which changes terms in the intrinsic impedance that are not due to radiation.
- changing the configuration of structural members relative to each other or the water surface, which affects both excitation coefficient and intrinsic impedance
- Changing the degrees of freedom of motion with respect to each other or the water surface, which affects both excitation coefficient and intrinsic impedance.

Geometry control works best when used in conjunction with PTO force control.

Stage 2: PTO force control

PTO force control determines the amount of power returned to the sea during the second stage of the power conversion chain. The amount of power returned to the sea also depends upon the intrinsic impedance, which is why geometry control works better when PTO force is also

controlled. PTO force is however usually studied independently of geometry control, as in many WECs, the hydrodynamic coefficients are fixed (terms defined in Chapter 3). In § 2.3.2 it is shown that, for linear control, PTO force control is equivalent to determining the PTO impedance.

Stage 3: Power regulation

Control of the third stage refers to regulation of the quality and quantity of the delivered electricity. Load shedding, voltage control or power factor control may be applied at this stage. In a buffered system, power conditioning may include storage management. In a direct drive system, power conditioning may include power smoothing (storage), and control of frequency, harmonic content, and voltage.

None of the parameters in the governing equation of motion are altered directly by this stage of control. However, good management of storage and load shedding can enable better strategies to be chosen in the power capture stage.

2.3.2 Control regimes

The operation of all three stages of control depends on the PTO regime. The PTO regimes are the different control aims that exist under different conditions.The focus here is on how the PTO regime determines the function of the second (PTO) stage of control, and of the combination of the first (geometry) and second stages of control. The PTO regime also determines the function of the third (power regulation) stage of control, but this topic is not within the scope of this research. The PTO regimes considered here are those that can be used to describe the operation in different types of sea states:

- Capture no power.
- Maximise generation of power.
- Maximise generation of power given constraints and limitations.
- Capture a set level of power.

There may be other control states, such as avoidance of storm damage, or diagnostic and test states. Control states that do not relate directly to normal power production are not within the scope of this thesis.

Set-point regime

Capturing a set power level has much in common with the conventional definition of control. Feedback can be used to minimise the difference between the desired power (set-point) and the

regime	Restriction	Details
maximum	none	upper limit set by acausal optimum control
maximum	causal	force feedback; variable coefficient
maximum	causal, linear	fixed coefficient sub-optimal impedance matching
limitation	causal, limits on reactive power	fixed coefficient limited range impedance matching
maximum	causal, no reactive power	latching
maximum	causal, linear, no reactive power	real sub-optimal control: damping only
limitation	causal, statistically low undesirable events	soft amplitude constraints: load-shedding, detuning
limitation	causal, preventing or reversing undesirable events	hard constraints: force clipping, end-stops
set-point	causal, power limitation	hard constraints: rated power generation

Table 2.5: ***PTO regimes and restrictions.***

actual power. The set-point could be chosen to be the instantaneous, peak, or running-average power. The choice of set-point is determined by factors such as generator rated power in a direct drive system, spare storage capacity in a buffered drive system, and the required quality of delivered power for grid integration.

Maximum regime

When the goal is to maximise power generation, the conventional approach of feeding back the error to minimise the difference between the set-point and the output has an extra level of complexity. The set-point is not known, so the control task includes its estimation. Estimation of the power set-point usually takes the form of finding the optimum velocity, PTO force, PTO impedance or total WEC (net) impedance, which are all different formulations of the same control problem. In fact the term *control* is often used in the wave energy community to indicate this task of determining the set-point.

The difference between the power maximisation and the amplitude limitation regimes is not straight-forward. Both have the goal of capturing as much power as possible for given constraints. In the power maximisation regime these constraints are built-in. They could be, for example, restraints due to the type of generator, the availability of advance information about approaching waves, or the ability to apply a varying PTO force that can be used to

implement linear control. These are all absolute constraints and are specific to a given WEC. For instance, if the hardware only allows unidirectional power flow (from the primary interface to the PTO), then the restriction of no reactive power flow always applies. Likewise, if there is no information about near future waves then the WEC is restricted to causal control. If the PTO force is limited to coulomb damping[1] [44], then the WEC is limited to non-linear control. These restrictions apply to all sea states.

Limitation regime

The amplitude limitation PTO regime involves conditional constraints. There are upper limits of allowable forces, displacements, reactive power or real power. As long as none of these upper limits have been reached, the control regime remains at generating maximum power. As soon as any of the upper limits are reached, then the PTO regime switches over to amplitude limitation.

The terms real and reactive power have the electrical engineering meaning, in the case where the PTO is an electrical generator (a direct drive system). This idea can be extended to other forms of energy carrier other than electricity. Real power is that due to response that is in phase with excitation. Reactive power is that due to response that is 90° out of phase with excitation. A PTO system that allows no reactive power (Table 2.5 on page 33) has unidirectional power flow; instantaneous power is always positive (or zero). A PTO system that allows reactive power has bi-directional power flow; instantaneous power is negative for part of a wave cycle. Limits on reactive power are either due to limits on instantaneous captured power (stage two) or self-imposed limits on the ratio of peak power to average power. The self-imposed limit is necessary because, as the ratio of peak to average power is increased, the loads contributing to fatigue get larger, while there are diminishing returns for energy production due to losses.

Limits on real power may include limits on instantaneous power and limits on average power. Limits on instantaneous power depend on the rating of the PTO plant (stage two) and spare storage capacity. Limits on average power depend on the chosen set-point of delivered power in stage three. This is usually the rated power, but may be less than the rated power for operational reasons. Although it is necessary to have a mechanism for dissipating any absorbed power that is surplus to the desired level of delivered power, it may nevertheless be desirable to limit the surplus absorbed energy. This surplus absorbed energy generates no income but invokes costs, as the loads contribute to fatigue.

There are many strategies for determining the set-point for power in the maximum and limitation regimes. Many of these are a specific solution to the absolute or conditional constraints imposed on the system. These strategies can be arranged roughly hierarchically,

[1] The PTO force only has three possible values: a negative value, zero, or a positive value. These are applied when the velocity is negative, zero or positive respectively

starting with the power maximisation regime with no restrictions. Many of the restrictions may apply simultaneously or hierarchically for one WEC. For example, two common types of limitation are upper limits placed on instantaneous power and displacement. In a build up to a storm, with progressively energetic sea states, one of these limits will probably be reached first, and when the second is reached the control system must then apply them simultaneously. The limit that is reached first will be specific to given WEC concepts, or even different versions of the same WEC, and may also depend on the sea state. The order of amplitude limits will also depend on the sea state.

In Table 2.5 the absolute and conditional constraints have been arranged hierarchically. The more a constraint restrains operation and power capture, the lower it is on the list.

No power capture

When the sea state contains insufficient energy then no power will be generated. If a sea state is very energetic it may be necessary to stop capturing power and to put into place procedures to limit the risk of storm damage. In a WEC with intermediate storage to smooth the power output, it may be desirable to allowed stored energy to reach a given level before switching to energy capture in the power maximisation regime.

2.3.3 Definitions of control

The word *control* has a specific meaning in wave energy literature that is different from the use of the word in control engineering. In control engineering the term means that there is a desired system state or set-point, and that it is possible to choose one of the system inputs in order to move the system towards the desired state. Furthermore, the term control often has the further implication of *closed-loop control*, where the difference between the desired state and measurements of the actual state are used to determine the controlled inputs.

In wave energy literature, the most common usage of the term *control* does not mean control in the classical sense at all, and is strictly an *optimisation* problem. It is typically used to mean the optimisation of the PTO settings, which corresponds to the second stage in the control classification by power flow. The most common usage also refers to a control regime that aims to maximise energy capture. This is optimisation rather than control because there are no set-points: the desired system state is to capture as much energy as possible, but it is not known how much is actually possible. There are however various ways of choosing the PTO settings that optimise the system, and these methods are the focus of much of this thesis.

In wave energy literature, the term *control* sometimes covers a broader scope. In § 2.3.2 control regimes with set-points were discussed. If there is a set-point then the term *control* takes on the meaning it has in classical control engineering. When operating at rated power, the set-point is the average or instantaneous power flow in any part of the power conversion chain. When

operating in a control regime that maximises power while limiting forces or displacement, then the control system is continually switching between optimisation and set-point control. In § 2.3.1 it was seen that *control* can also refer to geometry control, for example adjusting the water in ballast tanks, or to power regulation, for instance storage management. Geometry control is the optimisation of the device hydrodynamic and dynamic characteristics, while storage management usually involves control in the classical sense, where the set-point may be generator voltage or spare storage capacity. Some authors interpret WEC control as the control of electric generators [41]. Note however that a generator can perform the function of either the power capture (direct drive) or power regulation (buffered drive) stage. Some authors mean power regulation (stage three) when referring to control of WECs [45], but this is not the common usage of the term. As control of a generator in the power regulation stage is a more mature technology and less specific to wave energy, most of the research focus is on PTO force control. Most of the literature does not include geometry control when considering control of WECS. Reasons for this are that it is a less mature research area, and it is highly specific to a given design of WEC. While PTO force control is strictly an optimisation problem, the association of the term *control* with the problem of optimising PTO settings is so strong in wave energy literature, that this commonly understood usage has been continued here.

Control considered in this thesis

The thesis concerns the extent to which predictions can improve power capture. Here power capture refers specifically to primary power capture, so from the point of view of the thesis, PTO control is the most important. The research presented here focusses on PTO control, but the tools introduced to understand PTO control can also be used to understand geometry control and power regulation (Fig. 2.6).

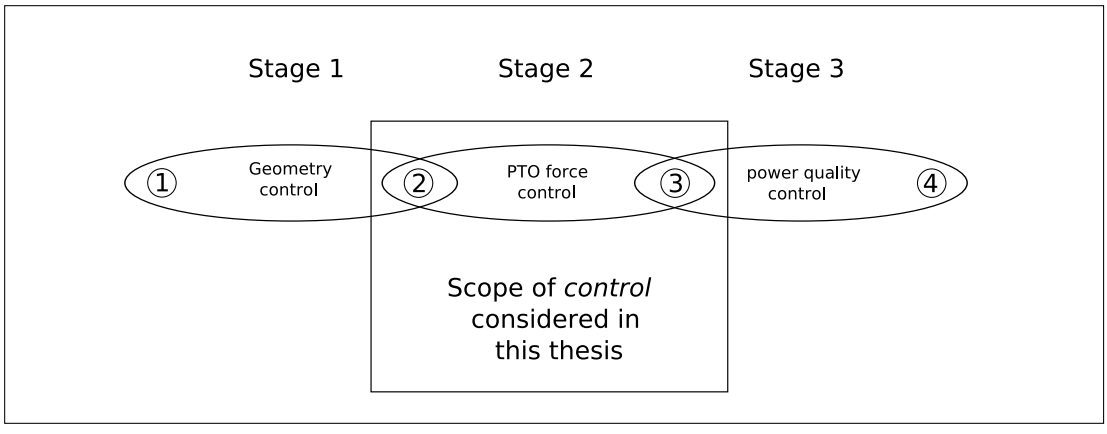

Figure 2.6: ***The scope of control considered in this thesis:*** *covers stage two of the classification of control according to power flow.*

2.3.4 Types of control used by commercial developers

The hierarchy described here (§ 2.3.1) is different to the classical concept of a control hierarchy. From the point of view of the physical implementation of a control system, it is more intuitive to define the hierarchy of various overseeing controllers, down to the blocks of code or embedded processors performing specific sub-tasks.

Nevertheless, the control hierarchy described in Table 2.5 is relevant to the practical implementation of control. There are choices that an overseeing controller might make. Once the PTO regime is chosen, there are further decisions about whether to achieve this aim via geometry control, PTO control, or power regulation; or a combination of these. Presently, commercial developers do consider all these three stages of control. Not much is published about geometry control, yet it is in use. AWS make use of air springs [43] that are designed to give an adjustable spring constant during operation. As elaborated in the case study which follows (§ 2.3.5), the angle of motion of the Pelamis can be controlled.

The weight of the water in the reservoir of the Wave Dragon contributes to its total mass, which functions as an inertial point of reaction, affects its floating height (the geometry of the wetted surface) and the height of the ramp. Here it is clear that management of reservoir levels and the motion of the superstructure affects all three stages of control. The geometry of the wetted surface and the total mass determine the intercepted power (geometry control). The height of the ramp above mean water level determines the captured power (PTO control). The spare (usable) reservoir capacity determines the delivered power (power regulation). In [46], the management of floating height is described as *slow control*, and is achieved by pumping air into open bottomed chambers. The use of data collected upstream to give forewarnings to aid reservoir management is described as *fast control*.

Power regulation and PTO force control are implemented to some degree by all developers of WECs. Details of the strategies used are generally difficult to come by because of commercial sensitivity [47]. There is some published information on the Pelamis device however, and the following section is devoted to a discussion of the control of this device.

2.3.5 Case study: Pelamis

Device concept

Pelamis Wave Power (PWP) is the commericial developer of the Pelamis WEC, shown in Fig. 2.7. This device is currently the industry leader in terms of investment capital raised, development program and installed capacity. It is also well documented, with many of the details of its operation discussed in academic publications [13, 14, 48–50]. For this reason, it has been chosen as a case study. Its power conversion chain and control strategies are reviewed here.

Pelamis is a semi-submerged, slack-moored, articulated WEC. A description of its operating principles is given in [48]. These are summarised in Table 2.3 (page 28), in terms of the newly introduced classification system. The second and third stages of power transfer correspond with the primary and secondary transmission described in [49].

Power is taken off by damping the relative angular motion between the long horizontal cylindrical modules. The modules move relative to each other with two degrees of freedom. In the present version of the Pelamis, the P1, the joints are on either end of a short cylinder known as the power module. If the joints about which the modules moved were parallel and perpendicular to the sea surface, movement about the joints would be in pitch and yaw. This allows the power modules to move in a combination of heave and sway. The joint axes have however been offset in the roll direction so that movement around each joint has components in both pitch and yaw. The advantage of this is that movement about either joint results in a restoring buoyancy force. There are additional advantages in terms of controllability. Numerical and experimental studies [51, 52] have shown that an inclined angle of coupling between two degrees of freedom also results in a broader and higher monochromatic capture width (see § 4.6.1 and § 5.2).

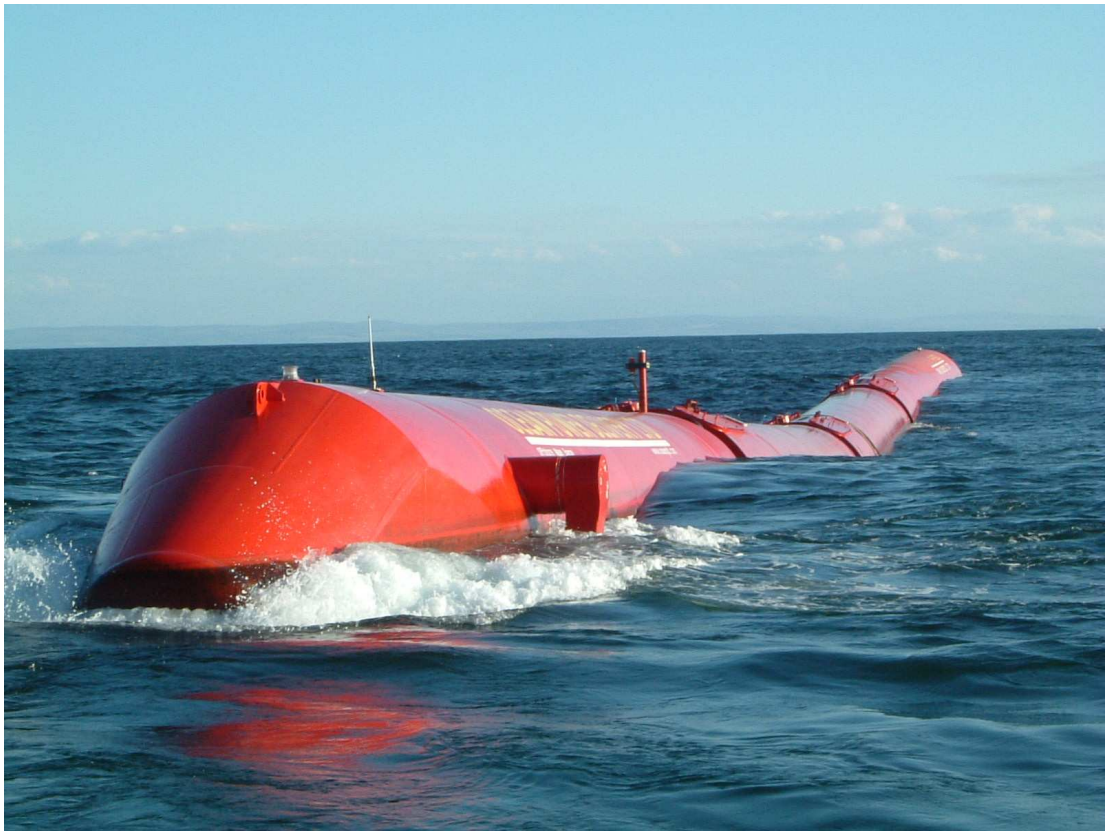

Figure 2.7: ***The Pelamis WEC:*** *The P1 prototype undergoing sea trials.*

Control strategies

For a system with translational degrees of freedom, power is defined by velocity and force. For a system with rotational degrees of freedom, such as Pelamis, these terms become angular velocity and moment of force (torque).

The offset angle of the joints sets the resonant frequency for the Pelamis by determining its angle of motion with respect to the water surface when it is oscillating freely. This can be chosen to match the dominant wave climate [49]. When the motion is damped, the angle of motion is determined by the ratio of PTO damping coefficients in the two orthogonal degrees of freedom [48]. This changes both the excitation and radiation hydrodynamic coefficients.

Control of the joint offset angle is geometry control; stage one in Fig. 2.6 (page 36). Pelamis also implements another type of geometry control: passive alignment with respect to the principal wave direction. This is presently used to limit forces rather than increase power, as the Pelamis is designed to operate in attenuator configuration.

PTO force control (stage two in Fig. 2.6) is also implemented. Details about PTO regimes have not been published, but it seems probable that there will be a maximum power regime based on fixed coefficient impedance matching (the sub-optimal causal reactive control described in Chapter 4), and amplitude limitations on reactive power and displacement.

Once the required ratio of the PTO damping coefficients in the two orthogonal joints is decided, the concept of impedance matching is used as a basis to decide the required PTO moments (angular version of force). Transducer measurements of any joint parameter, such as angle or angular velocity, can be used to choose the desired PTO settings. These settings are required to determine the set-point, as described in § 2.3.2. When modelled numerically, these are treated as fixed settings. They are in fact changed on a slow time-scale. Details of the method for finding the PTO settings are not published, but spectral analysis is probably used to choose the desired operating frequency, and the settings are then a function of this operating frequency. The settings could be found either using a mathematical function, or by using a look-up table with pre-calculated values.

The PTO settings are then multiplied by the instantaneous transducer motion measurements to give the desired moment, F_{ref1} in Fig. 2.8. If necessary, limits are implemented, giving F_{ref2} (Fig. 2.8). There are number of possible limits which could be applied individually or as a group. Limits on real and reactive power (as described in § 2.3.2) are imposed by accumulator capacity and the rating of the hydraulic pump. Angular displacement restraints are imposed by the range of the joint angles. Additional soft limits may be in place to restrict behaviour that shortens component lifespans. The required moment of force is then quantised, that is, several discrete levels of moment are available, and one of these levels is chosen to represent the required moment. The result is the PTO moment set-point, F_{ref3} in Fig. 2.8.

The actual PTO moment, F_{pto} in Fig. 2.8 is made to track the set-point as closely as possible.

The moment levels are actuated by choosing the number of cylinders in the pump that are open at any time. These cylinders are opened with electronically controlled valves. The moment level is adjusted many times during each cycle to give a stepped approximation to the smooth set-point. The PTO moment of force F_{pto} is thus a discretised approximation to F_{ref3}.

In the power maximisation regime, the resulting moment [49] contains too many harmonics to conform to many definitions of linearity, so time domain simulations are used to model real-time response. Nevertheless, it is linear enough for linear modelling to be useful in some instances. Frequency domain analysis was used to develop the Pelamis design [14].

The process for choosing the PTO force for one joint is shown in Fig. 2.8. The choice of PTO impedance (Z_{pto}) is updated relatively slowly, whereas the calculation of the moment set point F_{ref3} is made frequently, with [49] indicating updates every 0.5 seconds. The function that chooses the PTO impedance takes into account the ratio between the damping in the two orthogonal joints, as well as the impedance matching principle. This function may also impose

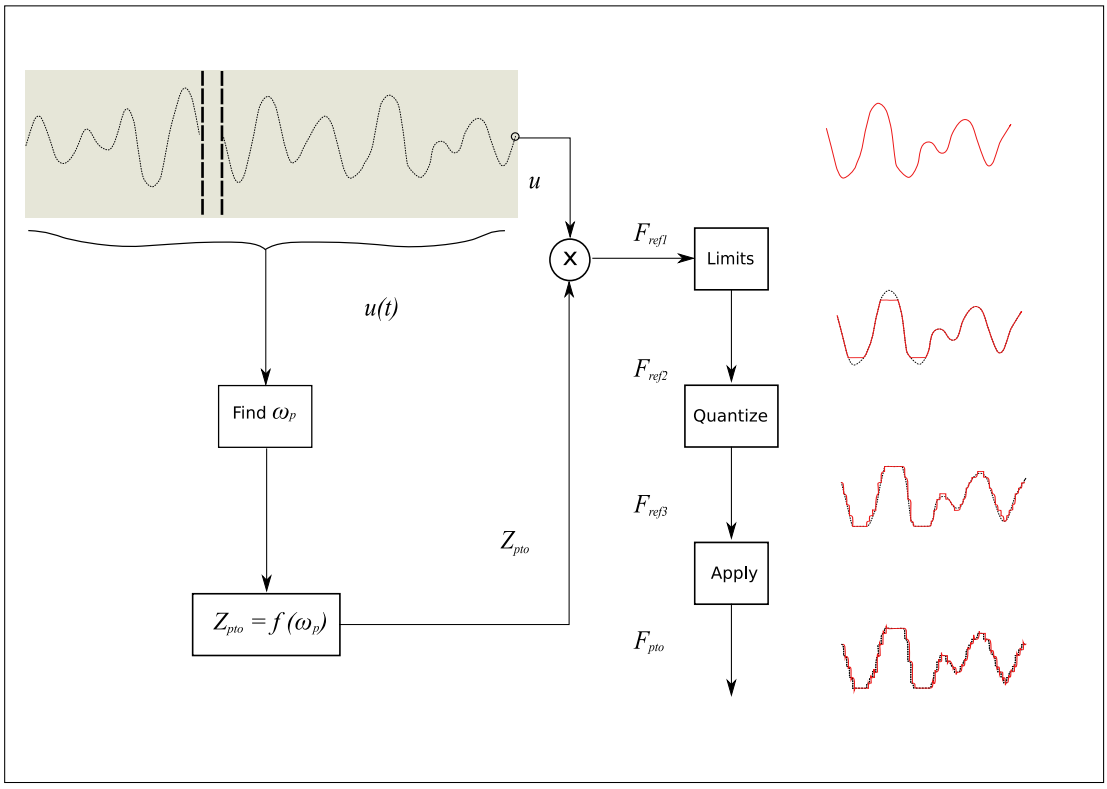

Figure 2.8: ***Possible implementation of control in the Pelamis WEC:*** *F_{ref1} is the instantaneous velocity multiplied by the PTO impedance Z_{pto}, which is a function of the operating frequency ω_p, i.e. $Z_{pto} = f(\omega_p)$. F_{ref2} is F_{ref1} with amplitude limits imposed (in this case force limits), F_{ref3} is a quantised version of F_{ref2}, and F_{pto} is the PTO force which is controlled to track the reference force, F_{ref3}, as closely as possible.*

limits on the value of the PTO impedance to limit the range of impedance matching. Each pair of joints is capable of real-time independent control. They are however linked to a centralised overseeing controller, which can co-ordinate the control of each pair of joints.

Power regulation (stage three in Fig. 2.6) is also implemented. The generator voltage is kept as smooth as possible. Changes to (peak) voltage are made using a slow ramp. Excess power is dumped using resistive heating [48].

2.3.6 The effect of classification on the dynamic equation

An important purpose of this classification exercise is to relate the physical design of a WEC to its equation of motion. This link between reality and the mathematical models used to describe it is useful as it allows different bits of theory to be related to different types of WEC. A dynamic equation can be used to describe any stage of the power conversion chain. The dynamic equation describing the PTO (second) stage is the most useful, and this is referred to as the governing equation of motion of a WEC in this research.

Stage one

The governing equation of motion described in this work assumes a system of constant mass. If a type of geometry control is used that alters the system mass, then the governing equation must be changed to include the time variance of the mass. A time domain equation will be required for this; however a frequency domain equation could be used to calculate the response for different values of total system mass.

The type of energy carrier in the last step of stage one is important. This is the type of primary interface, or if there are two interfaces, the type of secondary interface. The part of the primary interface that interacts with the PTO determines whether this equation of motion is written as a function of motion or volume flow.

In a fixed volume oscillating body, the excitation is a force (between the fluid and the body) and the response is the velocity (between the PTO mechanism and the means of reaction). The power generated is the product of this velocity and the PTO force (measured between the PTO mechanism and the means of reaction).

In a pulsating (solid or fluid) volume, the excitation is a pressure (between the fluid and the body) and the response is the volume flow rate (relative to the PTO system, and ultimately the means of reaction). The power generated is the product of this volume flow rate and the PTO pressure (measured relative to the pressure at rest). By considering the excitation force due to the excitation pressure, and the motion of the water surface that causes the volume flow rate, a pulsating volume WEC can also be modelled using force and motion [53]. Although the equations in this research refer to a WEC operating by motion of a fixed volume, the principles

apply to the operating principle of a pulsating volume. All statements about forces and velocity can be applied by analogy to pressures and volume flow rate.

The dynamic variables in the governing equation, velocity and wave elevation, are scaled by impedance and excitation coefficients. The impedance coefficient transforms the body motions to forces, while the excitation coefficient transforms the wave elevation to forces. The values of the hydrodynamic coefficients depend on the geometry, the modes of motion and the orientation of the primary interface. The impedance and excitation coefficients are influenced by the primary interface. For instance, the general characteristics associated with a submerged pulsating solid are different to those associated with a floating oscillating solid. The exact shape of the coefficients depend on the exact details of the geometry. The coefficients scale with geometry. There are also general characteristics associated with each mode of motion. For example, there is buoyancy spring (see § 3.5.4 on page 97) in the heave and pitch modes; and there is coupled motion between the pitch and surge modes. Not all WECs move with degrees of freedom corresponding to the modes described in Fig. 2.3. The axes of the degrees of freedom may be inclined to the vertical or horizontal. In this case a transformation matrix is required to move between the standard modes of motion and the degrees of freedom given by the inclined axes [51, 54]. The value of the excitation coefficient depends on the angle of incidence of the wave. In uni-directional seas, a terminator can absorb more power but will be subject to higher loads than an attenuator. A point-absorber diffracts (scatters) very little of an incoming wave (see Fig. 2.2), so a common modelling simplification is to neglect the diffraction force from the excitation force, so that it contains only the Froude-Krylov force (see page 160 of [55]).

In § 4.6 (page 143) a measure of efficiency, the capture width, is discussed. The upper bound of this capture width [56] is determined by the modes of motion. Intriguingly, the upper bound of capture width is not affected by the scale of the WEC, so a point absorber has the same upper bound as a scaled up version of itself. This means that, in theory at least, a small WEC (a point absorber) could absorb as much power as a large WEC. In Chapter 4, it will be shown that although the upper bound is not affected by scale, the capture width using a realisable control scheme is. While the width of the wave that can be captured is greatly influenced by the modes of motion and choice of PTO strategy, the energy contained within that captured wave is highly dependent on the directionality (attenuator or terminator configuration).

The same equation of motion can be used regardless of the number of degrees of freedom of a system. For n degrees of freedom, forces and motions are vectors with n terms; the excitation coefficient that transforms wave elevation into an excitation force is also an $n \times 1$ vector, and the impedance coefficients that transform motions into forces are $n \times n$ matrices. For a single degree of freedom, all the terms in the equation of motion represent scalar (single) values.

Stage two

The type of reference point will affect the values of the motion or pressure variables, which must be measured relative to the reference point. The equations presented in this research are for motion referenced to ground, but many of the principles and conclusions also apply to coupled motion. When the PTO force is relative to another moving body rather than a fixed position, the motion or pressure variables in the governing equation of motion become the relative motion of the moving bodies. The equation of motion must be extended to a two (or multiple) body system. The equation of motion will be written in the same form, but the velocity vector will contain up to six degrees of freedom for each body. The radiation of waves by each body in this system will result in radiation forces on all the bodies in the system. This effect is represented by terms in the impedance matrix.

Stage three

The design choices made for the final stage of power transfer (stage three) determine the control regime (§ 2.3.2) for any given sea state. Thus the third stage of power transfer has a significant influence on the efficiency and availability of the WEC. There is an indirect influence the governing equation of motion via the choice of PTO control strategy. However, if this strategy happens to be optimisation of power capture, then the power regulation stage has no influence on the PTO stage. It is only when the control regime includes the application of limits that decisions made at the power regulation stage are fed back to the PTO stage.

2.3.7 The relevance of this research to different types of WEC

The theory developed for this thesis is based on a governing equation of motion, which models the power capture stage (two) of power transfer in a WEC. The model presented is for a floating solid oscillator, with PTO referenced to ground. The equation of motion is therefore written in terms of the acceleration, velocity and displacement of the primary interface relative to ground. The impedance coefficients are taken from a published study of a scale-normalised geometry [57] (see Appendix A). The oscillator is not modelled as a point absorber, which means that the effects of diffraction are included in the excitation coefficient. The PTO force is modelled as linear. Amplitude constraints [58] have not been modelled.

This configuration results in the most conceptually simple equation of motion. Although specific geometries are considered, this model is nevertheless generic, as it serves the purpose of demonstrating universal principles rather than understanding a specific design of WEC. Many insights gained from the study of this model can be applied to other types of WECs, taking into account changes to the equation of motion due to the point of reference and the type of primary interface (oscillator or pulsator; modes of motion), and changes to the impedance and excitation coefficients due to the type of primary interface (oscillator or pulsator; scale; orientation).

Another way in which some WECs differ from the generic model presented in this research is the PTO. In many WECs it is possible to apply a linear PTO force when the waves are small. There are of course exceptions to this rule. In some WECs, non-linear PTO is an operational design choice, or is built-in to the design. The Oyster uses a constant PTO force as an operational design choice to reduce the capital costs and complexity of the system [59]. The Manchester Bobber and overtopping devices have inherently non-linear PTO, because there is built-in half-rectification at the PTO stage, in the form of a ratcheting clutch. In the Manchester Bobber the power from the primary interface is only captured when it is oscillating in one direction. Likewise, in an overtopping device, the power from the diagonally oscillating water column is only captured when the column reaches a certain height.

Governing equations of motion are often expressed in the frequency domain. This approach is only applicable for a linear equation of motion. The theory on the linear behaviour of a WEC is therefore suited to efficient operation in small seas (see § 6.2.8), and is not applicable to any of the following (see § 6.2.7):

- WECs with non-linear PTO,
- WECs excited by waves large enough to induce non-linear response,
- WECs excited by waves large enough to require non-linear PTO (amplitude or power limitation).

In the generic model used in this research, the PTO force opposes heave velocity. As heave is not coupled to other degrees of freedom, calculations of power capture can be performed by considering the heave response only. Nevertheless, equations are presented in such a way that they can be readily compared to equations for multiple degrees of freedom. When simplifications are made to the equation of motion that are valid only for heave motion, this will be stated.

2.4 Introduction to Fourier transforms

The frequency domain is used in many different ways in wave energy engineering. In order to describe the differences between these various approaches, it is necessary to first review the basic theory. This section draws the distinctions between different types of Fourier transform, and describes how these are used to model linear systems. The concept of convolution is briefly introduced as it will become important in later discussions. In § 2.5, this theoretical grounding is used to describe the different ways that Fourier analysis is used for theoretical modelling, measuring sea states, and experimental work.

Just as a signal can be represented as a function of time, it has an equivalent representation as a function of frequency (see § 2.4.2). The transformation between domains is performed using

the Fourier transform and its inverse. The Fourier transform analyses the time domain signal, decomposing it into a number of frequency dependent basis functions. There are two families of Fourier transform, namely the real Fourier transform, and the complex Fourier transform [60]. In the real Fourier transform, the basis functions are sine and cosine waves. The scaled amplitudes of the sinusoids are functions of frequency and are referred to as *the frequency domain*. In the complex Fourier transform, the basis functions are complex exponentials. Their magnitude and phase are referred to as *the frequency domain*. In the complex Fourier transform, both the time domain and the frequency domain are complex.

The complex, rather than real, family of Fourier transforms is used in this work as it is more mathematically rigorous, and so is becoming the standard in many fields. However, the concept of sinusoids as basis functions will still be used to discuss the frequency domain, as they are easier to visualise than complex exponentials.

The following notation will be used:

- A time domain signal is denoted with lower case letters, $x(t)$.
- The corresponding frequency domain function is denoted by capitals $X(\omega)$
- The curved bracket notation is used to denote continuous functions, $x(t)$,$X(\omega)$.
- The square bracket notation is used to denote discrete (sampled) functions: $x[t_n]$,$X[\omega_j]$, with n denoting the nth sample, taken at time t_n, and j denoting the jth *bin* at frequency ω_j.
- In the complex Fourier transform, $X(\omega)$ is complex and may be represented by an amplitude (or magnitude) spectrum, $|X(\omega)|$ and a phase spectrum $\angle X(\omega)$ or $\phi_X(\omega)$.

2.4.1 Types of Fourier transform

There are four categories of Fourier transforms, one for each type of (time domain) signal. A signal may be either continuous or discrete; and either periodic (repeating) or aperiodic. Fig. 2.9 shows the four different combinations, and the associated transform. Table 2.6 gives the time and frequency domain characteristics of each complex transform. The column titled *time domain* corresponds to Fig 2.9. A signal that is periodic in one domain is discrete in the other. Conversely, a signal that is aperiodic in one domain is continuous in the other.

The equations for the transforms have been listed in Table 2.6 because there are several versions. As discussed, there are real and complex versions of each transform. In addition, there are variations in scaling factors and notation. For instance, in the Fourier series (Table 2.6), the $1/2\pi$ term seen in front of the sum in the inverse transform is conventionally placed in front of the integral of the forward transform [61]. This form has been shown here for easy comparison

with the Fourier transform, the discrete time Fourier transform (DTFT) and the discrete Fourier transform (DFT), which conventionally have the scaling factor in the inverse transform [61].

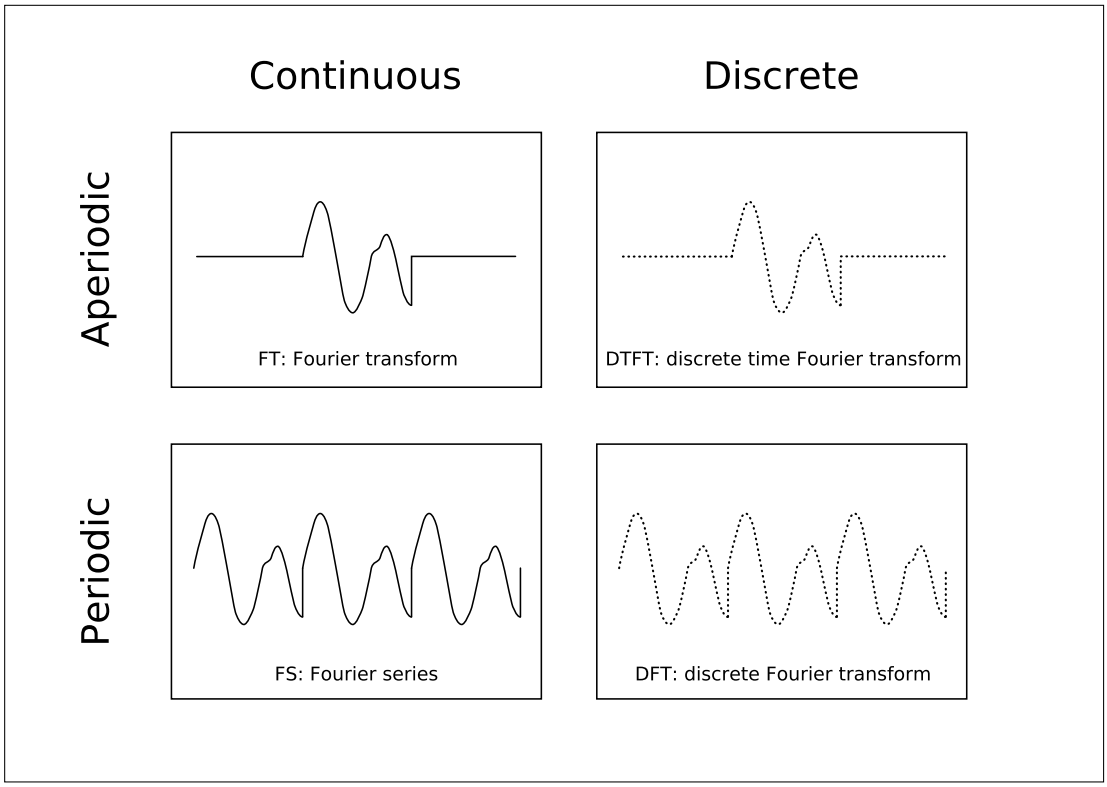

Figure 2.9: ***The family of Fourier transforms:*** *according to the continuity and periodicity of the time domain signal.*

In this research, the Fourier transform (FT) is used for the theoretical equations dealing with generalised properties, while the DFT is used to describe situations where the data is likely to be discrete, such as the analysis of experimental data.

The four types of signal shown in Fig. 2.9 are all infinite; they extend from negative to positive infinity. All categories of Fourier transforms are for infinite signals. This is not immediately clear because the transforms for periodic data are integrated or summed over a finite duration of time, one period. The signal being transformed is nevertheless infinite, as sinusoids are by definition infinite. The problem is that data is generally finite. To use a Fourier transform on data that is truly finite, we must assume that it is a snapshot of an infinite signal.

If the signal has a value of zero for all points outside of this viewing window, then the data is treated as an infinite aperiodic signal. To characterise an aperiodic signal, an infinite number of sinusoids is required. Given that the energy content will be contained within a finite band of frequencies, it follows that the frequency domain signal must be continuous. The FT or DTFT are used.

If the signal outside of the window is assumed to be a duplication of the snapshot data, then the data is treated as an infinite periodic signal. To characterise a periodic signal, a finite number of sinusoids is required, giving a discrete frequency domain. The Fourier series (FS) or DFT are used. Digital computers always use the DFT, because this transform allows both the time domain and the frequency domain signals to consist of data that is discrete and of finite length.

The complex DFT of a time signal of N points is a frequency signal of N points. Both the time and frequency domains are periodic, with the information repeating every N points. It is conventional to present only the DFT of a signal for the first N points. For the purposes of signal characterisation (§ 2.4.4) and finding the frequency response of a linear system (§ 2.4.5), this simplification is valid. These are two applications of the DFT that are commonly used in wave energy engineering.

The DFT $X[\omega_j]$ is defined over integer bin numbers over the interval $j = 0 \ldots N-1$. Positive frequencies are represented at points $j = 0 \ldots N/2$ and negative frequencies by the points $j = N/2 \ldots N-1$. Negative frequencies are thus included in the definition of the complex DFT. As the frequency domain signal is periodic, the information about negative frequencies could also be shown at $j = -N/2 \ldots 0$.

The complex DFT assumes that both the time signal and the frequency signal are complex. For many practical applications (including wave energy), the time domain is real, so the imaginary part is zero. For real time signals the magnitude of the DFT is symmetrical about zero. For this reason, the DFT is sometimes displayed between the limits of $j = 0 \ldots N/2$. This can be misleading because the real DFT is defined between these limits. The inverse real DFT synthesises the time domain signal differently to the inverse complex DFT, so it is important to be aware what type of transform was used to get to the frequency domain.

2.4.2 Conditions for the existence the Fourier transform

A time domain signal has an equivalent representation in the frequency domain, and vice versa, if it fulfils a number of conditions. For a continuous signal, one of these conditions is that it has no discontinuities (sudden jumps), and no discontinuities in slope (sharp corners). A well-known example of a function with discontinuities is a square wave. The Gibbs phenomenon describes how a time series reconstructed from the Fourier Series of the square wave differs from the original: at the edges of the steps there is an overshoot and oscillation. The requirement for a continuous signal with a continuous derivative does not apply to discrete signals: the Gibbs phenomenon does not occur for a discrete version of a square wave.

Another condition that be fulfilled in order for the Fourier transform and its inverse to exist is that the signal must be integrable. This condition applies to all members of the Fourier transform family. Where the domain is discrete (Table 2.6) then the discrete integral (summation) of the function must be possible.

These conditions apply to the Fourier transform of a function. It is also possible to perform a Fourier transform on a generalised function. A generalised function, also known as a distribution or measure, does not obey all the criteria for being a true function: for example it is not possible to find the square of a generalised function. However, they have a known integral and a measurable effect on other functions; The Dirac delta is a generalised function [62] used extensively in this work, and so is defined here.

The delta function

For an independent variable of x, the Dirac delta is an infinitely high and infinitely narrow pulse with an area of one located at $x = 0$, and is zero at all other values of x. Symbolically this is expressed as:

$$\delta(x) = \begin{cases} +\infty & x = 0 \\ 0 & x \neq 0 \end{cases}$$

$$\int_{-\infty}^{\infty} \delta(x)dx = 1 \tag{2.1}$$

The useful property of the Dirac delta is that it can be used to sample the value of a function at any point:

$$\int_{-\infty}^{\infty} f(x)\delta(x-a)dx = f(a) \tag{2.2}$$

From this it follows that it can be used as the identity function for convolution:

$$f(x) * \delta(x) = f(x) \tag{2.3}$$

and as the scaling function for convolution:

$$f(x) * c\delta(x) = cf(x) \tag{2.4}$$

The discrete version of the Dirac delta is a unit sample $\delta[x_n]$ with a value of one at $x_n = 0$ and a value of zero at all other samples:

$$\delta[x_n] = \begin{cases} 1 & x_n = 0 \\ 0 & x_n \neq 0 \end{cases} \tag{2.5}$$

It can be used to sample a discrete function, or as the identity or scaling functions when convolved with a discrete function.

Transform	Time domain	Forward transform	Frequency domain	Inverse transform
FT	continuous, aperiodic	$X(\omega) = \int_{-\infty}^{+\infty} x(t) e^{-i\omega t} dt$	aperiodic, continuous	$x(t) = \frac{1}{2\pi} \int_{-\infty}^{+\infty} X(\omega) e^{i\omega t} d\omega$
FS	continuous, periodic	$X[\omega_j] = \int_{0}^{2\pi} x(t) e^{-itj} dt$	aperiodic, discrete	$x(t) = \frac{1}{2\pi} \sum_{j=-\infty}^{+\infty} X[\omega_j] e^{itj}$
DTFT	discrete, aperiodic	$X(\omega) = \sum_{n=-\infty}^{+\infty} x[t_n] e^{-i\omega n}$	periodic, continuous	$x[t_n] = \frac{1}{2\pi} \int_{0}^{2\pi} X(\omega) e^{i\omega n} d\omega$
DFT	discrete, periodic	$X[\omega_j] = \sum_{n=0}^{N-1} x[t_n] e^{-i2\pi nj/N}$	periodic, discrete	$x[t_n] = \frac{1}{N} \sum_{j=0}^{N-1} X[\omega_j] e^{i2\pi nj/N}$

Table 2.6: ***The definitions of Fourier Transforms:*** *as used in this work.*

2.4.3 Important properties of the Fourier transform

Several properties of the Fourier transform family are listed here. The first is linearity; the Fourier transform is homogeneous and additive. This makes it useful for modelling linear systems. The homogeneity property indicates that a change in amplitude in one domain leads to a change in amplitude in the other. The additivity property indicates that addition in one domain leads to addition in the other.

A property of the Fourier transform that plays an important part in the arguments presented later in this research is the expansion - compression property. Expansion in one domain leads to compression in the other, and vice versa. This can be understood by considering a time domain pulse which is compressed. The same signal happens over a shorter period of time. Thus higher frequency basis functions are required to express the signal. This property is important because it explains why the bandwidth of a frequency signal is the inverse of the coherence time (§ 5.4.2 on page 229). The expansion/compression relationship holds for the extremes of a compressed signal (a Dirac delta function) and an expanded signal (a constant). A Dirac delta (impulse) in the time domain is a constant value in the frequency domain. Conversely, a constant value in the time domain (thought of as a DC offset in electronics) is a Dirac delta in the frequency domain.

Another property that plays an important role in the discussion presented is the relationship between multiplication and convolution. Multiplication in one domain is equivalent to convolution (§ 2.4.6) in the other. This is the reason why truncation of a signal with an infinite number of data points (§ 2.4.4) leads to a convolution in the frequency domain, and why the response of a linear system (§ 2.4.5) can be found by multiplication in the time domain.

2.4.4 Common Application of the DFT: characterisation of aperiodic signals

Although the DFT is defined for periodic signals, the most common engineering application of the DFT is to characterize aperiodic signals in terms of its frequency content. The signal being measured, for example wave elevation, is infinite. Only a finite window of the data is considered; this is known as the DFT record, and contains N points. The signal outside of the viewing window is not a duplication of the windowed data, but the DFT treats it as such. If the resulting Fourier coefficients were used to synthesise a time series, the result would be a signal that was periodic with the DFT record.

Leakage

Truncating an aperiodic signal with an infinite time domain introduces distortions in the frequency domain. Truncation can be thought of as multiplication of the time domain signal with a rectangular window of height one. This multiplication in the time domain is equivalent to convolution in the frequency domain of the DFTs of the signal and the rectangular window

[60]. The DTF of a rectangular window is a sinc function. Thus in a DFT of a truncated signal, each frequency component of the signal appears as a sinc function centred on that component. Each component appears to have side lobes, and the cumulative effect of these side lobes is known as *leakage*. The true frequency components are often hidden by leakage. For this reason, an alternative to the rectangular window is used, such as a tapered Hanning or Hamming window. They have Fourier transforms that are less spread out, so that there is less leakage of the frequency content of the signal.

Resolution

Another way of explaining leakage is to say that the true frequency components of a signal lie inbetween the chosen bins of the DFT. One frequency component then needs to be represented by several bins in the DFT. For this reason, leakage can also be reduced by considering more information: either using more of the input signal or a smaller sampling time on the original signal. This gives better resolution in the frequency domain: the frequency bins will be closer together, and it will be clearer which frequencies are carrying the signal. However, in general the true component of frequency will still lie inbetween bins, so although the resolution has increased, there is still the same problem with leakage.

When it is not possible to use more of the signal or a smaller sampling time, zero-padding (adding zeros to the end of the time domain signal before transformation) will result in frequency bins that are closer together, but they will not contain any extra information about the signal: they will clearly show the side lobes due to the chosen windowing function.

Noise

Aside from leakage, there is another reason why the true frequency content of a signal may not be clear in the frequency domain: the time domain signal may contain noise. This noise may be naturally present in the signal being measured, or it may be introduced during the process of measuring the signal. Common techniques for removing noise in the time domain signal are to filter the signal before the DFT, or to perform the DFT then filter (smooth) the frequency domain signal. Averaging is another method for removing noise due to leakage or present naturally in the system. Instead of doing one DFT with the entire windowed signal, the signal is divided into several overlapping DFT records. Each is windowed, and the DFTs are then averaged.

The disadvantages of noise reduction techniques

Windowing, averaging and zero-padding are commonly used techniques for identifying the frequency components in the DFT of an aperiodic signal. None of these techniques completely remove the signal noise or the distortion in the frequency domain due to leakage. Their use

also destroys the duality between the time domain and the frequency domain signals: the frequency domain signal is no longer the DFT of the chosen portion of the time domain signal. When techniques for noise reduction, increased resolution or leakage reduction are used, the DFT of an aperiodic signal is only an approximate representation of the time domain signal. However, if no steps are taken to reduce leakage, then the DFT of an aperiodic signal gives a poor approximation to the signal's frequency content.

2.4.5 Common Application of the DFT: frequency response of a linear system

Another common application of the DFT (and the Fourier transform family in general) is the analysis of linear systems.

Sinusoidal fidelity

Linear systems have sinusoidal fidelity, which means than if an input to a linear system is a sinusoid, then the output will be a sinusoid of the same frequency. The amplitude may have been scaled, and the phase may have changed, and so these two parameters characterise the response of the system at that frequency. The same holds for a complex exponential. A linear system will alter the amplitude and phase of the complex exponential that passes through it.

Thus if $X(\omega)$ represents the complex frequency components of the input, and $Y(\omega)$ the corresponding output, then the frequency response or transfer function $H(\omega)$ defines the relationship between the input and output in terms of gain and phase shift at each frequency:

$$Y(\omega) = H(\omega)X(\omega) \tag{2.6}$$

Superposition

As discussed in § 2.4.3, the superposition principle applies to the Fourier transform of a signal. Homogeneity and additivity, known collectively as superposition, also apply to linear systems. Homogeneity means that scaling an input signal, $x(t)$, results in an output, $y(t)$, scaled by the same factor, σ. So when considering the amplitudes of the frequency domain components, a linear system is homogeneous:

$$\sigma Y(\omega) = \sigma H(\omega)X(\omega) \tag{2.7}$$

Additivity means that individual responses to inputs can be added to give the response of the sum of these inputs. A linear system is additive in terms of the sinusoid's amplitude. Individual responses to inputs that can be decomposed into sinusoidal components($Y_1(\omega) = H(\omega)X_1(\omega)$ and $Y_2(\omega) = H(\omega)X_2(\omega)$) can be added to give the response of these components passing

through the system simultaneously:

$$Y_1(\omega) + Y_2(\omega) = H(\omega)\,(X_1(\omega) + X_2(\omega)) \tag{2.8}$$

From equations (2.7) and (2.8), it is clear that if an input to a linear system can be described as a sum of sinusoids, then knowing the change in amplitude and phase at each frequency (the transfer function) enables us to find the output. In terms of a discrete spectrum this is expressed as:

$$Y[\omega_j] = H[\omega_j]X[\omega_j] \tag{2.9}$$

The response of a linear system can be divided into a transient response and a steady state response. Note that the principle of sinusoidal fidelity holds only for the steady state response.

Frequency domain analysis

As sinusoidal fidelity and superposition apply to linear systems, the post-transient response to an input composed of superimposed sinusoids can be found using the transfer function (2.6). The Fourier transform is used to decompose a signal into constituent basis functions, which are complex functions based on sinusoids. The inverse Fourier transform is used to synthesise the time domain response from the frequency domain output of the transfer function.

Any infinitely long continuous signal with a continuous derivative can be decomposed into sinusoidal basis functions. A finite signal can also be represented by sinusoids if it is periodic. In this case, a finite number of sinusoids are required (see Table 2.6 on page 49; a periodic time domain signal is represented by a discrete function in the frequency domain). Each constituent sinusoid must be periodic with the repeat time (period) of the signal, so will complete an integer number of cycles within the repeat time. In the frequency domain, this means that each frequency bin will be an integer multiple of the lowest frequency, ω_1.

As discussed in § 2.4.4, a common application of the DFT is to estimate the frequency content of aperiodic signals. While this is useful to characterise a signal, the resulting spectral components are not equivalent to the original signal. Thus multiplying the DFT of an aperiodic signal with the known frequency response will only give an approximation to the (post-transient) response.

2.4.6 Convolution

Multiplication of frequency components with the transfer function is the preferred method of finding the response of a linear system to an input that can be decomposed into sinusoids. The reason for this is that it is much faster to compute than the equivalent calculation in the time domain. Multiplication in the frequency domain is equivalent to convolution in the time

domain. The time domain version of a linear system with a continuous input (2.6) is:

$$y(t) = h(t) * x(t) = \int_{-\infty}^{\infty} h(\tau)x(t-\tau)d\tau = \int_{-\infty}^{\infty} x(\tau)h(t-\tau)d\tau \tag{2.10}$$

while the time domain version of a linear system with a discrete input (2.9) is:

$$y[t_n] = h[t_n] * x[t_n] = \sum_{m=0}^{N-1} h[t_m]x[t_n - t_m]_N = \sum_{m=0}^{N-1} x[t_m]h[t_n - t_m]_N \tag{2.11}$$

Here the $[\ldots]_N$ notation indicates circular convolution. The inverse Fourier transform of the transfer function is the impulse response function, $h(t)$ or $h[t_n]$. This is the output of the system in response to an input of an impulse.

Whereas the frequency domain technique decomposes a signal into complex exponential basis functions, the time domain approach is to decompose the signal into impulsive basis functions. Thus a discrete input is treated as a series of discrete delta functions (2.5), each scaled and shifted in time. As a linear system is additive, the output to each component of the input is the impulse response, with the same scaling and time-shifting as the input components. The scaled and shifted impulse responses are added to give the output. This convolution process can be understood from the viewpoint of the input or output components. It can be thought of as a measure of how much a given input, for example $x[t_0]$, affects all future outputs, $y[t_n]$ or how much a given output, for example $y[t_{10}]$ is affected by past inputs, $x[t_0]..x[t_9]$. Both of these interpretations can be described as the *memory effect*. Present inputs are *remembered* in future outputs; outputs have a *memory* of preceding inputs.

Not all linear systems have memory. The memory depends on the impulse response function. If the impulse response function is itself an impulse, then the system has no memory. Convolution of any signal with a Dirac delta returns the original signal unchanged (2.3). The output depends only on the instantaneous value of the input; it does not *remember* past inputs. The frequency domain equivalent (transfer function) of the impulsive impulse response is a constant; it has the same value at all frequencies (see § 2.4.3).

Convolution of a signal with a scaled impulse is equivalent to multiplication of the signal with the scaling factor (2.4). This can be seen by considering the frequency domain equivalent of the convolution. It may either be viewed as the multiplication of two frequency domain functions (one of which has the same value over all frequencies) or as one frequency domain function multiplied by a constant. When the constant is treated as a scaling factor, the homogeneity property of the Fourier transform (2.7) gives the time domain as the original signal multiplied by the scaling factor.

2.5 The frequency domain in wave energy engineering

One of the problems with the term *frequency domain* is that it has many interpretations, applications and variations. As discussed in the previous section, not all these applications are compatible with each other. For example, two common applications of the DFT are the characterisation of aperiodic signals, and the analysis of linear systems. When the DFT is used for linear systems analysis, it is assumed that the input is periodic. However, the DFT is also used to characterise aperiodic signals such as wave elevation.

Any function of frequency can be referred to as a frequency domain signal. However, only the Fourier transform (or a member of the Fourier transform family) is the frequency domain equivalent of the time domain expression. A DFT of an aperiodic signal, incorporating noise reduction techniques such as windowing or averaging, is a frequency domain function, but is not the frequency domain equivalent of the original signal. Likewise, functions of the magnitude squared of the Fourier transform, such as the spectral density or incident power per metre, are frequency domain. However, they do not contain phase information, so cannot be used to reconstruct the original time series signal.

Another potential problem is that an approach commonly used in physics (for example 3.2.3 on page 75) can be confused with the frequency (Fourier) response. It is important to distinguish between Fourier transforms, and quantities which may be plotted as a function of frequency. Many wave parameters can be plotted against frequency, but are not the Fourier transform of a meaningful time domain function. Examples include the wavelength and group velocity. These properties are functions of uni-directional waves consisting of one frequency only: monochromatic waves. Many monochromatic properties apply to behaviour in monochromatic waves only, and do not describe behaviour in waves containing more than one frequency (polychromatic).

Different members of the Fourier transform family, and different applications of the Fourier transform, are used for theoretical modelling, measuring sea states and experimental work in wave energy engineering. This section describes the differences between these various approaches. This is to make mathematical arguments in later chapters more clear, and to provide background on the discussion of the limits of validity of frequency domain analysis in Chapter 6.

2.5.1 Theoretical modelling

When performing theoretical modelling using a linear equation of motion, as described in § 3.5.9 on page 101, a frequency domain system is the continuous Fourier transform of the time domain system. Functions of frequency and functions of time are continuous and infinite.

The linear equation of motion is treated as a linear system. In the time domain, an impulse response transforms the input into the output via convolution. In the frequency domain,

the transfer function transforms the input into the output via multiplication. The use of the frequency domain to analyse a linear system gives the post-transient response.

2.5.2 Characterisation and representation of sea states

The most common method of measuring wave elevation is to record discrete samples taken at one point in space, $\eta[t_n]$. Discrete measurements are used because digital processing is more powerful and versatile than analogue processing, so has become the standard tool for signal analysis. Sea states are routinely represented in the frequency domain. For a finite sampled wave record the transform used is the DFT: $H[\omega_j] = \mathcal{F}_{\mathcal{D}}\{\eta[t_n]\}$[2]. As wave elevation is not periodic with the wave record, the DFT only gives an approximation to its frequency content. The distortions introduced by the use of the DFT require techniques such as windowing or averaging for reducing spectral leakage. While these result in a more meaningful indication of the frequency content of the signal, they destroy the duality between the frequency and time domains. The exact original signal may no longer be reconstructed from the frequency domain representation.

There is a diversity in the use of the frequency domain signals to represent sea states. Fig. 2.10 gives some examples (A-C) of the ways that frequency domain signals are used to characterise, categorise or define the frequency domain of wave elevation.

Real seas

Here the word *real* means that the waves have not been artificially created in a basin. The surface elevation at any point is the result of waves converging from all directions. Some of these waves may have originated from distant storms and some from nearby winds. The energy flux of waves from a given source varies continuously over time. Ocean currents, local winds, wave steepness and bathymmetry will affect wave propagation. Wave elevation is a continuous function of time $\eta(t)$ defined at all values of time.

Measured spectra (A)

The sampled wave elevation $\eta[t_n]$ is read by a sensor, such as a wave rider buoy. A wave record of N samples taken at intervals of Δt has a duration of $T_{DFT} = N\Delta t$. This wave record may require cleaning to remove sensor errors. Spectral noise reduction techniques are required to minimise leakage of energy into neighbouring bins. Windowing is the standard solution [63]. Fig. 2.10 shows the use of a tapered window for this purpose. After multiplication with the tapered window, the record starts and ends at zero.

[2]Here $H[\omega_j]$ is not a generic transfer function but the Fourier transform of wave elevation, as the capital letter η is H.

The DFT is performed on the wave record and the resulting function has both magnitude and phase. The phases at each frequency will not be related to each other: they are random. The phase does not contain useful information for characterising the sea state. Often only the amplitude spectrum $|H[\omega_j]|$ (Fig. 2.10A) or the spectral density $|H[\omega_j]|^2$ (Fig. 2.10C) are displayed. However, the phase $\varphi_H[\omega_j]$ is essential for reconstructing a given time series, as in Fig. 2.11F. The spectrum could represent any time series with that frequency content; only when the phase is specified is the exact time series defined.

Regardless of the number of techniques used to reduce leakage or increase resolution, the DFT of an aperiodic signal will never clearly display its frequency content. The exact shape of the spectrum depends on the duration of the DFT record (T_{DFT}), its position in the time series, the number of samples within it (N), the type of windowing function used, and any other techniques used to reduce noise or improve resolution. In addition to problems associated with the DFT, there may be errors and noise in the time domain signal due to the limitations of the sensor and data acquisition systems.

Generalised spectra (B)

One way to use the measured spectra is to create a set of generalised spectra that describe the annual statistical distribution of a given location. Spectra with common shapes, as in Fig. 2.10A, are grouped together as one generalised spectrum. The phase information is discarded. A representative time series can later be synthesised using randomly generated phase, as in Fig. 2.11D. An example of a group of generalised spectra is the South Uist 399 data set [64], which represents the sea states over a year. The annual occurrence of each spectrum is known. The measured data may come from one year, in which case that year is assumed to be typical.

Artificial spectra (C)

Another way to use measured spectra is to derive artificial spectra. The spectrum is a function of heuristic parameters. These may be parameters that influence the development of a sea state, such as wind speed, in the case of the Pierson Moskowitz [19] (PM) spectrum, or the distance over which the wind blows, the *fetch*, in the case of the JONSWAP (JOint North Sea WAve Project) spectrum [65]. Some artificial spectra, such as the Bretschneider [66], are defined in terms of parameters commonly used to describe sea states (for example see Table 3.1). By convention the spectral density, $S(f) = |H(f)|^2$, is shown. Often this is referred to as simply *the spectrum*. The spectrum is a continuous function. If it is to be used to generate a time series of a finite duration of time, it must first be discretised. Fig. 2.10C shows that it can be discretised into a harmonic or a non-harmonic spectrum.

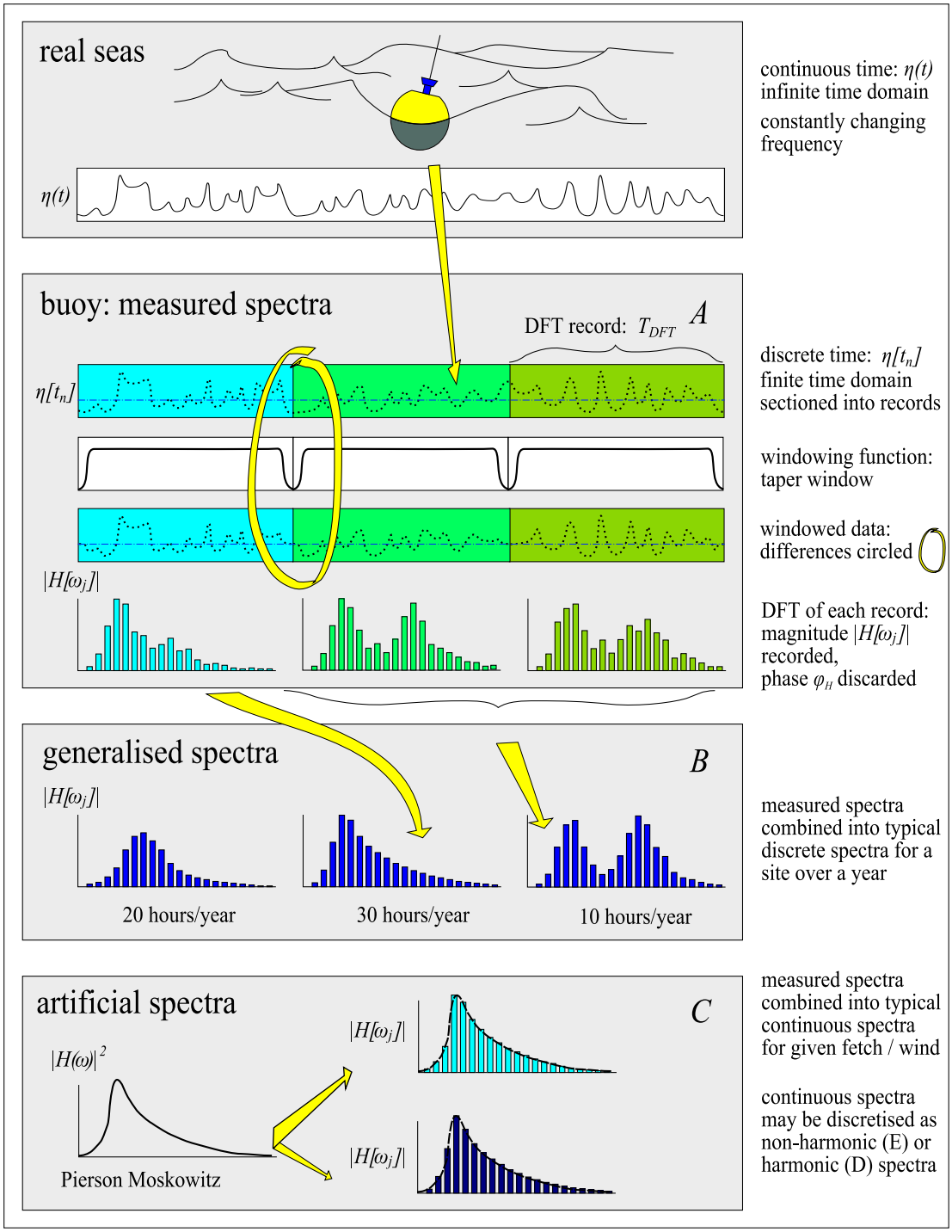

Figure 2.10: ***Representing sea states using spectra:*** *The frequency domain is used to (A): characterise measured wave elevation, (B): categorise and summarise measured spectra as generalised spectra, and (C): define artificial spectra as functions of parameters that influence the creation of a sea state, or parameters commonly used to describe sea states.*

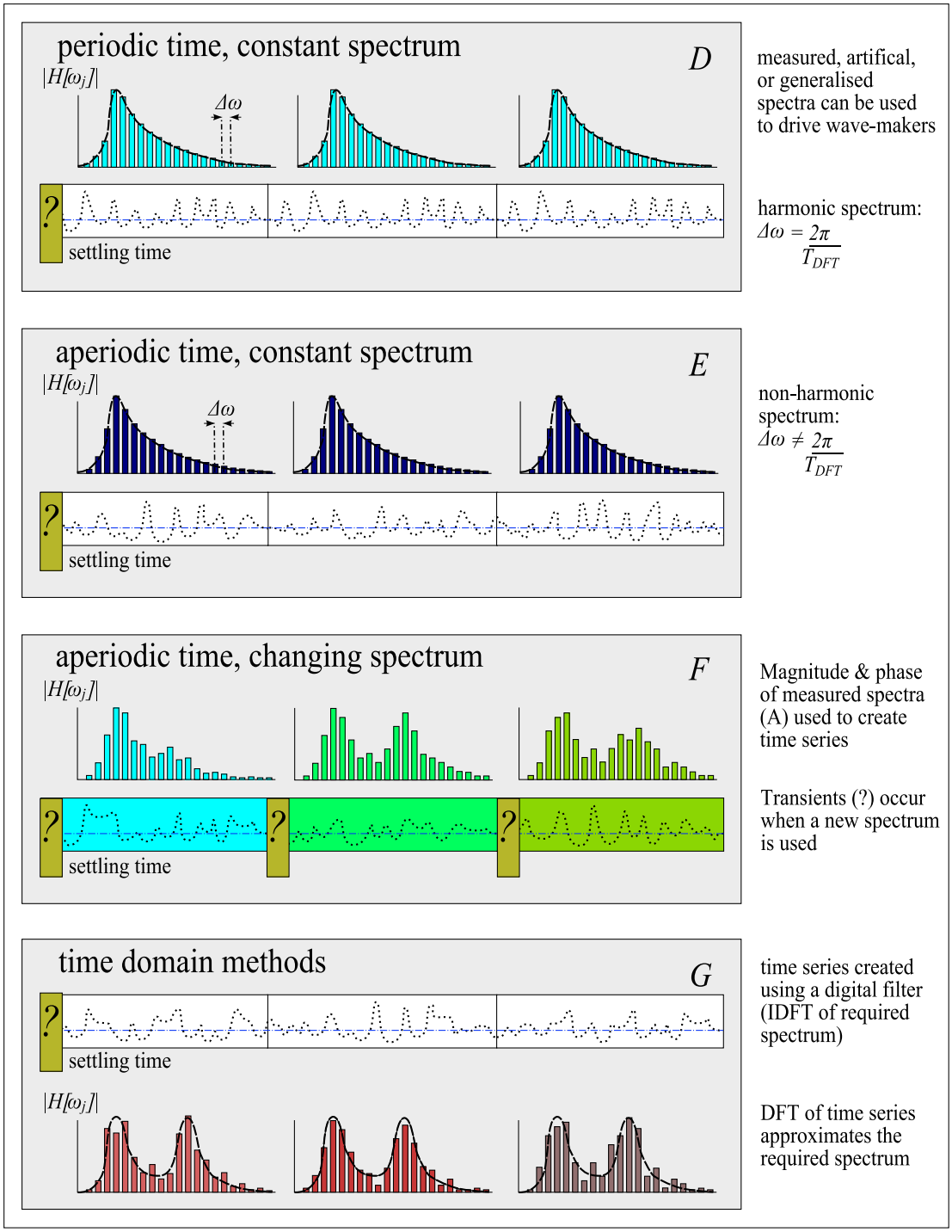

Figure 2.11: ***Synthesising sea states using spectra:*** *Measured, generalised, or artificial spectra (Fig 2.10 A - C) can be used to synthesise wave elevation $\eta[t_n]$. The IDFT generates periodic waves (D). Synthesis using non-harmonic discretisation of a continuous spectrum generates aperiodic waves (E). Synthesis using different spectra for each DFT record generates aperiodic waves (F). The IDFT of a spectrum is a filter which can be used to generate an aperiodic time series (G).*

2.5.3 Generation of wave time series characterised by a given spectra

There are various ways to synthesise a time series of wave elevation from a known spectrum [67, 68]. The resulting discrete time series may be used for a numerical simulation or to generate a drive signal for a wave maker in a tank. Fig. 2.11 shows that the time series can be periodic or aperiodic.

Tank waves: harmonic spectra (D)

The IDFT is a common way [69] of synthesising drive signals for wavemakers. For measured spectra, the amplitude and phase are used. This is known as deterministic synthesis. For generalised or artificial spectra, only the amplitude is known, so a randomly generated (but repeatable) phase is used. This is known as partially deterministic, or pseudo-random synthesis. A continuous spectrum such as a PM spectrum must first be discretised to look like a DFT. In a DFT, the frequency bins are harmonically related; each bin is an integer multiple of the first bin $\omega_j = j\omega_1$. The first bin, ω_1, is proportional to the reciprocal of the repeat time of the time series $\omega_1 = \frac{2\pi}{T_{DFT}}$. The term *harmonic spectrum* is used here to describe the harmonically related bins in a DFT.

The IDFT can also be used for non-deterministic synthesis. In the random Fourier coefficient method, the phase is chosen randomly, and a random number is added to the required Fourier magnitude.

Tank waves: non-harmonic spectra (E)

It may be desirable to generate waves that do not repeat, but which have particular spectral characteristics. In a DFT the bin number indicates the number of complete cycles made by a sinusoid of that frequency within the DFT record. For a non-repeating signal, sinusoidal components that do not repeat with the DFT record are required; that is, none of the component sinusoids must complete a full number of cycles with the chosen DFT record. This is done by choosing frequency components that are not integer multiples of the first bin $\omega_j \neq j\omega_1$ (not harmonically related). The resulting spectrum is described here as *non-harmonic*. When used to synthesise a time series, this is not the IDFT or any other member of the inverse Fourier transform family. It is nevertheless a useful group of methods [68] for synthesising aperiodic time series.

Tank waves: non-repeating spectra (F)

Wave elevation may be synthesised using a different spectrum for each successive record (T_{DFT}), although this is not a common technique. Fig.2.11F shows an attempt to reconstruct wave elevation from the magnitude and phase of successive measured spectra (Fig. 2.10A).

The original wave elevation can not be recreated, because the spectra represent the windowed time series, and new transients (indicated by a question mark: *?*) will arise when a different spectrum is used. It is better to use a single DFT with a T_{DFT} encompassing the entire time series to be replicated.

Tank waves: white noise filter (G)

To generate a drive signal for a wavemaker in the time domain, the white noise filtering method is used [70]. Noise is passed through a filter, which is the IDFT of the required spectrum. The resulting time series is similar to a real sea, as DFTs taken with a sliding window of successive overlapping records are different, but have the same general shape.

2.5.4 Presentation of experimental results

The phrase *doing experiments in the frequency domain* means the experimental set-up allows the results to be analysed in the frequency domain (see Fig. 2.12). The forcing function is defined in the frequency domain, as the DFT of the required signal. An IDFT is used to synthesise the time domain drive signal. The time series of the measured response, such as wave elevation, force or motion, is then converted back into the frequency domain using the DFT.

Fourier analysis is used in different contexts in experimental work (Table 2.7). In case 1, the system is driven with a sinusoidal wave. The response at that frequency (the fundamental) is recorded, and responses at any other frequencies (harmonics) are neglected. Measurements are taken at several frequencies and the ratio of response to input is logged to build up a frequency response or a transfer function. In case 2, the system is driven with a sinusoidal wave, and response is analysed at all frequencies to assess linearity in terms of harmonic content. In case 3, the system is driven with a bi-chromatic wave (containing two frequencies), and the response is analysed at all frequencies to measure cross components. In case 4, the system is driven with a polychromatic wave (containing many frequencies), and response expressed in the frequency domain.

The requirements for frequency domain experimental work depend on the purpose of the experiment. If the purpose is to determine the frequency response, the excitation must be periodic (§ 2.5.8), and the response linear (§ 2.5.7) and post-transient (§ 2.5.6). A transfer function can be characterised using either the monochromatic (case 1) or polychromatic (case 4) approach. The former is more common, as harmonics in a weakly non-linear system can be purposely removed. Here the DFT is used to analyse a linear system.

If the purpose of the experiment is to quantify non-linearities, then linearity is by definition not a requirement. Periodicity is nevertheless essential, otherwise harmonics will be obscured by leakage. Quantifying non-linearities is the purpose of cases 2 and 3. Non-linearities may also

Case:	Driven at:	Response at:	Results used to:
1	single frequency	that frequency	define a transfer function
2	single frequency	all frequencies	measure non-linearity
3	two frequencies	all frequencies	measure cross-components
4	many frequencies	many frequencies	find mixed-sea response

Table 2.7: ***Several uses of the frequency domain in experimental work.***

be quantified by comparing polychromatic (case 4) results with a transfer function derived from monochromatic experiments (case 1). Here the DFT is used to characterise the response of a non-linear system, so that it can be compared with that expected for a linear system.

If the purpose of the experiment is to characterise a typical response (another common application of case 4), rather than to analyse a linear system, the restrictions that apply to analysis of linear systems do not apply. There is nothing forbidding the inclusion of non-linear, transient, or aperiodic responses in the analysed signal. Indeed, aperiodic forcing (Fig. 2.11G) might be preferable as its statistical properties are more representative of real seas. A DFT of the response describes the frequency content of the results of a particular experiment, but does not characterise the frequency response.

2.5.5 Monochromatic experiments

In the monochromatic approach, a series of experiments are conducted; each driven with a pure sinusoidal wave. The result of each experiment is plotted against the frequency, ω_s, of the sinusoid. If the parameter being plotted is the DFT of the measured time series, and the system is linear and periodic, then this is the frequency response, as in case 1 of Table 2.7. If the parameter is the DFT, but the system is either non-linear or aperiodic, then this is a frequency domain signal, but not the frequency response of a linear system: results from monochromatic experiments are not accurate indicators of polychromatic response. If the parameter being plotted is derived from the time domain in any manner other than a Fourier transform, then the result is not the frequency response, and is valid only for the monochromatic case (Fig. 2.13).

The monochromatic approach is a valid and useful technique, based on the physics viewpoint of a wave. Ambiguity can arise because, it can be used to find the frequency response, which applies to polychromatic behaviour, and it can also be used to find parameters that apply only to monochromatic behaviour.

2.5.6 Ensuring Post-transient response

Frequency domain analysis of linear systems only applies to post-transient motion. When using the DFT to analyse linear systems (case 1 directly, and cases 2 and 3 for comparison with non-linear systems), a settling time must be allowed before measurements begin. The time required depends on the experimental set-up. It is measured from the time that the wavemakers start. Settling time includes the decay times of transients due to the motion of the wavemakers and the model, as well as the time required for the wave to travel from the wavemaker to the model. The model must be placed some distance from the wavemakers to avoid the standing waves created during the wave radiation process (§ 3.5.5 on page 98). The PTO settings must be constant throughout the experiment to avoid transients due to a sudden change in PTO force. It is good practice to use the same settling time for all experiments in a group of comparative tests.

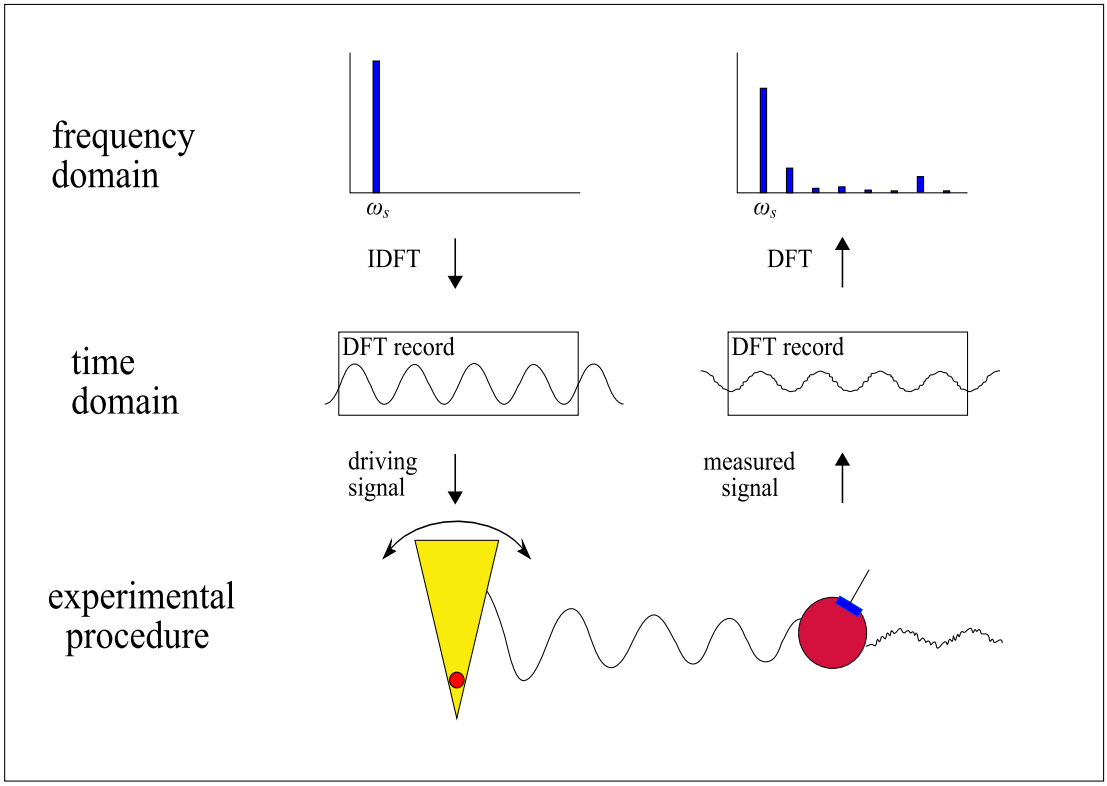

Figure 2.12: ***Representing experimental results in the frequency domain:*** *frequency domain spectra are used to define and synthesise (time domain) waves. Response is measured in the time domain and a DFT is performed to express this in the frequency domain. Case 1 in Table 2.7: only the fundamental frequency (ω_s) is recorded; harmonics are ignored. Case 2 in Table 2.7: fundamental and harmonics are compared to each other.*

2.5.7 Ensuring linear response

Non-linearities will always be present in waves and wave induced motions. The term *ensuring linear response* means choosing experimental conditions that result in weakly non-linear behaviour, which falls below a given linear limit. As there is no consensus on standardised limits, different groups choose different limits.

To ensure linearity, the amplitudes of both waves and motions must be limited. For waves to be within linear limits, the wave amplitude must be small in comparison to the wavelength and the wave depth (see § 3.2.3 on page 79). Steepness is one way to define a linearity limit. For mixed-seas, the steepness can be checked in the time domain to ensure the wave remains linear

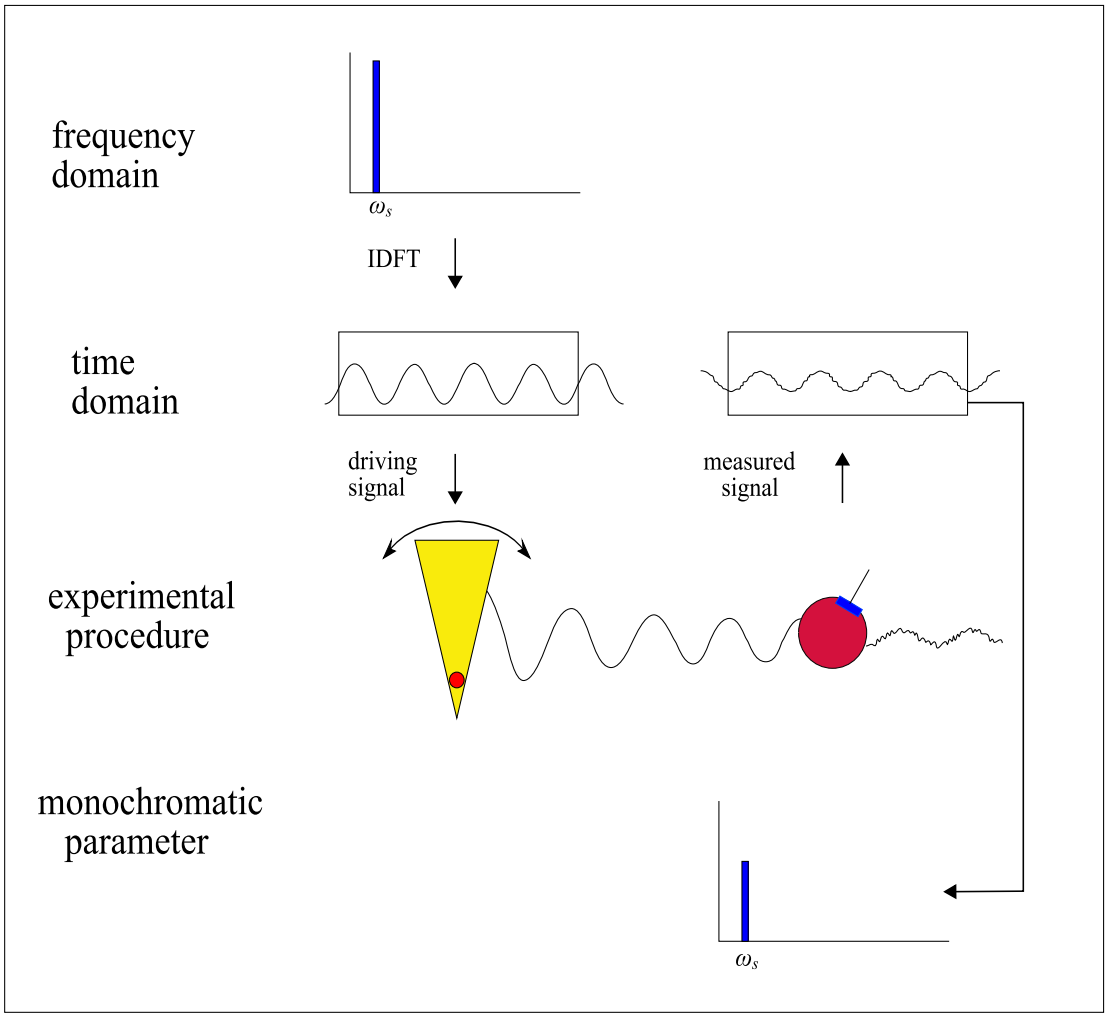

Figure 2.13: ***Representing experimental results from monochromatic tests:*** *frequency domain spectra are defined and used to synthesise (time domain) waves. Response is analysed using a non-Fourier method to give a single parameter and this is plotted against the driving frequency.*

at all positions and at all times.

The linear limits for motions are defined by maximum allowable displacements. Displacement limits can be defined as a function of geometry. For instance, Pizer [58] suggests that displacement of a heaving hemisphere should be limited to under a quarter of the radius. Alternatively, the limits to displacement can be defined by a limiting wave amplitude. For instance, Skyner [71] defined the monochromatic linear limit as the wave amplitude that resulted in a second harmonic of displacement that was 10% of the fundamental frequency (see Fig. 2.12, case 2). While it is clear that monochromatic limits are not to be interpreted as limits for each component of a mixed-sea, there are no guidelines as to how monochromatic limits do relate to those for mixed-seas. One way to measure non-linearity in a mixed-sea is to measure the difference between the mixed-sea response (for a harmonic spectrum) and the frequency response.

Linearity sets an upper limit on wave amplitude. Tank repeatability and sensor sensitivity place a lower limit on wave amplitude. Monochromatic waves are easier to fit into this range of suitable wave amplitudes than polychromatic waves. The amplitude of a sinusoidal wave must be below the linear limit, whereas the peak in the wave elevation $\eta[t_n]$ of a polychromatic wave must be below this limit.

Furthermore, linear wave theory (§ 3.2.3) is based on the assumption of inviscid flow. This assumption is only valid for high Reynold's numbers. In real seas, a large object in gravity waves will experience high enough Reynold's numbers for the assumption of inviscid flow to be valid. However, care must be taken with small scale models: the commonly used Froude scaling results in a higher viscosity (lower Reynold's number) than the full scale device [72].

2.5.8 Ensuring periodic response

If a discrete function is truly periodic with the DFT record, its (complex) DFT will be a delta function pair for each sinusoid and nothing else. The sampling interval Δt, and number of samples N, must be chosen so that the duration of the DFT record, $T_{DFT} = N\Delta t$, exactly equals the repeat period of the underlying continuous function, $T_{DFT} = T$. If the sampling interval or record duration are chosen so that the DFT duration does not equal the period of the underlying continuous function, $T_{DFT} \neq T$, then the function being transformed is different to the original signal. The DFT will contain not only the delta function pairs of the constituent sinusoids, but also smaller frequency components neighbouring these delta pairs.

The reason for this is that when $T_{DFT} \neq T$, the signal in the DFT record is represented by sinusoids that complete an integer number of cycles during the true period T, but do not complete an integer number of cycles during the imposed period T_{DFT}. The true frequencies of the constituent sinusoids lie in between the chosen frequency bins. This is known as the picket fence effect. Each constituent sinusoid is thus represented in the DFT by several bins

clustered about the true frequency. The picket fence effect is associated with leakage: a sinusoid that lies between bins will not complete an integer number of cycles within the DFT record, and the ends of the record will be discontinuous [60].

2.6 Chapter summary

This chapter discussed two main subject areas: the classification of WECs and their control; and the use of Fourier methods in wave energy engineering. In the discussion about classification, the important results, and the main points that relate to the remainder of this research are:

- A new classification system was introduced (§ 2.2.3). WECs were classified according to the three stages in the power conversion process (Fig. 2.1): power interception, capture, and delivery.
- Classification allows previously unclassifiable WECs such as overtopping devices to be compared to other WECs (§ 2.2.9).
- This classification system is linked to the governing equation of a WEC (§ 2.3.6).
- Control was also classified according to power flow. The three types of control corresponding to the interception, capture and delivery of power are geometry control, PTO control and power regulation (§ 2.3.1).
- Two common drive trains configurations were compared: direct and buffered drive (§ 2.2.7). The theory on PTO control in this research relates to either. In direct drive the PTO force is applied by the electrical generator. In a buffered drive, the PTO force is applied by an intermediate PTO mechanism such as a hydraulic pump. When comparing direct and buffered drives, all three stages of power flow must be considered (§ 2.2.7).
- A case study of a WEC under commercial development was undertaken to demonstrate how the three stages of control interact (§ 2.3.5).
- This thesis refers to the opportunities for improvement to PTO control. The leading device developers devote effort to geometry control, PTO control and power regulation (§ 2.3.4 and § 2.3.5).
- Frequency domain modelling of WEC dynamics, which is the basis for most of the work presented in this thesis, is only valid (§ 2.3.7) for post-transient response, and for behaviour where the relationship between excitation and response is linear during power production. The frequency domain cannot be used to model types of WECs for which it is not possible to apply linear PTO, such as overtopping devices. In WECs where linear behaviour is possible, the frequency domain model only applies the linear

operating regime. It cannot be used to model WECs which are experiencing high energy seas, moving with high velocities, or experiencing a non-linear PTO due to a control regime that limits forces, displacement or power.

In the discussion about Fourier methods, the main points that form the necessary background for the core of the research are:

- Equations for the family of complex Fourier transforms were given (Table 2.6). The continuous Fourier transform is used for theoretical modelling in most of the academic literature and in Chapter 3. The DFT is generally used for experimental and simulation work. Equations are expressed in DFT form from Chapter 4 onwards.
- The DFT is defined for discrete and periodic functions of time, and discrete and periodic functions of frequency.
- A common application of the DFT is the characterisation of an aperiodic signal (§ 2.4.4). Spectral noise reduction techniques are required to uncover the frequency information. This process destroys the equivalence between the time and frequency domain representation of the signal.
- Another common application of Fourier methods (including the DFT) is the analysis of linear systems (§ 2.4.5). In the time domain, the input convolved with the impulse response gives the output. The calculation is easier in the frequency domain. The Fourier transform of the input, multiplied by the Fourier transform of the impulse response (the transfer function), gives the Fourier transform of the output. When using the DFT, frequency domain analysis is only equivalent to time domain analysis when the input is periodic.
- In wave energy engineering, the DFT is commonly used to give the spectra of measured (aperiodic) wave records (§ 2.5.2).
- Generalised and artificial spectra, which are based on measured spectra, are often used to generate waves in tanks for experimental testing. It is possible to generate periodic or aperiodic waves using these spectra (§ 2.5.3).
- If these tests involve measuring (DFT) transfer functions, the waves must be periodic. Furthermore, the behaviour must be linear and post-transient (§ 2.5.4).
- There are many results that can be plotted against frequency that are the frequency response, which applies to polychromatic behaviour, but are instead specific to monochromatic behaviour at a given frequency (§ 2.5.5).

Chapter 3

Linear wave energy converter dynamics

3.1 Chapter overview

This chapter presents the dynamic model of a wave energy converter (WEC) that will be used in later chapters to extend theory on WEC control. The dynamic model is the well-known and widely used phenomenological approach, using hydrodynamic coefficients to model the interaction of the body with the fluid. The values of these coefficients depend on the size and shape of the body, referred to here collectively as *geometry*. The values can be derived analytically in special cases, for example the results given by Havelock [57], or numerically, for example the panel method used by the leading commercial software, WAMIT [73]. The dynamic model interacts with waves, and so this chapter begins with a review of wave theory (§ 3.2). The theory of ocean waves is an incredibly broad area, and by necessity this review focusses on topics that are relevant to the modelling of WECs. It is important to consider the different ways in which ocean waves are described because there is much room for ambiguity.

The discussion of the WEC model is preceded by a section describing the modelling process (§ 3.3). This discusses the relationship between a physical system and its model, and defines the concept of memory. Although the dynamic model of a WEC is widely used, there is also a wide variation in *how* it is used. For this reason the development of the model is given thorough treatment. The most general model is presented initially (§ 3.4), and justifications are given for the simplified frequency domain model that is used in later chapters (§ 3.5). The connection between the linear time domain model and the frequency domain model is discussed in (§ 3.6, and the physical meaning of individual terms in the equation of motion is explained in § 3.7.

Memory is the theme of the final section (§ 3.8). There are two ways in which the frequency domain dynamic equation, presented in § 3.5, is commonly interpreted and applied. There was no existing terminology in the wave energy literature for comparing these two schools of thought in an accessible way: descriptions such as *correct* or *incorrect* are imprecise and potentially alienating; terminology such as *frequency dependent* and *added mass* is conceptually linked to, and is thus interpreted according to, the school of thought to which the reader belongs. It was therefore necessary to introduce the wet and dry oscillator models as a tool to communicate the difference between these schools of thought. The cases and conditions for which these mathematical models are suitable representations of a WEC are described. This mathematical treatment shows in a precise manner the differences between these models,

and gives clues that suggests why the dry oscillator model has been used in wave energy literature under conditions for which it is not a good representation of WEC behaviour. This work leads in to a more detailed appraisal of the validity of the frequency domain equation in Chapter 6.

3.2 Ocean waves

The first step to modelling the dynamics of WECs is to consider the environment from which energy is extracted: ocean waves. The waves that contain the most energy are those which are of primary interest to wave energy engineering, and they are caused by wind blowing over the sea. There are several definitions and conceptual viewpoints of water waves. The definition of a *wave* is covered for the time domain, the frequency domain and the monochromatic approach. Using the monochromatic approach, the time and frequency domain signals are conceptually easy to relate to each other. It is important to clarify these definitions because some parameters, such as period, take on different meanings in different contexts.

Definitions of key terminology

The word *domain* is used in the context of its mathematical definition: it is the independent variable for which the function has a definition. If the function is plotted on Cartesian axes, then the domain is the x-axis. If a parameter is a function of time, its domain is time, and it is described as a time domain function. If a parameter is a function of frequency, its domain is frequency, and it is described as a frequency domain function.

A real time domain function can be considered a signal. Most signals have an equivalent representation in the frequency domain. A Fourier transform is used to change a time domain signal into its frequency domain representation, which is called the frequency domain signal, the spectrum, or sometimes simply the signal's Fourier transform. Considering a signal, such as wave elevation, in *the frequency domain* implies that it is the Fourier transform of a time domain signal. There is a subtle distinction between a frequency domain function and a frequency domain signal. As shall be shown, all Fourier transforms of signals are frequency domain functions, but not all frequency domain functions are Fourier transforms of meaningful signals. The broader definition of a frequency domain function will be used, which includes functions of frequency that are not Fourier transforms. Many functions of frequency that are not Fourier transforms are real, whereas the Fourier representation of a real time domain signal is complex.

The concepts of time and frequency domain are also used to describe systems. In a time domain system, the input and response are time domain signals. In a frequency domain system, the input and response are the Fourier transforms of these signals. The governing equations are known as the time domain and frequency domain equations. In this context, a frequency domain

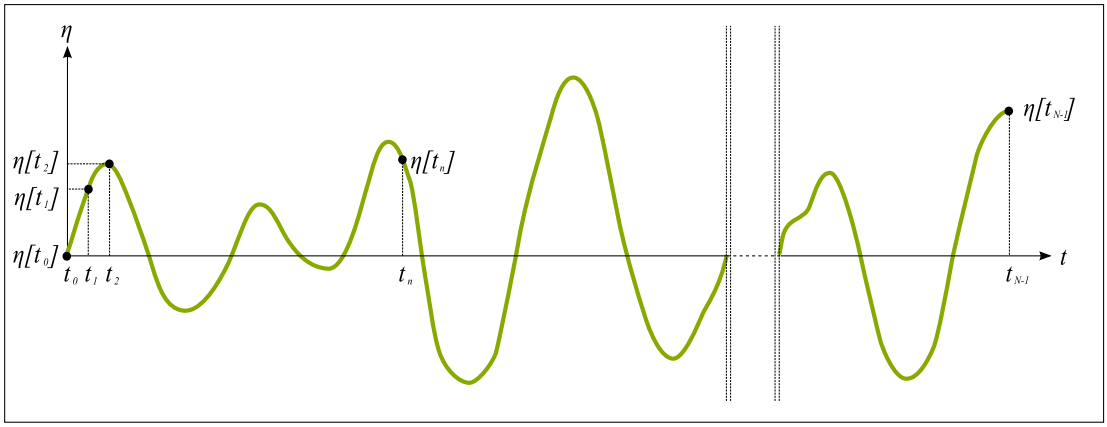

Figure 3.1: ***Time domain view of a wave:*** *a wave record containing samples of wave elevation,* $\eta[t_n]$.

equation always refers to the frequency domain representation of a time domain governing equation.

Another important term to define is *continuous*, which is used in different ways. A common use of the word in this chapter is to describe whether the function is continuous, rather than discrete. The other use of the word continuous is to describe whether a function is plotted against its whole domain contains any gaps or sudden jumps in value. Mathematically, the absence of gaps means the function must be defined over its entire domain. The absence of sudden jumps means that the value of $f(x \pm \Delta x)$ approaches $f(x)$ as Δx tends towards zero. A function fulfilling these criteria could be described as parametrically continuous.

3.2.1 Time domain definition of a wave

The time domain definition of a wave is that the surface elevation is a function of time. It may be considered at a single point in space $\eta(t)$, along a line in the direction of propagation of a uni-directional wave $\eta(t, x)$, or over the sea surface $\eta(t, x, y)$. Even when the domain includes distance or space, these definitions are thought of as time domain. The modelling of directional waves adds to the complexity of the problem, and so only uni-directional waves are considered here. The wave elevation at one point in space, $\eta(t)$, is a common representation because many wave measurements are taken at a fixed location, and because it is useful for modelling the dynamics of WECs. When dealing with measured or simulated waves, the wave elevation is discretised and expressed as $\eta[t_n]$. A group of N samples are considered; this is known as the wave record. Fig. 3.1 depicts a wave record, with wave elevation plotted against discrete values of time.

Information extracted from the time domain

The natural viewpoint for any wave probe is the time domain wave elevation signal. For people who interact with the sea, the natural tendency is to extract information from the time and space domain, $\eta(t, x, y)$. Thus when watching waves break on a beach, each crest is thought of as a separate wave. The traditional coastal engineering approach is a formalisation of this viewpoint: a *wave* is defined as one complete cycle of the wave elevation. There are various conventions for defining the portion of the wave record that is considered a *cycle*: one is between successive peaks; the most common is between two successive zero-crossings of the same direction. Some researchers consider zero up-crossings, while others consider zero down-crossings. The zero down-crossing method has the most official recognition [74].

The period is the time for a wave to pass a fixed point in space. The height of a given wave is then the distance between the highest and lowest points in the individual wave. A wave record can be split into K individual waves, where each is described by the period and height, T_k and H_k (see § 3.2.4 for discussion of notation). These parameters are commonly referred to as the time domain height and period. Strictly they are not time domain signals, but information extracted from a time domain signal. Fig. 3.2 shows how the zero up-crossing method is used to define individual waves from a wave record.

3.2.2 Frequency domain definition of a wave

The frequency domain is the natural viewpoint for engineers. Instead of viewing how wave elevation varies with time, its variation with frequency is of interest.

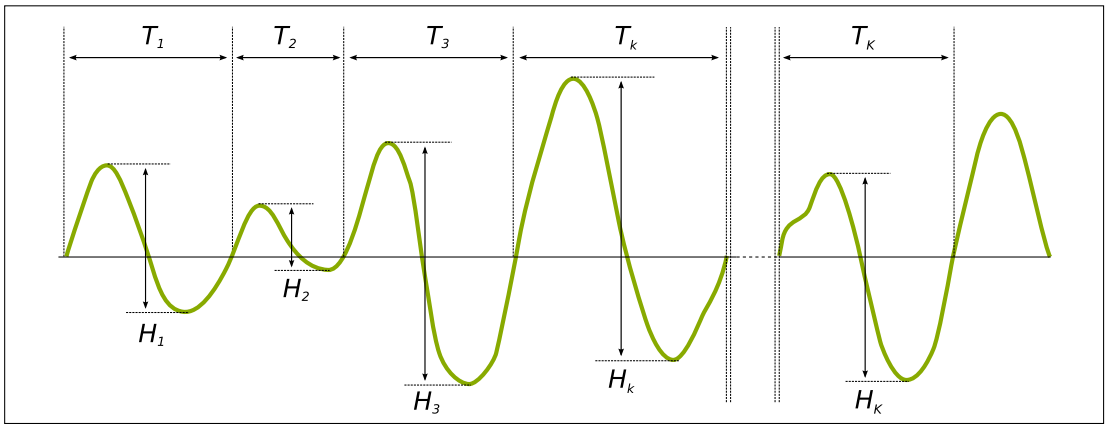

Figure 3.2: ***Information extracted from a time domain signal:*** *From the wave record, each cycle, defined here as the interval between successive upward zero-crossings, is defined as a wave. The wave parameters, T_k and H_k, describing the K waves in the wave record, are data extracted from the time domain signal $\eta(t, x)$.*

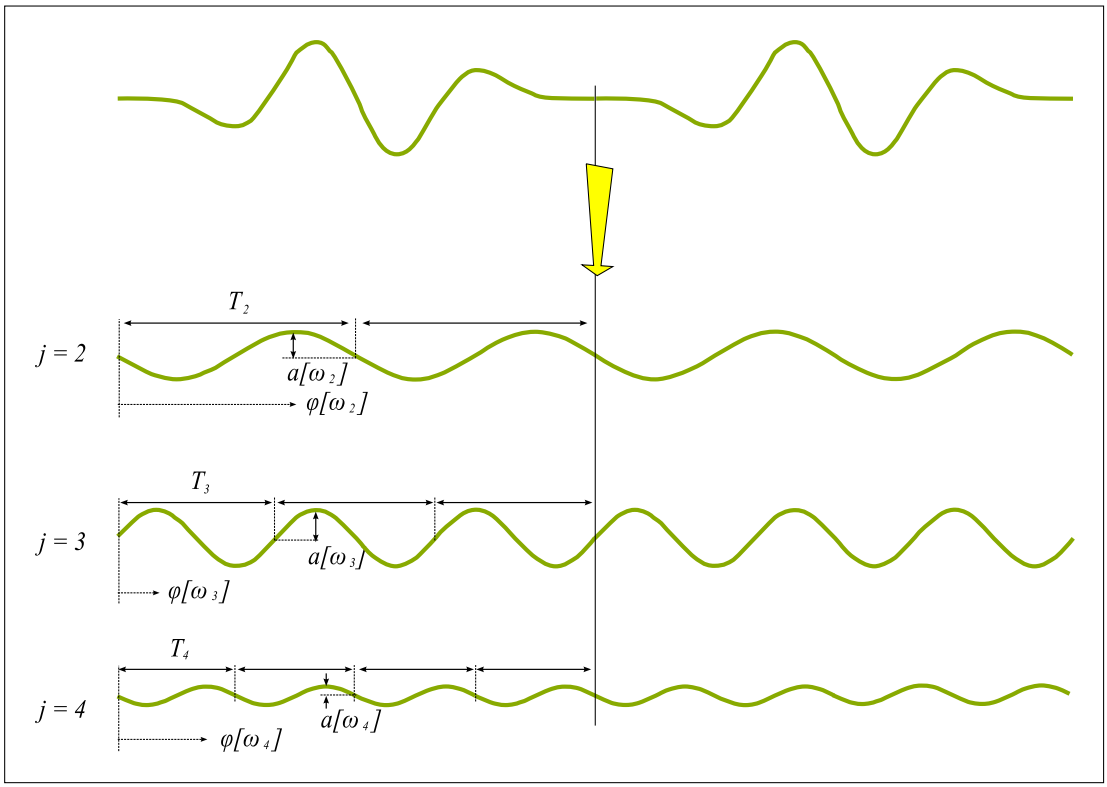

Figure 3.3: ***Decomposition of a time domain signal into sinusoidal components:*** *wave elevation is treated as the superposition of a number of sinusoidal waves. The amplitude and phase written as functions of frequency are a frequency domain representation of this signal (see left box in Fig. 3.4).*

The principle of sinusoidal decomposition

The principle behind frequency domain representation of a signal lies in expressing it as the sum of a series of building blocks known as basis functions. Basis functions are functions whose values are set by a small number of parameters. The basis functions used for frequency domain representation of signals can either be sinusoids or complex exponentials. In both cases, individual versions of the basis functions are defined by the angular frequency, ω. As discussed in § 3.2.4, the real Fourier transform is based on sinusoids, while the complex Fourier transform is based on complex exponentials. The theory presented here uses the complex Fourier transform because this is consistent with the widely used Fast Fourier transform (FFT). However, much processing of wave records uses the real Fourier transform.

To assist the reader, sinusoidal basis functions, rather than complex exponentials, are used to explain the principle of decomposition of a signal into basis functions. Fig. 3.3 shows how a time domain signal has been decomposed into three sinusoids. This example is contrived, as the signal is composed of just three sinusoids. However, any integrable parametrically continuous

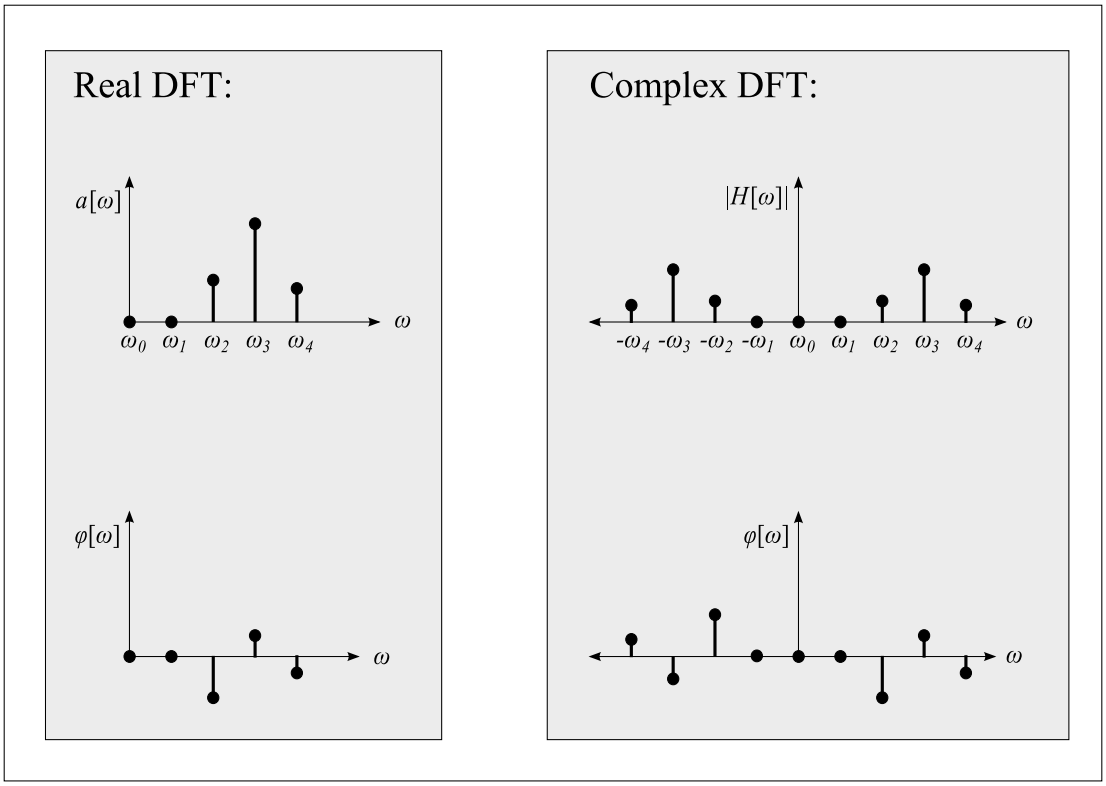

Figure 3.4: ***Frequency domain representation of a wave due to real (left) and complex (right) transforms:*** *These are frequency domain representations of the wave at the bottom of Fig. 3.3. The real DFT can be written as a sum of sines and cosines, or as a sum of cosines that have a specified phase shift. The complex DFT is the amplitude and phase of each complex exponential component. Note that the magnitude of the complex transform is half that of the real transform.*

signal with a parametrically continuous derivative can be decomposed into an infinite number of sinusoids (see § 2.4.2). If such a signal is also periodic, as in Fig. 3.3, then it can be decomposed into a finite number of sinusoids.

When there are a finite number of sinusoids, each is named a *bin* and is numbered according to how many cycles are completed within the repeat time of the signal. The top sinusoid in Fig. 3.3 completes two cycles within the signal's repeat time, so this sinusoid is represented by the second bin in the frequency domain signal. Thus the amplitude and phase of the top sinusoid in Fig. 3.3 correspond to values of amplitude (top) and phase (bottom) at ω_2 in the real transform (left in Fig. 3.4). Likewise, the second and third sinusoids in Fig. 3.3 complete three and four cycles within the signal's repeat time, and these sinusoids are represented by the amplitude and phase of the function at bins ω_3 and ω_4 in the left pair of plots in Fig. 3.4.

Real and complex Fourier transforms

The real Fourier transform decomposes a real, time domain, signal into sinusoids. For a periodic signal that is discrete with time, the DFT is used. The real DFT is:

$$\eta[t_n] = \sum_{j=0}^{N-1} a_j \cos(\omega_j t_n + \phi_j) \tag{3.1}$$

This decomposition is commonly used in coastal engineering (see for example [75]).

Less easy to visualise are the complex exponential basis functions used by the complex Fourier transforms. Using Euler's relation:

$$\mathrm{e}^{ix} = \cos x + i \sin x \tag{3.2}$$

a complex exponential is shown to be the sum of a real cosine wave and an imaginary sine wave. The time domain signal is treated as complex. When modelling waves, the time domain signal (wave elevation) is real, so the imaginary part is zero. In the complex transform (right in Fig. 3.4), there are values of magnitude and phase plotted for both positive and negative frequencies. When the time domain signal is real, the magnitude of the frequency domain signal has even symmetry, while the phase has odd symmetry. Another way of expressing this is to say that at positive frequencies the complex Fourier transform is the complex conjugate of the transform at negative frequencies: $H[\omega_j] = H^*[-\omega_j]$. The negative frequencies cancel out the imaginary (sine) components, and double the real (cosine) components, at the corresponding positive frequencies. For this reason, the amplitude of the complex Fourier transform is half that of the real Fourier transform [60]. Unless otherwise specified, the complex Fourier transform is used.

Continuous and discrete definitions

If the domain of time is infinite, and the signal is continuous, rather than discrete, the frequency domain signal is the continuous Fourier transform of the time domain signal: $H(\omega) = \mathcal{F}\{\eta(t)\}$. The continuous Fourier transform only exists if the signal is integrable (see § 2.4.2). Furthermore, if the time domain signal and its derivative are parametrically continuous, then the original signal can be reconstructed by taking the inverse Fourier transform (Table 2.6 on page 49) of the frequency domain signal:

$$\eta(t) = \int_{-\infty}^{+\infty} H(\omega) e^{i\omega t} d\omega \tag{3.3}$$

If the domain of time is finite and the signal is discrete, the frequency domain signal is the DFT of the time domain signal: $H[\omega_j] = \mathcal{F}_{DFT}\{\eta[t_n]\}$. The DFT only exists if the signal is

integrable (if its sum has a finite value). The time domain signal can be reconstructed from the inverse discrete Fourier transform (IDFT) (Table 2.6) of the frequency domain signal:

$$\eta[t_n] = \sum_{j=0}^{N-1} H[\omega_j] e^{i\omega_j n} \tag{3.4}$$

where $\omega_j = 2\pi j/N$.

Information extracted from the frequency domain signal

Information about ocean waves is often presented as parameters extracted from the frequency domain signal, rather than the frequency domain signal itself, which is the Fourier transform of the wave record. The first step in processing the frequency domain signal is to find the spectral density, or simply the *spectrum*. By convention it is expressed in terms of frequency $S(f)$, but it can also be expresses as a function of angular frequency $S(\omega)$ [55]. It is defined for positive frequencies only. For sea waves the phase information is often discarded, as it is random.

Various parameters can be used to describe the spectrum. The peak frequency is the frequency at which the spectrum has the highest value. The area under the spectrum is the zeroth moment. Other moments can be found using:

$$m_n = \int_0^\infty f^n S(f) df \tag{3.5}$$

where n, in this context, indicates the nth moment. For example, $m_0 = \int_0^\infty S(f)df$ is the area under the spectrum. By the definition of the spectrum, m_0 equals the variance of the signal, $\sigma(\eta)$. This is often written $m_0 = \sqrt{\overline{\eta^2}}$ [63, 75], for which the assumption of zero mean ($\overline{\eta} = 0$) is implicit. The use of spectral moments to define common sea state parameters such as energy period and significant wave height (H_{m_0}) has now superseded older definitions of these parameters [74], which used time domain data (see Table 3.1).

3.2.3 Monochromatic definition of a wave

The word *monochromatic* is borrowed from the science of optics, and means that only one frequency is present. Correspondingly, the word *polychromatic* means that many frequencies are present. In this study, only unidirectional waves are considered, so several waves of the same frequency, but travelling in different directions, are not considered. The time and frequency domains are alternative ways of representing polychromatic waves (§ 3.2.1 and § 3.2.2). Both domains can also be used to represent monochromatic waves, as shall now be described.

Modelling monochromatic waves is the natural viewpoint for physicists. This viewpoint focusses on the theoretical characteristics of waves, so wave elevation is usually considered to

be continuous and infinite. For a sinusoidal, unidirectional wave, the wave elevation is defined by:

$$\eta(t,x) = a_s \cos(\omega_s t - k_s x + \phi_s) \tag{3.6}$$

Here the amplitude a_s is the wave elevation at the top of a crest, ω_s is the frequency, k_s is the wavenumber, x is the distance along the direction of propagation and ϕ_s is the phase relative to an arbitrary historic start time. Here the subscript is used to distinguish the sinusoidal case at an arbitrary frequency, ω_s, from the polychromatic continuous frequency case, ω. Note that in the literature this subscript is not commonly used; it has been included here for the sake of clarity. When modelling waves from a physics point of view, the underlying assumption that the waves are monochromatic is so strong that it is rarely stated. When measured at one point in space, the wave elevation is simply:

$$\eta(t) = a_s \cos(\omega_s t + \phi_s) \tag{3.7}$$

A widely used alternative is phasor notation (see for example [55]). The time dependency of a sinusoid is hidden by expressing the sinusoidal function as a complex exponential:

$$\eta(t) = \Re\left\{a_s e^{i(\omega_s t + \phi_s)}\right\} = \Re\left\{\hat{a} e^{i\omega_s t}\right\} \tag{3.8}$$

The amplitude and phase are combined into one term, the complex amplitude, $\hat{a} = a_s e^{i\phi_s}$.

Fig. 3.5 shows the terminology associated with a monochromatic wave. Shown here are unidirectional sinusoidal waves considered for the domains of time (above) and space (below). The period is the time between two successive crests. Note that unlike the standard coastal engineering description of time domain waves, the time between each successive crest is identical. The angular frequency is the inverse of the period, scaled for the units of radians per second. The standard relation between T and ω, which is written $T = 2\pi/\omega$, usually refers to a monochromatic wave, in which case it pertains to an arbitrary frequency:

$$T_s = \frac{2\pi}{\omega_s} \tag{3.9}$$

There is an analogous relationship between wavelength (the distance between neighbouring crests), λ, and wavenumber, k. Once again this relationship usually refers to monochromatic waves and should be read as:

$$\lambda_s = \frac{2\pi}{k_s} \tag{3.10}$$

In Fig. 3.5 the wave elevation is shown for discrete values of time (above), $\eta[t_n]$, and for discrete values of space (below), $\eta[x_n]$.

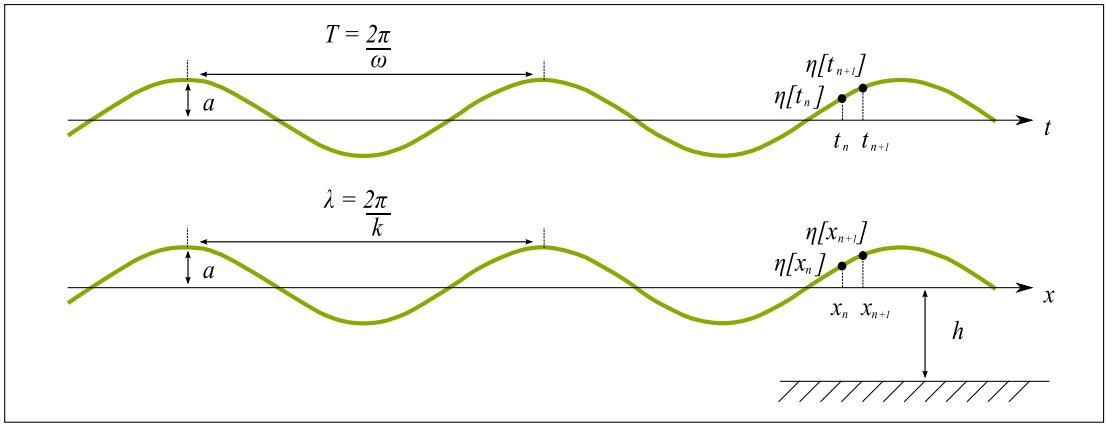

Figure 3.5: ***Physics view of a wave:*** *a sinusoid considered in time (above) and in space (below).*

Linear wave theory

Linear wave theory treats the propagation of waves through space and time as a linear system (§2.4.5). The input to the system is the wave elevation at one point in space, and the output is the elevation downstream of the direction of wave propagation. If the input to this linear system can be expressed as superimposed sinusoids, then the output involves only a change to the amplitudes and phases of these sinusoids.

Assuming that superposition applies, it is then useful to consider the properties of sinusoidal waves. A good introduction to linear wave theory can be found in Chapter 3 of [76], the main points of which are summarised here. The conservation of mass for potential flows is described by the Laplace equation [77], which assumes inviscid, irrotational, and incompressible flow. There are many solutions to this equation, and to find the unique solution to a specific problem, boundary conditions are required. These boundary conditions can include periodicity and linearisations, in which case superposition may later be used to add solutions of uni-directional sinusoidal waves.

The conditions at the boundaries of a region of interest are considered. There are boundary conditions at the bottom (no flow across this boundary), at the free surface (no flow across this boundary and no pressure variation along the boundary), and on the sides (no flow across solid boundaries, nor across fluid boundaries at right angles to the direction of wave propagation; periodic flow at boundaries parallel to the direction of wave propagation). The condition of no pressure variation along the free surface (the dynamic free surface boundary condition) results in an equation that is non-linear with respect to the wave elevation, η. The equation is linearised by assuming that the wave elevation and water particle velocity are infinitesimally small (Airy waves), and then removing any terms that are products or powers of these small terms. The substitution of the boundary conditions (including those linearised for infinitesimal waves) into

the Laplace equation gives the dispersion relation: the relationship between the wavenumber and angular wave frequency. The dispersion relation can manipulated to give the phase velocity.

The dispersion relation

Unlike electromagnetic waves, which have the same speed no matter the wavelength, deep water waves are dispersive, and the speed depends on the wavelength. The relationship between the frequency and the wavelength is the dispersion relation:

$$\omega_s^2 = g k_s \tanh(k_s h) \tag{3.11}$$

where g is acceleration due to gravity. Note that the dispersion relation also depends on the water depth, h, (see Fig. 3.5). In the deep water case, valid when $k_s h >> 1$, the dispersion relation simplifies to:

$$\omega_s^2 = g k_s \tag{3.12}$$

Group and phase velocity

The phase velocity (wave celerity) is the velocity of a particular wave feature such as a crest. In a monochromatic wave, a crest travels the distance λ_s during the time T_s so the phase velocity is:

$$c_p(k_s, h) = \frac{\lambda_s}{T_s} = \frac{\omega_s}{k_s} \tag{3.13}$$

Substituting the dispersion relation (3.11) into the above gives $c_p(\omega_s) = \sqrt{\frac{g}{k_s}\tanh(k_s h)}$

The group velocity is the velocity at which the energy in a monochromatic wave travels and is defined as:

$$c_g(\omega_s, h) = \frac{\partial \omega_s}{\partial k(\omega_s, h)} \tag{3.14}$$

Substitution of the dispersion (3.11) relation into the above gives:

$$c_g(\omega_s, h) = \frac{g}{2\omega_s} D(\omega_s, h) \tag{3.15}$$

with $D(\omega_s, h)$ denoting the depth function:

$$D(\omega_s, h) = \tanh(k_s h)\left[1 + \frac{2k_s h}{\sinh(2k_s h)}\right] \tag{3.16}$$

In the deep water case, valid when $k_s h >> 1$, the depth function approaches unity and

$$c_g(\omega_s) \approx \frac{g}{2\omega_s} \tag{3.17}$$

The limits of linear wave theory

Linear wave theory considers only the first order Stokes waves, and neglects the higher order components. For linear wave theory to be valid, the water must be deep ($k_s h >> 1$), and the amplitude of the second order Stokes wave (a_{s_2}) must be small compared to the amplitude of the first order Stokes wave (a_s). This condition gives the following relation (see pages 179 and 182 of [78]): This condition gives the following relation :

$$\frac{a_{s_2}}{a_s} = k_s a_s \frac{3 - \sigma^2}{4\sigma^3} << 1 \tag{3.18}$$

where a_s is the amplitude of the sinusoidal wave, $\sigma = \tanh(k_s h)$, and h is the water depth. In deep water, $\sigma \cong 1$, so the linearity condition is simply $k a_s << 2$. In simple terms, this means that in deep water the steepness of the wave determines the extent of its non-linearity. In shallow water, $\sigma \approx k_s h$, in which case the following approximation may be made:

$$\frac{a_{s_2}}{a_s} \approx k_s a_s \frac{3}{4(k_s h)^3} << 1 \tag{3.19}$$

This criteria was first highlighted by Stokes (see page 210 of [79]), and was later revised by Ursell [80]. A common form of this is the Stokes/Ursell number, $\frac{H\lambda_s^2}{h^3}$, which is found from (3.19) using $H = 2a_s$ and $k_s = 2\pi/\lambda_s$. The linearity limit is then given by :

$$\frac{H\lambda_s^2}{h^3} << \frac{32\pi^2}{3} \tag{3.20}$$

3.2.4 Clarification of potential ambiguities

Monochromatic definitions

In linear wave theory, wave properties are defined for monochromatic waves. In frequency domain equations of physical systems, these properties apply to each frequency component. Using Parseval's theorem, the values of power transported by an ocean wave at each component of frequency can be used to find the power for a polychromatic wave (Appendix B). However, for many wave properties, the values at each frequency bin cannot be used to find the overall value for a given wave spectrum. It is clear that while period, wavelength and wavenumber are defined at each frequency, so are by definition frequency domain properties, the time series given by the IDFT does not give any meaningful time domain measure of period, wavelength or wavenumber. It is less intuitive however that phase and group velocity are defined for a particular sinusoid, and cannot be used to give any meaningful measure of the velocity of polychromatic waves.

The name *group velocity* is particularly misleading as it suggests the combined velocity of several waves, where waves are defined either in the time domain sense, the velocity of a group

of crests, or in the frequency domain sense, the velocity of a number of sinusoidal waves. In fact, group velocity pertains to a monochromatic wave, or to a frequency component of a polychromatic wave.

The name group velocity arose because in cases where there is an obvious wave envelope that does not change shape, such as a bi-chromatic wave or a wave pulse, the energy travels at the speed of this envelope. However, in waves composed of three or more sinusoids, the shape of the envelope fluctuates over time, as it moves through space. When it is not possible to track one part of the envelope, it is not meaningful to define group velocity as the velocity of the energy of a group of waves, as it is not possible to define a group of waves.

Yet this is not always clear from the literature. The bi-chromatic case is often used to define group velocity [55, 76, 77] in the limiting case where the two sinusoids have the same frequency (a monochromatic wave). Furthermore, bi-chromatic waves allow a clear pictorial representation of the difference between the velocity of a crest (phase velocity) and of a group envelope (group velocity), as can be seen in an animation on Wikipedia [81]. This representation can obscure the fact that group velocity is defined for a monochromatic wave (3.14).

The definition of period

It is important to differentiate between the period of a monochromatic wave, T_s, the zero-crossing wave period of a polychromatic wave, T_k, and the period associated with a frequency component of a polychromatic wave, T_j.

The definitions of sea state parameters

A commonly used sea state parameter is the significant wave height, H_s or H_{sig}. This can be ambiguous as it has various definitions (see Table 3.1). The traditional definition, based on information extracted from the time domain signal, is known as $H_{1/3}$. The wave record is subdivided into individual waves according to the zero-crossing method (see Fig.3.2 which shows the zero up-crossing method), and the values of wave heights are treated as a set of numbers. This set is sorted by the value of wave height, rather than chronologically. From this set, a subset is extracted: it contains a third of the number of elements of the original set, and these consist of the largest numbers in the original set. The mean of this subset is found, and this gives $H_{1/3}$.

Another interpretation of H_s is four times the variance of the wave elevation signal: $H_\sigma = 4\sigma(\eta)$. The variance is the root mean square of the difference between the wave elevation and the mean wave elevation, $\sigma(\eta) = \sqrt{\left(\overline{\eta - \overline{\eta}}\right)^2}$. When the mean is zero ($\overline{\eta} = 0$), then the variance is the root mean square of the wave elevation, $\sigma(\eta) = \eta_{rms} = \sqrt{\overline{\eta^2}}$. H_σ can then

be calculated using frequency domain data because by definition the area under the spectrum is the variance in the signal $m_0 = \eta_{rms}$ [63, 75].

The official interpretation of H_s is H_{m_0}, which is defined as $H_{m_0} = 4.004\sqrt{m_0}$ [74]. The reason for the factor 4.004 is shown in Table 2.3 of Goda's textbook [75]. This table gives the ratio between $H_{1/3}$ and η_{rms} for various spectra and also for a sea state with a Rayleigh distribution of wave heights. This ratio is 4.004 for the sea state with the Rayleigh distribution but lower for other spectra. The coefficient 4.004 was used in the definition of H_{m_0} because this gives $H_{m_0} \approx H_{1/3}$ for a sea state with a Rayleigh distribution of wave heights. For some time, it was assumed that a Rayleigh distribution correctly described the distribution of wave heights in any sea state. It has since been shown that this only applies to very narrow spectra that are not typical of real sea waves [75]. While the origin of the factor 4.004 was based on the assumption of a Rayleigh distribution and on the historical importance of $H_{1/3}$, H_{m_0} has now become important in its own right and is interpreted by many to mean H_s. The definition $H_{m_0} = 4\sqrt{m_0}$ is commonly used [6, 63] and is equivalent to the definition of H_σ [74].

Table 3.1 shows why it is important to study literature on a case by case basis to interpret the meaning of the term H_s : its intended meaning could be $H_{1/3}$, H_{m_0} or H_σ. Although it is now understood that the calculations of $H_{1/3}$ and H_{m_0} will differ for typical sea waves, there was a time when $H_{1/3}$ and H_{m_0} were treated as being interchangeable. There are even cases where the notation $H_{1/3}$ has been used when the intended meaning was H_{m_0}: when spectra are defined in terms of $H_{1/3}$ (see (2.10) - (2.12) in [75]), this assumes the relationship $H_{1/3} = 4.004\sqrt{m_0}$.

Another widely used [82, 83], but not officially recommended [74] sea state parameter is the root mean square wave height. This is defined as the rms value of the crest to trough heights of individual waves in a wave record [75]:

$$H_{rms} = \sqrt{1/K \sum_{k=1}^{K} H_k^2} \tag{3.21}$$

Once again, if a Rayleigh distribution of wave heights were assumed then it is possible to estimate H_{rms} from the spectrum: $H_{rms} \approx \sqrt{8\, m_0}$ [84]. Although the assumption of a Rayleigh distribution is now not considered to be representative, it was historically believed to be, so it should be judged from the context whether H_{rms} has been calculated from time domain or frequency domain information.

Note that there is an alternative use of the term H_{rms}. In the annual reports of the Edinburgh Wave Power Project [85], and in work following this approach [6], wave elevation is referred to as wave height, and the rms of the wave height defined in this manner (η_{rms}) is referred to as H_{rms} .

Caution is required when interpreting literature, as similar notation is used to represent different things. For example the notation $n = 0$ to $N - 1$ is commonly used to describe a sampled

time domain function such as $\eta[n]$, which is equivalent notation for $\eta[t_n]$, as well as the height and period parameters of individual waves. It is for this reason that here different notations have been used to describe zero up-crossing heights and periods. Here the index k is used to describe zero up-crossing wave parameters, while the notation $[t_n]$ is used to indicate parameters sampled with time.

In the work presented here, the convention of using a lower case letter for the time domain signal, and the upper case for the corresponding frequency domain (Fourier) signal is applied where ever possible. The conventional notation for time domain wave elevation is η. The Greek capital Eta is H, so $H(\omega)$ is used to describe the Fourier transform of $\eta(t)$, and $H[\omega_j]$ to describe the DFT of $\eta[t_n]$. This is not standard practice in wave energy literature as H_{rms} and H_s are associated with wave height. However, the notation used here should not be a cause for ambiguity as the domain is clearly indicated by (ω) or $[\omega_j]$.

Real and complex Fourier transforms

It is important to note that the real and complex Fourier transforms are two different systems for representing frequency domain signals. The magnitude of the complex transform is half that of the real transform. It is not always clear whether the real or complex version of a transform has been used. If negative frequencies are shown, as in Fig. 3.4 (right), then the complex transform has been used. However, when dealing with time domain signals that are real, rather than complex, the information at the negative frequencies is redundant, so is often not included. All the graphs of frequency domain data presented in this thesis only show the data for positive frequencies. As noted in § 2.4, the complex Fourier transform is more rigorous than the real transform. An awareness of these two methods is important, as much of the theory of waves [55, 75, 86] uses the real Fourier transform (or sinusoidal motion, which represents one component of the real Fourier transform), while practical synthesis using the inverse fast Fourier transform (IFFT) uses the complex version of the DFT. Many measurements of sea spectra [64], sea state parameters derived from these spectra, formulae for calculating these sea state parameters (Table 3.1), formulae using spectra to calculate wave energy transport and absorbed power [55], and hydrodynamic parameters such as those used in this research [57] are expressed using the real DFT. However, any modelling work that requires conversion between the time and frequency domains will use the complex DFT. The treatment of hydrodynamic parameters to make them suitable for use with the complex DFT is discussed in § 4.6.6.

If the complex DFT version of Plancherel's theorem (B.3) is used with frequency domain signals derived with the real DFT, this will give an overestimation by a factor of two. This could apply to estimations of wave energy transport or absorbed power. Performance indicators such as capture width (4.6.1) are not at risk of this problem because any scaling factors due to Fourier transform definitions appear on both the denominator and numerator, and so cancel out.

Ambiguous parameter	Alternative definition	Explanation	Domain
H_s	$H_{1/3}$ [74]	mean highest third of crest to trough heights	time
H_s	$H_{m_0} = 4.004\sqrt{m_0}$ [74]	Rayleigh distribution :$H_{m_0} \approx H_{1/3}$	frequency
H_s	$H_\sigma = 4\sigma(\eta)$ [74]	Four times the variance of elevation.	time
H_s	$H_\sigma = 4\sqrt{m_0}$ [74]	if $\overline{\eta} = 0$ then $H_\sigma = 4\eta_{rms} = 4\sqrt{m_0}$	frequency
H_{rms}	H_{rms} [75]	rms of crest to trough heights	time
H_{rms}	$\sqrt{8\ m_0}$ [84]	Rayleigh distribution: $\sqrt{8\ m_0} \approx H_{rms}$	frequency
H_{rms}	η_{rms} [85]	rms of wave elevation	time
H_{rms}	η_{rms} [85]	if $\overline{\eta} = 0$ then $\eta_{rms} = \sqrt{m_0}$	frequency

Table 3.1: *Ambiguous sea state parameters associated with wave height: the first column shows how a sea state parameter might be written in the literature, while the second column gives the possible interpretations of these parameters.*

Systems analysis using phasor notation

In (3.8) wave elevation was expressed in phasor notation. If other sinusoidal quantities such as forces and velocities are also expressed in phasor notation, then an equation of motion containing only phasors can be built (see for example Chapter 2 of [55]). This governing equation will not be a general model of the system, and will only be valid when the input and response are sinusoids. In such a governing equation, the complex exponentials that appear on both sides of the equation can be cancelled. The resulting equation could contain terms that are functions of the sinusoidal frequency, but would contain no terms that are functions of time, giving it the appearance of a frequency domain equation. This is not the case however, as the frequency terms, such as the frequency of the sinusoid, or the value of a parameter at that frequency, are in fact constants. These constants have different values depending on the frequency of the sinusoid, but within the phasor equation (for a given frequency) they are nevertheless constants. A frequency domain equation is different because it is a general system model, and is valid for inputs and response signals containing many frequencies. The difference between models suitable for only sinusoidal inputs or for a general input is dealt with in more depth later in this chapter (§ 3.8).

Limitations of the DFT

When an integrable signal and its derivative are parametrically continuous, the signal can be represented equally well in the time or frequency domain; either can be reconstructed from the other using the continuous Fourier transform or its inverse. In the real world however, we work with finite length signals, such as a wave record, and usually discrete values are required. From Table 2.6 it can be seen that a discrete signal in one domain leads to a periodic signal in the other. When it is a requirement for both the time and frequency domain signals to be discrete, they both need to be periodic too. Discretised time and frequency domain signals are only equivalent to each other if the time series repeats with the wave record.

A DFT can be used to express an aperiodic signal as a sum of sinusoids, but these sinusoids cannot be treated as the monochromatic components of the wave. As discussed in § 2.4.4, some of these sinusoids are due to leakage and do not represent the true frequency content. Spectral noise reduction techniques inevitably involve throwing away information. Thus wave elevation that is aperiodic with the wave record cannot be accurately expressed as the sum of monochromatic waves. Modelling the excitation of a WEC however relies on the ability to decompose waves into sinusoids. There are two ways to get around this. Either the aperiodicity is ignored: wave elevation is treated as though it were periodic, and any calculations made using this assumption are then approximations (see § 6.2.5). Alternatively, the periodicity is forced: in numerical simulations and tank tests waves that are periodic can be created (see § 2.5.3). When presenting equations for discrete time and frequency, the DFT, and hence the periodicity of the time and frequency domain signals, is implicitly presumed.

3.3 Modelling systems

It is important to separate a physical system and its model [87]. A physical system is subjected to various external excitations and internal (intrinsic) responses to the system's state. A model is used to analyse a physical system. It breaks the response into individual components, attributes physical meaning to them, and describes dependencies between excitation, response and state. These dependencies are often not fully known or understood, and are, in general, non-linear. Behaviour that is difficult to model is neglected for the sake of a simpler model. If the behaviour neglected is negligible then this is a *good model* (accurate). If the behaviour neglected is significant, then this is a *poor model*. There is often a need for compromise between accuracy and simplicity.

3.3.1 Linear models

A common simplification is only to model linear dependencies. Real physical systems are never linear[1]. While some systems, such as mass-spring-damper or inductor-capacitor-resistor systems, are described as linear, they are in fact weakly non-linear systems for which a linear model is an adequate approximation. WECs are highly non-linear, but for very small motions the behaviour is only weakly non-linear. Fig. 3.6 shows a system (top) which has behaviour ranging from highly non-linear to weakly non-linear.

Non-linear behaviour in WECs has several possible causes, including steep waves, large motions or a non-linear PTO force. Non-linear behaviour could be due to any combination of these. The linear operating regime is the sub-set of behaviour for which a linear approximation is a good model. Non-linear models are required to model behaviour outside the linear operating regime. These non-linear models will also involve simplifications, and may also be limited to specific behaviours. For example, it may be possible to model non-linear PTO while the hydrodynamic response remains linear, or vice versa.

The linear operating regime of the physical system is modelled as a linear system. Linear systems analysis may then be applied. The linear system is treated as the transformation an input (excitation) into an output (response). In the time domain system representation, the input must be convolved with the impulse response to give the output: $x(t) * h(t) = y(t)$. Here $h(t)$ is the standard systems analysis notation for the impulse response of an arbitrary system. This equation models both the transient and steady state responses. The steady state response can also be found by solving the frequency domain representation of a linear system: the input is multiplied by the transfer function to give the output: $X(\omega)H(\omega) = Y(\omega)$. Here $H(\omega)$ is the standard systems analysis notation for the transfer function of an arbitrary system. In these equations the output is on the right hand side as this ordering corresponds to the standard diagrammatic representation of a linear system shown in Fig. 3.7.

[1] Linear in the sense that superposition may be applied.

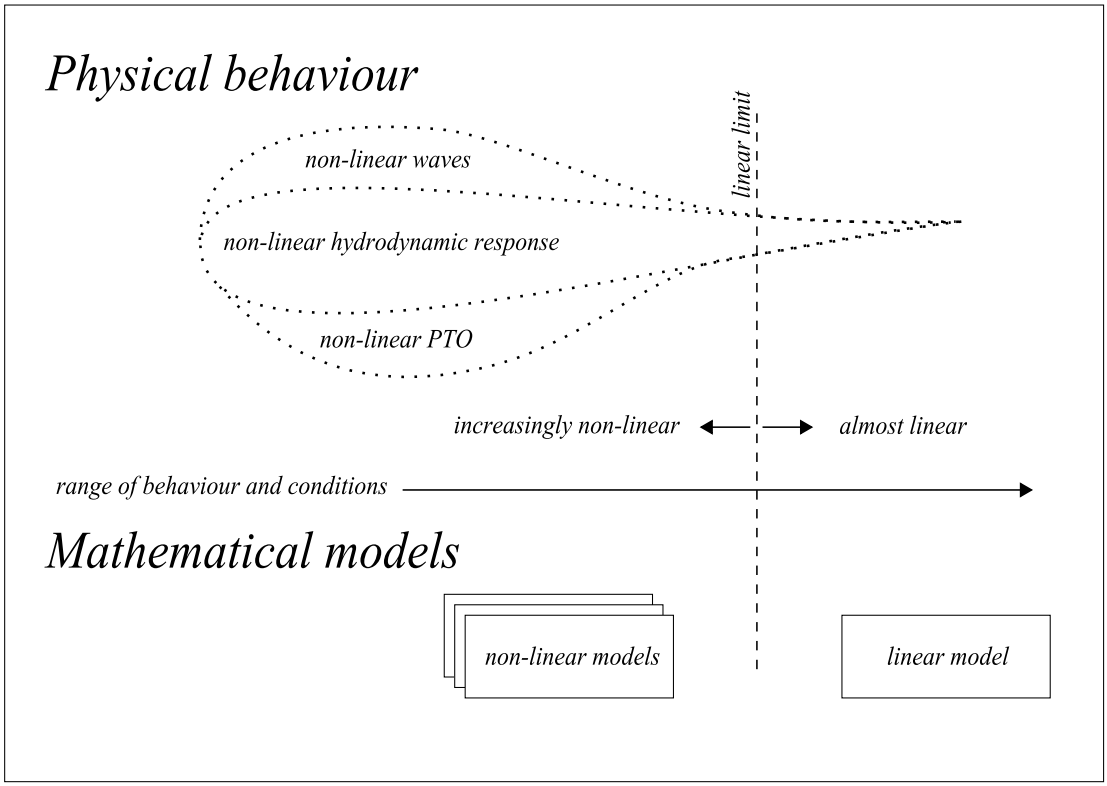

Figure 3.6: ***The difference between a physical system (top) and the mathematical model (bottom):*** *the mathematical model represents a simplification of the behaviour of the real system. A linear model is only appropriate for a sub-set of the behaviour.*

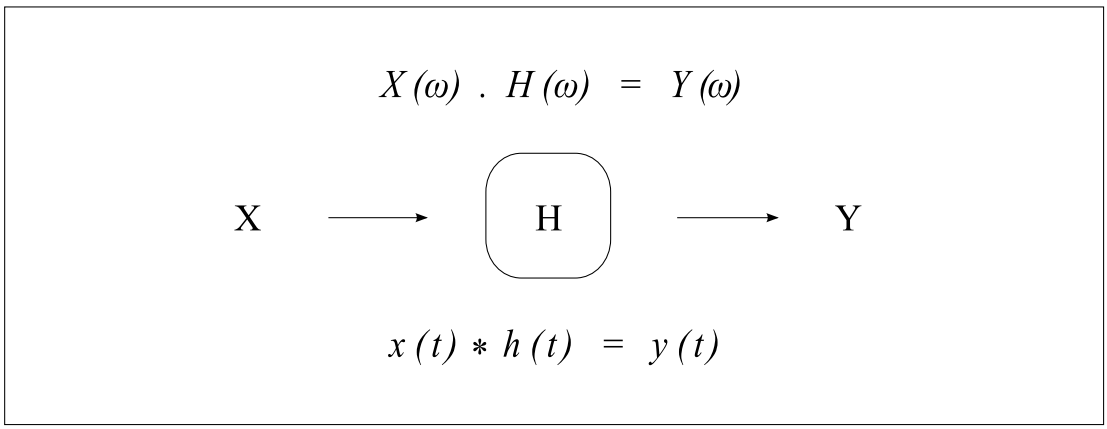

Figure 3.7: ***The standard diagrammatic representation of a linear system (middle):*** *in the frequency domain representation this corresponds to multiplication (top) and in the time domain representation this corresponds to convolution (bottom).*

3.3.2 System order

The order of a system is another useful description. It is the highest derivative of the dynamic variable seen in the equation of motion. A system containing a mass, spring and damper is a second order system because the dynamic variable is displacement and the mass acceleration is proportional to the second derivative of displacement. It is possible to find a solution for either the displacement, velocity or acceleration. No matter which derivative of the dynamic variable is considered the response, the system remains a second order system.

3.3.3 Memory and Causality

Memoryless systems

The viewpoint presented in this section up to this point has been borrowed from a branch of electrical engineering called systems analysis. The concepts of memory and causality are crucial concepts in systems analysis. These concepts are also used to describe the control of WECs. The wave energy engineering and systems analysis definitions of a memoryless system are different.

The systems analysis definition of a memoryless system is a system where past values of the response have no effect on the present value of response. The history of response determines the system's state: the values of the dynamic variable and its derivatives. In a mass-spring-damper system, the past values of velocity (response) determine the present value of acceleration and displacement (state), which influence the present value of response. According to this definition of system memory, a mass-spring-damper system has memory, because past values of response are *remembered* in the state. Thus only first order systems, such as a mass subject to an exciting force (without any spring or damping) or a resistor with a voltage across it, are described as *memoryless* in systems analysis. The response depends only on the (instantaneous) value of excitation. Thus there is no transient response due to initial conditions; the response does not depend on the state of the system.

The terminology of systems analysis is not consistent because a causal system is often described as a system with memory. A causal system is one that contains a term that depends directly on past values of the dynamic variable (or its derivatives). A convolution of an impulse response with a dynamic variable would lead to a so called history, or memory, term. The inclusion of such a term in an equation of motion makes this a system with memory. It would then seem logical that the absence of such a memory term would indicate a memoryless system. This would make a mass-spring-damper system memoryless, which does not fit with the standard definition of memoryless given in systems analysis textbooks [61].

In wave engineering, the terminology is more consistent. A mass-spring-damper is understood as memoryless, because it contains no memory term. At any instant, the response depends only on the excitation and the state of the system; past values of system state are not important.

In this research, the standard wave energy engineering meaning will be attributed to the term memoryless. The standard systems analysis definition of memoryless will be referred to an instantaneous system.

Causality

In systems analysis the exact definitions of causal, acausal and anticausal systems vary. A causal system is defined as containing a term that depends on the past state of the system: a memory term. Often however, the word causal is used to describe a system that is not affected by values of future state, that is, to indicate it is not acausal. For example, if the electrical equivalent of a mass-spring-damper system, an inductor-capacitor-resistor circuit, were described as causal, this would indicate that it is a filter which does not require information about future inputs.

An acausal system is defined as containing a term that depends on future values of state. By analogy, this has been named the premonition term [88]. When the system contains a term that depends on past, present and future states, it is sometimes called an acausal system with memory, and sometimes simply an acausal system. The formal definition of an anticausal system is one that depends on future inputs only. However it is now common practice in systems analysis to describe systems that depend on present and future inputs as anticausal.

Definitions of terminology

A second order linear equation of motion is of the following general form:

$$f_e(t) = ma(t) + bu(t) + cx(t) + h(t) * x(t) \tag{3.22}$$

where

f_e is a generalised excitation
m is the physical mass
b is a generalised damping coefficient
c is a generalised spring coefficient
h is a convolution kernel
x is the dynamic variable; for a solid WEC with translating motion this is displacement
u is the first derivative of the dynamic variable; for a solid WEC with translating motion this is velocity
a is the second derivative of the dynamic variable; for a solid WEC with translating motion this is acceleration

The types of terms on the right hand side of the equation define the type of system it describes. The first three terms are instantaneous terms: they are directly proportional to the dynamic variable or one of its derivatives.

The last term is a convolution[2]. The value of the convolution kernel $h(t)$ defines whether this term is instantaneous, a memory term, a premonition term, or both a memory and a premonition term. Fig. 3.8 shows the kernels that characterise the four different types of terms:

- a) Instantaneous term: $h(t)$ is a delta function: non-zero at $t = 0$; zero at all other times.
- b) Memory term : $h(t)$ is non-zero at $t \geq 0$ (decaying for large values of $|t|$), and is zero for $t = \infty$ and $t < 0$.
- c) Premonition term: $h(t)$ is non-zero at $t \leq 0$ (decaying for large values of $|t|$), and is zero for $t = -\infty$ and $t > 0$.
- d) Memory/premonition term: $h(t)$ may have non-zero values at any value of t, but decays for large values of $|t|$), and is zero for $t = \pm\infty$.

The reason why a memory term has values for $t \geq 0$ is that during convolution, it is time reversed and multiplied by the dynamic variable forming the other term of the convolution. The reason why a delta function leads to an instantaneous term is that convolution with a delta function simplifies to a constant multiplied by the dynamic variable. If $h(t)$ in the final term of (3.22) was instantaneous, it could be incorporated into one of the first three instantaneous terms, and the equation would then be a second order, linear, ordinary differential equation.

In this thesis, the definitions for words are those in common use in wave energy engineering rather than systems analysis. This is not only because these definitions are familiar to the target audience, but also because the definitions are more consistent. Systems can be described as:

- Instantaneous: contains one instantaneous term, so depends on present input only, not present state.
- Memoryless: contains multiple instantaneous terms of different orders, but no memory or premonition terms, so depends on present input and state.
- Causal: contains a memory term in addition to any number of instantaneous terms, so depends on present and past inputs and states only.
- Anticausal: contains a premonition term in addition to any number of instantaneous terms, so depends on present and future inputs and states.
- Acausal: contains either one term that has both memory and premonition, or separate memory and premonition terms, in addition to any number of instantaneous terms, so depends on past, present and future inputs.

[2]A linear equation of motion may contain such a term because convolution is a linear operator. Here the convolution is with the dynamic variable, but it could also take place with a derivative of the dynamic variable.

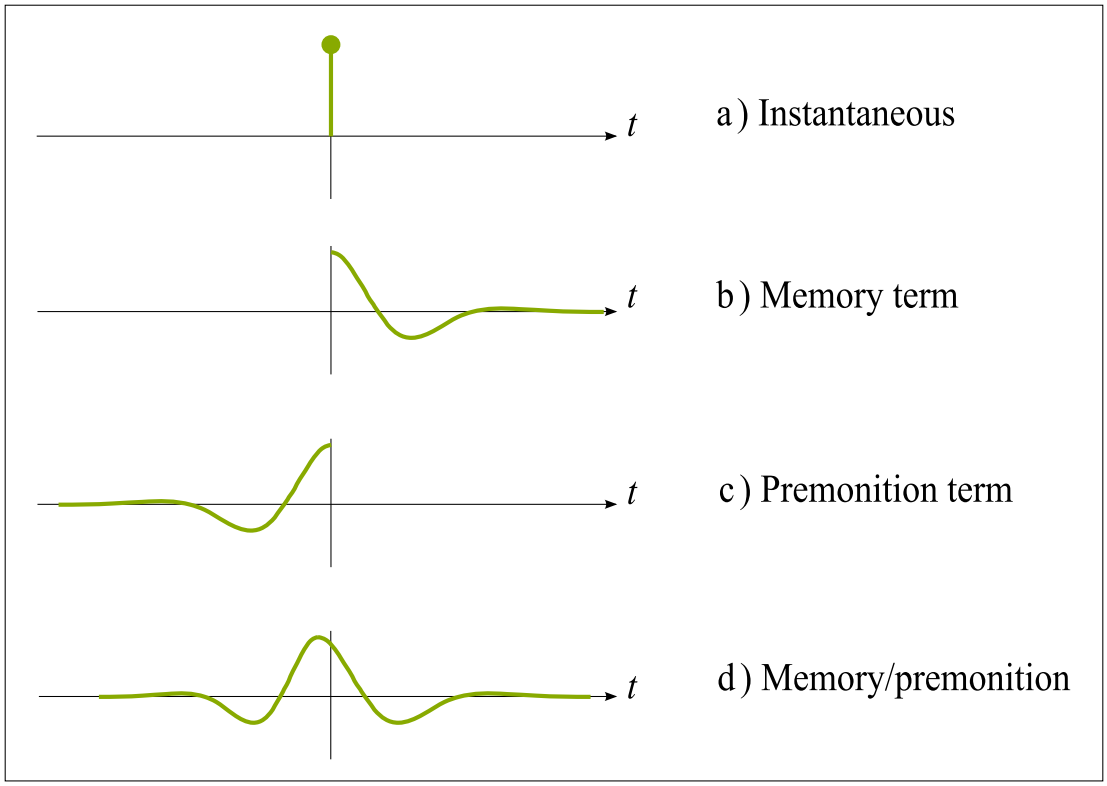

Figure 3.8: ***Kernel functions characterise the type of term:*** *a) an instantaneous term b) a memory term c) a premonition term d) a memory/premonition term.*

An immersed oscillating solid, pulsating solid, or pulsating fluid (see § 2.2.4), excited by ocean waves, is a causal system. The dynamic model that describes it contains a memory term[3].

In Chapter 4 the terminology for describing systems will also be used to describe types of control. It has become standard practice in wave energy engineering to distinguish between causal and acausal control. In causal control, the PTO term [4] that gives the best performance without future knowledge is memoryless; it does not contain a memory term. When this PTO term is included in the causal equation of motion, the resulting system remains causal. In acausal control, the PTO term that gives the best performance is anticausal: it contains a premonition term. When this PTO term is included in the causal equation of motion, the resulting system becomes acausal, because it contains a memory term and a premonition term. Thus the terminology *causal* and *acausal control* refer to the type of system resulting from this control.

[3]The input to the system is the excitation (force or pressure), rather than the wave elevation. The acausal relationship between wave elevation and excitation does not make the system acausal; it is the nature of the terms containing the dynamic variable that determine the causality of the relationship.

[4]If the PTO system opposes the motion of an oscillating solid then the PTO term is a force; if it opposes fluid flow, it is a pressure differential.

3.4 Generalised dynamic model

This section presents the governing equation of motion for a simple WEC. This governing equation can be modified to suit specific types of WEC, as described in §2.3.6. For this reason it is known as the generalised equation of motion. For a WEC that works by translation of a solid working surface, the excitation is a force and the response is a motion (either displacement, velocity, or acceleration). The governing equation is hence known as the equation of motion. Other types of WEC can be represented by replacing force and motion with the appropriate excitation and response terms. For example, where the response is a rotational (angular) motion, the excitation is a moment; where the response is fluid flow, the excitation is a pressure.

The equation of motion is a time domain representation of the system by default. Following convention, and to make the equations more readable, the time dependency is not indicated. Equation (3.23) is valid for an arbitrary excitation, including an impulse, a sinusoid or anything else in between. There are no restrictions on the impedance (see § 3.5.2) that the WEC offers to this excitation. The impedance may be non-linear and may vary with time.

The model that is valid for all cases is then linearised (§ 3.4.3). It is then valid only for the subset of behaviour that can be described by a linear governing equation. Solution of this equation gives a transient and post-transient response. The easiest way to find the post-transient solution to this linearised model is to solve the equation of the frequency domain representation of the system, which is described in § 3.5. The frequency domain equation is easier to solve as it is an algebraic equation, rather than the differential equation given by the time domain formulation.

The representation of a system in the frequency domain limits the input to a signal that is the superposition of sinusoids. When an integrable signal of infinite length and its derivative are parametrically continuous, the signal can be equivalently represented by sinusoids using the continuous Fourier transform. However, if the excitation is modelled as a discrete signal of finite length, and if a finite number of frequency bins are required, then the DFT must be used. This limits the excitation to periodic signals.

The frequency domain equation is introduced first, as it is simpler than the time domain equation, and is useful for explaining the meaning of individual terms. However, the corresponding linear time domain equation is necessary for modelling transients and explicitly describing causality. The time and frequency domain equations in common use contain different notation, so the link between the terms in the time and frequency domain equations is shown in § 3.6.

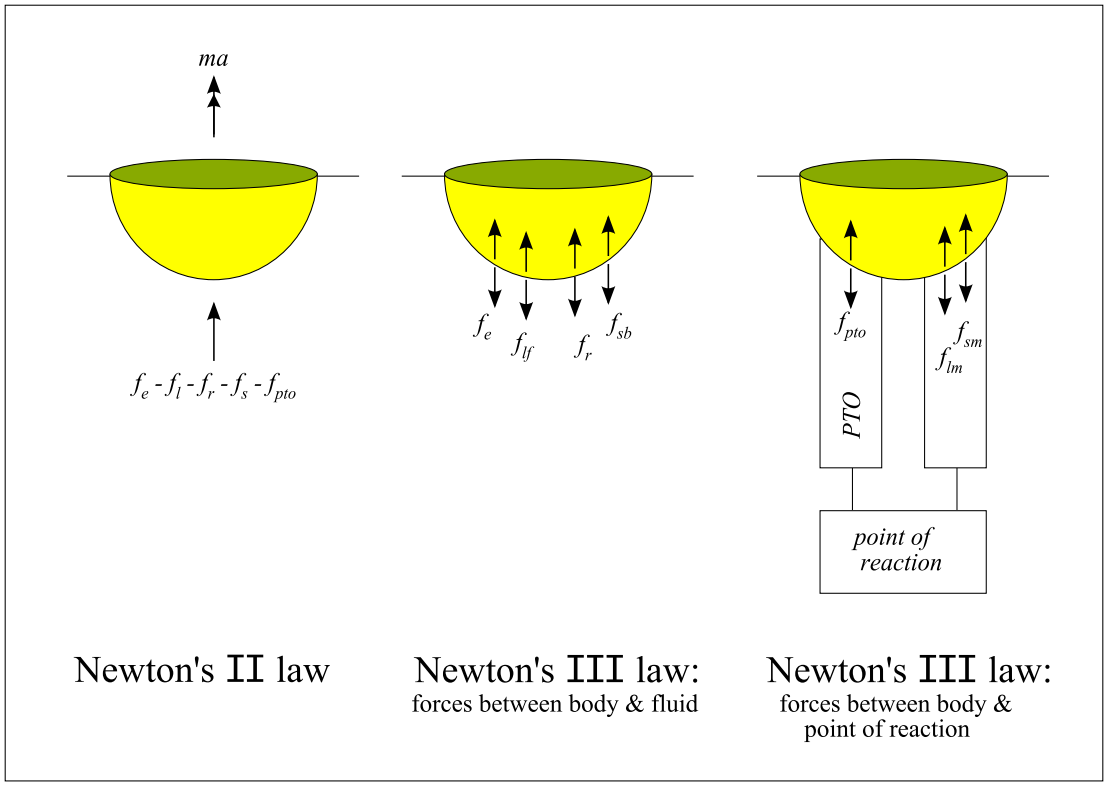

Figure 3.9: ***Newton's second and third laws applied to a WEC moving in heave:*** *Newton's second law: the sum of the forces on the WEC equals the mass acceleration (left). Newton's third law: each force is matched by a equal and opposite reaction force. There are forces between the body and the fluid (centre), and between the body and the point of reaction (right).*

3.4.1 Newton's second law

Any equation of motion begins with Newton's second law: the sum of all the forces on the body equals the mass acceleration, $f = ma$. For a WEC, the total force f can be expanded to give:

$$f_e - f_{loss} - f_r - f_s - f_{pto} = ma \tag{3.23}$$

where

f_e is the wave excitation force

f_{loss} is the net force due to energy losses

f_r is the force due to radiation of waves

f_s is the net restoring (spring) force, which includes the effects of gravity

f_{pto} is the external force provided by the PTO system

The diagram on the left in Fig. 3.9 depicts equation (3.23) for motion in one degree of freedom (heave). This equation applies to a system with a constant mass.

3.4.2 Newton's third law

Newton's third law states that every force has a reaction force equal in magnitude and opposite in direction. All the forces experienced by the body (3.23) must have associated reaction forces. It is the force on the body that is of interest when modelling the motion of WECs, so in later diagrams the reaction forces are not included; only the forces felt by the body are shown.

Nevertheless, clarification of where these reaction forces are placed is a useful way of checking the origin of the forces on the body. Knowledge of where the reaction forces lie is also essential when using measured forces as control data (§ 6.3.1).

It is useful to divide the body forces into those between the body and the surrounding fluid, and those between the body and other points of reaction. The loss f_{loss} and spring f_s terms contain both types of forces. The force due to losses can be sub-divided thus:

$$f_{loss} = f_{lf} + f_{lm} \tag{3.24}$$

with contributions from the fluid f_{lf} (drag and viscosity) and from the point of reaction f_{lm} (friction and losses associated with the PTO stage of a WEC, as described in § 2.2.3). The spring force can be sub-divided thus:

$$f_s = f_{sb} + f_{sm} \tag{3.25}$$

with contributions from the fluid f_{sb} (dynamic buoyancy) and from the means of reaction f_{sm} (mooring spring and mechanical springs).

Forces between the body and the fluid

In addition to the loss f_{lf} and spring f_{sb} forces exerted by the body and the surrounding fluid on each other, there are forces due to the radiation of created waves, f_r, and the interaction with incoming waves, f_e. The diagram in the centre of Fig. 3.9 shows these fluid forces. A force sensor between the body and the fluid would sense the sum of these forces. As described in § 3.5.4, the hydrostatic force is felt via the buoyancy spring, f_{sb}.

Forces between the body and point of reaction

The forces between the body and the point of reaction are the PTO force, f_{pto}, and any restoring f_{sm} or friction f_{lm} forces. In Fig. 3.9 (right), the restoring and spring forces are shown reacting against the same point as the PTO. They may in fact react against different points, but they often react against the same point. Examples of both cases will now be given.

As described in § 2.2.3, the point of reaction could be the sea-bed, another body subjected to different hydrodynamic forces, or a coupled inertia. When losses represent friction in the PTO

system, f_{lm} and f_{pto} react against the same point. When the losses represent friction in a mode of motion where there is no PTO, f_{lm} and f_{pto} react against different points.

The mechanical spring f_{sm} is a restoring force that is not applied using the PTO mechanism (thus it is not a component of f_{pto}). It, however, can be applied in parallel to the PTO system, and use the PTO system's point of reaction. An example of this is the AWS, the motion of which is impeded by a PTO force and an independent air spring [89]. It is also possible for f_{sm} and f_{pto} to react against different points. In a slack-moored attenuator such as the Pelamis, the restoring force due to mooring does not share the point of reaction of the PTO force, which is experienced between neighbouring modules. The restoring force due to mooring may have multiple reaction points, and these depend on the type of mooring system. For a typical slack moored system, the means of reaction is a combination of the sea-bed, the surrounding fluid (due to the buoyancy of a mooring line float) and coupled inertia (due to the mass of a mooring line sinker).

3.4.3 Linearisation

Equation (3.23) is linearised by writing all the forces, apart from the excitation, as linear functions of the response. It is conventional to group terms that are functions of dynamic variables on one side, and keep the excitation on the other, to give an equation of motion of the form (3.22). Rearranging (3.23) into the conventional form for an equation of motion gives:

$$f_e = ma + f_{loss} + f_r + f_s + f_{pto} \tag{3.26}$$

Note that each of these terms is now considered to the linearised version of those in (3.23).

3.5 Frequency domain dynamic model

Equation (3.26) can be expressed in the frequency domain by taking the Fourier transform of each term:

$$F_e(\omega) = mA(\omega) + F_{loss}(\omega) + F_r(\omega) + F_s(\omega) + F_{pto}(\omega) \tag{3.27}$$

This transformation can be made because (3.26) was defined as linear. The frequency domain equation (3.27) can be easily rearranged to give the post-transient solution for any of the dynamic variables (displacement, velocity or acceleration).

Capital letters have been used to indicate that a term is the Fourier transform of the corresponding term expressed in lower case. Constant terms, such as mass, remain lower case. In a multiple degree of freedom system, mass would be a matrix, and acceleration a vector. Each element of the mass matrix would be a constant, while each element of the acceleration vector would be a function of frequency.

3.5.1 Excitation force

The excitation force is the fluid force experienced by the body when it is held motionless in the presence of oncoming waves. It is composed of the Froude-Krylov force and the diffraction force. The Froude-Krylov force is the pressure field of the undisturbed incident wave integrated over the body. It is often named the incident wave force. The diffraction force is the pressure field of the diffracted wave integrated over the body.

It can be useful to relate the excitation force to the wave elevation. The transfer function between the elevation $H(\omega)$ of the undisturbed incident wave and the excitation force is the excitation coefficient, $W(\omega)$, also known as the wave force coefficient or the diffraction coefficient:

$$F_e(\omega) = W(\omega)H(\omega) \tag{3.28}$$

3.5.2 Mass-spring-damper representation

The linearisation of the equation of motion means that each of the terms on the right hand side of (3.27) can be expressed as a function of displacement or its derivatives. It is common to express each term as a function of velocity, so that the equation can be solved for velocity. This aids in the calculation of power, and facilitates the use of a concept borrowed from the analysis of electrical circuits, *impedance*. Impedance is the complex version of resistance; it describes how a system opposes velocity. For a generalised force $F_g(\omega)$, the impedance $Z_g(\omega)$ is the transfer function between force and velocity: $F_g(\omega) = Z_g(\omega)U(\omega)$. Note the sign convention used here; the sign convention that considers $-Z_g(\omega)$ to be the transfer function is also seen in the literature.

In a frequency domain representation of a system, the operator $i\omega$ indicates differentiation. Acceleration is given by $i\omega U(\omega)$ and displacement by $\frac{1}{i\omega}U(\omega)$, which can also be written $-\frac{i}{\omega}U(\omega)$. The equation of motion can be expanded to:

$$F_e(\omega) = i\omega m U(\omega) + b_{loss}U(\omega) + Z_r(\omega)U(\omega) + \frac{c_s}{i\omega}U(\omega) + Z_{pto}(\omega)U(\omega) \tag{3.29}$$

where

b_{loss}	is the damping loss coefficient
$Z_r(\omega)$	is the radiation impedance
c_s	is any source of spring in the system.
$Z_{pto}(\omega)$	is the PTO impedance

In a mechanical oscillator, it is useful to separate the problem into individual terms that are either masses, dampers, or springs. These are defined as components that are directly proportional to acceleration, velocity and displacement, at each point in time. In this model, (3.29) the linearised spring term c_s is a constant, so the restoring force can be represented by a

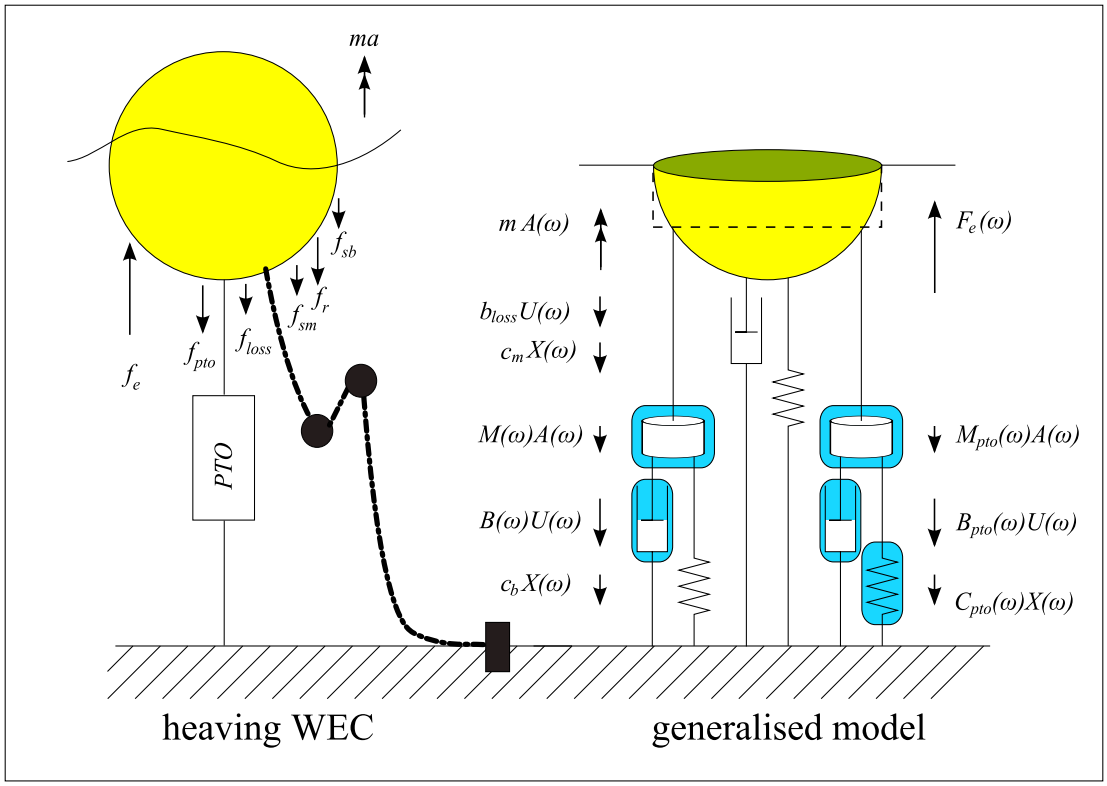

Figure 3.10: ***Forces and mass acceleration experienced by a heaving buoy:*** *Left - The generalised non-linear forces (3.23) on a WEC and the resulting mass acceleration. Right - Assuming a linear model, the post-transient response can be expressed as a frequency domain equation (3.29). The components with shaded backgrounds look like mass, spring and damping in the frequency domain equation, but not in time domain equation (§ 3.5.2).*

spring, as in Fig. 3.10. The linearised loss term b_{loss} is likewise a constant, so the force due to losses is represented by a damper in Fig. 3.10.

The radiation and PTO impedance are however frequency dependent. Although both impedances can be decomposed into components directly proportional to motion (acceleration, velocity and displacement) at each frequency, these terms are not directly proportional to instantaneous values of motion at each point in time. The radiation and PTO impedances cannot be expressed as a combination of masses, springs and dampers, according to the definition given above. In Fig. 3.10, the shaded backgrounds are used to indicate forces that are functions of motion (acceleration, velocity and displacement), but are not directly proportional to motion, and thus not true masses, springs and dampers. In § 3.8, it is shown that, in the time domain representation of a system, the shaded backgrounds indicate a form of memory or anticipation (premonition) in the system.

3.5.3 Damping losses

The damping losses in (3.29), b_{loss}, represent the linear components of any form of damping in the system other than the radiation damping, $\Re\{Z_r(\omega)\}$, and PTO damping, $\Re\{Z_{pto}(\omega)\}$. The radiation and PTO damping are both necessary for energy capture (see § 4.4.1 on page 129), so the losses represent any mechanisms for doing work that do not contribute to energy capture. The non-linear loss force as defined in (3.23), f_{loss}, can be divided (3.24) into fluid losses and mechanical losses, which are represented by damping coefficients b_{lf} and b_{lm} respectively. The fluid losses represent mechanisms for losing energy other than radiation of waves. This includes losses to viscosity and drag. Viscous losses are often modelled as being proportional to the square of the velocity. The mechanical losses represent mechanisms for losing energy other than the PTO damping. This includes PTO losses and friction in modes of motion where there is no PTO.

Both the fluid and mechanical losses are generally non-linear. The linearised equation includes the linear components of these losses. As the linear components are small (compared to the non-linear loss components, and compared to other body forces), the loss force is often not included in linear models of WEC.

3.5.4 Intrinsic Spring

The spring coefficient c_s is an intrinsic part of the body's impedance. Intrinsic means it is present even when there is no PTO force. It is made up of buoyancy spring c_b, and mechanical spring c_m. These are linearised spring coefficients associated with the spring forces that react against the fluid, f_{sb}, or any other point of reaction, f_{sm}, as defined in (3.25) and shown in Fig. 3.9.

Buoyancy spring

As described by the Archimedes principle, a fluid exerts a buoyancy force equal to the weight of the displaced fluid. At equilibrium, the weight of the body, mg, is balanced by the weight of the displaced fluid, $\rho g v$, where v is the submerged volume, ρ the water density, and g gravitational acceleration. The net force on the body is the resultant of these two forces:

$$f_b = mg - \rho g v \tag{3.30}$$

At rest, the weight of the displaced fluid $\rho g v$ equals the weight of the body mg, and there is no net force on the body. If the body is moved away from its equilibrium position, the body's weight will no longer be equal to the weight of the displaced fluid. The net force is applied in the direction required to restore the body to its equilibrium position. This net force is the dynamic buoyancy force, f_b. Note that in wave energy research, it is conventionally referred to as simply

the buoyancy force, whereas in discussions of the Archimedes principle, the buoyancy force is the weight of the displaced fluid, $\rho g v$.

The dynamic (net) buoyancy force is equal to the weight of the fluid in the dynamic variation in submerged volume Δv. Given an equilibrium volume of v_e, $\Delta v = v - v_e$. Equation (3.30) may then be written as: $f_b = \rho g \Delta v$. The dynamic buoyancy and Δv are both time varying quantities. The frequency domain representation gives the post-transient case for harmonic excitation:

$$F_b(\omega) = \rho g \Delta V(\omega) \tag{3.31}$$

To linearise the buoyancy force, the water plane area, a_W, is modelled as constant. The buoyancy force $F_b(\omega)$ is then proportional to displacement $X(\omega)$ (Fig. 3.10 - right), and the buoyancy spring c_b is the constant of proportionality:

$$F_b(\omega) = \rho g a_W X(\omega) = c_b X(\omega) \tag{3.32}$$

For this assumption to be valid, either the operating regime is restricted to the region where buoyancy is only weakly non-linear (small amplitude displacement; see §2.5.7), or a simplified problem with a constant water plane area, such as a heaving cylindrical buoy, is considered.

In Fig. 3.10 (left) the cross-section of the spherical buoy decreases with vertical distance from the equilibrium water level. In Fig. 3.10 (right) the buoyancy spring has been linearised. The cross-section is modelled as constant (shown by the dashed line) over the range of heave displacement for which the model is valid.

Mechanical spring

Mechanical spring includes any means of opposing displacement apart from buoyancy and the PTO force. A mechanical spring that reacts against the same reaction point as the PTO system is not the same as PTO spring. The mechanical spring term forms part of the intrinsic impedance of the WEC, rather than part of its PTO impedance. This distinction is important for the theory of the control of WECs, as discussed in Chapter 4.

The mechanical spring can take many physical forms. The AWS device for example has an air-spring [43], which, along with the PTO system, reacts against the sea bed. As discussed in § 3.4.2, mooring results in a spring force whose point of reaction is different from that to the PTO force.

3.5.5 Radiation impedance

An oscillating body and the surrounding water apply a *radiation force* to each other as waves are created. In frequency domain representation, the linearised part of this force can be written

as a function of the velocity:

$$F_r(\omega) = Z_r(\omega)U(\omega) \tag{3.33}$$

The transfer function between the velocity and the radiation force, $Z_r(\omega)$, is the radiation impedance. It is a complex function of frequency. The imaginary part is approximately proportional to frequency, particularly in heave where the variation in added mass is small. When decomposing the radiation impedance into its real and imaginary parts, it is conventional to write:

$$Z_r(\omega) = B(\omega) + i\omega M(\omega) \tag{3.34}$$

where $M(\omega)$ is known as the added mass, and $B(\omega)$ is known as the radiation (or added) damping. The descriptions damping and mass are used because this choice of decomposition leads to components that are functions of velocity and acceleration (recalling that $i\omega$ indicates differentiation in a frequency domain representation of a system):

$$F_r(\omega) = B(\omega)U(\omega) + i\omega M(\omega)U(\omega) \tag{3.35}$$

The physical meaning of the added mass and damping coefficients is discussed in § 3.7.

The relationship between excitation and radiation

The excitation coefficient is related to radiation damping via the Haskind relations [77]. For a heaving body with a vertical axis of symmetry:

$$|W(\omega)|^2 = \frac{4\rho g c_g(\omega, h)}{k(\omega, h)} B(\omega) \tag{3.36}$$

where $c_g(\omega, h)$ is the group velocity, $k(\omega, h)$ is the wave number, and h is the water depth.

3.5.6 Intrinsic impedance

Including all the terms introduced so far gives:

$$F_e(\omega) = i\omega[m+M(\omega)]U(\omega)+[b_{lm}+b_{lf}+B(\omega)]U(\omega)+\frac{c_m + c_b}{i\omega}U(\omega)+Z_{pto}(\omega)U(\omega) \tag{3.37}$$

All the terms associated with the intrinsic behaviour of the body, i.e. behaviour that exists in the absence of a PTO force, are grouped according to whether they oppose acceleration, velocity or displacement. As each of these terms can also be written as a function of velocity, they can be grouped yet again to give: $F_e(\omega) = Z(\omega)U(\omega) + Z_{pto}(\omega)U(\omega)$, where $Z(\omega)$ is the intrinsic impedance:

$$Z(\omega) = [b_{lm} + b_{lf} + B(\omega)] + i\left(\omega\left[m + M(\omega)\right] - \frac{c_m + c_b}{\omega}\right) \tag{3.38}$$

3.5.7 Power take off impedance

The presence of a PTO force is what turns an oscillating body (or column of fluid) into a WEC. For inclusion in a linear second order model, the generalised linear PTO force is:

$$F_{pto}(\omega) = i\omega M_{pto}(\omega)U(\omega) + B_{pto}(\omega)U(\omega) + \frac{C_{pto}(\omega)}{i\omega}U(\omega) \tag{3.39}$$

where $M_{pto}(\omega)$, $B_{pto}(\omega)$ and $C_{pto}(\omega)$ are the mass, damping and spring PTO coefficients respectively. Note that this is the force on the WEC due to the PTO system. Consequently, the point of reaction will place a force equal in magnitude and opposite in direction on the PTO mechanism. Equation (3.39) can be expressed as $F_{pto}(\omega) = Z_{pto}(\omega)U(\omega)$, where

$$Z_{pto}(\omega) = B_{pto}(\omega) + i\left(\omega M_{pto}(\omega) - \frac{C_{pto}(\omega)}{\omega}\right) \tag{3.40}$$

Equation (3.39) represents a generalised linear external force between the body and the point of reaction. The PTO coefficients may have any value. If the PTO impedance is real ($\omega M_{pto}(\omega) - \frac{C_{pto}(\omega)}{\omega} = 0$) then the PTO force will be in phase with velocity at each frequency. The power generated depends on the damping coefficient:

- If the PTO damping is zero ($B_{pto}(\omega) = 0$) then no power is generated.
- If the PTO damping is negative ($B_{pto}(\omega) < 0$) then the PTO force experienced by the WEC will always be in the opposite direction to velocity. Instantaneous power will always be greater than or equal to zero.
- If the PTO damping is positive ($B_{pto}(\omega) > 0$) then the PTO force experienced by the WEC will always be in the same direction as velocity. Instantaneous power will always be less than or equal to zero.
- When the PTO damping is a constant ($B_{pto}(\omega) = b_{pto}$) then it is a true damper in the sense that the instantaneous PTO damping force is directly proportional to the instantaneous velocity ($f_{pto}(t) = b_{pto}u(t)$).

If the PTO impedance is complex ($\omega M_{pto}(\omega) - \frac{C_{pto}(\omega)}{\omega} \neq 0$) at any frequency, then the PTO force will not be in phase with velocity at that frequency. The instantaneous power will oscillate between positive and negative values. The average generated power depends on the damping coefficient:

- With $B_{pto}(\omega) = 0$, non-zero PTO mass and spring coefficients are still possible. Assuming no losses, the average power will be zero.
- With negative damping ($B_{pto}(\omega) < 0$) the average power will be greater than zero.

- With positive damping ($B_{pto}(\omega) > 0$) the average power will be less than zero.
- With constant PTO coefficients, m_{pto}, b_{pto} and c_{pto}, the PTO force can be represented by a true mass-spring-damper system, with force components proportional to acceleration, displacement and velocity at each point in time (see Fig. 3.12).

3.5.8 Net impedance

The equation of motion can be written more concisely by combining the PTO and intrinsic impedances, which become the net impedance:

$$\begin{aligned} F_e(\omega) &= [Z(\omega) + Z_{pto}(\omega)]\, U(\omega) \\ &= Z_{net}(\omega) U(\omega) \end{aligned} \tag{3.41}$$

3.5.9 Simplified equation of motion

For the purpose of the work in this thesis, a simpler version of the generalised frequency domain equation of motion (3.37) is used. Terms that are not crucial to the development of the theory are not included, namely the net force due to energy losses, f_{loss}, and the mechanical spring force f_{sm} that might represent mooring or a physical spring. This results in a simpler equation:

$$F_e(\omega) = i\omega[m + M(\omega)]U(\omega) + B(\omega)U(\omega) + \frac{c}{i\omega}U(\omega) + Z_{pto}(\omega)U(\omega) \tag{3.42}$$

where the only spring in the system is buoyancy: $c = c_b$. There are a number of reasons for removal of the b_{lm}, b_{lf} and c_m terms:

- The purpose of this study is to investigate theory, rather than to give performance estimates. These terms were removed to simplify the equation.
- High values of mechanical spring occur in specific designs of WECs, but it is possible to consider a WEC that does not have mechanical spring. As the system considered has the PTO system reacting against the sea-bed, there is no spring from a mooring line.
- The linear components of the loss terms are small compared to the terms retained.
- The value of b_{lf} found from experiments depends upon the definition of the limit of the linear regime.
- The value of b_{lm} depends more on the mechanical and electrical design and choice of components than on the underlying concept.

While the linear components of the damping losses are small, the non-linear components may be significant. Thus losses are important to consider in general, but are not significant in a

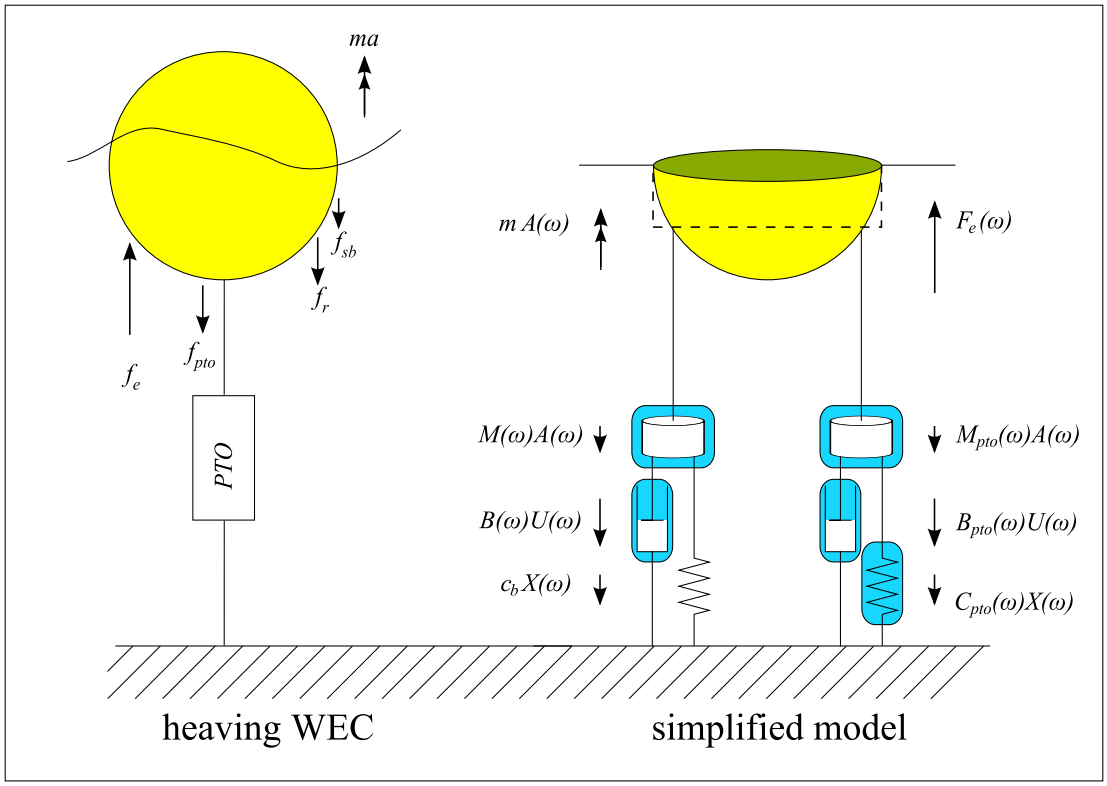

Figure 3.11: ***Simplified model of a heaving buoy:*** *Left - The generalised non-linear forces on a WEC and the resulting mass acceleration (3.23). Right - Assuming a linear model, the post-transient response can be expressed as a frequency domain equation (3.29). Mechanical spring and damping losses are not included in this simplified model. The components with shaded backgrounds are not true masses, springs and dampers (§ 3.5.2).*

linear model. There may be some types of losses that are entirely non-linear and have no linear component. An example is the PTO losses when reactive PTO coefficients ($C_{pto}(\omega) \neq 0$ and/or $M_{pto}(\omega) \neq 0$) are used. To apply a reactive PTO force, the PTO system must switch between generating and motoring with each wave. When generating, the force due to losses would be in the same direction as the PTO force, $f_{pto}(t)$. When motoring, the force due to losses would be in the opposite direction to the PTO force. Thus it is not possible to model the PTO losses due to a reactive PTO force, using a linear model.

In the simplified model, equation (3.41) still holds, but the intrinsic impedance has been simplified to:

$$Z(\omega) = B(\omega) + i\left(\omega\left[m + M(\omega)\right] - \frac{c}{\omega}\right) \tag{3.43}$$

This is the intrinsic impedance as shown in Fig. 3.11.

Degrees of freedom

For simplicity, the equations presented in this thesis are given for the single degree of freedom case. Unless otherwise stated, these results all generalise to multiple degrees of freedom. For higher orders (3.42) would be expressed $F_{e,i}(\omega) = F_{pto,i}(\omega) + \sum_j Z_{i,j}(\omega)U_j(\omega)$, or alternatively $\mathbf{F}_e(\omega) = \mathbf{F}_{pto}(\omega) + \mathbf{Z}(\omega)\mathbf{U}(\omega)$. Both these notations are seen in the textbooks on wave-body interactions [36, 37, 55]. For the six degree of freedom expansion of the impedance terms see equations (2.49) - (2.50) in [37]. For the three degree of freedom expansion of the equation of motion, see [71]. For n degrees of freedom, forces and motions are vectors with n elements, and the coefficients that transform motions into forces (mass, damping and spring) are $n \times n$ matrices. Simplifications to the equation of motion that are valid for only for one degree of freedom are explicitly stated.

3.6 Linear time domain modelling of WECs

3.6.1 Conversion into the time domain representation of a system

The inverse (complex) Fourier transform ($\mathcal{F}^{-1}$) is used to transform the frequency domain equation into the time domain. Note that the inverse Fourier transform:

- Is indicated by the lower case : $g(t) = \mathcal{F}^{-1}[G(\omega)]$,
- Is linear, so each term in an equation can be transformed separately,
- Of a product of functions of frequency is the convolution of their inverse transforms: $\mathcal{F}^{-1}[G(\omega)H(\omega)] = g(t) * h(t)$,
- Requires integrating with respect to frequency, so the function must be integrable,
- Of a constant is a constant: $\mathcal{F}^{-1}[c] = c$,
- Of a straight line $G(\omega) = c$ is a scaled impulse: $\mathcal{F}^{-1}[G(\omega)] = c\delta(t)$.

The last two points appear to be in conflict: how can the inverse Fourier transform of a constant be both the constant and a delta function scaled by the constant? The answer follows from the second and third points in this list. As the transform is linear, the inverse Fourier transform of a function multiplied by a constant is the inverse Fourier transform of the original function scaled by the constant: $\mathcal{F}^{-1}[cG(\omega)] = cg(t)$. As multiplication in the frequency domain gives convolution in the time domain, the inverse Fourier transform of a straight line, $H(\omega) = c$, multiplied by an arbitrary function is the convolution of a scaled delta function and the inverse Fourier transform of the original function $\mathcal{F}^{-1}[H(\omega)G(\omega)] = [c\delta(t)] * g(t)$. By the definition of a delta function (§ 2.4.2), this convolution simplifies to the inverse Fourier transform of the original function scaled by the constant $\mathcal{F}^{-1}[H(\omega)G(\omega)] = [c\delta(t)] * g(t) = cg(t)$.

There are two terms in (3.42) that involve multiplications of functions of frequency: the terms involving damping $B(\omega)U(\omega)$ and mass $[m + M(\omega)]U(\omega)$. A multiplication of two frequency functions becomes a convolution of the corresponding functions of time. Combining added mass and damping into one term reduces the problem to only one convolution. The most common arrangement is to express them as radiation impedance (3.34):

$$\begin{aligned} F_e(\omega) &= i\omega m U(\omega) + [i\omega M(\omega) + B(\omega)]U(\omega) + \frac{c_m}{i\omega}U(\omega) + F_{pto}(\omega) \\ &= i\omega m U(\omega) + Z_r(\omega)U(\omega) + \frac{c_m}{i\omega}U(\omega) + F_{pto}(\omega) \end{aligned} \tag{3.44}$$

However, it is not possible to perform an inverse Fourier transform on Z_r because it does not drop to zero when frequency is infinite. For a body with no forward speed [90], this is due to added mass (see Fig. 4.7): at high frequencies, radiation damping $B(\omega)$ approaches zero, while added mass $M(\omega)$ approaches m_∞. The presence of m_∞ means that there is a component of the radiation impedance that is frequency independent. If the reactance due to m_∞ is removed from Z_r, the remaining impedance, K, will be zero as the frequency approaches infinity. This is the portion of radiation impedance that is frequency dependent:

$$\begin{aligned} K(\omega) &= Z_r - i\omega m_\infty \\ &= B(\omega) + i\omega\left[M(\omega) - m_\infty\right] \end{aligned} \tag{3.45}$$

Removing m_∞ from Z_r and regrouping it with the physical mass gives:

$$F_e(\omega) = i\omega\left[m + m_\infty\right]U(\omega) + K(\omega)U(\omega) + \frac{c}{i\omega}U(\omega) + F_{pto}(\omega) \tag{3.46}$$

3.6.2 Time domain formulation

The inverse Fourier transform may now be performed on each term of (3.46) to give:

$$f_e(t) = [m + m_\infty]a(t) + k(t) * u(t) + cx(t) + f_{pto}(t) \tag{3.47}$$

The convolution term is the force due to the radiation of waves (§ 3.7). In general, convolutions are between infinite limits, so the convolution in (3.47) could be written: $k(t) * u(t) = \int_{-\infty}^{\infty} k(\tau)u(t-\tau)d\tau = \int_{-\infty}^{\infty} k(t-\tau)u(\tau)d\tau$. These limits can be reduced by examining conditions that apply to the given problem.

It is well known that radiation force is only affected by present and past velocity, which means it is causal [91]. A causal convolution is given when the convolution kernel is zero at times less than zero: $k(t < 0) = 0$, giving it the form shown in Fig. 3.8 (b). The convolution may then be divided into integrals with limits above and below t: $\int_{-\infty}^{\infty} k(t-\tau)u(\tau)d\tau = \int_{-\infty}^{t} k(t-\tau)u(\tau)d\tau + \int_{t}^{\infty} k(t-\tau)u(\tau)d\tau$. As $k(t-\tau)$ equals zero for $\tau < t$, the value of

the second integral is zero, leaving $k(t) * u(t) = \int_{-\infty}^{t} k(t-\tau)u(\tau)d\tau$.

Furthermore, if the initial velocity is assumed to be zero, i.e. for $u(t < 0) = 0$, then, using the same technique of dividing integrals, the limits can be narrowed yet again to $0 < \tau < t$ [55, 92]. Given these assumptions, (3.47) may be written as:

$$f_e(t) = [m + m_\infty]a(t) + \int_0^t k(\tau)u(t-\tau)d\tau + cx(t) + f_{pto}(t) \tag{3.48}$$

Limits of $[0, t]$ give equivalent results to those of $(-\infty, t]$ once transients have decayed. When performing numerical simulations, it is not possible or useful to model velocity at all times in the past, and so the limits $[0, t]$ become a necessity. Note that the $\int_0^t k(\tau)u(t-\tau)d\tau$ form of the convolution, rather than the $\int_0^t k(t-\tau)u(\tau)d\tau$ form, has been used in (3.48). Mathematically they are equivalent, and both forms appear in the literature. The form used in (3.48) is preferred

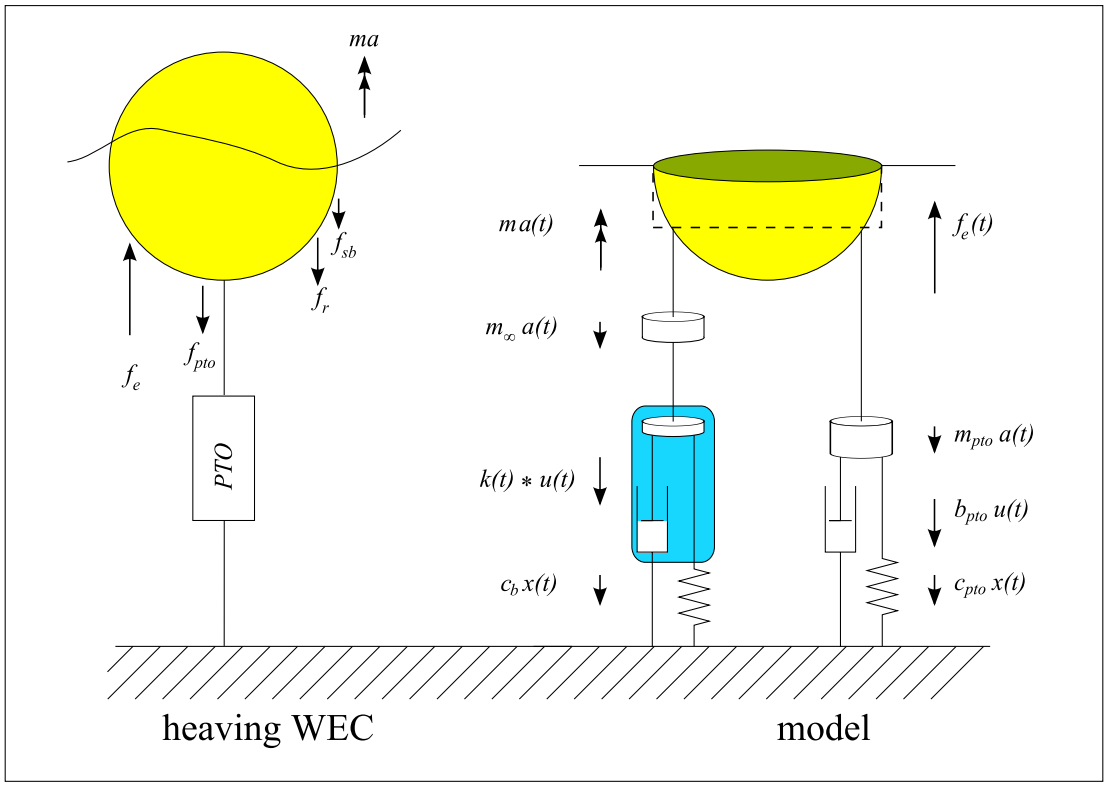

Figure 3.12: ***Time domain model of a WEC with a causal control force:*** *Added mass at infinity (m_∞) acts like additional mass in the system. The memory due to wave radiation is determined by the memory kernel, which is the inverse Fourier transform of the frequency dependent radiation impedance ($k(t) = \mathcal{F}^{-1}\{B(\omega) + i\omega[M(\omega) - m_\infty]\}$). Note that the PTO force shown here consists of mass, spring and damper components.*

as this makes it clear that the instantaneous and past values of velocity are required.

The time domain formulation was suggested by Cummins [90] for modelling ship motion and by Jefferys [93] and Count [44] for modelling wave energy conversion. The convolution is sometimes arranged for displacement or acceleration. The convolution with velocity is now the most commonly used. Useful discussions of the time domain formulation can be found in [92, 94].

3.7 Physical meaning of hydrodynamic coefficients

3.7.1 Excitation force

Assuming that superposition applies, the excitation force can be decomposed into terms due to the undisturbed incident wave (the Froude-Krylov force) and due to the diffracted wave (the diffraction force). The excitation force is sometimes described as the exciting force, wave force, or diffraction force, the latter term being ambiguous. The component of the excitation force called the diffraction force results from (and causes) the diffraction (change of direction, such as reflection) of incoming waves. The Froude-Krylov component is due to the pressure of the undisturbed incident wave. Using a Taylor series expansion, the leading order term is the hydrostatic force due to the oscillating wave elevation (see page 302 of Newman [36]).

3.7.2 Excitation coefficient

The relationship between wave elevation and excitation force is not causal [91]. When describing excitation force as a linear function of wave elevation: $f_e(t) = w(t) * \eta(t)$, the convolution kernel $w(t)$ (the inverse Fourier transform of the excitation coefficient $W(\omega)$) has memory and premonition qualities, and is of the form shown in Fig. 3.8 (d). The lack of a causal relationship between wave elevation and excitation force seems counter-intuitive, because for bodies with dimensions much smaller than the wavelength, the acausal convolution has such a short duration, it approaches an impulsive function seen in Fig. 3.8 (a) [91]. When objects are small compared to the wavelength of the incident waves, the excitation force is dominated by the Froude-Krylov force (§ 3.5.1), which means that the dominant term is directly proportional to wave elevation. Thus the acausal relationship between wave elevation and exciting force does not relate to human experience. A human body, attempting to stand still while being hit by sea waves, experiences a force that appears to be directly proportional to, and caused by, the wave elevation.

3.7.3 Wave elevation

It is important to highlight a potential ambiguity in the interpretation of the term *wave elevation*. When referring to the relationship between wave elevation and exciting force (3.28), wave

elevation is the elevation of the undisturbed incident wave. Measurements of surface elevation in the absence of a WEC will give the elevation of the undisturbed incident wave, whereas measurements of the surface elevation in the presence of a WEC will measure the superposition of the incident, radiated and diffracted waves (Fig. 2.4 on page 17). In the context of the excitation relationship (3.28), it seems more intuitive to think of the wave elevation as the surface elevation in the presence of the device. Nevertheless, this relationship refers to the surface elevation at the central position of the device, in the absence of the device. This highlights yet another problem: if the WEC is surface piercing, the water-air interface will not exist at the position of the device.

3.7.4 Buoyancy force

In § 3.5.4, buoyancy was defined as the restoring force proportional to the body's own motion. The restoring force arises when the body's motion causes its weight to be different from that of the displaced fluid. So the restoring force is the difference between the hydrostatic force and the body's weight. There is a potential for ambiguity here because the hydrostatic force also includes a component due to the change in water level caused by the incident wave. In classical texts (see page 291 of Newman [36]) this is dealt with by assuming the wave elevation to be small, in which case this component is neglected. Note however that the excitation force includes a component that is directly proportional to the wave elevation, and this can be attributed to the component of the hydrostatic force due to the oscillating wave elevation, as discussed in § 3.7.2.

3.7.5 Radiation force

When defining the generalised equation of motion (§ 3.4), all the fluid-body forces caused by forced motion on calm water were grouped together and referred to as the radiation force, f_r. The buoyancy force was treated separately as it is only present in certain modes of motion, and can be easily calculated. The force due to fluid losses was not included, because for a linearised problem, this is negligible. The frequency domain representation of the radiation force was defined as $F_r(\omega) = [B(\omega) + i\omega M(\omega)]U(\omega)$ (3.35).

Radiation damping

It can be seen that $B(\omega)$ is the real part of radiation impedance. The real part of an impedance causes work to be done and energy to be transferred out of the system. The mechanism for this energy loss is a radiated (propagating) wave. The energy in a radiated (post-transient, polychromatic) wave equals the energy used to drive the motion (assuming negligible losses).

Radiation damping has different values at different frequencies. This means that radiation damping is not proportional to instantaneous velocity, so is not a true damper. Instead it forms

part of the memory convolution. If a discrete version of the convolution is considered, it can be seen that the memory convolution contains components proportional to instantaneous and past values of velocity, with different values of proportionality at different times in the past.

Time domain radiation force

The time domain equation for radiation force is required to find both the transient and post-transient solutions:

$$f_r(t) = m_\infty a(t) + \int_0^t k(\tau)u(t-\tau)d\tau \tag{3.49}$$

The first term on the RHS is proportional to instantaneous acceleration. Apart from the fact that it is a fluid force, $m_\infty a(t)$ acts exactly like additional added mass that has been included in the system. In a mass-spring-damper diagram, it could be represented by additional mass attached to the body (see Fig. 3.12 - right). The second term on the RHS depends on previous values of velocity (and hence acceleration). As $k(t)$ includes a contribution from radiation damping, it is clear that this term is associated with the past and present (instantaneous) radiation of waves. It cannot be represented by conventional masses and dampers, as indicated by the shaded background in Fig. 3.12 (right).

The memory kernel

The kernel of the convolution integral, $k(t)$, is called, among many things, the memory term [95] and the memory function [96]. Here the name *memory kernel* will be used to differentiate it from the memory convolution.

Another common name for the memory kernel is the radiation impulse response function [97]. Actually, if the radiation force is defined conventionally, as in (3.35), then the radiation impulse response function is $m_\infty\dot{\delta}(t) + k(t)$, which is convolved with $u(t)$ to give (3.49). If however $K(\omega)$ were defined as the transfer function for radiation force, then $k(t)$ would indeed be the radiation impulse response function.

Added mass

From (3.49) it can be seen that m_∞ contributes to a fluid-body force that has the same dynamic effect on the WEC as additional mass. In fact, by grouping it together with mass in (3.48) to give $[m + m_\infty]a(t)$, it is being implicitly treated as additional mass in the system.

In the frequency domain definition of radiation force, $F_r(\omega) = B(\omega)U(\omega) + i\omega M(\omega)U(\omega)$ (3.35), the first term on the RHS is proportional to velocity, is thus a damping force which does work; and the energy transfer is in the form of a radiated wave. The second term on the

RHS is proportional to acceleration ($i\omega$ indicates differentiation). Analogously, this force acts like inertia; it stores energy in the system. Added mass is often described as the mass of the entrained water. However it is more than this: it is also a way of storing energy. The means of this energy storage is an evanescent wave attached to the oscillating body.

Linear wavemaker theory [68] confirms that a driven immersed body produces both propagating (radiated far-field) and non-propagating (evanescent near-field) waves, which are responsible for the real and imaginary components of the fluid-body force experienced during radiation (the radiation force). The reason for the formation of this evanescent wave is the mismatch between the displacement profiles of the wavemaker (the body radiating the waves) and the water particles. The horizontal component of the displacement of the water particles decays exponentially with distance from the water surface. The rate of this decay depends upon the wave frequency.

If a wavemaker is given a shape so that the paddle surface moves with exactly the same velocity profile as the water particles in the propagating wave (as in Fig. 3.13), then at this frequency, the added mass will be zero: $M(\omega_s) = 0$. Furthermore, once the motion is steady-state, there will be no evanescent wave attached to the surface of the paddle [98]. This assumes that the depth of the water has been taken into account when calculating the water particle velocity profile, and that the paddle is moving with steady-state sinusoidal motion. At all other frequencies $M(\omega)$ will be positive and sinusoidal motion at these frequencies will produce an evanescent wave. This shows that the added mass at any frequency $M(\omega_s)$ is associated with the evanescent wave at ω_s [68].

The time domain equation for radiation force (3.49) is also valid for post-transient behaviour. It is clear that even in the case where $M(\omega_s) = 0$, the added mass due to entrained water (m_∞) still exists, as does the memory term. The memory term contains a contribution from $M(\omega) - m_\infty$. In post-transient sinusoidal motion only the value at ω_s has any effect on the motion, and this equals $-m_\infty$. For steady-state sinusoidal motion, the opposition to acceleration afforded by the memory term and m_∞ cancel each other out.

To summarise:

- m_∞ represents the additional mass due to entrained water.
- $i\omega M(\omega_s)U(\omega_s)$ is the force due to the evanescent wave at a given frequency.
- $M(\omega) - m_\infty$ describes the interaction between forces due to entrained water and the standing wave.

Reasons for ambiguity surrounding added mass

The term *added mass* is ambiguous because many fluid dynamicists refer to m_∞ as the added mass (and to $k(t) * u(t)$ as the history term), while in wave energy and ship engineering, the

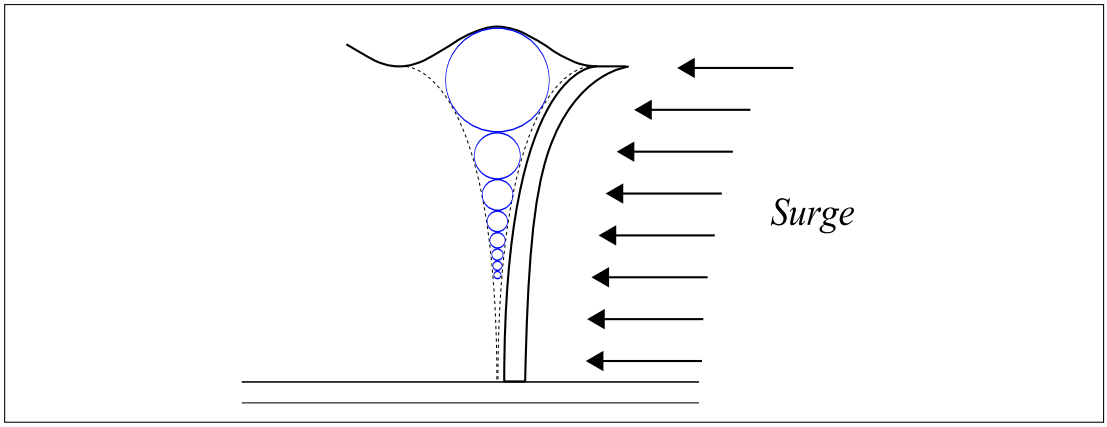

Figure 3.13: ***Surging wave paddle with the same displacement profile as a progressive wave of a given frequency:*** *When undergoing steady state motion at the design frequency, ω_s, no evanescent wave is formed.*

frequency domain coefficient $M(\omega)$ is referred to as the added mass. Furthermore, as linear wave theory reduces the problem to studying one sinusoid at a time, many references to added mass in wave energy literature in fact mean the added mass at a specific frequency, $M(\omega_s)$.

Stokes [99] reported that the term had been coined by Friedrich Bessel. Both conducted experiments whereby a pendulum was swung under water. As the oscillation period was longer than expected, Bessel concluded that the surrounding fluid had *added mass* to the system. Stokes measured this added mass and included it in an equation describing the sinusoidal motion of an immersed pendulum. It is significant that added mass was first used to describe sinusoidal motion, as this set the precedent for using added mass to mean $M(\omega_s)$.

The historical precedent for referring to m_∞ as the added mass was set by Basset [100] who described a force expression of the form given in (3.49). On page 267 of [100] he describes the terms due to m_∞ and the memory effect with the following comment:

> The effect of the first term is simply to produce an apparent increase in the inertia of the sphere; the second term would produce a gradual diminution of the arc of oscillation if the sphere were left free.

In § 3.8 it is shown that the equation describing sinusoidal motion has a different form from the general equation of motion. In particular, it is seen that in the general equation of motion, the component of the fluid-body force directly proportional to acceleration is m_∞, while in the equation describing steady state sinusoidal motion it is $M(\omega_s)$. This potential ambiguity in the description *added mass* was noted by Odar and Hamilton [101], who stated:

> If the force expression derived by Basset [100] ... is applied to an oscillating sphere and if the integral term is calculated for the oscillation after a long period of time

> ... the same expression found by Stokes [99] can be obtained. This shows that, in a force expression valid for a specific motion, the quantity which is multiplied by acceleration does not necessarily represent the added mass as defined for an inviscid and irrotational motion.

3.8 The difference between wet and dry oscillators

There are two commonly used time domain models that appear in wave energy literature. Conventionally they are described respectively as the model for monochromatic behaviour (regular waves), and the model for polychromatic behaviour (irregular waves); see for example Wehausen's paper [92], or equations (194) - (195) in [36]. There are difficulties in discussing these models because frequency domain equations of the form (3.42) may be interpreted as pertaining to either. Furthermore, commonly used terminology has different interpretations depending on whether monochromatic or polychromatic behaviour is assumed. As discussed in § 3.7.5; the concept of added mass due to entrained water is interpreted as $M(\omega_s)$ when modelling steady state sinusoidal motion [99], and as m_∞ when modelling polychromatic motion [100]. As the interpretation of terminology is so tightly bound to the modelling viewpoint, the existing terminology does not lend itself to making apparent the differences between these viewpoints. Thus it became necessary to find a new way of presenting these two viewpoints that did not rely on any ambiguous terminology.

The concepts of the wet and dry oscillator are introduced here. They are described as a paradigm because they neatly classify two different approaches using a point of division that is mathematically meaningful. They are subtly distinct from the previous approach [36, 92] of defining equations that are 'correct' or 'incorrect' polychromatic motion. Instead, the wet and dry oscillators are both defined for polychromatic motion, but the dry oscillator is a valid description of a linear oscillator immersed in fluid, only for steady-state sinusoidal motion. The wet and dry oscillators are a tool for understanding how these two modelling approaches compare. An examination of the cases where the wet and dry oscillators are equally valid models is instructive. They are used later (§ 6.2) as a tool for debunking a common myth held about modelling of WECs.

Both the wet and dry oscillator models are second order linear differential equations. The wet oscillator is an integro-differential equation, and the dry oscillator is an ordinary differential equation. As before, the equations presented are for a solid semi-immersed body constrained to move only in heave, but the principles are applicable to WECs with other modes of motion or types of primary interface (as described in § 2.2.4). The PTO force is not included in the wet and dry oscillator models. The differences between these models, as seen in Fig. 3.14 shall now be discussed.

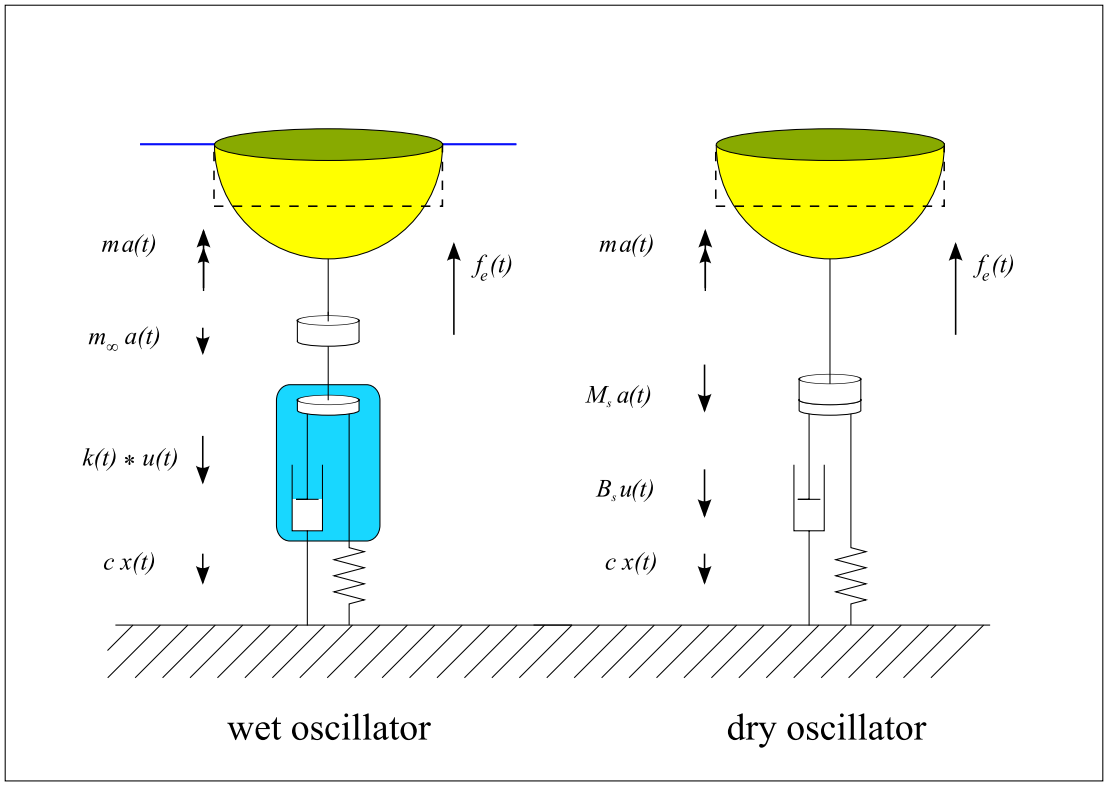

Figure 3.14: ***Wet and dry oscillators:*** *time domain models of a wet oscillator (left) and a dry oscillator (right).*

3.8.1 Definition of a wet oscillator

The wet oscillator model is a mass-spring-damper system where the damping is provided by a memory term. The presence of this memory term (a convolution with a kernel of the form shown in Fig. 3.8 (b)) makes it a causal system (or a system with memory). The damping term is not directly proportional to instantaneous velocity. It is a function of past values of velocity. In Fig. 3.14 (left) the shaded background indicates the memory term. The presence of a mass component in this memory term can be explained by studying the equation of motion. Comparing Fig. 3.14 (left) to Fig. 3.12, it can be seen that the wet oscillator model is the simplified generalised equation of motion given by (3.48), but without any PTO force. the governing equation of motion for the wet oscillator model is:

$$f_e(t) = [m + m_\infty]a(t) + \int_0^t k(\tau)u(\tau)(t-\tau)d\tau + cx(t) \tag{3.50}$$

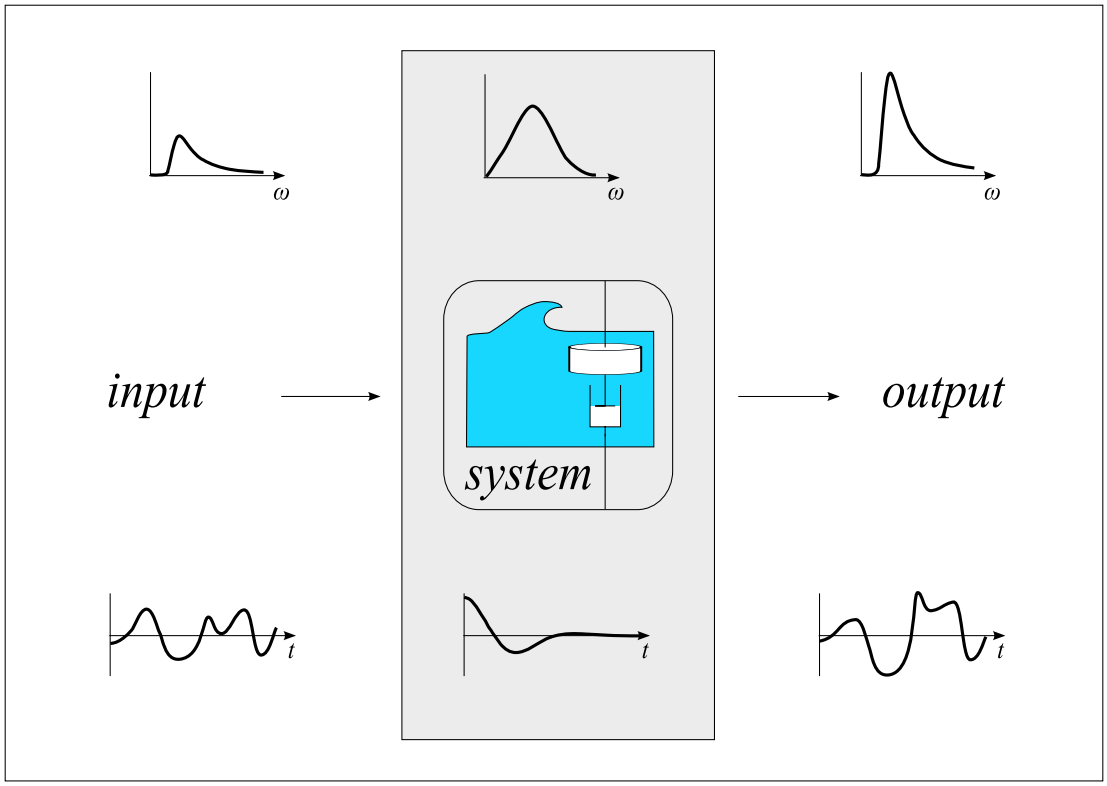

Figure 3.15: ***A wet oscillator (a linear system with memory) for a polychromatic input (middle row):*** *correctly models the memory effect of radiation. Frequency domain (top row):* $U(\omega)K(\omega) = F_{rm}(\omega)$. *Time domain post-transient (bottom row) :* $u(t) * k(t) = f_{rm}(t)$ *(3.52).*

Solution of this equation gives the transient and post-transient response. The post-transient response can also be found by solving the frequency domain expression of this model:

$$\begin{aligned} F_e(\omega) &= i\omega[m + m_\infty]U(\omega) + (B(\omega) + i\omega[M(\omega) - m_\infty])\,U(\omega) + \frac{c}{i\omega}U(\omega) \\ &= i\omega[m + M(\omega)]U(\omega) + B(\omega)U(\omega) + \frac{c}{i\omega}U(\omega) \end{aligned} \tag{3.51}$$

A wet oscillator correctly models the memory effects of radiation. To make this clear, the relationship between the radiation memory force f_{rm} and velocity is considered. In the time and frequency domains this relationship is:

$$\begin{aligned} u(t) * k(t) &= f_{rm}(t) \\ U(\omega)K(\omega) &= F_{rm}(\omega) \end{aligned} \tag{3.52}$$

The positions of the terms within these equations is intentional: they show that in a linear system the velocity is the input and the radiation memory force is the response. In the frequency

domain, the velocity multiplied by the transfer function, $K(\omega)$, gives the response. In the time domain, the velocity convolved with the impulse response, $k(t)$, gives the response.

The time and frequency domain representations of radiation damping (3.52) are shown diagrammatically in Fig. 3.15. The central row is a schematic of how the input (velocity) is transformed into the output (radiation memory force). The top row shows this transformation in the frequency domain, and the bottom row is the equivalent representation in the time domain. The post-transient radiation memory force (bottom right) could be found by convolving the velocity (bottom left) with the memory kernel (bottom centre). It is often more computationally efficient to take the Fourier transforms of the velocity (top left) and memory kernel (top centre), and then find the inverse Fourier transform of their product (top right).

Both the time and frequency domain versions of the radiation memory force (3.52) correctly model the post-transient radiation memory force. The memory effect is not experienced in a mechanical mass-spring-damper system, only in an oscillator that is in contact with water. For this reason, the name *wet oscillator* has been chosen to describe a model that includes memory due to radiation.

3.8.2 Definition of a dry oscillator

The dry oscillator is a mass-spring-damper system that does not include a memory term. The absence of a memory term means that this model is classified (according to the system defined in § 3.3.3) as memoryless. It contains only terms that are instantaneous, i.e. directly proportional to either acceleration, velocity or displacement.

When using a dry oscillator to model a WEC, the values of the mass, spring and damper are those that would be found in the wet oscillator model at one given frequency, ω_s. Thus the added mass is M_s, where $M_s = M(\omega_s)$, and the radiation damping is $B_s = B(\omega_s)$ (see Fig. 3.15 (right)). The frequency domain representation of the governing equation of motion is:

$$F_e(\omega) = i\omega \left[m + M_s\right] U(\omega) + B_s U(\omega) + \frac{c}{i\omega} U(\omega) \tag{3.53}$$

Whereas in (3.51) the added mass and damping, $M(\omega)$ and $B(\omega)$, have different values at each frequency (Fig. 4.7), in (3.53) the added mass and damping, M_s and B_s, are constants. The inverse Fourier transform of a constant is a constant. Hence the time domain equation of motion is:

$$f_e(t) = \left[m + M_s\right] a(t) + B_s u(t) + cx(t) \tag{3.54}$$

It is not immediately obvious how to compare (3.54) to (3.50) as the terms are different. Fig. 3.14 depicts these differences. In the wet oscillator there is a term that acts like additional system mass (m_∞) and another that forms part of the memory kernel: $k(t) = \mathcal{F}^{-1}\left\{B(\omega) + i\omega\left[M(\omega) - m_\infty\right]\right\}$. In the dry oscillator both components of

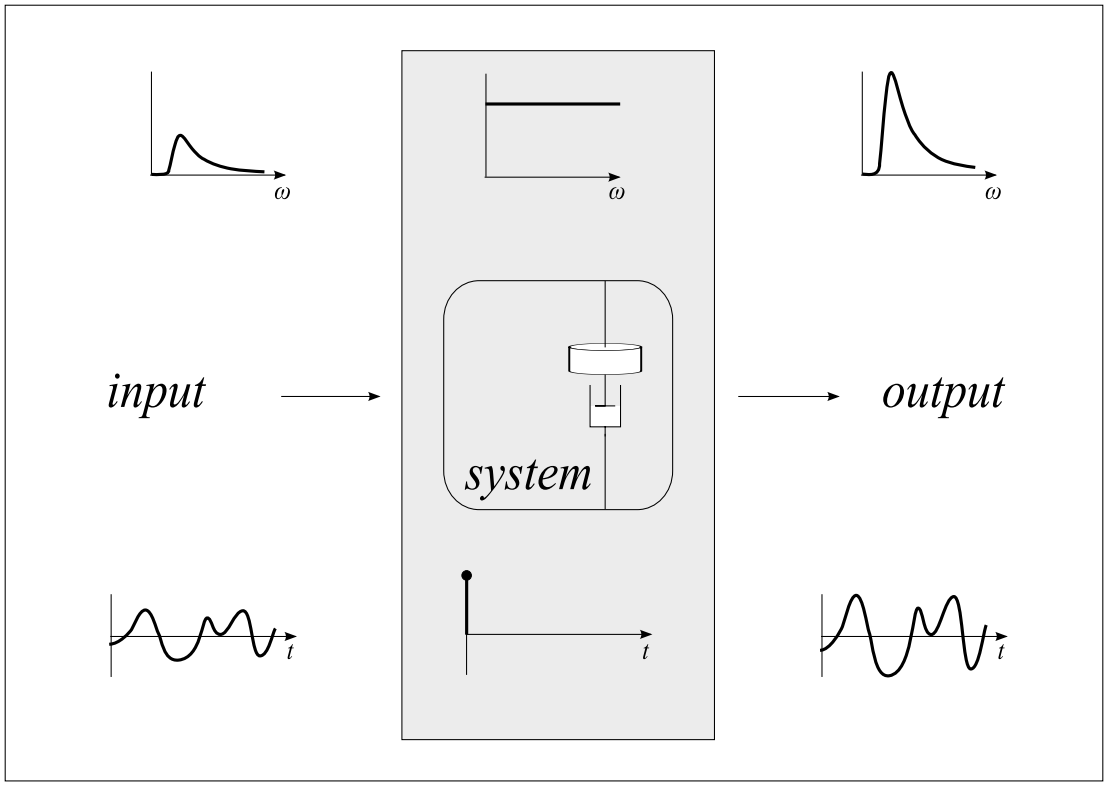

Figure 3.16: ***A dry oscillator (memory-less linear system) for a polychromatic input (middle row):*** *models radiation damping as pure damping (no memory). Frequency domain (top row):* $U(\omega)K_s(\omega) = F_{rd}(\omega)$. *Time domain (bottom row) :* $u(t) * \delta K_s = f_{rd}(t)$.

mass combine and act like additional system mass (directly proportional to instantaneous acceleration): $M_s = \mathcal{F}^{-1}\{m_\infty + [M_s - m_\infty]\}$.

The other difference between these equations is that in the wet oscillator radiation damping is given by a convolution (shaded background in Fig. 3.15), while in the dry oscillator, radiation damping is given by a multiplication (pure damper in Fig. 3.15 right). The convolution in (3.50) was necessary as both $K(\omega)$ and $U(\omega)$ were functions of frequency. In (3.54) however, the damping term $B_s u(t)$ is a multiplication, as in the frequency domain equation this was a product of a constant and a function of frequency.

In the dry oscillator model, as added mass M_s is a straight line when plotted against frequency, its value at infinitely high frequencies is $m_\infty = M_s$. This leaves $K_s = B_s$, which is a straight line if plotted against frequency. The inverse Fourier transform of a straight line is a delta function, $\delta(t)$. In the dry oscillator model, the radiation damping force f_{rd} is given by the

following frequency and time domain expressions:

$$\begin{aligned} U(\omega)K_s &= U(\omega)B_s &= F_{rd}(\omega) \\ u(t) * K_s\delta(t) &= u(t)B_s &= f_{rd}(t) \end{aligned} \tag{3.55}$$

The simplification in the second equation follows from the definition of a delta function. Convolution with a delta function is equivalent to multiplication by a constant (2.4). Writing (3.54) as $f_e(t) = [m + M_s]\, a(t) + [B_s\delta(t)] * u(t) + cx(t)$ makes it easier to compare to (3.50).

The radiation damping force (3.55) is shown diagrammatically in Fig. 3.16. The central row is a schematic of how the input (velocity) is transformed into the output (radiation damping force). The top row shows the model of the system in the frequency domain, and the bottom row is the equivalent representation in the time domain. Both the time and frequency domain equations are suitable for modelling post-transient linear response of a pure memoryless damper. Neither of these equations (3.52) correctly model the post-transient radiation memory force. The memory effect due to radiation is not experienced in a mechanical mass-spring-damper system. For this reason, the name *dry oscillator* has been chosen to describe this model.

3.8.3 The validity of the wet and dry oscillator models

Monochromatic behaviour

Both the dry oscillator (memoryless) and wet oscillator (memory) systems correctly represent the post-transient response of an immersed body to monochromatic excitation. Fig. 3.17 shows the post-transient response of a dry (memory-less) oscillator with sinusoidal excitation.

Polychromatic behaviour

Neither the frequency (3.53) nor time (3.54) domain equations for the dry oscillator correctly model the post-transient response of an immersed body in the general case of polychromatic excitation. A dry oscillator is not suitable for modelling an immersed body with polychromatic excitation, as it cannot model the memory inherent in the system due to the radiation of waves (§3.5.5).

The wet oscillator model correctly represents the memory due to wave radiation. Both the time and frequency domain equations for the wet oscillator correctly model the linearised post-transient response of an immersed oscillator to polychromatic excitation.

Transient response

Frequency domain representation of a linear system is only suitable for modelling post-transient response. The time domain equation of the wet oscillator correctly models transient and post-transient response to polychromatic excitation.

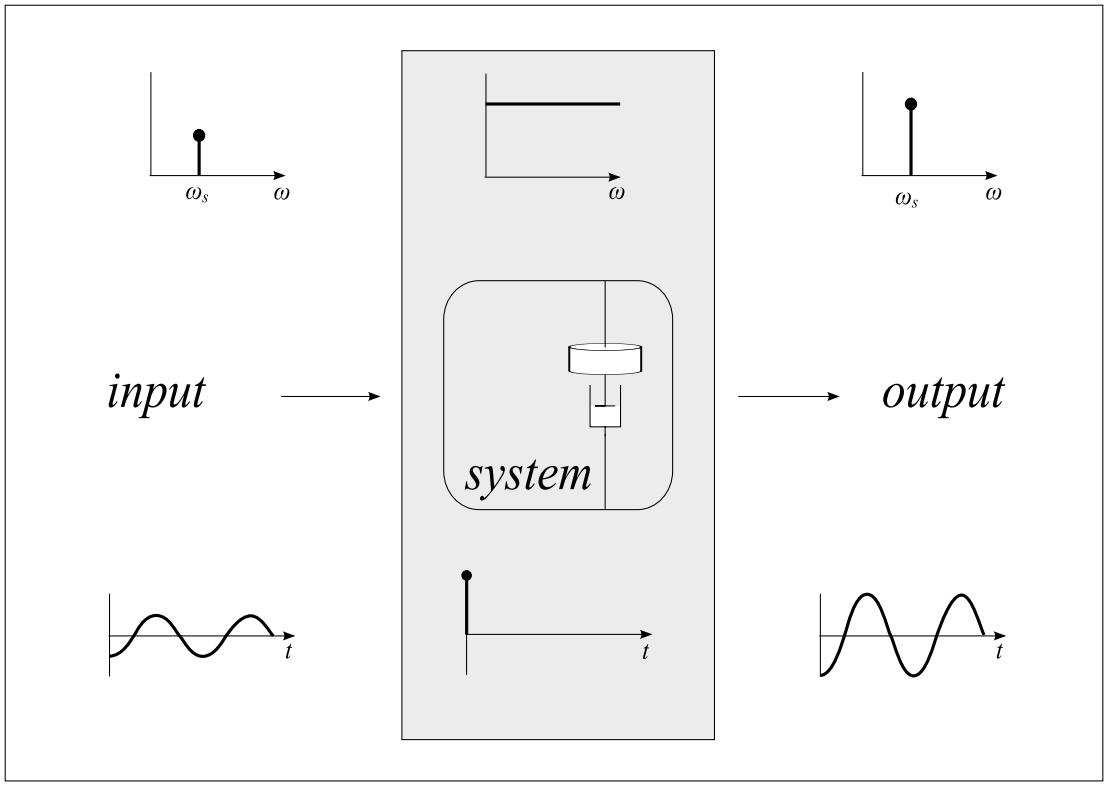

Figure 3.17: ***A dry oscillator (memory-less linear system) for a monochromatic input (middle row):*** *correctly models steady-state damping force due to radiation, as there is no memory effect for monochromatic behaviour. Frequency domain (top row):* $U(\omega)K_s(\omega) = F_{rd}(\omega)$. *Time domain (bottom row) :* $u(t) * K_s\delta(t) = f_{rd}(t)$.

The dry oscillator models a mass-spring-damper system whose values of added mass and damping equal to those of an immersed body with monochromatic excitation. The time domain model correctly represents the transient response of this equivalent system. This transient response would result in a velocity that was not initially sinusoidal, so the time domain equation of the dry oscillator cannot be used to give the transient response of an immersed body, even for monochromatic excitation.

Time varying response

Any model that can suitably represent transients can be adapted to describe time varying response. Thus only the time domain model of the wet-oscillator can be used to represent an immersed body with time varying behaviour.

An example of a time varying system is a WEC controlled using latching. One way to model latching is to treat the PTO force as piece-wise linear. When the WEC is unlatched, the PTO damping coefficient (the constant of proportionality between the PTO force and the velocity)

is a chosen constant, $B_{pto}(\omega) = b_{pto}$. When the WEC is latched, the PTO damping coefficient can be modelled as infinite. The time domain equation of a wet oscillator correctly models a system (impulse response) that changes how it responds to inputs (time variant), and correctly represents transients. Frequency domain representation of a linear system is not suitable for modelling transients and time variance. Thus the frequency domain equation of a wet oscillator is not suitable for modelling latching. Here latching has been described as piece-wise linear, with different linear relationships between PTO force and velocity applied at successive intervals in time. In reality there is a non-linear transition between the latched and unlatched state. The wet oscillator time domain model can model time variant and transient response, but is nevertheless a linear model. It does not model the non-linear aspects of latching PTO. It can however be extended to include these effects.

Validity of wet and dry models

Table 3.2 shows the cases for which the time and frequency domain versions of the dry and wet oscillator models are valid. The time domain model of a wet oscillator is the most versatile. It can model post-transient response, polychromatic excitation and a time varying system. The frequency domain of the wet oscillator cannot model transients or time variance, but can model post-transient response to polychromatic excitation. The dry oscillator model (both time and frequency domain equations) is only suitable for modelling steady-state monochromatic behaviour.

Convergence of models for point absorbers

The duration (length of time for which there is a non-zero value) of the radiation impulse response increases as a device is scaled up. This is clear from any normalised plot of added damping (and mass) or radiation impulse response [102]: the frequency and time axes are scaled by a function of the geometry; for a sphere or vertical cylinder this is the radius.

For very small geometries, the impulse response of a wet oscillator (Fig. 3.15 bottom row, shaded box) has a very short duration, and is very similar to the delta function of the dry oscillator model (Fig. 3.16 bottom row, shaded box). As the geometry is scaled down towards zero radius, the dry and wet oscillator models converge. The dry oscillator can be considered a model of an infinitely small point absorber.

	Monochromatic post-transient	Monochromatic transient	Polychromatic post-transient	Polychromatic transient	Time varying
Wet oscillator - time domain	×	×	×	×	×
- frequency domain	×		×		
Dry oscillator - time domain	×				
- frequency domain	×				

Table 3.2: ***The validity of the time and frequency domain versions of wet and dry oscillator models:*** *validity indicated with a cross.*

3.9 Chapter summary

This chapter introduced the equation of motion that will be used to develop theory in later chapters. This is a well-known and widely used equation, yet it is used in different manners and so in this chapter the meaning of the equation and each of its terms is given thorough treatment. The model is for a specific heaving WEC, chosen to yield the most simple equation of motion. Yet the model also represents a generic WEC; the theory introduced in subsequent chapters, which is demonstrated using this model, can be applied to the linear regime of all other types of WECs. Important points raised in this chapter were:

- There exist different viewpoints for modelling water waves: time domain, frequency domain, and monochromatic modelling, which considers the signal in both time and frequency domain, and is valid only for sinusoidal waves.
- Monochromatic behaviour was indicated by use of a subscript to indicate an arbitrary frequency: ω_s
- The interpretation of terminology, for example wave period and added mass due to entrained water, depends upon that viewpoint.
- The historic precedents for different interpretations of added mass were discussed: for polychromatic and monochromatic behaviour respectively the terms that act like additional mass in the system are m_∞ and $M(\omega_s)$.
- There exist conflicting definitions of wave height.
- Both the real and complex versions of the Fourier transform are in use.
- The group velocity is defined for a single frequency of wave, despite the name suggesting otherwise.
- The points of reaction of the forces on a WEC were noted. The forces between the fluid and the body are the excitation force, the radiation force, the fluid losses and the buoyancy spring force.

This chapter covered water waves, systems theory, modelling of WECs and the introduction of a new way of describing WEC models in common use in the literature. The theme that ties all these subjects together is the concept of monochromatic modelling. A signal such as wave elevation can be decomposed into sinusoidal components, which can be considered separately. When modelling a system, sinusoidal (monochromatic) motion results in different behaviour, and has a different equation, from polychromatic (containing many sinusoids) behaviour. Even fundamental concepts such as added mass have different treatment for monochromatic behaviour.

The wet and dry oscillator paradigm was introduced to separate the distinctions between time domain and frequency domain models, from the distinction between an equation of motion suitable for general motion, and an equation representing a specific type of motion. The wet and dry oscillator models give the same results for post-transient monochromatic response. They also give the same response for a theoretical point absorber (an infinitely small body). This means that for a body that is very small compared to the wavelength, that the dry oscillator model will give a close approximation to the actual behaviour.

Chapter 4

Control of wave energy converters

4.1 Overview

This chapter discusses the control of wave energy converters (WECs). It begins by extending the classification method introduced in Chapter 2 into a full classification system. Following on from the distinction made in the previous chapter between wet and dry oscillators, it is shown how for monochromatic motion the control problem is fundamentally different to that for polychromatic motion. To demonstrate this difference, one of the steps in the classification process is to describe control as either causal or acausal, and as either optimal or sub-optimal. Acausal sub-optimal control is not described in the literature, so its significance is described here. The relationship between causality and optimal control is described in terms of the number of frequency components at which the optimal control condition is applied.

The final step in the classification process is the combination of PTO settings used to make up the PTO force in linear causal sub-optimal PTO control. Four configurations are considered: a scheme using mass, damping and spring coefficients, another using damping and spring coefficients, another using mass and damping coefficients, and finally a scheme that uses only a damping coefficient.

The worked examples for a specific geometry presented in § 4.7 - 4.8 on pages 149 - 170 are used to compare the performance of these schemes at different values of operating frequency. A significant point that is demonstrated by this work is that the scheme with three PTO coefficients (mass-damping-spring) gives superior performance to schemes using two PTO coefficients (mass-damping or damping-spring). In fact, its performance is very close to that given by causal optimal (ideal) control, particularly at frequencies near the operating frequency.

In § 4.9 on page 183 the four types of causal sub-optimal control are again studied, this time for examples of different sizes of the same WEC. This gives surprising results. For the scheme with three PTO coefficients (mass-damping-spring), the larger WEC has a wider bandwidth performance. The implications of this are discussed in more detail in Chapter 6.

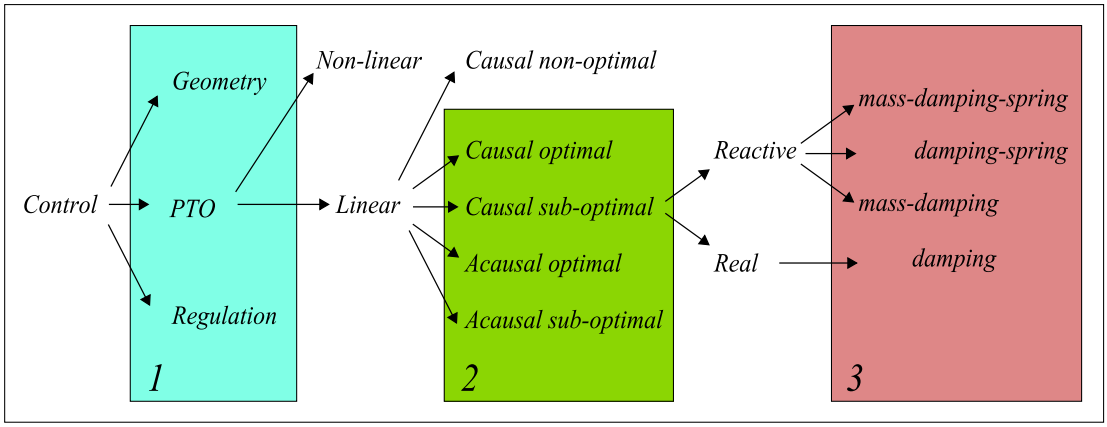

Figure 4.1: ***Full classification of control:*** *Classification of control by power flow, linearity, causality and optimality, real or reactive PTO impedance, and the types of PTO coefficients. Box 1 is the classification described in Chapter 2; Box 2 is described in § 4.3, and Box 3 is described in § 4.8.*

4.2 Full classification of control

Before it is possible to review the theory on linear sub-optimal PTO control of WECs, it is first necessary to define what is meant by this. Fig. 4.1 is one possible way of classifying different types of control. Starting from the left, control is subdivided into various subgroups. The first subdivision, shown highlighted by Box 1, was introduced in § 2.3.

Classification by power flow

Classification by power flow considers how each stage of the flow of power from the wave to the final energy carrier can be controlled. Geometry control determines how much of the incident power is intercepted. PTO control determines how much of the intercepted power is captured. Power regulation determines the quality (and to a lesser extent the quantity) of the delivered power. This chapter focusses primarily on PTO control, but the results show that geometry control and power regulation are both important.

Classification by linearity

In Fig. 4.1 the next step is to classify PTO control as linear or non-linear. The placement of this distinction in the classification order is purely for convenience: this research happens to consider linear control only so it is worth excluding non-linear control early on in the classification process. In this context, linear PTO control means a PTO force that has a linear relationship to the velocity it is opposing[1]. Linear is not used to refer to a translating motion

[1]As in Chapter 3, all references to force and velocity in a WEC with an oscillating primary interface can be applied to pressure and flow in a WEC with a pulsating primary interface.

along a straight line, as opposed to rotation, nor does it refer to a linear generator [103], as opposed to a conventional rotary generator.

Classification by causality and optimality

The next step in the classification of linear PTO control is to describe whether it is causal or optimal. The definitions of these terms and the meanings of these groupings are described in § 4.3.3. The highlighted Box 2 shows the types of control that are described in depth in § 4.5.

Classification of the PTO impedance as real or reactive

In Fig. 4.1 the next step is to classify causal, sub-optimal, linear, PTO control into real and reactive control. Here the terms *real* and *reactive* describe the nature of the PTO impedance. A real PTO impedance results in real control, while a complex PTO impedance results in reactive control.

Classification according to types of PTO coefficients

When applying causal, sub-optimal, linear, PTO control, and using the common assumption that the PTO force is a second order differential equation, the PTO impedance takes the general form of a mass-spring-damper system (Fig. 3.12). Damping is essential for power capture (§ 3.5.7) so the possible sub-categories are those shown in Box 3: damping combined with mass and spring (mass-damping-spring), damping combined with spring (damping-spring), damping combined with mass (mass-damping), and damping applied on its own. The performance resulting from these four combinations is explored in this chapter from § 4.7 onwards.

4.3 Terminology and notation

4.3.1 Definitions of causal and optimal control

Using the definitions of *memoryless*, *causal*, *acausal* and *anticausal* described in § 3.3.3, the meanings of the classifications shown in Fig. 4.1 are as follows:

Causal The control scheme results in a causal equation of motion, so the PTO force may be causal or memoryless. In practice it will be memoryless, as this gives better performance.

Acausal The control scheme results in an acausal equation of motion, so the PTO force may be acausal or anticausal. In practice it will be anticausal, as this the requirement for applying the ideal control conditions at more than one frequency.

Optimal The ideal conditions are applied at every frequency of the excitation. This results in complete absorption of the incident wave.

Sub-optimal Power capture is optimised at one or more (but not all) frequencies. This results in as much absorption of the incident wave as is possible for given restrictions on the values of the PTO coefficients.

Non-optimal The control scheme does not aim to optimise power capture at any one frequency.

4.3.2 Types of control not within the scope of this thesis

Table 2.5 includes types of control that are not within the scope of this thesis. These include non-optimal linear control, and non-linear control, both of which are shown in Fig. 4.1, but are not described by further layers of classification.

Non-optimal linear control is used as a soft constraint on power, displacement or force. Non-linear control could include latching control or hard constraints on power, displacement or force. It could be sub-optimal or non-optimal, and it could be causal or acausal. None of these details are shown in Fig. 4.1, as the purpose of this diagram is to relate the types of control discussed in this chapter, highlighted in Boxes 2 and 3, to the bigger picture of the control problem.

4.3.3 Types of control considered in this chapter

Using the definitions of causality and optimality given in § 4.3.1, the four different combinations shown in Box 2 in Fig. 4.1 were identified. Three of these are well known, but often not clearly differentiated in the literature. The fourth, acausal sub-optimal control, has not yet been described in the literature. It will be shown that it describes linear control that uses forecasts that are only accurate for a short time in the future. The differences between these schemes are depicted in Fig. 4.6.

The main distinction between these four types of control is the number of frequencies at which the optimal control condition (also known as impedance matching) is applied:

- Causal optimal: applies to the special case of monochromatic motion; impedance matching at every (the only) frequency (§4.5.1).
- Causal sub-optimal: applies to the general case of polychromatic motion; impedance matching at one (not every) frequency (§4.5.2).
- Acausal optimal: applies to the general case of polychromatic motion; impedance matching at all frequencies (§4.5.3).
- Acausal sub-optimal: applies to the general case of polychromatic motion; impedance matching at several (not all) frequencies (§4.5.4).

4.3.4 Terminology used in the literature

In the literature, several terms are used to indicate that the ideal condition for linear PTO control has been applied. These include the terms phase control, reactive control, complex conjugate control, impedance matching, and the condition whereby velocity is in phase with excitation force. The reasons why all these terms describe the ideal condition is as follows. The ideal condition at any given frequency is that the PTO impedance must equal the complex conjugate of the intrinsic impedance at that frequency. Choosing a PTO impedance that is the complex conjugate of the intrinsic impedance is known as impedance matching. In order to apply the ideal conditions at an arbitrary frequency, the PTO impedance must be complex, and as it contains reactive terms, is known as reactive control. The ideal conditions are that the velocity has the correct amplitude (the amplitude condition) and that it has the correct phase (the phase condition). Real control is sometimes called amplitude control as it is only possible to satisfy the amplitude condition. Reactive control is sometimes called phase control because a complex PTO impedance can be used to implement both the amplitude and the phase condition. The phase condition is that the velocity should have the same phase as the excitation force.

These terms all refer to the ideal condition at a given frequency. They are all used, depending on the context, as shorthand for causal optimal control (the special case of monochromatic motion where complete absorption does not require future knowledge), or acausal optimal control (the upper limit: complete absorption of a polychromatic wave, which requires future knowledge). In addition to these interpretations, each of these terms tends to get used in slightly different ways.

Falnes [55] interprets *phase control* as finding the optimum velocity, and *reactive control* as finding the optimum PTO impedance. As the velocity is determined by the PTO impedance (see (4.1) in § 4.4), control for optimum PTO impedance and optimum velocity are equivalent ways of approaching the same problem. *Phase control* is also now commonly used to describe latching control. This is the application of a time-varying damping (real) impedance, which results in a non-linear PTO force which has some of the advantages of linear phase (reactive) control.

The terms *reactive control* and *impedance matching* are sometimes used to describe causal sub-optimal control (where the ideal condition is applied at one frequency and does not occur at any other frequencies). This is because in causal sub-optimal control the impedance matching still occurs, albeit at one frequency only, the operating frequency. At all values of operating frequency other than the natural frequency, this requires a complex PTO impedance. In fact, when physically applying causal sub-optimal control, the PTO settings are identical to those required for causal optimal control (Fig. 4.4), the only difference being whether the input is sinusoidal or not. However, the terms *phase control* and ensuring *the velocity is in phase with excitation* are rarely used to describe causal sub-optimal control. When studying the time domain velocity and excitation force, they will not (in general) appear to be 'in phase'. It

will only be apparent that there is one frequency for which they are in phase if velocity and excitation are narrow bandwidth signals. As the excitation approaches sinusoidal, this type of control approaches causal optimal control.

The term *complex conjugate control* is commonly associated with the complete absorption of a polychromatic wave by applying the ideal conditions at every frequency. However this interpretation is not consistent. As discussed in § 6.2.4, some authors [71, 104] have described both causal and acausal optimal control as complex conjugate control, often in the same document, and often without clearly distinguishing between these cases. At the time, differentiating between causal and acausal optimal control was not considered to be important, and hence the term *complex conjugate control* was used loosely to refer to both.

4.3.5 Notation distinguishing between optimal and sub-optimal control

It is important to distinguish between PTO impedance in its general form, and PTO impedance where the settings (m_{pto}, b_{pto} and c_{pto}) have been assigned values required for a given control scheme. The following notations are used:

- Z_{pto} is used to indicate the general PTO impedance.
- $\tilde{Z}_{pto}$ is used to indicate the PTO impedance required for optimal control. This is used for both causal and acausal optimal control.
- $\breve{Z}_{pto}$ is used to indicate the PTO impedance required for sub-optimal control. This is used for both real and reactive sub-optimal control.

This notation also applies to the PTO settings (m_{pto}, $\tilde{b}_{pto}$ and $\breve{c}_{pto}$), and to any parameter that is a function of PTO impedance. Sub-optimal control requires that an operating frequency, ω_p, is chosen. The added mass and damping at this frequency, $M[\omega_p]$ and $B[\omega_p]$, are written M_p and B_p to emphasise that they are constants and not frequency domain functions.

4.3.6 Notation distinguishing between monochromatic and polychromatic cases

As shall be discussed in § 6.2.4, it is important to distinguish between functions that apply to monochromatic motion and those that apply to the polychromatic case. The notation used in Chapters 2 and 3 to indicate the monochromatic case is continued here. An arbitrary sinusoidal frequency is indicated by ω_s. The added mass and damping at this frequency, $M[\omega_s]$ and $B[\omega_s]$, are written M_s and B_s to emphasise that they are constants and not frequency domain functions.

In § 5.2 the distinction will be made between capture width calculated for the cases of monochromatic and polychromatic behaviour. In the literature, both are usually referred to as capture width. The notation C_W is used to indicate capture width under polychromatic

conditions and C_W^s indicates capture width under monochromatic conditions. Monochromatic capture width is commonly used as a performance indicator and is plotted against frequency.

4.3.7 Notation distinguishing between continuous and discrete data

The equations in this chapter describing PTO impedance are continuous with time and frequency, so the transform between the domains is the continuous Fourier transform. This is consistent with convention in wave energy research. The equations of the performance indicators used for this chapter are given in discrete form in § 4.6, so the transform between domains is the DFT. As the results of the case studies in this thesis are based on hydrodynamic parameters at discrete frequencies, the results have been plotted in such a way that this is clear. This makes the nature of the data more transparent, and allows easy repetition of results. It is hoped that the ideas discussed here will be useful to those conducting experimental work, or numerical work using discrete hydrodynamic parameters calculated for specific geometries. Most numerical and experimental work is now conducted using discrete time and frequency domain signals.

Any frequency domain equation of a linear system (input $\times$ transfer function = output) can be changed from continuous Fourier transform notation to DFT notation by simply replacing (ω) with $[\omega_j]$. Note that frequency decompositions of power are not linear systems, but expressions using Parseval's or Plancherel's equation. Changing the domain from continuous to discrete also requires a change to the scaling factor (Appendix B.1). Capture width is a ratio of power decompositions using Plancherel's equation, so the scaling factor cancels. It can be changed from Fourier transform to DFT notation by replacing (ω) with $[\omega_j]$.

4.4 PTO force control

When using a PTO force that is a linear function of velocity, $F_{pto}(\omega) = Z_{pto}(\omega)U(\omega)$, the choice of PTO impedance has an impact on the velocity. This can be seen by rearranging (3.41) as:

$$U(\omega) = \frac{F_e(\omega)}{Z(\omega) + Z_{pto}(\omega)} \tag{4.1}$$

Note that here the PTO impedance is a general value and has not yet been assigned a value, optimal or otherwise. Velocity and PTO impedance are inversely related. Velocity is at a maximum when there is no impedance from the PTO, and decreases as PTO impedance rises. Instantaneous power is the product of the PTO force and the velocity. The total work done, W, is the instantaneous power integrated over the interval of interest. This can be written in the

frequency domain using Plancherel's equation (B.14):

$$W = \int_{-\infty}^{+\infty} f_{pto}(t)\ u(t)dt = \frac{1}{2\pi}\int_{-\infty}^{+\infty} F^*_{pto}(\omega)U(\omega)d\omega \tag{4.2}$$

As shown in [55] this can be rearranged in terms of velocity and PTO damping coefficient:

$$W = \frac{1}{\pi}\int_{0}^{+\infty} b_{pto}\,|U(\omega)|^2\,d\omega \tag{4.3}$$

In this equation, an increase in the first term, the PTO damping, results in a decrease in the second term, the velocity. This is due to their inverse relationship, which is shown in (4.1). Thus it is intuitive that there is some value of PTO damping that maximises the amount of work done (the energy captured). It is also clear that work is quadratically related to velocity (4.3). For any frequency, a plot of work against the magnitude of the velocity would yield a parabola [105]. The peak of this parabola is the magnitude of velocity that maximises energy capture. Substituting (4.1) into (4.3) gives work as a function of PTO impedance. The maxima of this can be found by setting its derivative to zero and solving for PTO impedance [106]. This gives the optimum PTO impedance as the complex conjugate of the intrinsic impedance [56, 77, 106].

4.4.1 A good wave absorber must be a good wave-maker

The observation that *a good wave absorber must be a good wave-maker* was first noted by Falnes and Budal [105]. They explained the principle of complete absorption of a sinusoidal wave by considering the interaction of the incident, transmitted, diffracted and radiated waves. Each of these propagating waves carries energy. Using the principle of conservation of energy, it can be shown that the mechanism for wave absorption is wave radiation.

This initially appears contradictory. How is it that radiated waves are required for absorbing waves when they in fact transport energy away from the body? The key to making sense of this is to think of energy transport in terms of waves, as opposed to particles. Energy absorbed from an incoming wave is related to the square of the elevation of the net outgoing waves [77]. The radiation of waves due to body motion is one source of outgoing waves. However, diffracted and transmitted waves can also be thought of as outgoing; they travel away from the body and also transport energy away from it. However, if the radiated waves cancel the diffracted and transmitted waves then there is no net outgoing wave, and hence no energy carried away from the body.

Fig. 2.4 in §2.2.5 shows how the captured power relates to the power in the incident, diffracted, transmitted and radiated waves. For there to be absorbed power, the radiated wave must reduce the height of the net outgoing (diffracted and transmitted) wave. In the diagram the wave

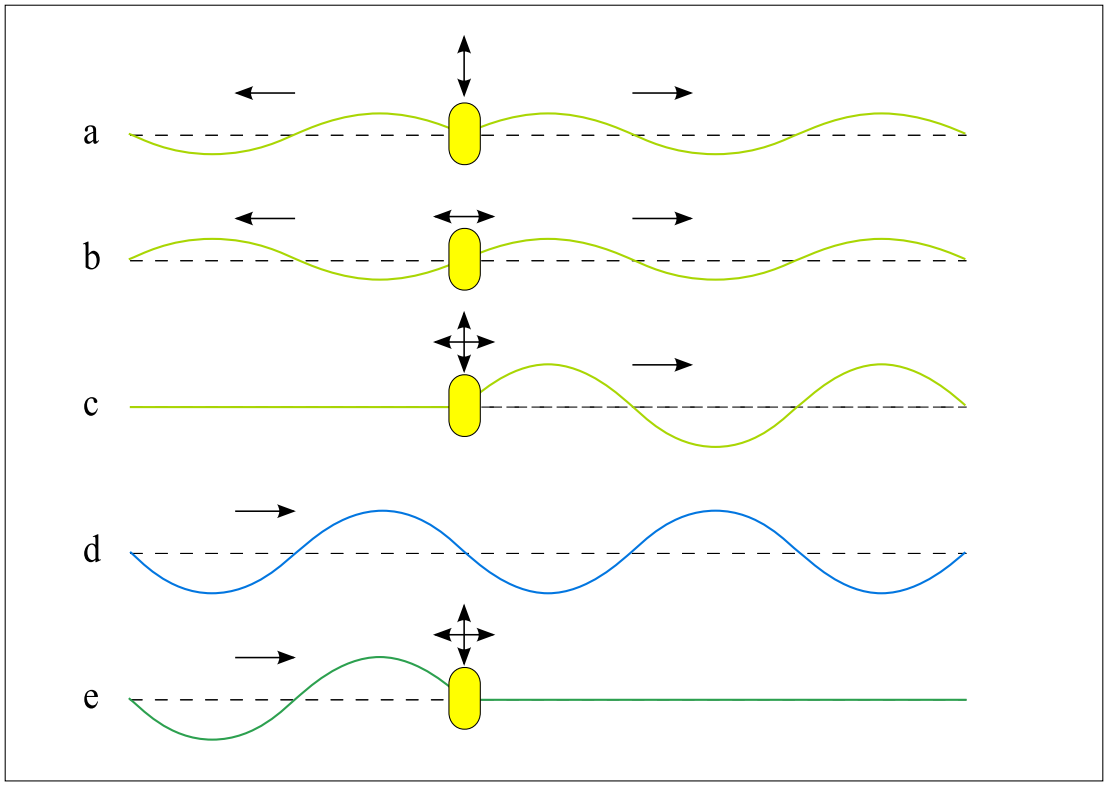

Figure 4.2: ***Full cancellation of the transmitted wave by the radiated wave****(after Fig. 6 in [105]): a) radiated wave due to heave motion. b) radiated wave due to surge motion. c) radiated wave due to heave and surge. d) incident wave in the absence of point absorber. e) incoming wave not transmitted due to cancellation by point absorber's heave and surge radiation.*

symbol for the radiated power is shown as being in counter-phase with that of the diffracted and transmitted waves.

It can be helpful to consider the cancellation of transmitted and diffracted waves separately. Fig. 6 in [105], reproduced here in Fig. 4.2, shows the case of where there are no diffracted waves, only transmitted waves (a point absorber). Complete absorption would occur if a point absorber were moved in such a way that it radiated no waves towards the oncoming waves, yet produced waves behind it to cancel out the passing (transmitted) wave. A terminator, as shown by the solid wall in Fig. 1 of [105] does not transmit any waves, but diffracts waves. For a terminator, complete absorption requires movement that radiates waves towards the oncoming waves to cancel diffracted waves, yet radiates no waves behind it. In the general case of a WEC that transmits and diffracts waves, complete absorption involves motion that produces radiated waves that cancel both the transmitted and diffracted wave.

Fig. 4.2 demonstrates the two conditions required for complete absorption of the incident wave: the amplitude and the phase conditions. The amplitude condition is that the amplitude of the

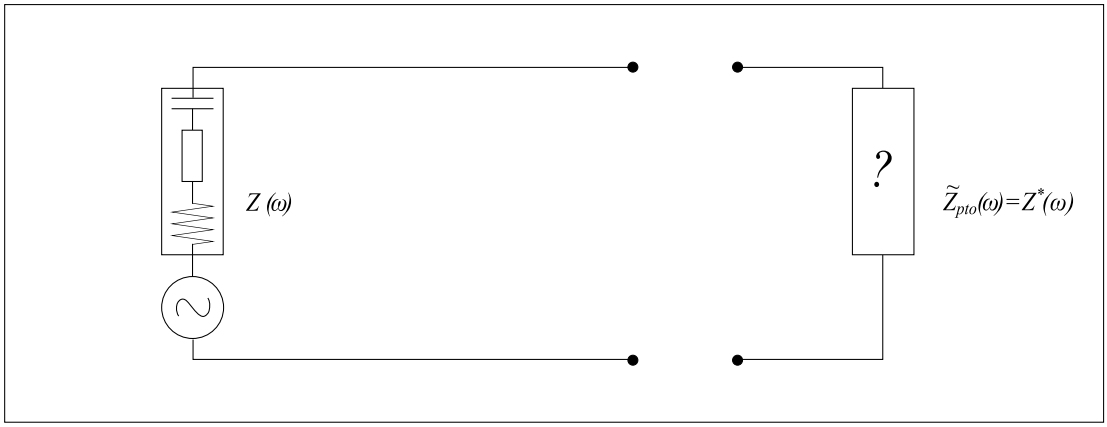

Figure 4.3: ***The electrical analogy:*** *in an electrical circuit, the load impedance resulting in the greatest power transfer is the complex conjugate of the source impedance. The control problem is causal (can be solved using information available in real time) only when the load impedance is a combination of inductance, resistance and capacitance.*

radiated wave must be the same as the (diffracted or transmitted) wave it needs to cancel. The phase condition is that the radiated wave should be in counter-phase (180° out of phase) with the wave to be cancelled. The amplitude condition was first noted by [56], as well as [77, 106] who also explicitly stated the phase condition. The amplitude and phase conditions are equivalent to impedance matching. The amplitude condition is achieved by choosing PTO damping equal to the intrinsic damping. The phase condition is achieved by choosing PTO reactance that cancels the intrinsic reactance.

4.4.2 Impedance matching

The optimum condition for controlling a WEC has a well-known analogy in electrical engineering (see Fig. 4.3). In an electrical circuit, maximum power transfer between a source and a load occurs when the load impedance is the complex conjugate [107] of the source impedance (see "maximum power theorem" and "impedance matching" in [108]).

Note that this is only true for an electrical circuit with a source impedance that is a combination of capacitances, resistances and inductances. This type of circuit is known as a linear circuit. A circuit composed of capacitances, resistances and inductances is analogous to a mass-spring-damper system, which is a dry oscillator (§ 3.8), rather than analogous to a WEC, which is a wet oscillator. While the concept of impedance matching is useful, it can be misleading to think of a WEC's intrinsic impedance as being made up of resistance-capacitance-inductance circuit.

4.5 Four types of impedance matching

The four types of impedance matching described in § 4.3.3 are now discussed, with reference to both the time and frequency domain. The cases to which they apply are noted.

4.5.1 Causal optimal control

When applying impedance matching at one frequency only, and when the WEC is moving monochromatically at that frequency, ω_s, then the control is causal (no future information required) and the performance is optimal (resulting in complete absorption of the wave). The optimal PTO impedance at ω_s is the complex conjugate of the intrinsic impedance:

$$\tilde{Z}_{pto}[\omega_s] = Z^*[\omega_s] \tag{4.4}$$

Here the presence of the *tilde* indicates the optimal value, rather than the general value. The capital letters indicate that here impedance is considered in the frequency domain. The net (combined PTO and intrinsic) impedance at that frequency will be twice the radiation damping at the frequency of interest, ω_s:

$$\begin{aligned} \tilde{Z}_{net}[\omega_s] &= Z[\omega_s] + Z^*[\omega_s] \\ &= 2B[\omega_s] \end{aligned} \tag{4.5}$$

Given a PTO impedance containing mass, damping, and spring terms, $Z_{pto}[\omega_s] = i\omega m_{pto} + b_{pto} + c_{pto}/i\omega$ (3.39), the following PTO coefficients till give the ideal condition at the frequency ω_s (4.4):

$$\begin{aligned} \tilde{m}_{pto}[\omega_s] &= -[m + M_s] \\ \tilde{b}_{pto}[\omega_s] &= B_s \\ \tilde{c}_{pto}[\omega_s] &= -c \end{aligned} \tag{4.6}$$

While the use of $i\omega$ in (3.39) indicates that the PTO impedance has been defined as a frequency domain parameter, each of the PTO coefficients are constants. The subscripted letter *s* indicates that the value of the constant is defined only for a sinusoid of one frequency. The notation $[\omega_s]$ indicates that the value of the PTO coefficients are not defined at frequencies other than ω_s. In order to define the PTO force in the time domain, an inverse Fourier transform is needed, and for this it is necessary to define these coefficients at all frequencies. This simply means that the values of the coefficients at ω_s are used to define the coefficients at all other frequencies. This is the definition given in (4.9) for causal sub-optimal control. It is sub-optimal because the ideal conditions are not applied at many frequencies, these being frequencies other than the operating frequency, ω_p.

While the PTO coefficients for causal control of sinusoidal motion (4.6) and causal control of polychromatic motion (4.9) look deceptively similar, the important distinction is that for sinusoidal motion this leads to optimal control. The ideal conditions are applied at all frequencies of interest, which happen to be only one frequency, ω_s.

Fig. 4.4 shows that the same physical method and PTO coefficients are used for applying optimal and sub-optimal causal control to a WEC with linear behaviour. The only difference is whether the motion is monochromatic or polychromatic. When the displacement $x(t)$ is sinusoidal, the PTO force is:

$$\tilde{f}_{pto}(t) = -\left[m + M_s\right] a(t) + B_s u(t) - c x(t) \tag{4.7}$$

4.5.2 Causal sub-optimal control

The use of PTO coefficients that are constants, rather than having a different value at each frequency bin, gives a time domain PTO force that is memoryless. This means that no future information is required, and the equation of motion, including the PTO force, is causal. The connection between causal control and a memoryless PTO force shall be discussed in § 4.5.5. When motion is polychromatic and the impedance is matched at only one component of frequency, then the performance is necessarily sub-optimal. This type of causal sub-optimal control is now considered.

Choosing peak frequency

A frequency at which optimum absorption will occur must be chosen. A common approach is to find the peak of the power spectrum of wave elevation [109]. Measuring wave elevation for a full-scale WEC in real seas is not practical, as the value of wave elevation required is at the position of the WEC, and the surrounding wave field will have been altered by radiation and diffraction. A more realisable approach is to measure the peak in power spectrum of measured velocity [49]. As the operating frequency is usually the peak of some spectra or other, it is often referred to as the peak frequency and will be denoted ω_p. Another commonly used name is tuning frequency, which evokes the analogy of tuning an antenna [107] to have maximum power transfer at one frequency, and low power transfer at all others.

PTO impedance for arbitrary PTO settings expressed in the frequency domain

The PTO impedance (3.39) at the operating frequency ω_p is chosen to be the complex conjugate of the intrinsic impedance at that frequency (3.43):

$$\begin{aligned} \breve{Z}_{pto}[\omega_p] &= Z[\omega_p]^* \\ &= B_p - i\left(\omega_p\left[m + M_p\right] - \frac{c}{\omega_p}\right) \end{aligned} \tag{4.8}$$

Here the *breve* indicates that a property has a value determined by sub-optimal control. The frequency dependency of the PTO impedance, $\breve{Z}_{pto}(\omega)$, depends on the available PTO coefficients. By convention, systems up to second order are considered, which means a causal control force could consist of a combination of mass, spring and damping, as shown in Fig. 3.12. In fact, for a causal control force only the damping component is compulsory; the mass and spring components are optional. The combination of PTO coefficients that is chosen has an important effect on the frequency dependency of the PTO and net impedance, as discussed in § 4.8, and ultimately on the performance of the WEC, as discussed in § 4.8 and § 5.3.

PTO impedance for specific PTO settings expressed in the frequency domain

As shall be discussed in § 4.7, when mass, damping and spring PTO coefficients are chosen to satisfy (4.8), there is some freedom in the choice of chosen values. It shall be shown that the values resulting in the best performance are:

$$\begin{aligned} \breve{M}_{pto}(\omega) &= \breve{m}_{pto} &&= -\left[m + M_p\right] \\ \breve{B}_{pto}(\omega) &= \breve{b}_{pto} &&= B_p \\ \breve{C}_{pto}(\omega) &= \breve{c}_{pto} &&= -c \end{aligned} \tag{4.9}$$

As a memoryless PTO force is required, the PTO coefficients are constants, indicated by lower case, rather than functions of frequency indicated by the upper case notation and the specification of the domain (ω). Here the notation B_p is used to indicate that it is a constant value and not frequency dependent. Although the PTO coefficients are constants, the resulting PTO impedance is not.

PTO force for specific PTO settings expressed in the time domain

As the PTO coefficients are constant, conversion of PTO force into a time domain signal is easy and does not involve any convolutions. For general values of PTO coefficient the PTO force is:

$$\breve{f}_{pto}(t) = \breve{m}_{pto}a(t) + \breve{b}_{pto}u(t) + \breve{c}_{pto}x(t) \tag{4.10}$$

Using the specific values of PTO coefficient given in (4.9), the PTO force for impedance matching at one frequency, ω_s is:

$$\breve{f}_{pto}(t) = -\left[m + M_p\right]a(t) + B_p u(t) - cx(t) \tag{4.11}$$

This equation appears similar to (4.7) but is different in that it is a general equation, where $x(t)$ may be any function of time. In (4.7) $x(t)$ is limited to a sinusoid of frequency ω_s.

The physical realisation of the PTO force for impedance matching at one frequency is simple.

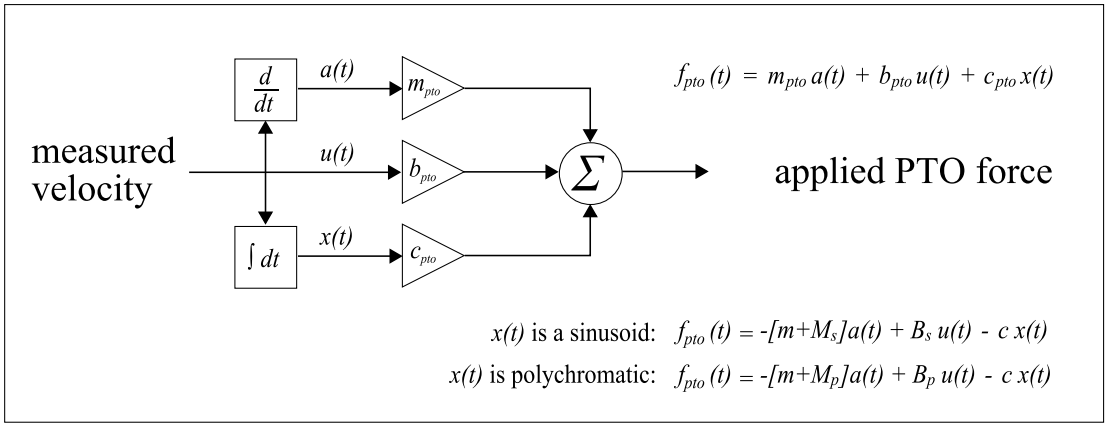

Figure 4.4: ***Circuit for impedance matching at one frequency:*** *a signal representing the measured velocity is integrated to give displacement, and differentiated to give acceleration. Various gains, determined by the PTO coefficients, are applied to the acceleration, velocity and displacement signals. Summation gives a signal proportional to the required PTO force. This circuit gives optimal control for monochromatic excitation and sub-optimal control for polychromatic excitation.*

When mass, spring and damping coefficients are used, the PTO force is that given in (4.11). Its implementation as an electrical circuit is shown in Fig. 4.4. The velocity (or displacement or acceleration) is sensed with a transducer and represented as an electrical signal. This signal is processed so that electrical signals representing displacement, velocity and acceleration are available. The PTO coefficients are the values of gain chosen to amplify each of these signals. The sum of the amplified components gives an electrical signal proportional to the required PTO force. This can be used to drive the mechanism applying this force, for instance an electrical machine that can operate as either a motor or a generator.

The resulting PTO force (4.10) only matches the intrinsic impedance at one frequency. It gives the optimal PTO force for monochromatic motion (4.7) and a sub-optimal PTO force when $x(t)$ contains more than one frequency (4.11).

The PTO spring coefficient, c_{pto}, is constant for a given geometry, and does not need to be adjusted. The physical circuit requires adjustable values of m_{pto} and b_{pto} so that it can be used with different values of ω_s (for monochromatic waves) or ω_p (for polychromatic waves). Once the value of ω_s or ω_p is known, the values of the PTO mass and damping coefficients remain fixed. Although their values are set by a given frequency, they are nevertheless constant values. To be precise, when modelling linear post-transient response of a WEC due to causal control, the chosen model (see Fig. 3.6) is valid for constant PTO coefficients.

4.5.3 Acausal optimal contol

When applying impedance matching at every frequency of a polychromatic excitation, the control is acausal (future information is required) and the performance is optimal (the wave is completely absorbed). The PTO impedance equals the complex conjugate of the intrinsic impedance at every frequency:

$$\tilde{Z}_{pto}(\omega) = Z(\omega)^* \tag{4.12}$$

For a PTO impedance containing mass, damping, and spring terms (3.39) the following settings are required:

$$\begin{aligned} \tilde{M}_{pto}(\omega) &= -\left[m + M(\omega)\right] \\ \tilde{B}_{pto}(\omega) &= B(\omega) \\ \tilde{C}_{pto}(\omega) &= \tilde{c}_{pto} = -c \end{aligned} \tag{4.13}$$

The mass and damping PTO coefficients are frequency dependent, as they are required to match the frequency dependent hydrodynamic radiation coefficients. Using these PTO coefficients, the frequency domain representation of the optimal control force is:

$$\tilde{F}_{pto}(\omega) = -i\omega\left[m + M(\omega)\right]U(\omega) + B(\omega)U(\omega) + \frac{ic}{\omega}U(\omega) \tag{4.14}$$

For acausal optimal control the net impedance is:

$$\tilde{Z}_{net}(\omega) = 2B(\omega) \tag{4.15}$$

Time domain representation of the acausal optimal PTO force

In the same way that m_∞ is separated from the radiation impedance in the equation of motion (3.46), the constants and frequency dependent terms in the PTO force (4.14) must first be separated:

$$\tilde{F}_{pto}(\omega) = -i\omega\left[m + m_\infty\right]U(\omega) + K^*(\omega)U(\omega) - c/i\omega U(\omega) \tag{4.16}$$

The middle term on the right hand side is the complex conjugate of the frequency dependent radiation impedance, $K(\omega)$. Given that the time domain PTO force must be real, $K^*(\omega) = K(-\omega)$, so $\mathcal{F}^{-1}\left\{K^*(\omega)\right\} = k(-t)$ [60]. The time domain function corresponding to (4.16) is:

$$\tilde{f}_{pto}(t) = -[m + m_\infty]a(t) + k(-t) * u(t) - cx(t) \tag{4.17}$$

The middle term is the convolution of velocity with the time reversed memory kernel, $k(-t)$. As the memory kernel is a causal function (such as case (b) in Fig. 3.8), it is anticausal when time reversed (such as case (c) in Fig. 3.8); thus future knowledge of velocity is required. This result was first presented by Niato and Nakamura in 1985 [110]. Although not explicitly stated,

this paper described the ideal control force as:

$$\tilde{f}_{pto}(t) = -[m + m_\infty]a(t) + \int_0^\infty k(\tau)u(t+\tau)d\tau - cx(t) \tag{4.18}$$

The particular form of the integral can be explained by writing the convolution out in full, noting that convolution with $k(-t)$ gives the term $k(-\tau)$:

$$k(-t) * u(t) = \int_{-\infty}^{\infty} k(-\tau)u(t-\tau)d\tau \tag{4.19}$$

then substituting a dummy variable $\acute{\tau} = -\tau$, and noting that this dummy variable could stand for τ itself: $\acute{\tau} = \tau$. Finally, as $k(t)$ is causal, the limits can be changed, using the same method of splitting integrals shown in 3.6.2:

$$\begin{aligned} k(-t) * u(t) &= \int_{-\infty}^{\infty} k(\acute{\tau})u(t+\acute{\tau})d\acute{\tau} \\ &= \int_{-\infty}^{\infty} k(\tau)u(t+\tau)d\tau \\ &= \int_0^{\infty} k(\tau)u(t+\tau)d\tau \end{aligned} \tag{4.20}$$

Just as $k(t)$ and $k(t) * u(t)$ are referred to in this work as the memory kernel and the memory convolution, by analogy $k(-t)$ and $k(-t) * u(t)$ are referred to as the premonition kernel and the premonition convolution. The memory convolution is a force that is a function of past values of velocity so can be thought of as containing a memory of the past. Analogously, the premonition convolution is a force that is a function of future values of velocity, so can be thought of as requiring a premonition of the future.

The acausality of optimal control explained in terms of radiated waves

The memory convolution in (3.49) indicates that the radiation force depends on the present (instantaneous) and past values of velocity. Consequently, the present velocity affects the radiation force in the future. The connection between the present velocity and the future radiation force has implications for control. Perfect absorption of waves can be thought of as the radiation of a wave that is in anti-phase with the diffracted and transmitted waves so that these are completely cancelled. The radiated wave field depends on the past and present values of velocity. To achieve perfect cancellation of the diffracted and transmitted waves in the present instant, the control system would have needed to know about the waves requiring

cancellation in advance to attain the correct value of damping in the present moment. Likewise, control decisions need to be made in the present moment to produce the required radiation force to cancel future waves, and so knowledge of the future waves is required. To summarise:

- Choice of PTO coefficients now determines instantaneous velocity.
- Instantaneous velocity influences future radiation force.
- Future radiation force determines the radiated wave field in the future.
- These radiated waves should cancel the diffracted and transmitted waves.
- Future diffracted and transmitted waves result from future (unknown) incident waves.
- Thus choice of PTO coefficients determines whether waves radiated in the future will cancel diffracted and transmitted waves due to incident waves that have yet to arrive.

The theoretical implementation of optimal acausal control

Fig. 4.4 shows how causal mass-damping-spring control is implemented in terms of an analogue circuit. This shows that the force has components proportional to instantaneous values of acceleration, velocity and displacement. The question that follows naturally from this figure is how the analogue circuit implementing acausal optimal control would look. If the circuit in Fig. 4.4 was used, but the PTO coefficients were varied over time, it may be possible to implement the required control force. However, there are several problems with this. If the PTO coefficients are varied over time, then this is actually non-linear control. Also, it is not clear where the future knowledge comes in. The reason for these problems is that the memoryless equation representing this circuit is not adequate for describing the optimal control force. The equation of optimal acausal control is better represented by Fig. 4.5. Rather than having a time varying PTO damping coefficient, there is instead an acausal filter. It is an impulse response, so is a function of time. However, it is time invariant, so it is always the same function of time. Into this acausal filter are fed the instantaneous value of velocity and future values of velocity. The future values originate from an icon of a crystal ball. This indicates that they are not values which can be derived from the system, and also that their availability is purely hypothetical. This diagram shows where the future knowledge fits in. It also demonstrates that this system is linear; integration, and hence convolution, is a linear operation. Of course the PTO force given by Fig. 4.5 could also be produced by using time varying PTO coefficients with the circuit representing mass-damping-spring control, Fig. 4.4. While this may be quantitatively correct, it is qualitatively incorrect.

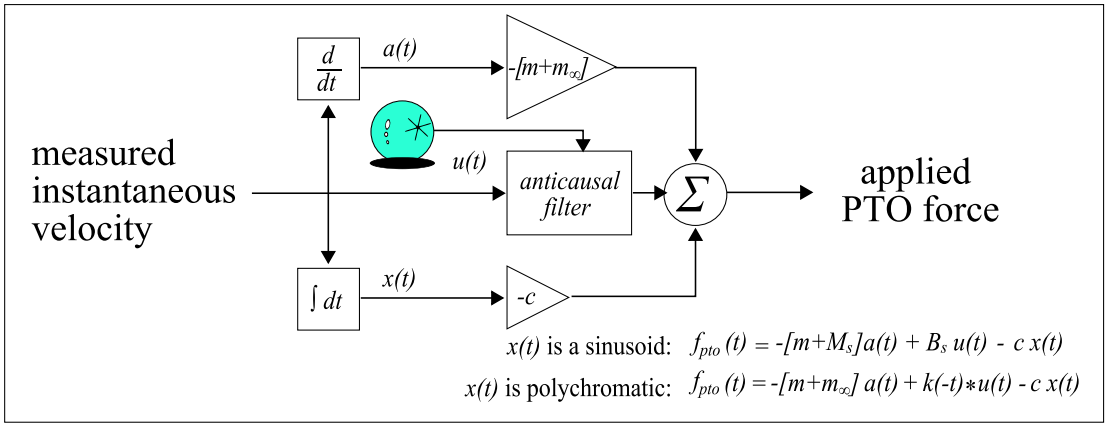

Figure 4.5: ***Circuit for impedance matching at all frequencies:*** *future values of velocity, indicated by the crystal ball, as well as the instantaneous velocity, are fed into a linear acausal filter. Summation of the filtered velocity, and the scaled displacement and acceleration signals, gives a signal proportional to the required PTO force. This circuit gives optimal control for polychromatic excitation.*

4.5.4 Acausal sub-optimal control

In Fig. 4.6 the three types of control discussed so far are those without highlighted backgrounds. The distinctions between these three types of control suggests the existence of a fourth type, which is highlighted with a coloured background: acausal sub-optimal control. This type of control has not been previously discussed in the literature. Extrapolating what is known about acausal optimal control, and causal sub-optimal control, the characteristics of this type of control can be deduced. It is then possible to postulate what the nature of this type of control may be.

The difference between acausal and causal control lies in whether the PTO force is anticausal or memoryless. In order to have a memoryless PTO force, the PTO coefficients must be constants. If the PTO coefficients vary with frequency, then the time domain expression of PTO force will include a convolution with an anticausal premonition kernel. The highlighted control results in acausal behaviour, so it will have an anticausal term in the time domain expression of PTO force, and PTO coefficients that are functions of frequency in the frequency domain expression of PTO force.

The difference between optimal and sub-optimal control lies in whether or not the performance has been optimised for all relevant frequencies. This can be seen by comparing causal optimal and causal sub-optimal control. Both optimise the PTO impedance at one frequency. The distinction is that for causal sub-optimal control there are many frequencies where the PTO impedance has not been optimised. The highlighted control scheme is sub-optimal so it is clear that there are frequencies at which the PTO impedance will not be optimal.

The descriptions *acausal* and *sub-optimal* dictate that the highlighted control requires future knowledge, has PTO coefficients that are functions of frequency, and has a PTO impedance that is not optimised for all frequencies of interest. The interaction of these defining characteristics gives more information about this type of control. With acausal optimal control, it can be seen that the ability to apply the ideal conditions at more than one frequency requires that the PTO coefficients are not constants, but functions of frequency. Thus it is clear that while acausal sub-optimal control does not apply the ideal conditions at all frequencies, it provides the means of applying the ideal conditions at several frequencies. Although impedance matching at several frequencies is not explicit from the definition of acausal sub-optimal control, it is the only reason why acausal sub-optimal control could be of interest. It is an upgrade from sub-optimal causal control, where the impedance is matched at only one frequency, in the direction of acausal optimal control, where the impedance is matched at all possible frequencies.

The concept of a control scheme that lies between causal sub-optimal control and acausal optimal control is useful and interesting. It acknowledges that accurate predictions may not be available for a sufficiently long time horizon. It suggests the means for improving on impedance matching at one frequency only. The mechanism of impedance matching at several but not all relevant frequencies fits into the existing pattern seen in the three existing types of control.

It is interesting to speculate what sort of behaviour would arise from impedance matching at several frequencies. The discussion of capture width in Chapter 5 will show that for good performance it is not sufficient for the PTO impedance to be the ideal value at the operating frequency; it is also important that the PTO impedance be as close as possible to the ideal values at frequencies neighbouring the operating frequency. A useful application of a scheme where it is possible to set the PTO impedance to the ideal values at several frequencies would be to apply impedance matching over a band of frequencies surrounding the operating frequency. For a range of frequencies defined by the lower bound ω_{p1} and the upper bound ω_{p2}, the PTO impedance would be equal to those for acausal optimal control, while outside this frequency band, it would be equal to those for causal sub-optimal control:

$$Z_{pto} \begin{cases} = \tilde{Z}_{pto}(\omega) = Z^*(\omega) & \text{for all } \omega_{p1} < \omega < \omega_{p2} \\ = \check{Z}_{pto}(\omega) = f(Z^*(\omega_p)) & \text{for all } \omega < \omega_{p1} \text{ and } \omega > \omega_{p2} \end{cases} \tag{4.21}$$

4.5.5 Comparison between different types of impedance matching

The type of the kernel used in the premonition convolution

The type of the kernel used in the premonition convolution is a useful way of showing the differences between the four groups of impedance matching described in Fig. 4.6. In § 4.5.3 it was shown that the optimal PTO force includes an anticausal term, the premonition convolution. This term is an anticausal premonition kernel (case (c) in Fig. 3.8) convolved with past values

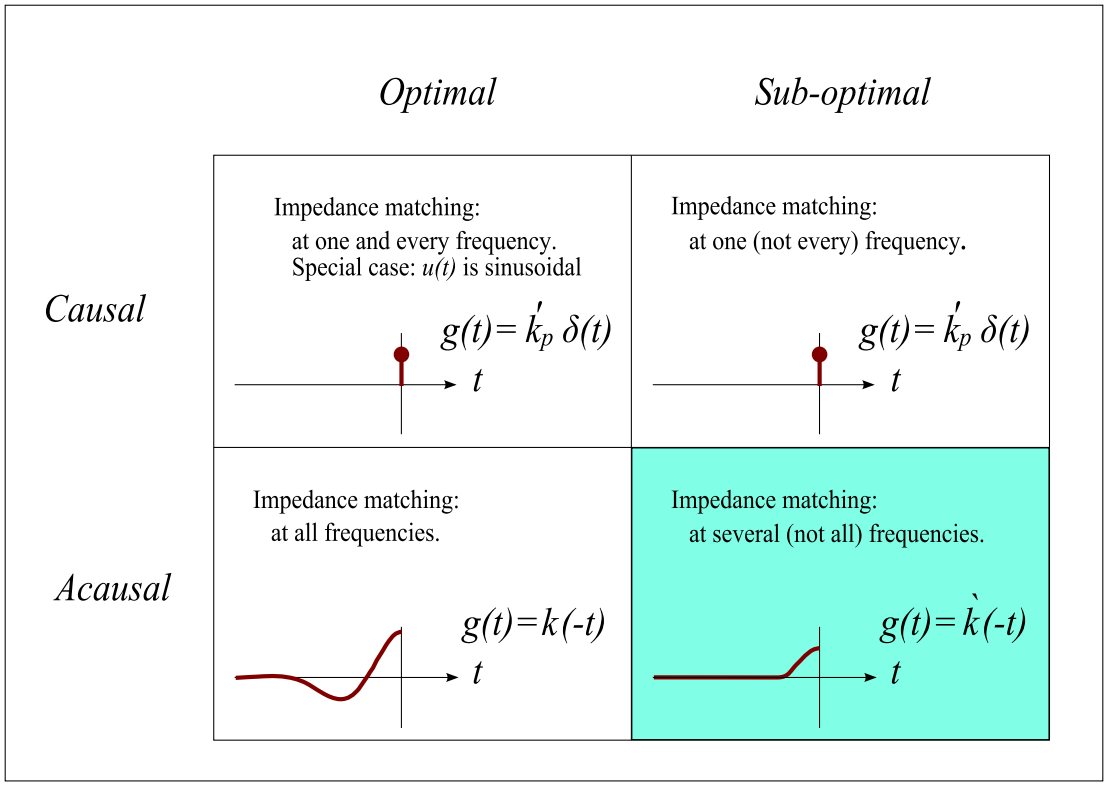

Figure 4.6: ***The types of impedance matching:*** *Optimal control for impedance matching at all excitation frequencies; sub-optimal control for one or more, but not all frequencies; causal control for an instantaneous kernel; acausal control for an anticausal kernel.*

of velocity (4.19). Replacing the premonition kernel with a general kernel $g(t)$:

$$g(t) * u(t) = \int_{-\infty}^{\infty} g(\tau)u(t-\tau)d\tau \tag{4.22}$$

Optimal control occurs when the general kernel used in this convolution is the time reversed memory kernel: $g(t) = k(-t)$, which is the premonition kernel. Whenever the general kernel used has non-zero values for $t <= 0$ and is zero for $t > 0$ (as is the case for the premonition kernel), the convolution (4.22) is anticausal. The WEC equation of motion (inclusive of this anticausal PTO force) is acausal, so this is known as acausal control.

If the value of the general kernel is set to be an instantaneous term, case (a) in Fig. 3.8, rather than an anticausal kernel, the premonition convolution becomes memoryless. Choosing an instantaneous term for the general kernel gives $g(t) = \acute{k}_p\delta(-t) = \acute{k}_p\delta(t)$. This is a Delta function scaled by the constant $\acute{k}_p$. The reason for the resulting memoryless premonition convolution is that the convolution $\acute{k}_p\delta(t) * u(t)$ can be reduced to the multiplication $\acute{k}_p u(t)$.

The WEC equation of motion (inclusive of this memoryless PTO force) is causal, so this is known as causal control.

The value of the constant $\acute{k}_p$ is chosen so that it is possible to implement the optimal value at one frequency, ω_p. This means that the convolutions $\acute{k}_p\delta(t) * u(t)$ and $k(-t) * u(t)$ give equivalent results, after transients have decayed, when the velocity $u(t)$ is sinusoidal with frequency ω_p. This is the reason why for sinusoidal motion it is possible to have optimal control that is causal. However, for causal ($g(t) = \acute{k}_p\delta(t)$) control with $\acute{k}_p$ optimised at ω_p, and for velocity $u(t)$ that contains more than one frequency, then this is only sub-optimal control.

Suppose adequately accurate predictions were available for Δt seconds into the future. In this case, instead of replacing the anticausal premonition kernel with an instantaneous term, it could be replaced with an anticausal kernel that had a shorter duration. If the time over which the new kernel had a significant value (its duration) was Δt, then, depending on the accuracy of the velocity predictions, this offers a possibility of an improvement over causal sub-optimal control.

A general kernel that is an anticausal function of short duration $g(t) = \grave{k}(-t)$, nevertheless leads to acausal control. The PTO coefficients are functions of frequency. For frequencies neighbouring the operating frequency, this could result in values of PTO impedance that are closer to the ideal values. Alternatively, it could lead to the situation discussed in § 4.5.4, where the ideal condition has been implemented over a narrow band of frequencies. If such a system is excited by waves that contain only frequencies in the optimised band then this is optimal control: the convolution $g(t) * u(t)$ will give the same result regardless of whether $g(t) = \grave{k}(-t)$ or $g(t) = k(-t)$ is used. If the system excitation contains frequencies other than those in an optimised band, then this is sub-optimal, but nevertheless still acausal, control.

Acausal sub-optimal control is the type of control being referred to when speaking about 'using predictions of oncoming waves to improve control'. Predictions of oncoming waves can only be used for optimal control if these predictions are completely accurate over the duration of the general kernel $g(t)$ used. This is not a type of control that is presently being used in commercial devices. It describes the type of control that would result if predictions are ever used to apply linear PTO control.

Fig. 4.6 shows the four different combinations of causality and the optimal condition discussed here. The values of $g(t)$ for each case are given and sketches of the type of function expected are given.

Conditions for acausality and sub-optimal control

Optimal control occurs when the impedance is matched at every frequency present in the sea state. Sub-optimal control is a consequence of not matching the intrinsic impedance at every frequency. To match the impedance at more than one frequency, PTO coefficients that

are functions of frequency are required, and these result in an anticausal generalised kernel, and hence PTO force. Acausality is the consequence of impedance matching at more than one frequency. For causal control, the generalised kernel must be instantaneous. This leads to constant PTO coefficients, with which it is only possible to match the impedance at one frequency. Impedance matching at one frequency is a consequence of causal control.

The relationship between impedance matching, causality and optimality can be seen in Fig. 4.6. Impedance matching at the one and only frequency present in the sea state results in control that is both causal and optimal. Impedance matching at one but not all frequencies gives causal sub-optimal control. Impedance matching at several but not all frequencies gives acausal sub-optimal control. Impedance matching over all of the many frequencies present in a sea state gives acausal optimal control.

4.6 Performance indicators

With a clear distinction between acausal optimal control (impedance matching at all frequencies) and causal sub-optimal control (impedance matching at only one frequency), it is now possible to compare the performance, as given by the theory, due to these types of control. The performance of various causal sub-optimal schemes are compared to the upper limit given by acausal optimal control from § 4.7 onwards. The present section gathers together all the information about these plots, and is intended as a reference for later sections.

4.6.1 Monochromatic capture width

Capture width is a widely used performance indicator. The theory behind capture width is explored in depth in § 5.2. However, in the present chapter it is used to show how the choice of geometry or PTO coefficients can affect the performance of a WEC. The property most commonly called capture width (or efficiency) in the literature (for example [52, 53, 111]), is referred to as the monochromatic capture width in this thesis, so as to distinguish it from the polychromatic capture width (see § 5.2). Many authors (for example [58, 112, 113]) use the relative capture width, which is the monochromatic capture width normalised by the width of the WEC. Some authors have used the term *efficiency* to describe the two dimensional version (for a given segment of a terminator device in uni-directional waves) of capture width [52, 114] or relative capture width [111]. The notation $C_W^s[\omega_j]$ is used to show that the monochromatic capture width is a function of discrete frequency. The monochromatic capture width at a given frequency ω_j is defined as (5.10) the ratio between the component of the power absorbed by the WEC, $P_A[\omega_j]$, and the component of wave energy transport, $P_{IW}[\omega_j]$. This definition is only valid when meaningful decompositions can be made of absorbed power $P_A = \sum P_A[\omega_j]$ and wave energy transport $P_{IW} = \sum P_{IW}[\omega_j]$. Given these assumptions (§ 5.2.2 and § 5.2.4), and

the assumption of deep water (3.17), monochromatic capture width can be written as:

$$C_W^s[\omega_j] = \frac{2\omega_j B_{pto}[\omega_j] \left|Z_{net}^{-1}[\omega_j]\right|^2 \left|W[\omega_j]\right|^2}{\rho g^2} \tag{4.23}$$

If the WEC is vertically symmetrical and moving in one degree of freedom: heave (3.36) in deep water (3.12); then the monochromatic capture width reduces to:

$$C_W^s[\omega_j] = \frac{4gB_{pto}[\omega_j]\ B[\omega_j]}{\omega_j^2 \left|Z_{net}[\omega_j]\right|^2} \tag{4.24}$$

This equation is a version of (4.23) specifically for heave motion. Thus all the impedance terms are scalars, rather than the matrices required for multiple degrees of freedom. Equation (4.24) was used to calculate all the monochromatic capture width results presented in this thesis.

4.6.2 Normalised capture width

The upper limit of (monochromatic) capture width is independent of the scale of a WEC, and depends only on the modes of motion. For a WEC with motion in heave, it is well known [56] that the upper limit is $\tilde{C}_W^s[\omega_j] = \frac{\lambda}{2\pi}$. Here λ is the wavelength. As wavelength is a function of frequency, the upper limit may also be written as a function of frequency. Substituting in deep water values (3.12), the upper limit of monochromatic capture width becomes $\tilde{C}_W^s[\omega_j] = g/\omega_j^2$. The resulting function is a (rectangular) hyperbola, with asymptotes on the x and y axes.

All the plots presented here generally compare causal control for a number of influential factors (indicated by the coloured open markers), with the upper limit given by acausal optimal control (indicated by the solid black markers). For instance, the capture width graphs show monochromatic capture width due to causal control ($\breve{C}_W[\omega_j]$), and due to acausal optimal control ($\tilde{C}_W[\omega_j]$). At some frequencies of interest, such as the operating frequency ω_p, or the natural frequency ω_n, these values of capture width can be very close together and difficult to distinguish. At high frequencies the upper limit is low and it can be difficult to see how close a particular line is to this upper limit. For this reason, an alternative representation of capture width can be useful. Here the normalised capture width is introduced. This is defined as the monochromatic capture width as a percentage of the ideal value of monochromatic capture width:

$$\breve{C}_{Wn}^s[\omega_j] = \frac{\breve{C}_W^s[\omega_j]}{\tilde{C}_W^s[\omega_j]} \times 100\% \tag{4.25}$$

4.6.3 PTO Impedance

Plots of PTO impedance are also given, for instance Fig. 4.8. Once again, causal control for several influential factors are compared to an ideal value. The ideal PTO impedance, $\tilde{Z}_{pto}[\omega_j]$,

is the complex conjugate of the intrinsic impedance at each frequency (4.12). The causal control procedures are sub-optimal, so are indicated by $\breve{Z}_{pto}[\omega_j]$.

The PTO impedance is a complex property and can be displayed as either its real and reactive parts, or its magnitude and phase. In all the impedance graphs, the top pair of plots are the real and imaginary parts, and the bottom pair of plots are the magnitude and phase. The real and imaginary parts of the PTO impedance are useful because they relate to the real and imaginary parts of intrinsic impedance. The magnitude is important for visualising the impact of some of the influential parameters. The magnitude is also important because it contributes to the magnitude of the net impedance. The real part of the PTO impedance ($B_{pto}[\omega_j]$) and the magnitude of the net impedance are both terms that make up the capture width.

4.6.4 Net impedance

The magnitude of the net impedance appears in the formula for capture width. Net impedance can be used as a stepping stone to understand the impact of the PTO impedance on the capture width. The net impedance is plotted to compare the performance of different control schemes (see for instance Fig. 4.9).

The solid markers show the ideal net impedance for the monochromatic case (§ 4.5.1), which is also the ideal net impedance for acausal optimal control (§ 4.5.3). Recalling that $\tilde{Z}_{net}(\omega) = 2B(\omega)$ (4.15), the real part of the ideal net impedance (top plot), and the magnitude of the ideal net impedance (third plot), are double the value of the radiation damping. As all the reactance has been cancelled, the imaginary part and the phase of the ideal net impedance is zero.

Each of the coloured open markers shows the net impedance for causal (realisable) sub-optimal control. The net impedance is shown for impedance matching at three different operating frequencies (ω_p). The vertical lines indicate the operating frequencies. In all four plots it can be seen that the net impedance for causal control equals the ideal value (for acausal control) only at the operating frequency.

For impedance matching at single frequencies, the real parts of net impedance (the solid lines) have similar shapes, for example Fig. 4.9. This is because the real part of the net impedance is the radiation damping plus a constant $\Re\left\{\breve{Z}_{net}(\omega)\right\} = B(\omega) + B_p$. Likewise, the imaginary parts of net impedance (the solid lines) follow a similar pattern.

4.6.5 Controlled displacement response amplitude

The controlled displacement response amplitude is the magnitude of the displacement due to a given control scheme normalised with respect to the magnitude of the wave elevation. It can be thought of as a transfer function between wave elevation and controlled displacement, or as an amplification factor. The terms in (3.42) can be written as functions of displacement rather

than velocity: $F_e(\omega) = -\omega^2[m + M(\omega)]X(\omega) + i\omega B(\omega)X(\omega) + cX(\omega) + i\omega Z_{pto}(\omega)X(\omega)$. This can be rearranged in the following manner:

$$\begin{aligned} \frac{X(\omega)}{H(\omega)} &= \frac{W(\omega)}{c - \omega^2[m + M(\omega)] + i\omega B(\omega) + i\omega Z_{pto}(\omega)} \\ &= \frac{W(\omega)}{G(\omega) + G_{pto}(\omega)} \end{aligned} \tag{4.26}$$

where $G(\omega) = c - \omega^2[m + M(\omega)] + i\omega B(\omega)$ is the intrinsic transfer function [55] and $G_{pto}(\omega) = i\omega Z_{pto}$ is the PTO transfer function. The ratio of the magnitudes of the controlled displacement and wave elevation is therefore defined as:

$$RAO_c = \frac{|W(\omega)|}{|G(\omega) + G_{pto}(\omega)|} \tag{4.27}$$

It is denoted RAO_c, as the response amplitude operator (RAO) is defined as the ratio of the uncontrolled displacement and wave elevation, i.e. for $Z_{pto} = 0$. In the work presented here, the discrete version of the controlled displacement response amplitude was used:

$$RAO_c = \frac{|W[\omega_j]|}{|G[\omega_j] + G_{pto}[\omega_j]|} \tag{4.28}$$

4.6.6 Hydrodynamic parameters used in this thesis

Worked examples make the principles discussed here easier to visualise. The purpose of the worked examples presented is to demonstrate the theory. It is important to emphasise that only a small sub-set of data is considered, so the results should in no way be taken to demonstrate universal principles. The worked examples are useful for showing that existing theory needs to be extended to take into account the interaction between the geometry, control scheme, and sea state. However, some of the specific details about this interaction that will be highlighted in the present and following chapter, may be artifacts of the particular examples chosen.

All the worked examples presented in this thesis are based on radiation hydrodynamic coefficients taken from Havelock [57]. These are for a heaving spherical buoy, which has a hemispherical wetted surface when there is no motion and no waves. The PTO system reacts against the sea-bed. A simplified linearised equation of motion is used (3.48) and the intrinsic impedance is that described by (3.43). There is no mechanical spring, and losses are not included in the model. The buoyancy is linearised by assuming that the water plane area is always that of the sphere at its diameter.

Havelock's hydrodynamic coefficients were published in normalised form. The formulae for turning these into coefficients for a specific size (radius) of buoy are described in Appendix A. The radius used in the sections comparing various control schemes and operating frequencies, § 4.7 and § 4.8, is 2.5 m. In the section that compares performance for different sized buoys,

§ 4.9, radii of 1.9 m, 2.5 m and 3.5 m, are used. The hydrodynamic coefficients for these sizes of buoy are shown in Fig. 4.7.

In Fig. 4.7 it can be seen that the hydrodynamic data is incomplete. At the highest frequencies shown, the added mass is lower than the value given by Havelock for m_∞. The added mass is in fact at its lowest value. At frequencies above those shown, the added mass will rise asymptotically to m_∞, while the radiation damping will fall to zero. Note in particular that because the independent variable (frequency) also scales with the radius, there is less high frequency data available for the larger buoys. Despite being incomplete, these hydrodynamic coefficients are suitable for demonstration purposes, as their use by other authors [36, 58, 115] shows that they are widely considered to be accurate, as well as providing an opportunity to verify results. The purpose of this study was to provide proof of concept of the analysis conducted here, and hence it was vital to use data that was known to be correct, both for rigour and for credibility.

The parameters were captured from a digital copy of Havelock's paper using free software called Tracer [116]. The accuracy was limited by the thickness of the line in Havelock's plot. An error the thickness of the line in Havelock's plot would amount to a 1% error for added damping and an error of $1/2$ % for added mass, taking into account the highest points of these hydrdynamic parameters. When digital versions of the traced coefficients and the plot from [57] were superimposed, the lines appeared to be identical, so it is likely that the errors are less than these values.

Havelock's hydrodynamic coefficients are plotted against the product of the wavenumber and the radius. By convention, plotting parameters against the product of wavenumber and the radius implies that they are for sinusoidal motion. Application of these radiation coefficients to a sinusoidal velocity gives the relative magnitude and phase of the corresponding sinusoidal radiation force. Thus these coefficients can be considered to be the real DFT, as discussed in § 3.2.2. For compatibility with time domain work, the complex DFT has been assumed in this research. To convert the coefficients of the DFT to the complex DFT, the magnitude is divided by two, and symmetrical coefficients at corresponding negative frequencies are considered. As the time domain signals considered in this research are all real, the information at the negative frequencies is redundant. None of the graphs here show the negative frequencies, however, the theory does take them into account, as can be seen in Appendix B. Fig. 4.7 thus shows values that are half the magnitude given by the standard denormalisation procedures.

The choice of presenting worked examples in real DFT or complex DFT form does not make a difference to the meaning and interpretation of the results, although there is an effect on the numerical values of some of the results. It does not affect the value of monochromatic capture width for ideal control, because the factor of two appears in both the denominator and the numerator. It does affect the values of monochromatic capture width for causal control, but not the values of polychromatic capture width. All the equations presented here assume that

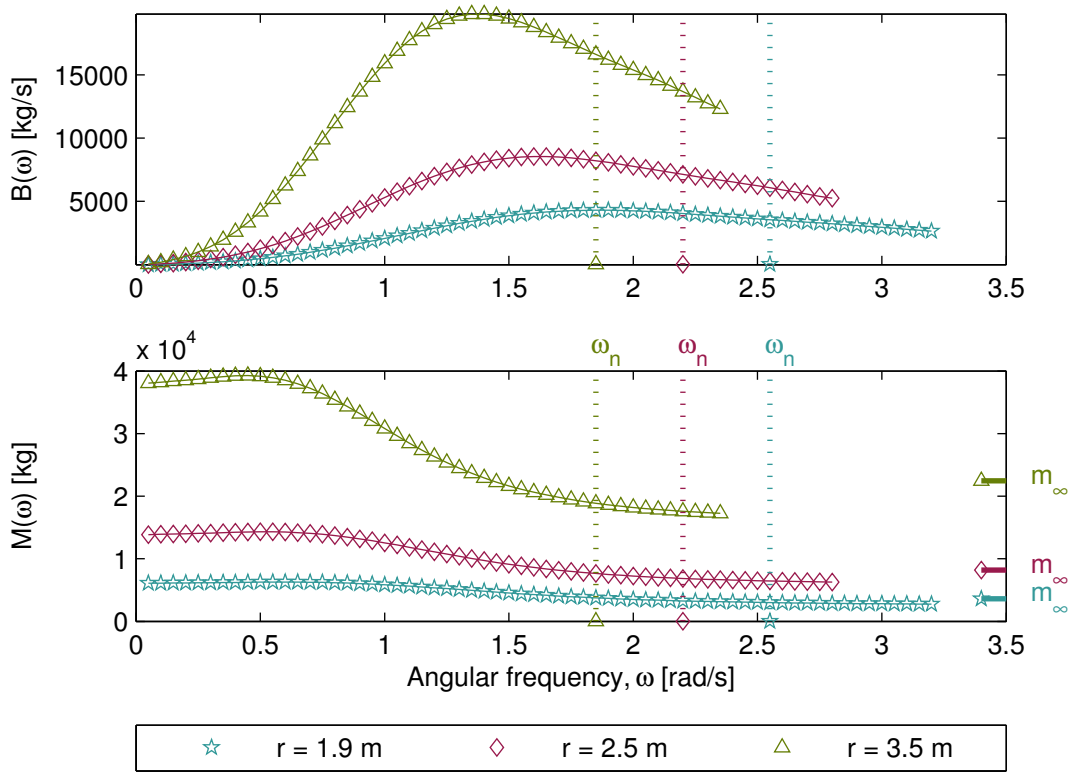

Figure 4.7: ***Radiation coefficients of case studies:*** *Havelock's [57] coefficients for radiation damping $B(\omega)$ and added mass $M(\omega)$ of heaving spherical buoys with radii of 1.9 m, 2.5 m and 3.5 m. At high frequencies the added mass approaches m_∞. The natural frequency ω_n for each size is indicated.*

the complex DFT is being used. Slightly different versions of the equations are required if the real DFT is used. For this reason it is important that one of these systems is chosen and used consistently.

4.6.7 Interpretation of plots

Sections 4.7 - 4.9 graph performance indicators in a way that is different to that currently seen in the literature. The approach taken here is to plot the performance indicator for a given sub-optimal control scheme $\breve{Y}[\omega_j]$ on the same plot as the performance parameter for the optimal scheme $\tilde{Y}[\omega_j]$. Here Y is an arbitrary performance indicator, and the *tilde* and *breve* over-bars indicate values due to optimal and sub-optimal control respectively.

In all the plots in this chapter the vertical lines indicate the position of the operating frequency ω_p or the natural frequency ω_n. In addition the following symbols have been used:

Solid black markers Discrete values of performance for optimal control $\tilde{Y}[\omega_j]$.

Open coloured markers Discrete values of performance for sub-optimal control $\breve{Y}[\omega_j]$; each colour indicates a different scheme, choice of ω_p or ω_n.

Solid black vertical line The ω_p; applies to all cases of sub-optimal control.

Solid coloured vertical lines The ω_p; applies to the case of sub-optimal control of the same colour and symbol.

Dashed black vertical line The ω_n; applies to all cases of sub-optimal control.

Dashed coloured vertical lines The ω_n; applies to the case of sub-optimal control of the same colour and symbol.

The natural frequency is the frequency at which the intrinsic impedance is real. In this study frequencies were considered at discrete bins, so the frequency bin closest to the natural frequency is treated as the natural frequency.

Sections 4.7 - 4.8 consider one size of buoy and three choices of ω_p. For instance, Fig. 4.33 on page 151 compares the PTO impedance for mass-damping-spring schemes using different values of ω_p (open coloured markers), to the ideal PTO impedance for optimal control (solid black markers). The dashed vertical black line at 2.2 rad/s indicates the ω_n. The solid vertical coloured lines indicate the position of the ω_p for each version of this control scheme.

Section 4.9 considers three sizes of buoy and one choice of ω_p. For instance, Fig. 4.27 on page 184 compares the monochromatic capture width for the mass-damping-spring scheme for three sizes of buoy (coloured open markers) to the ideal value of monochromatic capture width for all three sizes of buoy (closed black markers). The dashed vertical coloured lines indicate the ω_n of each sized buoy, while the solid black vertical line indicates the ω_p.

4.7 The impedance due to causal sub-optimal control schemes

The linear, causal version of impedance matching is implemented using PTO settings that are constants, resulting in a PTO force of the form (4.30). The PTO impedance at the operating frequency ω_p is chosen to be the complex conjugate of the intrinsic impedance at that frequency (4.8). At ω_p the ideal PTO impedance is:

$$\breve{Z}_{pto}[\omega_p] = B_p - i\left(\omega_p\left[m + M_p\right] - \frac{c}{\omega_p}\right) \tag{4.29}$$

Assuming a generalised PTO force with mass, damping and spring PTO coefficients, m_{pto}, b_{pto} and c_{pto}:

$$f_{pto}(t) = m_{pto}a(t) + b_{pto}u(t) + c_{pto}x(t) \tag{4.30}$$

then the PTO impedance expressed in the frequency domain then has the following general form:

$$Z_{pto}(\omega) = b_{pto} + i\left(\omega m_{pto} - \frac{c_{pto}}{\omega}\right) \tag{4.31}$$

Equating this to (4.29) and associating real and reactive terms gives $\breve{b}_{pto} = B_p$ and:

$$\omega_p \breve{m}_{pto} - \frac{\breve{c}_{pto}}{\omega_p} = \omega_p \left[m + M_p\right] - \frac{c}{\omega_p} \tag{4.32}$$

This is an equation with two unknowns, $\breve{m}_{pto}$ and $\breve{c}_{pto}$, and is as such indeterminate [117]. Any arbitrary value can be chosen for one of these PTO coefficients, and this will set the value of the other coefficient. While any pair of reactive PTO coefficients chosen in this manner will satisfy the ideal condition at ω_p (4.29), they will differ in how close they come to the ideal condition at frequencies other than ω_p. In the study presented here, three possible solutions of (4.32) will be presented. The first solution defines $\breve{c}_{pto} = c$, from which it follows that $\breve{m}_{pto} = m + M_p$. These give the PTO coefficients listed in (4.9). It must be emphasised that (4.9) is not the only solution of (4.32). It is the best solution because $\breve{c}_{pto} = c$ cancels the c/ω term in the net impedance at all frequencies (4.34), while $\breve{m}_{pto} = m + M_p$ cancels the ωm term in the net impedance (4.34). When speaking about the mass-damping-spring in the remainder, this refers to the best control possible using mass, damping, and spring terms (4.29). However, it is important to keep in mind that other pairs of values of $\breve{m}_{pto}$ and $\breve{c}_{pto}$ are nevertheless valid.

When considering alternative pairs of $\breve{m}_{pto}$ and $\breve{c}_{pto}$, two extreme cases are of interest. When $\breve{m}_{pto} = 0$ then this is known as the sub-optimal damping-spring scheme. When $\breve{c}_{pto} = 0$ then this is known as the sub-optimal mass-damping scheme.

When operating under monochromatic conditions, the mass-damping-spring, mass-damping, and damping-spring schemes are all equivalent. The damping-spring scheme is the most commonly used (for instance [118, 119]). It is important to note that the reason for this is convention and convenience, rather than the other options being incorrect. In much of the early work PTO impedance was written as damping and spring [110, 114], and this has set a precedent. While all the reactive control schemes are equivalent for monochromatic operation, under polychromatic operation the different types of reactive PTO coefficients result in different values of PTO impedance $Z(\omega)$ at frequencies other than ω_p.

The effects of the type of reactive PTO coefficient on the PTO is discussed in this section. First, the three types of reactive control are discussed: using three PTO settings: mass-damping-spring, or only two PTO settings: mass-damping or damping-spring. Lastly, real control is discussed: this is a sub-optimal technique which uses only damping. For each of these four types of causal sub-optimal control, equations for PTO and net impedance are derived. They are then plotted, in Fig. 4.8 - 4.15 for three values of operating frequency, $\omega_p = 1.5$ rad/s, $\omega_p = 2.2$ rad/s and $\omega_p = 2.6$ rad/s. For this particular size of WEC (2.5 m

radius), the natural frequency is $\omega_n = 2.2$ rad/s. These three operating frequencies were chosen because they are less than, equal to, and greater than the natural frequency, respectively. The plotting conventions described in § 4.6.7 are used.

4.7.1 Impedance due to a mass-damping-spring scheme

Equation (4.32) shows that when mass, damping and spring PTO coefficients are all available to make up the PTO impedance (4.31), then there is some freedom in the choice of the reactive PTO coefficients, m_{pto} and c_{pto}. Choosing the values of PTO coefficients defined in (4.9) to meet the ideal condition at ω_p (4.29) gives the following PTO impedance:

$$\breve{Z}_{pto}(\omega) = B_p - i\left(\omega\left[m + M_p\right] - \frac{c}{\omega}\right) \tag{4.33}$$

which results in a net impedance of:

$$\begin{aligned} Z_{net}(\omega) &= Z(\omega) + Z_{pto} \\ \breve{Z}_{net}(\omega) &= B(\omega) + i\left(\omega\left[m + M(\omega)\right] - \frac{c}{\omega}\right) + B_p - i\left(\omega[m + M_p] - \frac{c}{\omega}\right) \\ &= B(\omega) + B_p + i\omega\left[M(\omega) - M_p\right] \end{aligned} \tag{4.34}$$

Ideal values of impedance

Fig. 4.8 and Fig. 4.9 show the PTO impedance (4.33) and the net impedance (4.34) of the heaving WEC described above. The ideal value of PTO damping, the solid black markers in the top plot of Fig. 4.8, is the radiation damping $B(\omega)$, as shown in Fig. 4.7. The ideal value of the net damping, in the top plot of Fig. 4.9 is twice the radiation damping, which is the expected ideal condition (4.15).

The imaginary part of PTO impedance is the PTO reactance shown in the second plot of Fig. 4.8. Its ideal value is the intrinsic reactance, as shown in Fig. 4.16, multiplied by -1. The ideal value of net reactance, in the second plot of Fig. 4.9, is zero. This is because the ideal PTO impedance is the complex conjugate of the intrinsic impedance so cancels the intrinsic reactance at all frequencies (4.15). In all four plots of both these figures it can be seen that the impedance for a particular choice of ω_p equals the ideal value at ω_p, and remains close to the ideal value for frequencies near ω_p.

Impedance matching with the mass-damping-spring scheme

In (4.34) it can be seen that the physical mass and spring have been cancelled by the PTO reactance. In Fig. 4.9 it can be seen that, at frequencies neighbouring ω_p, the value of added mass does not vary too much from M_p and the added mass is almost entirely eliminated from the net impedance. For heave motion, the added mass does not vary much with frequency, that

is, $M(\omega) - m_\infty < m_\infty$. As a result, the PTO reactance, shown in the second plot in Fig. 4.8, is very close to its ideal value over all the frequencies shown, for any choice of ω_p. The resulting net impedance has an imaginary part, shown in the second plot in Fig. 4.9, that has values which are close to the ideal of zero reactance for frequencies close to ω_p.

The good fit of the PTO reactance to the ideal value in the second plot in Fig. 4.8 is the reason why the PTO coefficients defined in (4.9) are better than choosing a damping-spring or mass-damping scheme, and indeed why they are better than other pairs of m_{pto} and c_{pto} which satisfy the ideal conditions at ω_p (4.32). Any other choice of PTO coefficients would not completely cancel the physical mass and spring terms. This would make it necessary to cancel some of the intrinsic mass with a PTO spring term, or some of the intrinsic spring with a PTO mass term. The sections that follow show the extreme cases of this situation, the damping-spring and the mass-damping schemes. It will be shown that using PTO spring to cancel intrinsic mass, or PTO mass to cancel intrinsic spring, does not lead to a good fit of the PTO reactance to the ideal value for frequencies other than the ω_p.

In the plots of the net impedance, Fig. 4.9, the important result is the magnitude (the third plot), as the monochromatic capture width is a function of the net impedance magnitude. It can be seen that the magnitude of net impedance is close to the ideal value, at frequencies neighbouring the ω_p.

It is important to recall that the good performance of this scheme is in part due to the small variation in added mass in heave. While the conclusions do not apply directly to other modes of motion, the analysis presented here is a useful tool that can be applied to any mode of motion.

The points of note in Fig. 4.8 and Fig. 4.9 are that the mass-damping-spring scheme (4.9) gives a close fit of PTO reactance with the ideal value, by cancelling all the physical mass and spring (4.34), which gives a good fit of the net impedance magnitude with the ideal value at frequencies neighbouring ω_p.

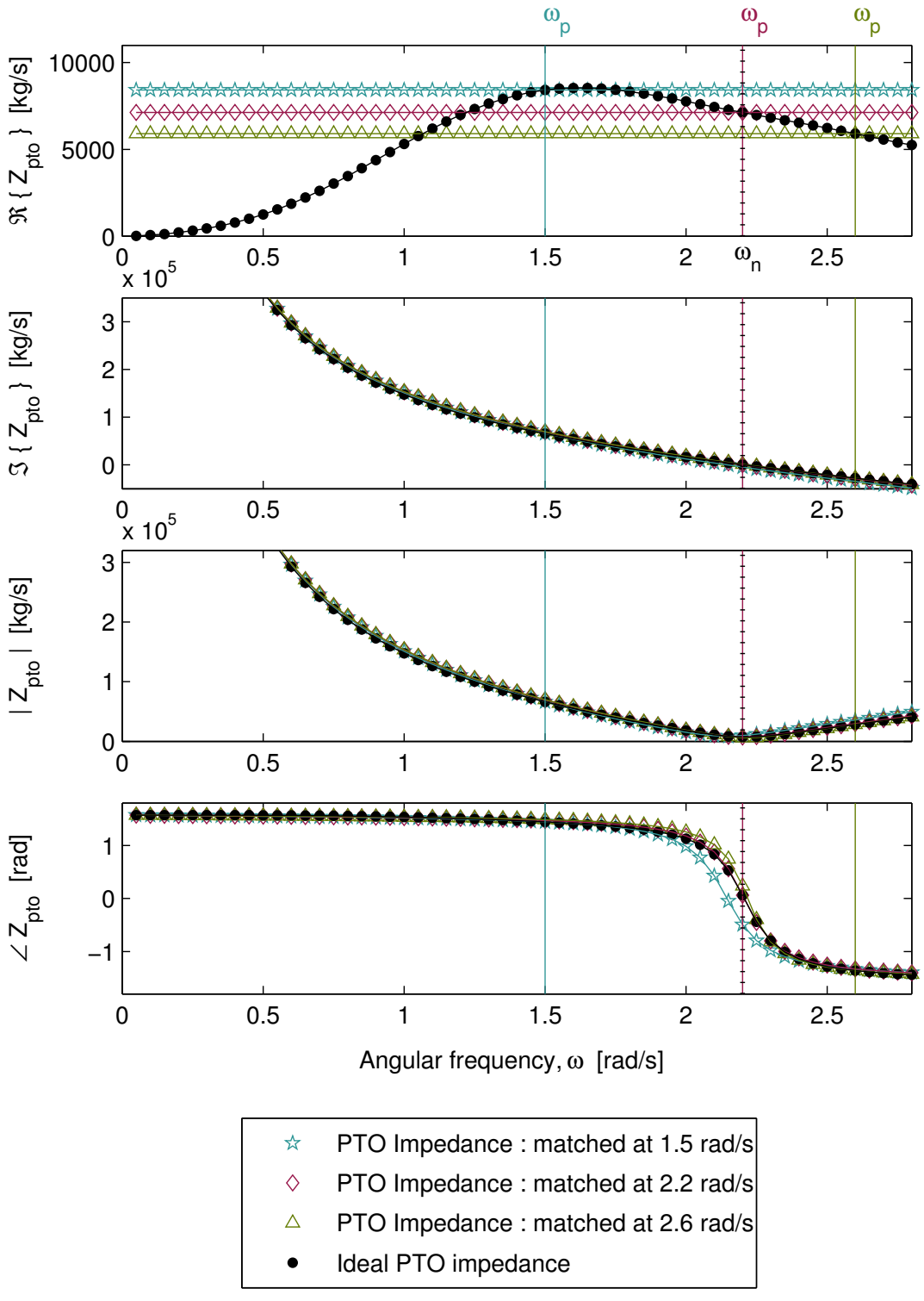

Figure 4.8: ***PTO impedance using mass, damping and spring PTO terms:*** *causal sub-optimal control (open markers) with impedance matched at three different operating frequencies is compared to acausal optimal control (solid markers).*

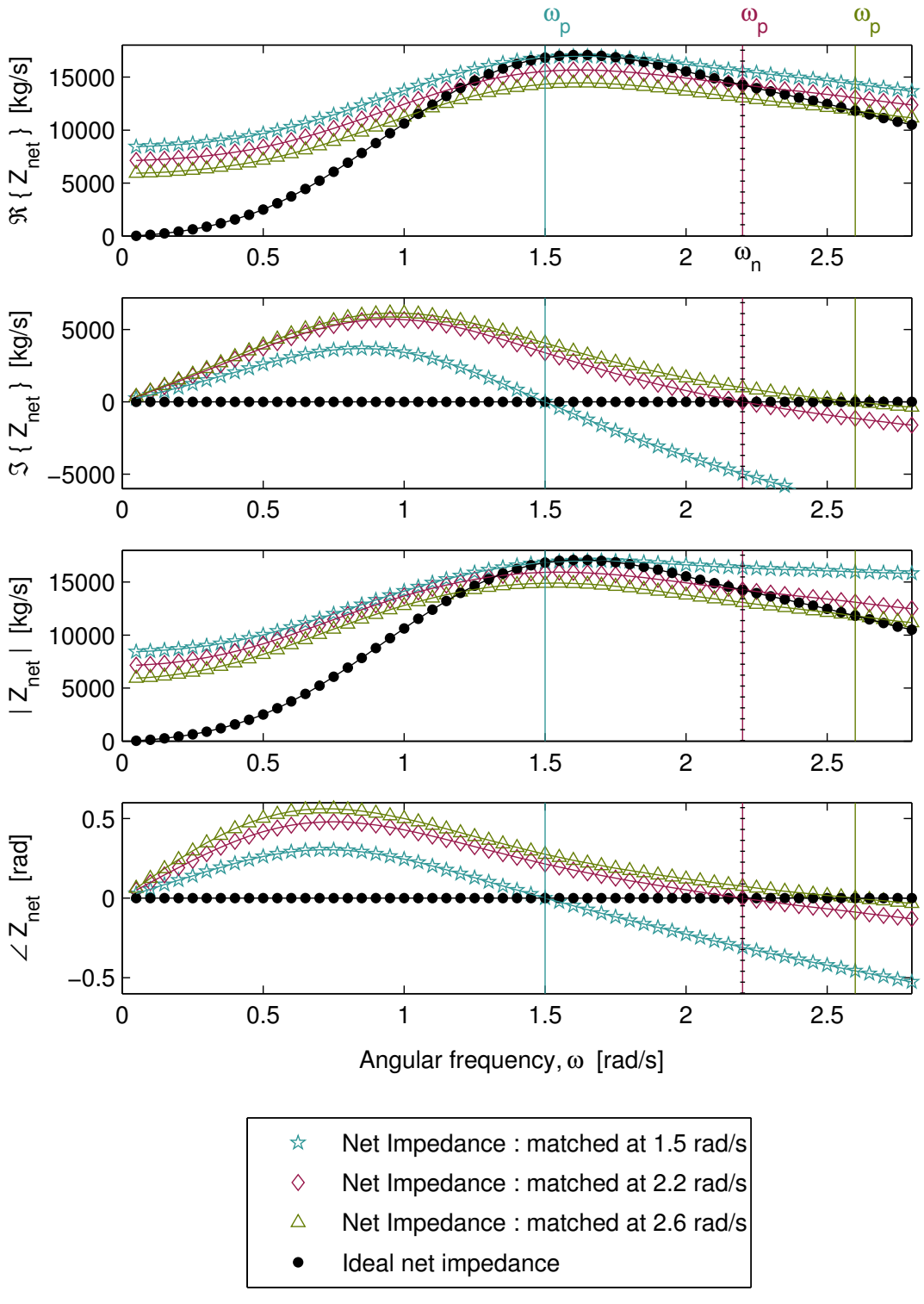

Figure 4.9: ***Net impedance using mass, damping and spring PTO terms:*** *causal sub-optimal control (open markers) with impedance matched at three different operating frequencies is compared to acausal optimal control (solid markers).*

4.7.2 Impedance due to a damping-spring scheme

If only the damping and spring PTO settings, b_{pto} and c_{pto}, are used, then the PTO force is:

$$f_{pto}(t) = b_{pto}u(t) + c_{pto}x(t) \tag{4.35}$$

In the frequency domain, the PTO impedance then has the following general form:

$$Z_{pto}(\omega) = b_{pto} + \frac{c_{pto}}{i\omega} \tag{4.36}$$

Setting the PTO impedance at ω_p to the ideal values (4.29) gives the following PTO settings:

$$\begin{aligned} \breve{b}_{pto} &= B_p \\ \breve{c}_{pto} &= \omega_p^2 \left[m + M_p\right] - c \end{aligned} \tag{4.37}$$

For monochromatic behaviour, these settings result in $Z_{pto}[\omega_p]$ as given by (4.29). For polychromatic behaviour, these settings give the following PTO impedance:

$$\breve{Z}_{pto}(\omega) = B_p - \frac{i}{\omega}\left(\omega_p^2 \left[m + M_p\right] - c\right) \tag{4.38}$$

which results in a net impedance of:

$$\begin{aligned} \breve{Z}_{net}(\omega) &= Z(\omega) + Z_{pto} \\ &= B(\omega) + i\left(\omega\left[m + M(\omega)\right] - \frac{c}{\omega}\right) + B_p - \frac{i}{\omega}\left(\omega_p^2\left[m + M_p\right] - c\right) \\ &= B(\omega) + B_p + i\left(\omega\left[m + M(\omega)\right] - \frac{\omega_p^2}{\omega}\left[m + M_p\right]\right) \end{aligned} \tag{4.39}$$

Fig. 4.10 is the PTO impedance and Fig. 4.11 is the net impedance. The first point of note is that the values of PTO reactance in the second plot of Fig. 4.10 largely depend on whether the ω_p is less than, equal to , or greater than the natural frequency ω_n. The reason for this is that the ideal PTO reactance $\Im\left\{\tilde{Z}_{pto}[\omega_j]\right\}$ passes through zero at ω_n, as the ω_n is by definition the frequency for which $\Im\{Z[\omega_n]\} = 0$. For a control scheme where $\omega_p = \omega_n$, the required PTO reactance is zero, so this is identical to real control, which will be described in § 4.8.4.

For a control scheme where $\omega_p > \omega_n$, the reactance required to attain the ideal value at ω_p is negative. As the PTO reactance consists only of spring, the hyperbolic shape characteristic of the spring coefficient is seen. This gives a poor fit to the ideal value at frequencies below the natural frequency. So when ω_p is at a frequency where the intrinsic reactance is dominated by inertia (as shown in Fig. 4.16), then a PTO reactance consisting of spring does not give a good fit to the ideal value at frequencies where the intrinsic reactance is dominated by spring.

For a control scheme where $\omega_p < \omega_n$, the reactance required to attain the ideal value at ω_p is

positive. Once again the hyperbolic shape due to a PTO reactance consisting of only spring can be seen. This gives a poor fit to the ideal value at frequencies above the natural frequency. So when ω_p is at a frequency where the intrinsic reactance is dominated by spring (as shown in Fig. 4.16), then a PTO reactance consisting of spring does not give a good fit to the ideal value, particularly at frequencies where the PTO reactance is dominated by inertia.

As the capture width is a function of the magnitude of the net impedance, the third plot in (Fig. 4.11) is important. For all three schemes with different values of ω_p, the net impedance is greater than the ideal value except at ω_p, where it equals the ideal value.

The points of note in Fig. 4.10 and Fig. 4.11 are that the damping-spring scheme (4.37) gives a poor fit of PTO reactance with the ideal value, in comparison with the mass-damper-spring scheme. Physical spring is cancelled (4.39), but there are errors when cancelling mass at frequencies different from ω_p. The magnitude of the net impedance is much higher than the ideal value at frequencies different from ω_p.

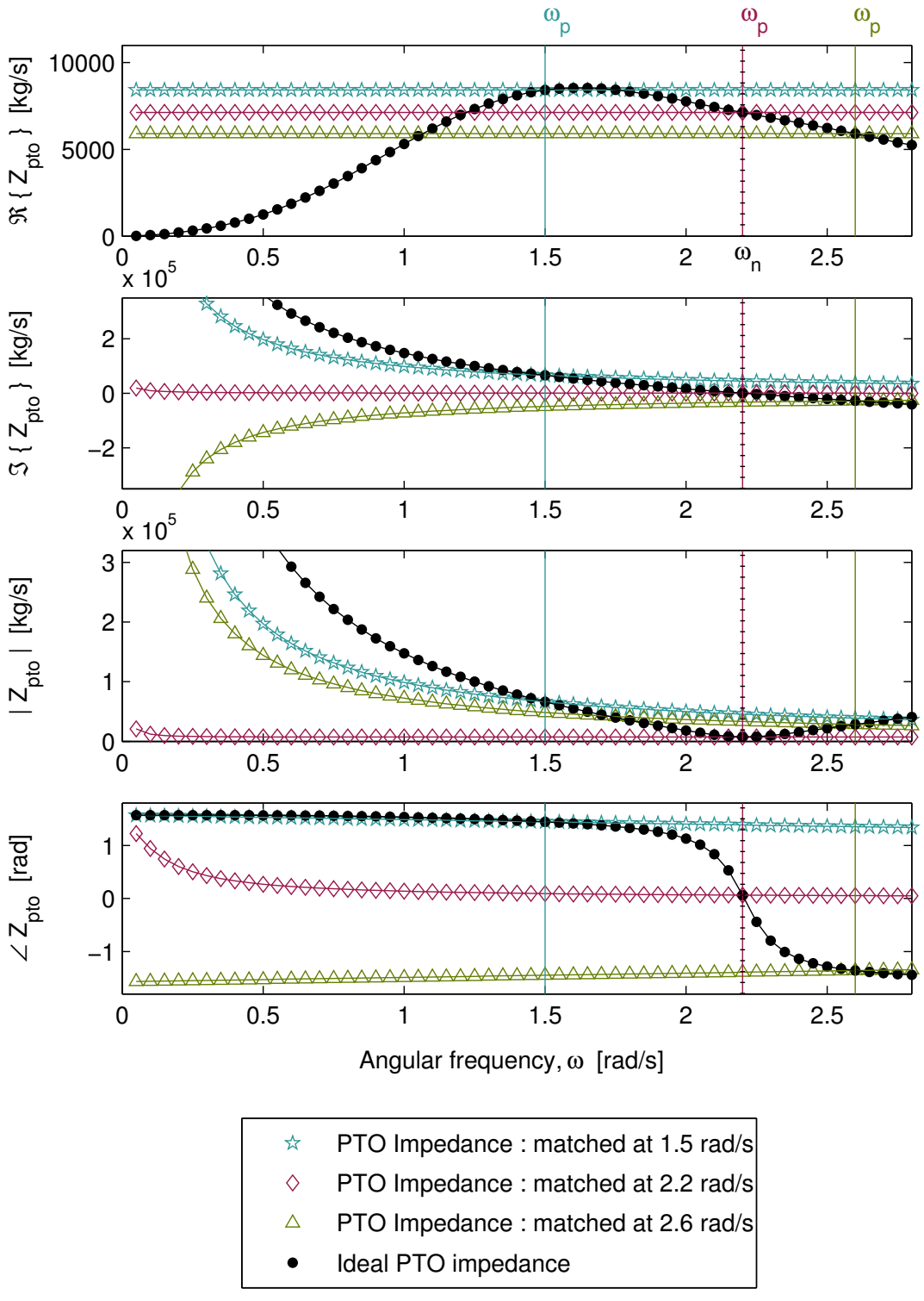

Figure 4.10: ***PTO impedance using damping and spring PTO terms:*** *causal sub-optimal control (open markers) with impedance matched at three different operating frequencies is compared to acausal optimal control (solid markers).*

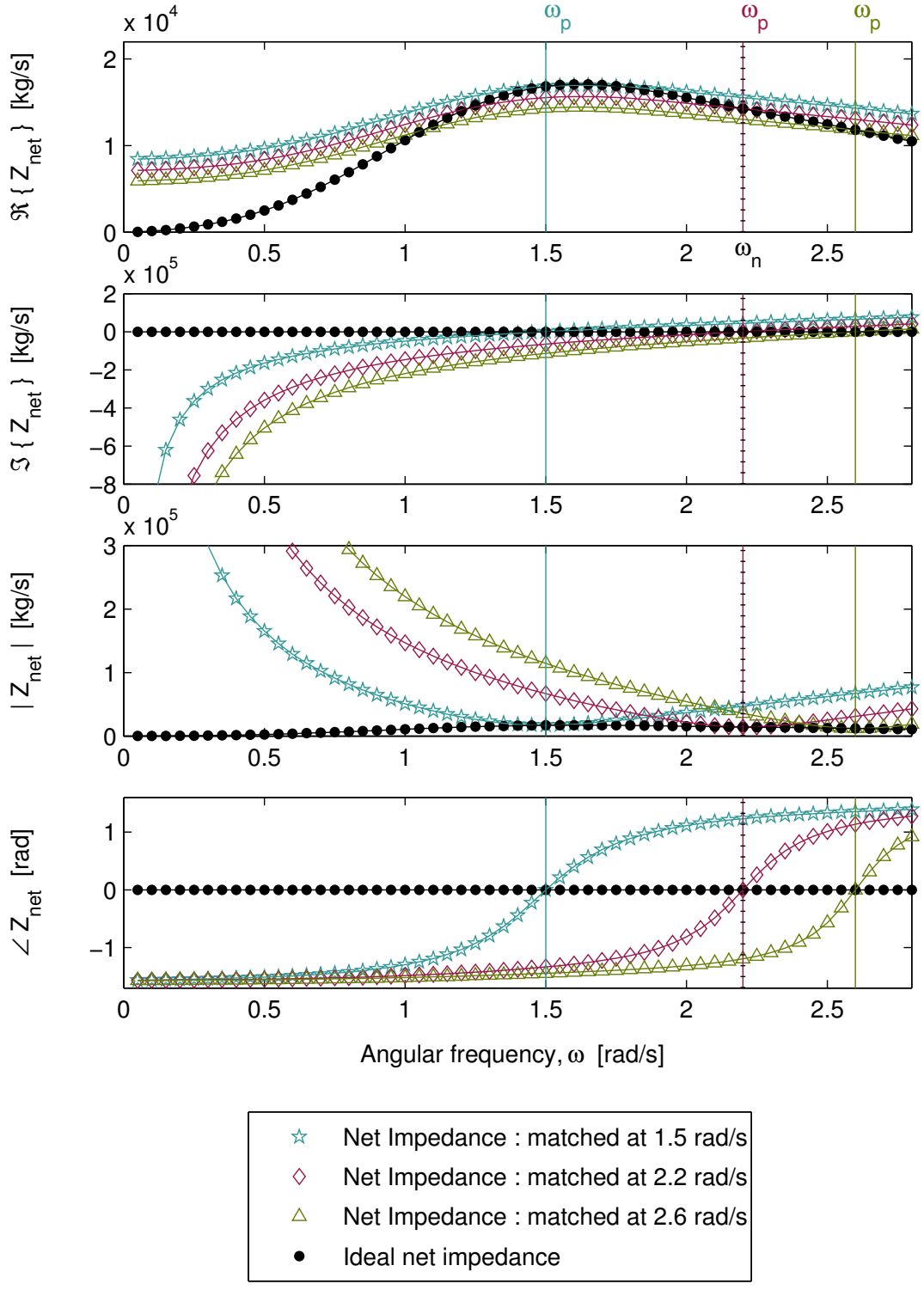

Figure 4.11: ***Net impedance using damping and spring PTO terms:*** *causal sub-optimal control (open markers) with impedance matched at three different operating frequencies is compared to acausal optimal control (solid markers).*

4.7.3 Impedance due to a mass-damping scheme

If only the mass and damping PTO settings, m_{pto} and b_{pto}, are used, then the PTO force is:

$$f_{pto}(t) = m_{pto}a(t) + b_{pto}u(t) \tag{4.40}$$

In the frequency domain, the PTO impedance then has the following general form:

$$Z_{pto}(\omega) = b_{pto} + i\omega m_{pto} \tag{4.41}$$

Setting the PTO impedance at ω_p to the ideal values (4.29) gives the following PTO settings:

$$\begin{aligned} \breve{m}_{pto} &= -\left(m + M_p - c/\omega_p^2\right) \\ \breve{b}_{pto} &= B_p \end{aligned} \tag{4.42}$$

For monochromatic behaviour, these settings result in $Z_{pto}[\omega_p]$ as given by (4.29). For polychromatic behaviour, these settings give the following PTO impedance:

$$\breve{Z}_{pto}(\omega) = B_p - i\omega\left(m + M_p - c/\omega_p^2\right) \tag{4.43}$$

which results in a net impedance of:

$$\begin{aligned} \breve{Z}_{net}(\omega) &= Z(\omega) + Z_{pto} \\ &= B(\omega) + i\left(\omega\left[m + M(\omega)\right] - \frac{c}{\omega}\right) + B_p - i\omega\left(m + M_p - c/\omega_p^2\right) \\ &= B(\omega) + B_p + i\left(\omega\left[M(\omega) - M_p\right] - \frac{c}{\omega} + \frac{c\omega}{\omega_p^2}\right) \end{aligned} \tag{4.44}$$

In this equation it can be seen that the physical mass has been cancelled, and that the added mass is adequately cancelled only where the added mass has a value close to M_p. At frequencies other than ω_p, spring is not cancelled, and the departure from the ideal value is larger the further the frequency is from ω_p. So while the damping-spring scheme cancels the intrinsic spring, but does not manage to cancel the intrinsic mass, the mass-damping scheme cancels only the physical mass, and does not manage to cancel the added mass and the intrinsic spring.

The imaginary part of the PTO impedance (second plot in Fig. 4.12) shows an interesting property of this control technique. As the PTO reactance is proportional to frequency, it is a straight line passing diagonally through zero. The ideal PTO impedance however has a shape (especially below ω_n) that is much closer to spring, i.e. inversely proportional to frequency. For $\omega_p \leq \omega_n$ (the scheme optimised at $\omega_p = 1.5$ rad/s), the bandwidth of the capture width (Fig. 4.21) is very narrow. This is largely because the gradients of the PTO impedance and the ideal PTO impedance have different signs. As a result, the net impedance magnitude (third plot in Fig. 4.13) differs greatly from the ideal value at frequencies other than ω_p.

For $\omega_p < \omega_n$ the gradient of the imaginary part of PTO impedance is positive; for $\omega_p = \omega_n$ it is zero; for $\omega_p > \omega_n$ it is negative. The gradient of the imaginary part of the ideal PTO impedance is negative, so this scheme favours operating frequencies higher than ω_n. Fig. 4.12 and Fig. 4.13 do not have enough data points to show clearly what happens at $\omega > \omega_n$. However, for $\omega_p > \omega_n$ (the scheme optimised at $\omega_p = 2.6$ rad/s) it can be seen that the PTO and net impedance magnitudes approach the ideal value at a much more shallow angle.

The points of note in Fig. 4.12 and Fig. 4.13 are that the mass-damping scheme (4.42) gives a poor fit of PTO reactance with the ideal value, compared to the mass-damping-spring scheme. Physical mass is cancelled (4.39), but there is poor cancellation of spring at frequencies far from ω_p. The magnitude of the net impedance is much higher than the ideal value at frequencies different from ω_p.

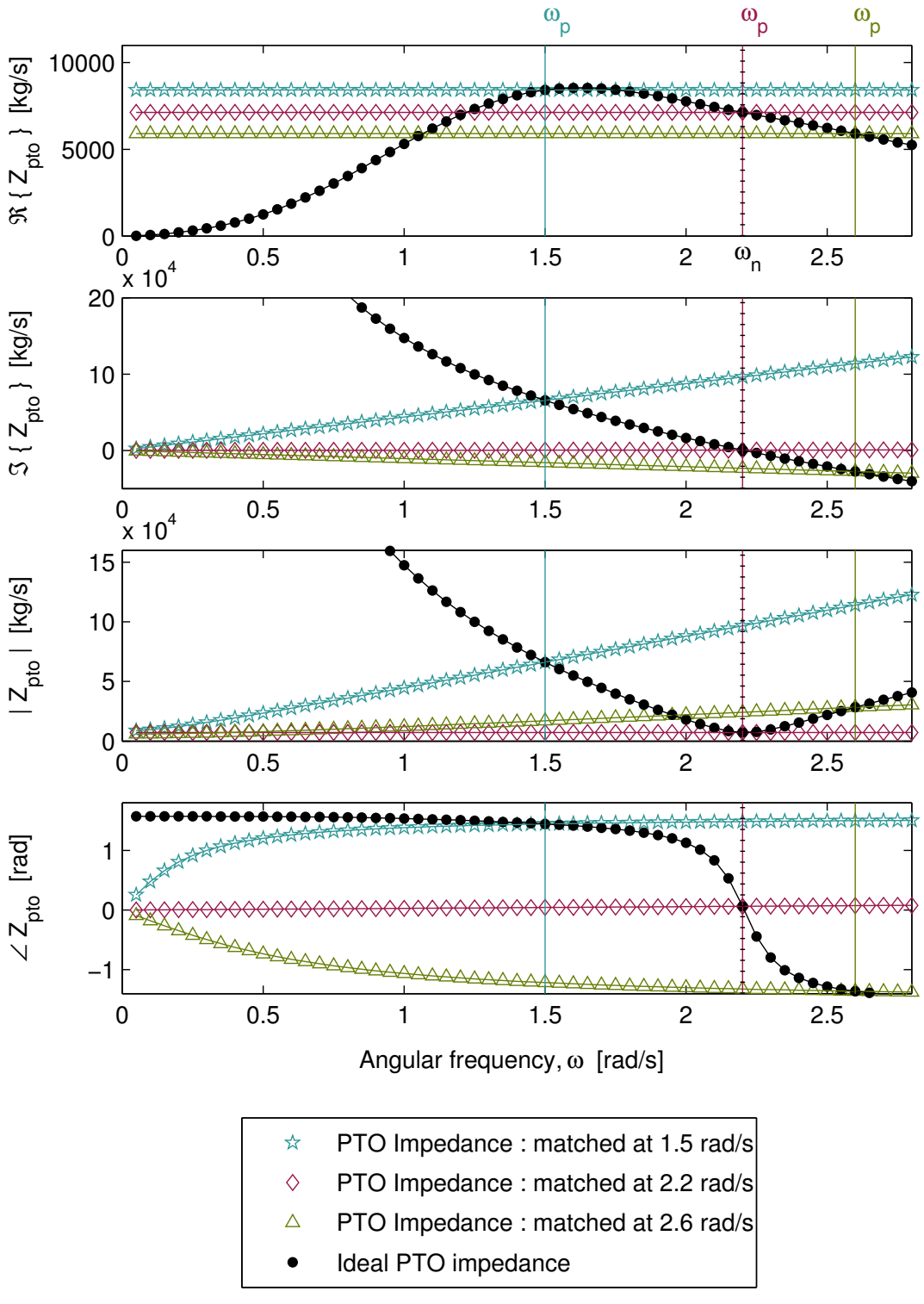

Figure 4.12: ***PTO impedance using mass and damping PTO terms:*** *causal sub-optimal control (open markers) with impedance matched at three different operating frequencies is compared to acausal optimal control (solid markers).*

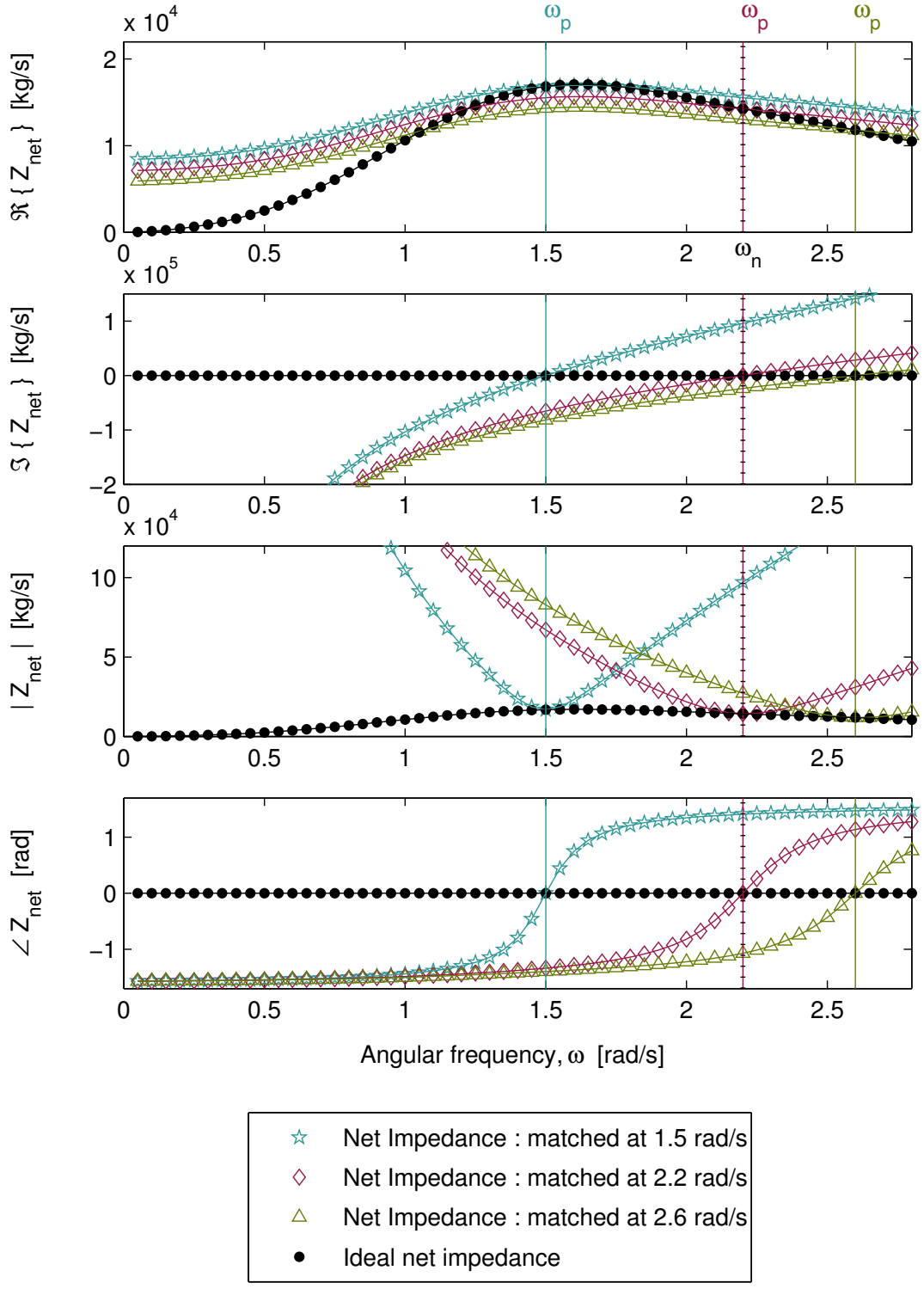

Figure 4.13: ***Net impedance using mass and damping PTO terms:*** *causal sub-optimal control (open markers) with impedance matched at three different operating frequencies is compared to acausal optimal control (solid markers).*

4.7.4 Impedance due to a causal damping scheme

It is particularly important to investigate PTO systems that provide only damping, as damping PTO is cheaper and less complex (easier to design) than a PTO system that provides reactive elements (such as mass and spring). For this reason, it is an attractive option for developers who wish to get sea-trial experience without the cost and risk of a reactive PTO system. Indeed, it is currently being considered by one of the leading commercial devices under development, the AWS [47]. Given that this technique is suitable for testing full-scale prototypes, it is important to understand how much additional energy could be absorbed by upgrading to a reactive PTO system.

When there is only a PTO damping coefficient b_{pto} available:

$$f_{pto}(t) = b_{pto}u(t) \tag{4.45}$$

and the (frequency domain) PTO impedance is always real:

$$Z_{pto}(\omega) = b_{pto} \tag{4.46}$$

For this reason, sub-optimal control using only PTO damping is often known as real control. With a real PTO impedance, is not possible to achieve impedance matching at an arbitrary frequency $\tilde{Z}_{pto}[\omega_p] = Z^*[\omega_p]$, as there is no PTO reactance with which to cancel the intrinsic reactance. The optimum condition at ω_p when only damping is available is [120]:

$$\tilde{Z}_{pto}[\omega_p] = |Z[\omega_p]| \tag{4.47}$$

Setting the PTO impedance (4.46) at ω_p to (4.29) gives the following value of PTO damping:

$$\breve{b}_{pto} = \sqrt{B_p^2 + \left(\omega_p \left[m + M_p\right] - c/\omega_p\right)^2} \tag{4.48}$$

This is also the value of $Z_{pto}[\omega_p]$ and indeed the impedance at all frequencies, $Z_{pto}(\omega)$:

$$\breve{Z}_{pto}(\omega) = \sqrt{B_p^2 + \left(\omega_p \left[m + M_p\right] - c/\omega_p\right)^2} \tag{4.49}$$

Although indicated as a function of frequency, the PTO impedance is a constant, as shown by the straight lines in Fig. 4.14. This PTO impedance results in a net impedance of:

$$\breve{Z}_{net}(\omega) = B(\omega) + \sqrt{B_p^2 + \left(\omega_p \left[m + M_p\right] - c/\omega_p\right)^2} + i\left(\omega\left[m + M(\omega)\right] - \frac{c}{\omega}\right) \tag{4.50}$$

Fig. 4.14 is the PTO impedance (4.49) and Fig. 4.15 is the net impedance (4.50). The magnitude of the net impedance is particularly interesting. Like the damping-spring and the mass-damping schemes, the magnitude of the net impedance is roughly U-shaped. However, unlike the

damping-spring and mass-damping schemes where the minima are the ideal values at each ω_p, the minima of the net impedance magnitudes for the damping schemes are all at the natural frequency, regardless of choice of ω_p. The scheme with $\omega_p = \omega_n$ has a minima that is the ideal value of net impedance. For $\omega_p \neq \omega_n$, the minima is higher than the ideal value.

Likewise, it should be noted that for the real part of the PTO impedance, shown in the first plot of Fig. 4.14, the damping only equals the ideal value at ω_p when $\omega_p = \omega_n$. For $\omega_p \neq \omega_n$, the PTO damping is higher than the ideal value at ω_p. Noting that the performance indicator monochromatic capture width is a function of both the magnitude of the net impedance and the real part of the PTO impedance, it can be seen that the ideal performance will only be met when $\omega_p = \omega_n$.

The points of note in Fig. 4.14 and Fig. 4.15 are that the damping scheme is not able to match the ideal value of PTO reactance at an arbitrary operating frequency. Instead the ideal *magnitude* of the PTO impedance is ensured at ω_p by the choice of the damping PTO coefficient (4.48). The magnitude of net impedance has a minima at ω_n, and its value at this minima only equals the ideal value at $\omega_p = \omega_n$.

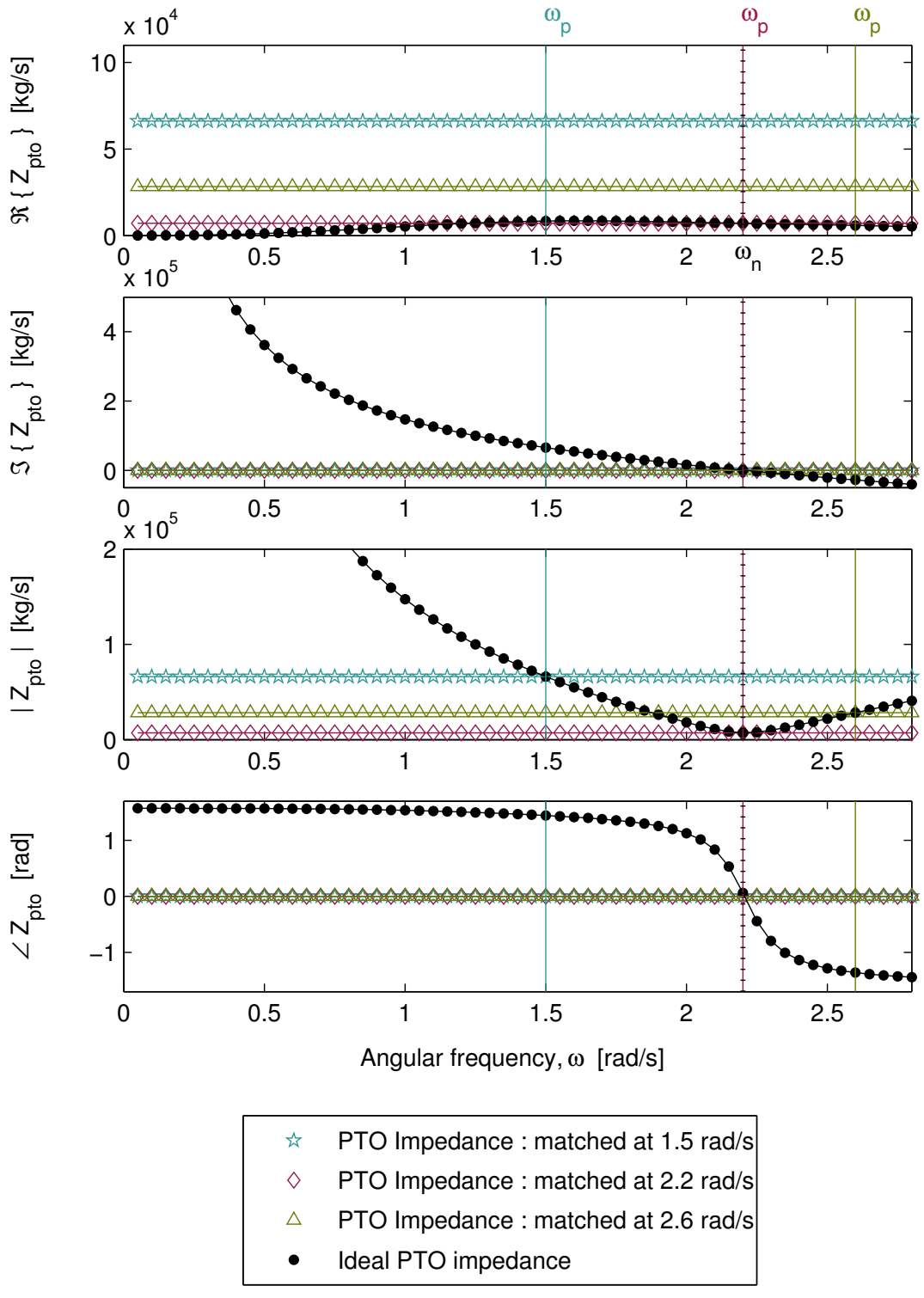

Figure 4.14: ***PTO impedance using damping PTO term only:*** *causal sub-optimal control (open markers) with impedance matched at three different operating frequencies is compared to acausal optimal control (solid markers).*

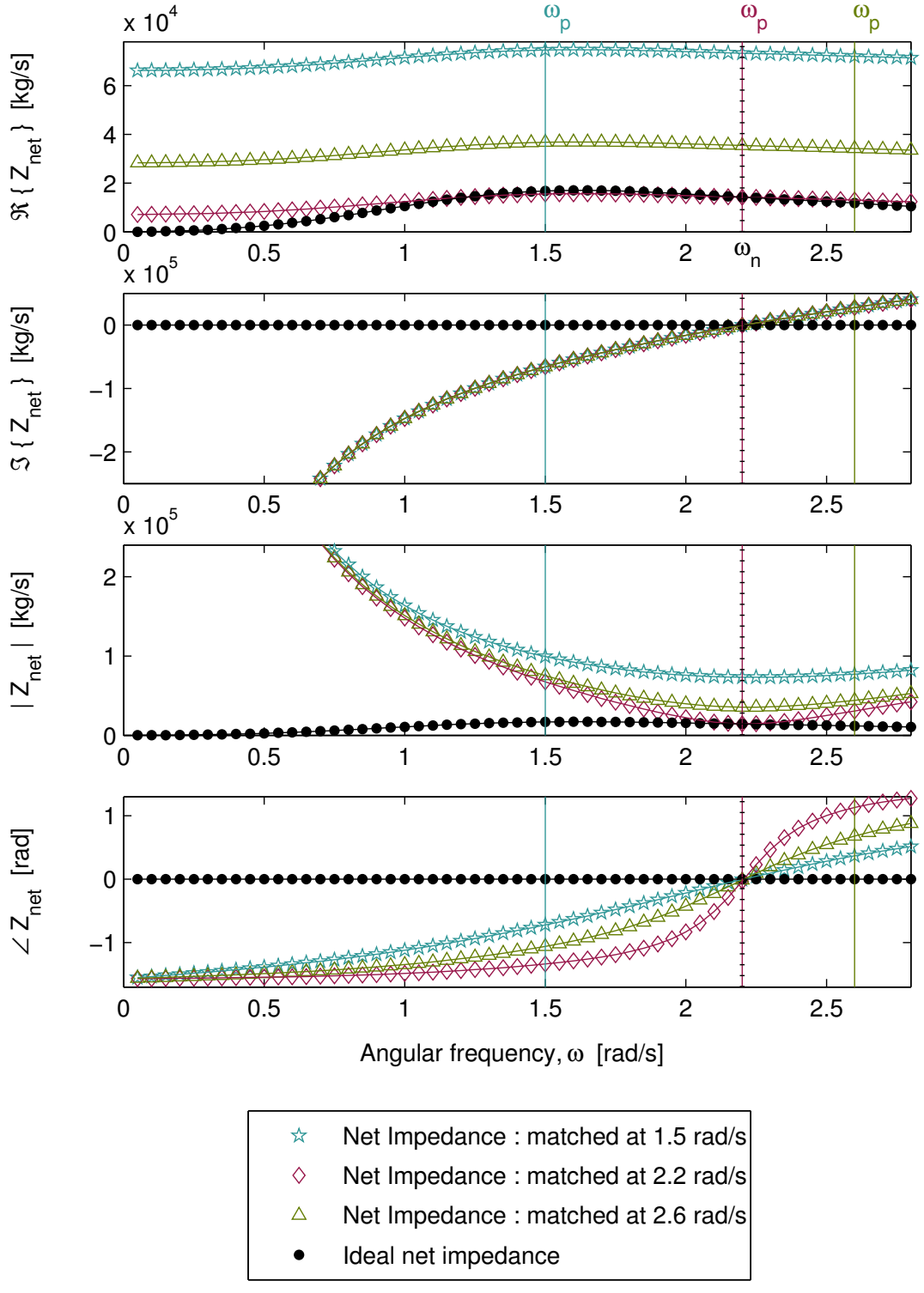

Figure 4.15: ***Net impedance using damping PTO term only:*** *causal sub-optimal control (open markers) with impedance matched at three different operating frequencies is compared to acausal optimal control (solid markers).*

4.7.5 Comparison of the effects of impedance matching schemes on impedance

The PTO impedance was shown for a particular geometry (Appendix A), using the mass-damping-spring scheme (Fig. 4.8), the damping-spring scheme (Fig. 4.10), the mass-damping scheme (Fig. 4.12), and the damping only scheme (Fig. 4.14). It can be seen that the mass-damping-spring scheme is superior because it is possible to achieve close to the reactive part of the ideal PTO impedance. This method is not very sensitive to the choice of operating frequency (ω_p): three very different values of ω_p gave values of PTO and net impedance Fig. 4.9 very close to each other. In contrast, the schemes using only one or two PTO coefficients are very sensitive to the choice of operating frequency. For frequencies far from the ω_p, the schemes with two PTO coefficients do not achieve close to the reactive part of the ideal PTO impedance. For frequencies far from the natural frequency, ω_n, the scheme with only one PTO coefficient does not achieve close to the reactive part of the ideal PTO impedance.

Another good way to compare these impedance matching schemes is to examine the equations of PTO impedance. Table 4.1 summarises these equations. The first line is for impedance matching at all frequencies. This is the optimum value of PTO impedance, against which all causal control schemes must be measured. The mass-damping-spring reactive control is the most effective because it has the correct value of spring reactance (c/ω) at all frequencies, and close to the correct value of inertial reactance at most frequencies. The inertial reactance,

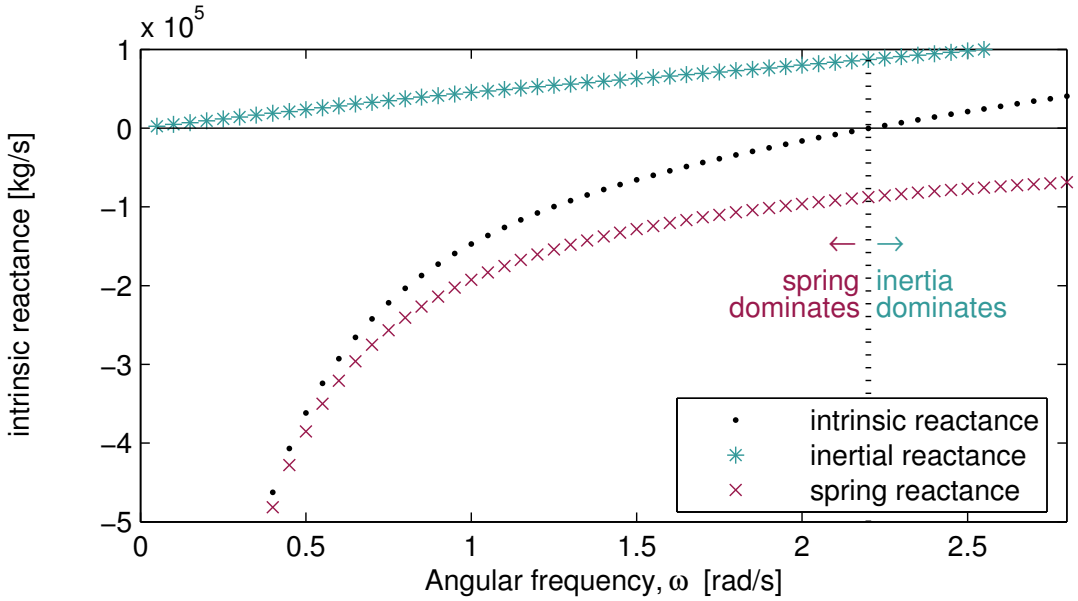

Figure 4.16: ***Inertial and spring contributions to intrinsic reactance:*** *below the natural frequency, intrinsic reactance is dominated by spring, while above the natural frequency, it is dominated by inertia.*

$\omega\,[m + M_p]$, only differs from the ideal value, $\omega\,[m + M(\omega)]$, by the small amount with which $M[\omega_p]$ deviates from $M(\omega)$. For many geometries, and certainly for the one studied here, the range of values of added mass does not vary much (over its domain of frequency) from the average value.

The damping-spring reactive control has the correct value of spring reactance (c/ω), but inertial reactance ($\frac{\omega_p^2}{\omega}\,[m + M_p]$) that differs from the ideal value $\omega\,[m + M(\omega)]$ at frequencies far from ω_p. This form of control is thus good at operating frequencies where the intrinsic reactance is dominated by spring. In Fig. 4.16 it can be seen that spring dominates the intrinsic reactance above the natural frequency.

The mass-damping reactive control has spring reactance $c\frac{\omega}{\omega_p^2}$ that differs from the ideal value $\frac{c}{\omega}$ by a large amount at frequencies far from ω_p. The inertial reactance $\omega\,[m + M_p]$, only differs from the ideal value, $\omega\,[m + M(\omega)]$, by the small amount with which $M[\omega_p]$ deviates from $M(\omega)$. This form of control is thus better at operating frequencies where the intrinsic reactance is dominated by inertia. In Fig. 4.16 it can be seen that inertia dominates below the natural frequency.

Impedance matching scheme	$Z_{pto}(\omega) =$	**real part** $+$	**reactive part**
(1) optimal	$\tilde{Z}_{pto}(\omega) =$	$B(\omega)$	$-i\left(\omega\left[m+M(\omega)\right]-\frac{c}{\omega}\right)$
(2) mass-damping-spring	$\breve{Z}_{pto}(\omega) =$	B_p	$-i\left(\omega\left[m+M_p\right]-\frac{c}{\omega}\right)$
(3) damping-spring	$\breve{Z}_{pto}(\omega) =$	B_p	$-i\left(\frac{\omega_p^2}{\omega}\left[m+M_p\right]-\frac{c}{\omega}\right)$
(4) mass-damping	$\breve{Z}_{pto}(\omega) =$	B_p	$-i\left(\omega\left[m+M_p\right]-c\frac{\omega}{\omega_p^2}\right)$
(5) damping	$\breve{Z}_{pto}(\omega) =$	$\sqrt{B_p^2+\left(\omega_p\left[m+M_p\right]-c/\omega_p\right)^2}$	

Table 4.1: ***Comparison of PTO impedance due to impedance matching schemes:*** *(1) PTO impedance due to optimal control; the impedance is matched at all ω. (2) PTO impedance due to sub-optimal control (the impedance is matched at ω_p) using mass, damping and spring PTO settings (reactive control). (3) PTO impedance due to sub-optimal control (the impedance is matched at ω_p) using damping and spring PTO settings (reactive control). (4) PTO impedance due to sub-optimal control (the impedance is matched at ω_p) using mass and damping PTO settings (reactive control). (5) PTO impedance due to sub-optimal control (the impedance is matched at ω_p) using a damping PTO setting only (real control).*

4.8 The performance of causal sub-optimal control schemes

The definitions of PTO and net impedance given in § 4.7 are now used to define capture width. Monochromatic capture width (4.24) and normalised capture width (4.25) are plotted for the same geometry and the same three values of operating frequency used in § 4.7. Results are compared to the capture width for the ideal case, which is indicated by the solid black markers on the plots. Substituting the ideal values of PTO damping $\tilde{B}_{pto}[\omega_j] = B[\omega_j]$ and net impedance magnitude $\left|\tilde{Z}_{net}[\omega_j]\right| = 2B[\omega_j]$ into capture width (4.24) gives:

$$\tilde{C}^s_W[\omega_j] = \frac{4g}{\omega_j^2}\,\frac{B[\omega_j]B[\omega_j]}{(2B[\omega_j])^2} = \frac{g}{\omega_j^2} \tag{4.51}$$

which is the upper limit [56], as discussed in § 4.6.2.

4.8.1 Performance of a causal mass-damping-spring scheme

Substituting the PTO (4.33) and net impedance (4.34) due to the mass-damping-spring scheme into capture width (4.24) gives:

$$\breve{C}^s_W[\omega_j] = \frac{4g}{\omega_j^2}\,\frac{B_p B[\omega_j]}{\left(B_p + B[\omega_j]\right)^2 + \left(\omega_j\left[M[\omega_j] - M_p\right]\right)^2} \tag{4.52}$$

Fig. 4.17 shows this function plotted for three different values of operating frequency ω_p. To show more clearly the differences between sub-optimal and optimal control, a plot of the normalised capture width has also been provided (Fig. 4.18). This expresses the performance due to sub-optimal control as a percentage of the performance of optimal control. The upper limit is no longer a hyperbola but the horizontal line at 100%. The bandwidth is at its broadest when $\omega_p = \omega_n$. This is not immediattely obvious from Fig. 4.18 because high frequency data is not included, and must be inferred by studying the gradient of the normalised capture width at the highest frequency shown on the plot.

In Chapter 5 it will be shown that it is the performance at frequencies around the ω_p that is particularly important. Fig. 4.17 shows that, at frequencies neighbouring the ω_p the capture width is very close to the ideal value. Thus the potential for improving performance by using a control scheme that requires forecasts is not very large. This has been commented on by Niato [121]. Next it will be shown that the conclusion that acausal control does not give large improvements over causal control only holds for the mass-damping-spring scheme. The other reactive control schemes do not perform as well.

The points of note in Fig. 4.17 and Fig. 4.18 are that the mass-damping-spring scheme (4.9) has a monochromatic capture width close to the ideal value at a broad range of frequencies close to ω_p. The bandwidth of the normalised capture width is broadest for $\omega_p = \omega_n$

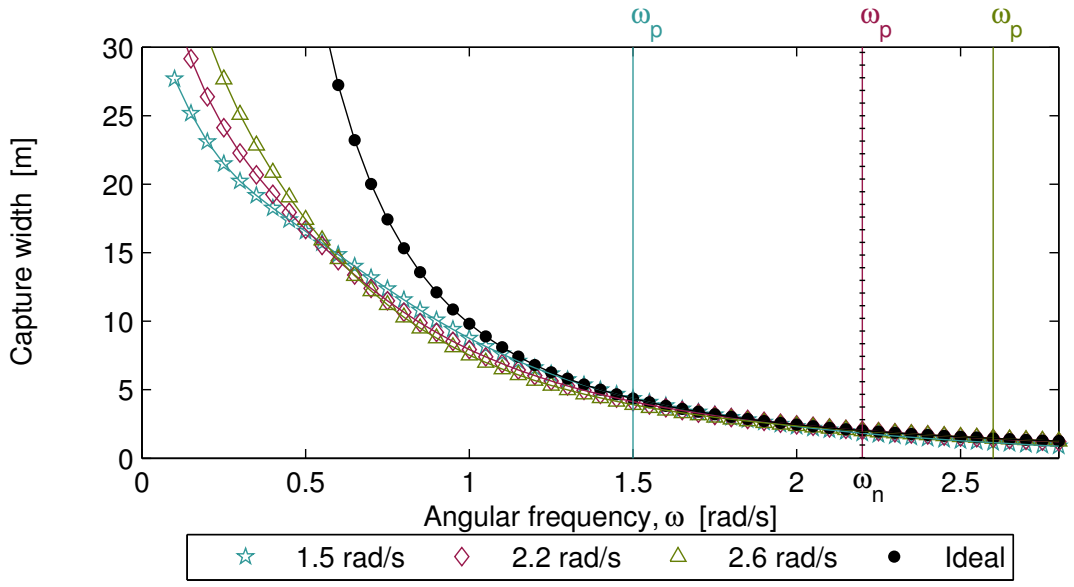

Figure 4.17: ***Capture width using a mass-damping-spring scheme:*** *causal sub-optimal control (open markers) with impedance matched at three different operating frequencies is compared to acausal optimal control (solid markers).*

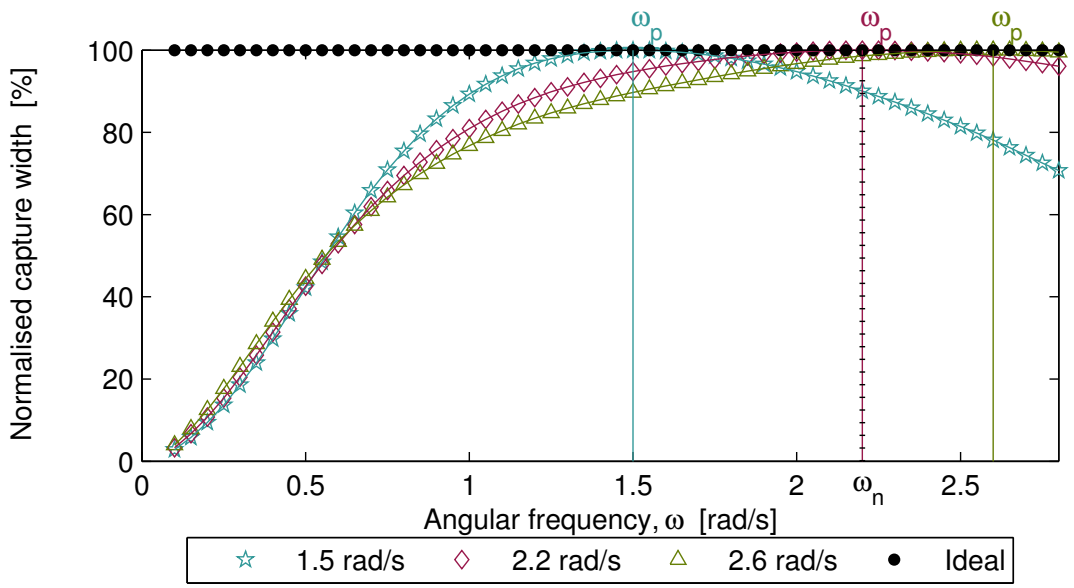

Figure 4.18: ***Normalised capture width using a mass-damping-spring scheme:*** *causal sub-optimal control (open markers) with impedance matched at three different operating frequencies is compared to acausal optimal control (solid markers).*

4.8.2 Performance of a causal damping-spring scheme

Substituting the PTO (4.38) and net impedance (4.39) for a damping-spring scheme into capture width (4.24) gives:

$$\breve{C}_W^s[\omega_j] = \frac{4g}{\omega_j^2} \frac{B_p B[\omega_j]}{\Big(B_p + B[\omega_j]\Big)^2 + \Big(\omega\left[m + M[\omega_j]\right] - \frac{\omega_p^2}{\omega}\left[m + M_p\right]\Big)^2} \tag{4.53}$$

Fig. 4.19 is the monochromatic capture width defined in (4.53) and Fig. 4.20 is the associated normalised capture width. Comparing the performance of the damping-spring scheme (Fig. 4.19 - 4.20) to that of the mass-damping-spring scheme (Fig. 4.17 - 4.18), it can be seen that the latter is far superior. Using only two PTO settings results in a much narrower bandwidth of capture width. This means that while there is good performance at the operating frequency, there is poor performance at frequencies remote from the operating frequency. In fact, there is poor performance even for small values of $|\omega_p - \omega_n|$.

In § 5.2 it will be shown that the (monochromatic) capture width does the job of a filter that acts on the wave spectrum. When the monochromatic capture width is very narrow, it acts like a bandpass filter, so that only energy within the passband (of frequencies) is intercepted. Wave energy that is not within the passband is not captured. Using only two PTO settings results in performance that is far more *tuned* to the operating frequency than when using three PTO settings. In fact, causal sub-optimal control using impedance matching is often referred to as tuning a WEC to a given operating frequency. Salter [21] objected to the term *tuning* on the grounds that it implied a narrow bandwidth was a desirable quality, when in fact a broad bandwidth (centred on the spectrum of the sea state) is preferable.

In Fig. 4.19, the scheme with the lowest ω_p has a maxima of monochromatic capture width not at the ω_p, but at a frequency lower than the ω_p. This is not an error but simply a consequence of the steep slope of the ideal value of monochromatic capture width at that point. As the frequency bins are sufficiently close together and the bandwidth of the damping-spring monochromatic capture width is broad enough, this effect is shown on the graph. In fact the maxima for all the damping-spring plots are at frequencies slightly lower than the ω_p. It is not noticeable for the schemes with higher values of ω_p because the frequency bins are not close enough to show this. This can be seen by comparing the more symmetrical normalised capture width plots with the corresponding plots of monochromatic capture width, and noting the position of the points before and after the ω_p.

The points of note in Fig. 4.19 and Fig. 4.20 are that the performance of the damping-spring scheme (4.37) touches the ideal value of monochromatic capture width at the ω_p, but drops to zero on either side. This acts like a pass-band filter. The peak frequency of this filter is may be slightly lower than the ω_p.

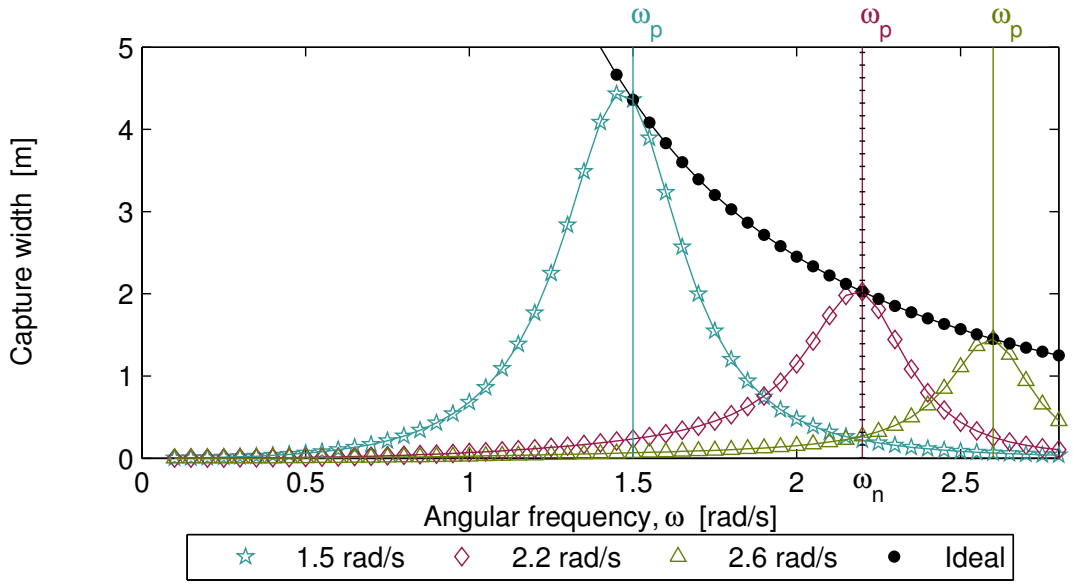

Figure 4.19: ***Capture width using a damping-spring scheme:*** *causal sub-optimal control (open markers) with impedance matched at three different operating frequencies is compared to acausal optimal control (solid markers).*

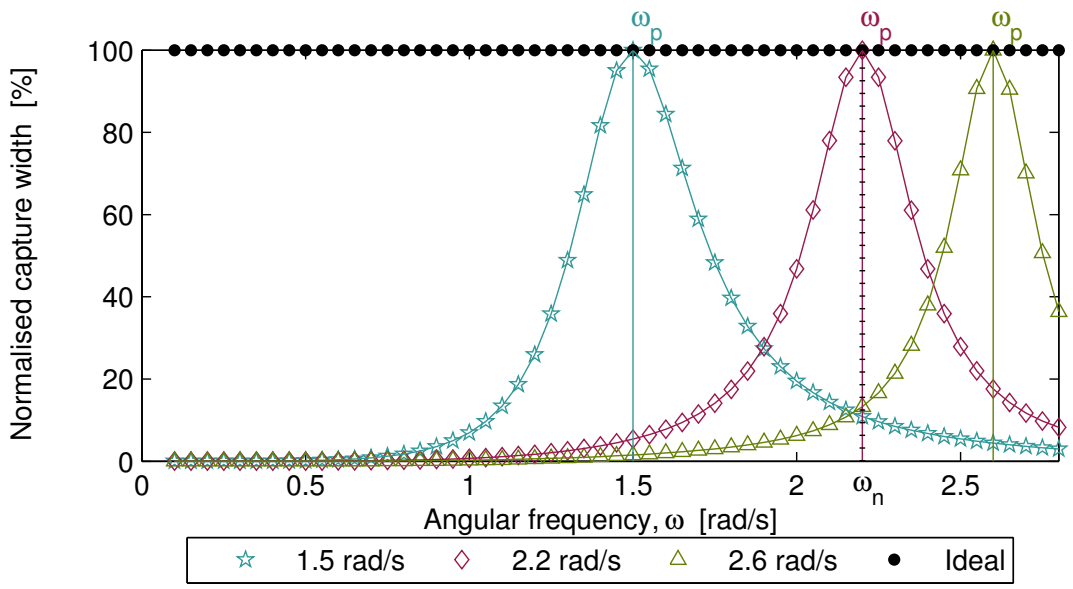

Figure 4.20: ***Normalised capture width using a damping-spring scheme:*** *causal sub-optimal control (open markers) with impedance matched at three different operating frequencies is compared to acausal optimal control (solid markers).*

4.8.3 Performance of a causal mass-damping scheme

Substituting the PTO (4.43) and net impedance (4.44) resulting from a mass-damping scheme into capture width (4.24) gives:

$$\breve{C}_W^s[\omega_j] = \frac{4g}{\omega_j^2} \frac{B_p B[\omega_j]}{\Big(B_p + B[\omega_j]\Big)^2 + \Big(\omega\left[M[\omega_j] - M_p\right] - \frac{c}{\omega} + \frac{c\omega}{\omega_p^2}\Big)^2} \tag{4.54}$$

Fig. 4.21 is the (monochromatic) capture width given by (4.54) and Fig. 4.22 is the associated normalised capture width. Comparing the performance of the mass-damping scheme (Fig. 4.21 - 4.22) to that of the mass-damping-spring scheme (Fig. 4.17 - 4.18), it is clear that the scheme with three PTO settings is far superior. Once again, using only two PTO settings results in a much narrower bandwidth of capture width.

In Fig. 4.21 the peak of the monochromatic capture width appears to be at the ω_p, rather than slightly below it, as seen for the lowest ω_p of the damping-spring scheme in Fig. 4.19. This is only because the frequency bins are spaced too far apart and the bandwidth is not broad enough. If the frequency bins were closer then the maxima would always be at a frequency slightly lower than the peak frequency. Once again, this can be seen by comparing the more symmetrical normalised capture width plots with the corresponding plots of monochromatic capture width, and noting the position of the points before and after the ω_p.

The points of note in Fig. 4.21 and Fig. 4.22 are that the mass-damping scheme (4.42) also has a monochromatic capture width that touches the ideal value at ω_p, then drops to zero on either side. The bandwidth for the $\omega_p < \omega_n$ scheme is narrower than is seen in the damping-spring scheme.

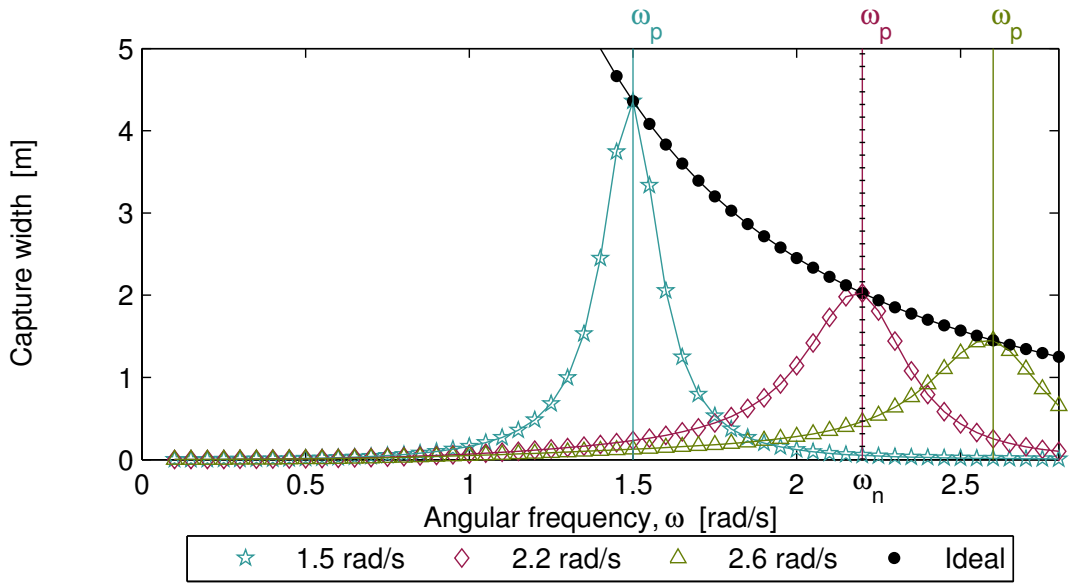

Figure 4.21: ***Capture width using a mass-damping scheme:*** *causal sub-optimal control (open markers) with impedance matched at three different values of operating frequency ω_p is compared to acausal optimal control (solid markers).*

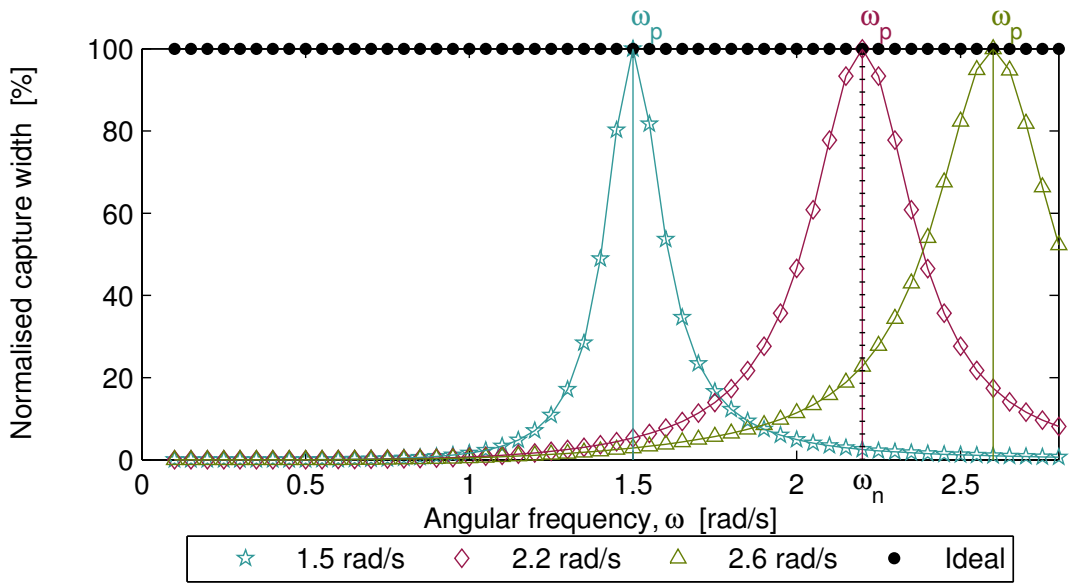

Figure 4.22: ***Normalised capture width using a mass-damping scheme:*** *causal control (open markers) for three different values of operating frequency ω_p is compared to acausal optimal control (solid markers).*

4.8.4 Performance of a causal damping scheme

Substituting the PTO (4.49) and net impedance (4.50) due to real control into capture width (4.24) gives:

$$\breve{C}_W^s[\omega_j] = \frac{4g}{\omega_j^2} \frac{B[\omega_j]\sqrt{B_p^2 + \left(\omega_p\left[m + M_p\right] - \frac{c}{\omega_p}\right)^2}}{\left(B[\omega_j]\sqrt{B_p^2 + \left(\omega_p\left[m + M_p\right] - \frac{c}{\omega_p}\right)^2}\right)^2 + \left(\omega\left[m + M[\omega_j]\right] - \frac{c}{\omega}\right)^2} \tag{4.55}$$

Fig. 4.23 is the monochromatic capture width for (4.55) and Fig. 4.24 is the associated normalised capture width. When using reactive control, the ideal capture width can be attained at the chosen operating frequency. However, when using real control, the capture width only reaches the ideal value at the operating frequency ω_p, when this is also the natural frequency ω_n (see the scheme with $\omega_p = 2.2$ rad/s in Fig. 4.23). In Fig. 4.24 it can be clearly seen that the optimisation for a given ω_p has been effective: at $\omega_j = \omega_p$, the highest capture width is given by the control scheme that has optimised for that frequency. While (4.49) is the best scheme possible when the PTO system can provide damping only, it is clear that reactive control (Fig. 4.18) will lead to more energy capture, particularly at operating frequencies far from the natural frequency (high values of $|\omega_p - \omega_n|$).

Fig. 4.24 shows an interesting peculiarity of real control: the control scheme using an operating frequency that is on the natural frequency ($\omega_p = \omega_n = 2.2$ rad/s) has a narrow bandwidth compared to the control schemes with operating frequencies not at the natural frequency. For schemes where the operating frequency is close to the natural frequency ($\omega_p = 2.6$ rad/s), the peak value of capture width remains close to the natural frequency. In sea states with broad spectra that are centred near the natural frequency, choosing an operating frequency nearby the natural frequency (triangles), rather than at the natural frequency (diamonds), may result in more overall energy capture.

The reasons for the broader bandwidth can be traced back to the magnitude of the PTO impedance (third plot in Fig. 4.14). The ideal PTO impedance is U-shaped, with a minimum at the natural frequency. Matching the impedance at either side of the natural frequency gives a PTO impedance that also equals the ideal value on the other side of the natural frequency. For example, matching the impedance at $\omega_p = 2.6$ rad/s (triangles) also results in the ideal PTO impedance magnitude at $\omega = 1.9$ rad/s.

It is interesting to note that the peak in monochromatic capture width appears to be lower than the natural frequency for all values of ω_p. For $\omega_p = \omega_n$, the peak appears to be at ω_p, but study of the points before and after ω_p shows that the peak is probably slightly lower than the ω_p. This is not clear because the bins are not closely enough spaced. The peak in monochromatic

capture width for $\omega_p < \omega_n$ lies between ω_p and ω_n. What is surprising however is that the peak for $\omega_p > \omega_n$ does not lie between ω_p and ω_n but instead is lower than ω_n.

The points of note in Fig. 4.23 and Fig. 4.24 are that the damping scheme (4.48) only touches the ideal performance at ω_p when $\omega_p = \omega_n$. The peak in monochromatic capture width is neither at ω_p nor ω_n. It appears to be lower than the natural frequency, whether the ω_p is higher or lower than the ω_n.

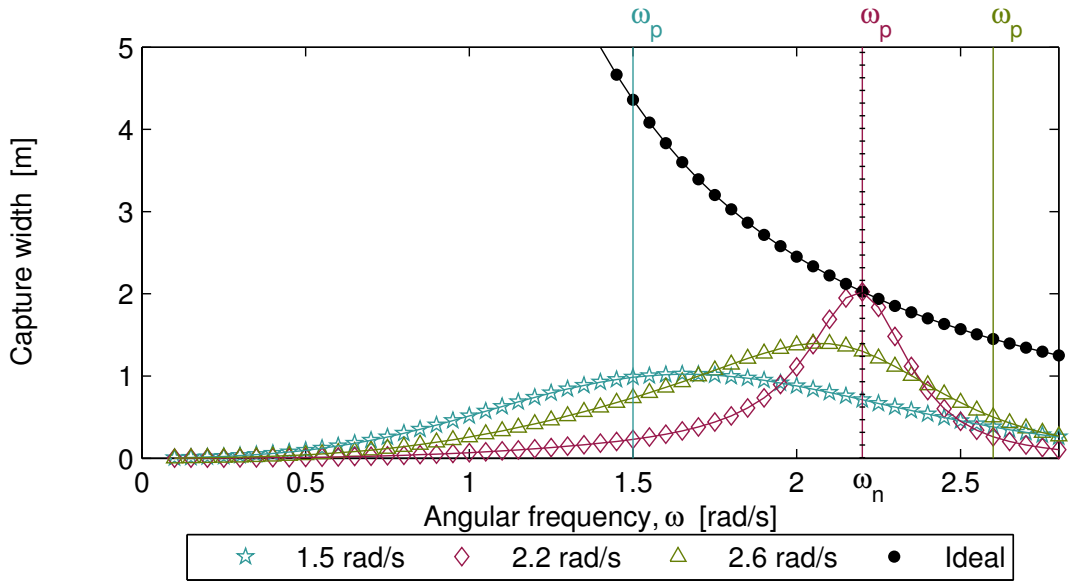

Figure 4.23: ***Capture width using a damping PTO term only:*** *causal sub-optimal control (open markers) with impedance matched at three different operating frequencies is compared to acausal optimal control (solid markers).*

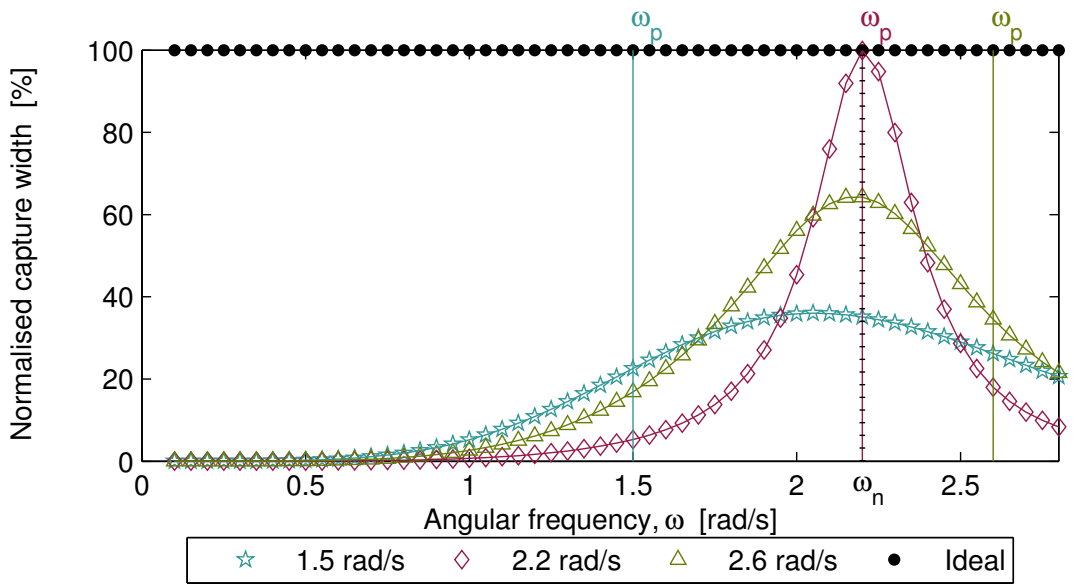

Figure 4.24: ***Normalised capture width using a damping PTO term only:*** *causal sub-optimal control (open markers) with impedance matched at three different operating frequencies is compared to acausal optimal control (solid markers).*

4.8.5 Comparison of the effects of impedance matching schemes on performance

The performance (monochromatic capture width) was shown for a particular geometry (Appendix A), using the mass-damping-spring scheme (Fig. 4.17), the damping-spring scheme (Fig. 4.19), the mass-damping scheme (Fig. 4.21), and the damping only scheme (Fig. 4.23). It can be seen that the mass-damping-spring scheme is superior because it is possible to achieve close to the ideal capture width for a broad band of frequencies around the operating frequency (ω_p). This method is not very sensitive to the choice of ω_p: three very different values of ω_p gave values of performance very close to each other. In contrast, the schemes using only one or two PTO coefficients are very sensitive to the choice of operating frequency.

To aid the comparison of these four PTO schemes, Fig. 4.25 shows the normalised capture width for three types of reactive control (m b c, b c, and m b), and for real control (b). Each plot is for a different operating frequency. It can be seen that the scheme using three PTO settings (m b c) is far superior to all the other schemes, whatever the operating frequency.

When the operating frequency is equal to the natural frequency (third plot), reactive control using only two PTO settings (m b, and b c) gives the same performance as real control (b). Real control has its highest peak value and its narrowest bandwidth when the operating frequency is chosen to be the natural frequency. As the operating frequency moves away from the natural frequency (the progression from the third plot, to the second, and then to the first plot) the peak of the performance for real control reduces, and the bandwidth broadens. For all three types of reactive control however, progression of the operating frequency away from the natural frequency results in a narrowing of the bandwidth, and a peak value that remains the same.

It is interesting to note the symmetry between the two types of reactive control that do not make use of both reactive PTO settings. In the first and second plots, it can be seen that for $\omega_p < \omega_n$, the damping-spring combination (b c) gives a broader bandwidth performance than the scheme using the mass-damping combination (m b). In the last plot, it can be seen that for $\omega_p > \omega_n$, the mass-damping combination gives a broader bandwidth performance than damping-spring combination.

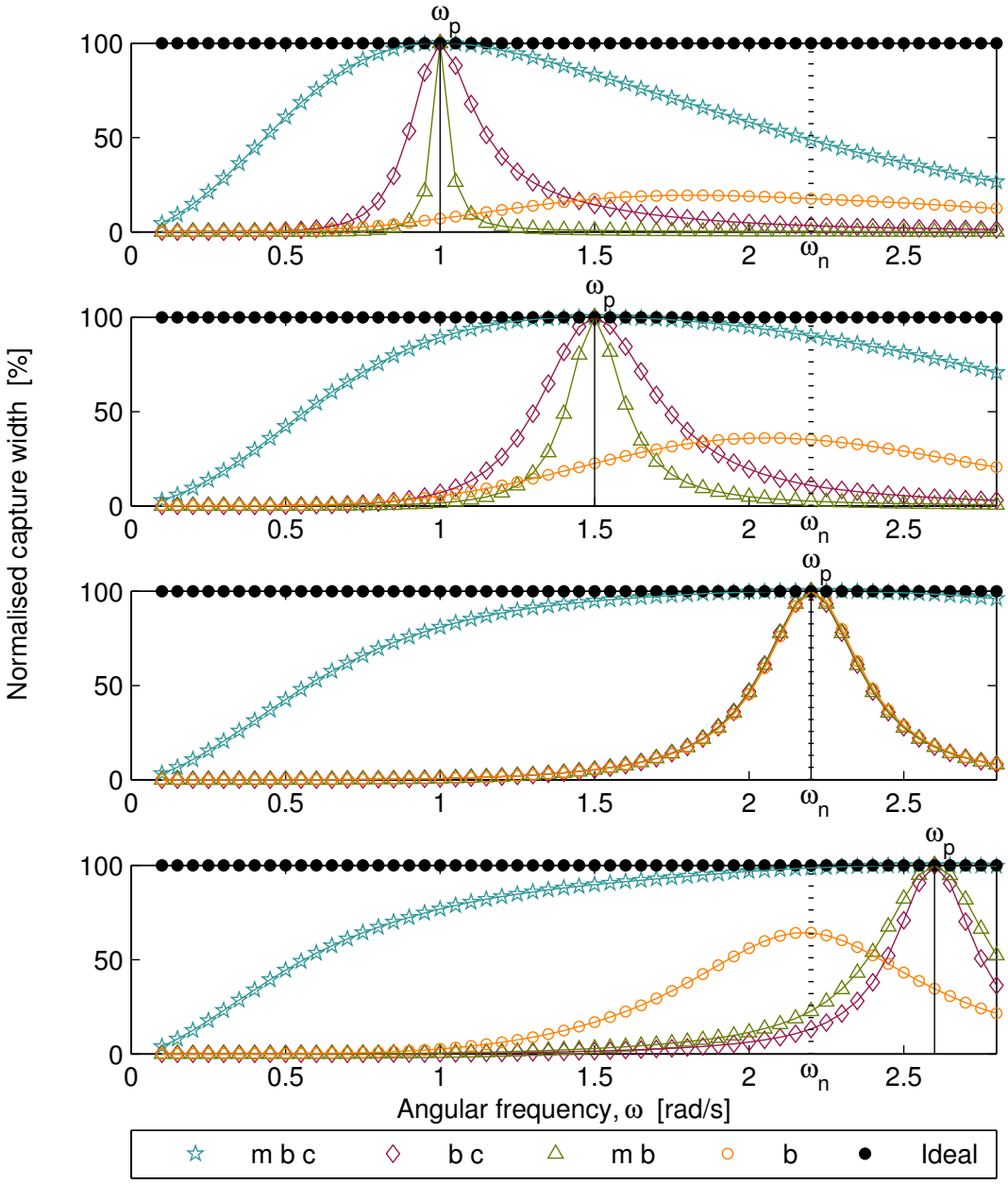

Figure 4.25: ***Normalised capture width for four impedance matching schemes:*** *reactive control with mass, damping and spring PTO settings (m b c), reactive control with damping and spring PTO settings(b c), reactive control with mass and damping PTO settings (m b), and real control with a damping coefficient (b). Each plot shows impedance matched at a different operating frequency:* $\omega_p = 1$ *rad/s (first plot),* $\omega_p = 1.5$ *rad/s (second plot),* $\omega_p = 2.2$ *rad/s (third plot), and* $\omega_p = 2.6$ *rad/s (last plot).*

4.8.6 Comparison of the effects of impedance matching schemes on displacement

For a more complete comparison of the different impedance matching schemes, it is informative to also consider the displacement as a result of each scheme. The magnitude of the displacement at each frequency is the product of the magnitude of the wave elevation, $|H(\omega)|$, and the controlled displacement response amplitude, $RAO_c(\omega) = \frac{|W(\omega)|}{|G(\omega)|+|G_{pto}(\omega)|}$ (see equation(4.28)on page 146). Fig. 4.26 shows the controlled displacement response amplitude for the same cases considered in Fig. 4.25. The values of $G_{pto}(\omega)$ used are given in Table 4.2.

The solid black markers in Fig. 4.26 indicate the $RAO_c(\omega)$ that would result if linear acausal optimal control were implemented. Note that this generally results in high values of displacement. However, unlike capture width where the value due to acausal optimal control is an upper limit that is never surpassed by the capture width due to sub-optimal control, the displacement response due to acausal optimal control is not the upper limit of displacement. For instance, in the top plot of Fig. 4.26, at some frequencies, the displacement due to the mass-damping-spring control scheme is larger than that for optimal control.

It can be seen that high values of capture width in Fig. 4.25 correspond generally to high values of $RAO_c(\omega)$ in Fig. 4.26. The first point of note is that the ideal case results in very high values of $RAO_c(\omega)$, particularly at low frequencies. The second point of note is that the mass-damping-spring scheme, which Fig. 4.25 shows is vastly superior to the other causal impedance matching schemes, also has very high values of $RAO_c(\omega)$. The controlled displacement response amplitude is very similar to that for ideal control, and also has very large values at low frequencies. This means that a WEC controlled with the mass-damping-spring scheme will require displacement restraints for spectra that contain even small amounts of power at lower frequencies. Thus it can be seen that the highly tuned capture widths of the mass-damping and damping-spring schemes also result in highly tuned controlled displacement response amplitudes.

Impedance matching scheme	$G_{pto}(\omega)$
(1) optimal	$\tilde{G}_{pto}(\omega) = 2i\omega B(\omega)$
(2) mass-damping-spring	$\breve{G}_{pto}(\omega) = -c + \omega^2(M_p + m) + i\omega B_p$
(3) damping-spring	$\breve{G}_{pto}(\omega) = -c + \omega_p^2(M_p + m) + i\omega B_p$
(4) mass-damping	$\breve{G}_{pto}(\omega) = \omega^2[m + M_p - \frac{c}{\omega_p^2}] + i\omega B_p$
(5) damping	$\breve{G}_{pto}(\omega) = i\omega\sqrt{B_p^2 + (\omega_p[m + M_p] - \frac{c}{\omega_p})^2}$

Table 4.2: ***Comparison of PTO transfer function due to impedance matching schemes.***

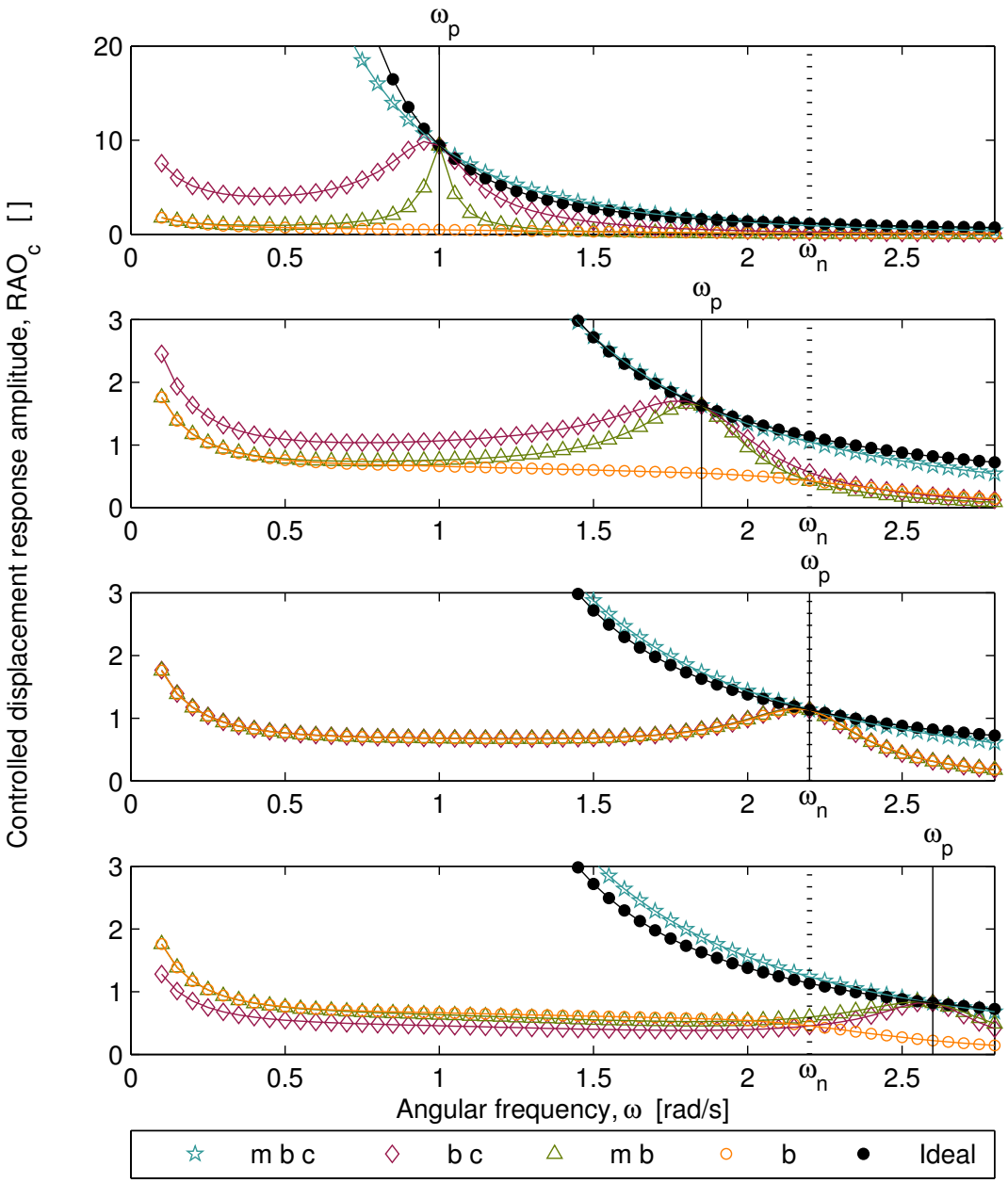

Figure 4.26: ***Controlled displacement response amplitude for four impedance matching schemes:*** *reactive control for a mass-damping-spring scheme (m b c), reactive control for a damping-spring scheme (b c), reactive control for a mass-damping scheme (m b), and real control with damping only (b). Each plot shows the magnitude of displacement with respect to magnitude of wave elevation, RAO_c, for schemes with different operating frequencies: $\omega_p = 1$ rad/s (first plot), $\omega_p = 1.5$ rad/s (second plot), $\omega_p = 2.2$ rad/s (third plot), and $\omega_p = 2.6$ rad/s (last plot). Note that the first plot has a different y-axis scale.*

4.9 The effects of scaling on performance

While the upper limit of monochromatic capture width is independent of the scale of a WEC, the monochromatic capture width due to causal control is not. It depends on the size of the WEC (scale) and on the operating frequency, ω_p. Furthermore, the type of impedance matching strategy used, i.e. the combination of mass, damping and spring PTO settings as described in § 4.8.1 - § 4.8.4, also plays an important role.

This section presents results of a study of the interaction of WEC size, the operating frequency, and the control strategy. The same general shape is considered; the spherical buoy described by Havelock [57]. It is scaled up by the choice of radius, r. WECs with radii of $1.9m$, $2.5m$ and $3.5m$ were investigated. These choices of size were influenced by the need to have clear plots. The values of natural frequency, ω_n, needed to be close enough together for easy comparison of results. Although the size difference between WECs with diameters of $3.8m$ and $7m$ is not comparable with the size difference between point-absorbers and large (terminator or attenuator) WECs, the effects of scaling are demonstrated. Thus the results can be used to draw conclusions about the suitability of various sub-optimal control techniques to point-absorbers and large WECs.

The added mass, radiation damping, dry mass and buoyancy spring are all functions of the radius. More importantly, the natural frequency (§ 4.6.7) is a function of radius. This study shows how the relationship between ω_n and ω_p affects performance. The effect on performance depends on the impedance matching strategy, so each is considered in turn. Figs. 4.28 - 4.33 show the performance for each control strategy in turn. The ω_n of each size of WEC is indicated by a dotted line. As expected, large physical size corresponds to a low ω_n. Performance is indicated by the normalised capture width (4.25), which is the capture width due to causal control as a percentage of capture width due to acausal optimal control (the upper-limit).

Within each figure, each plot shows the normalised capture width for a different value of ω_p, indicated by the solid line. The first plot in each figure uses a value of ω_p much lower than the ω_n of any of the three sizes of WEC studied. The second plot in each figure is for an ω_p that is equal to the ω_n of the largest WEC. In the third plot, the ω_p falls between the natural frequencies of the largest and medium sized WEC. The fourth plot is for the ω_n of the medium WEC. In the fifth plot, the ω_p falls between the natural frequencies of the medium and smallest WEC.

4.9.1 The effect of size on performance of a mass-damping-spring scheme

In § 4.8.1 it was shown that using the mass-damping-spring scheme (4.52) was the best type of reactive control in terms of performance. Here this scheme is considered for three sizes of WEC (see Fig. 4.7). Fig. 4.27 compares the performance (monochromatic capture width) for the mass-damping-spring scheme to that for acausal optimal control (black solid markers). The

upper limit of the performance is the same regardless of the size of WEC, while the performance for causal control depends on the size of the WEC. Fig. 4.28 shows the interaction between the scale of a WEC and the choice of operating frequency. Each plot is for the same sized WECs as in Fig. 4.27, but shows the normalised capture width. A different choice of ω_p is used in each plot. The fourth plot is for the same ω_p as Fig. 4.27. The most noticeable trait seen in Figs. 4.27 and 4.28 is that the performance of all three sizes of WEC appears very similar, apart from at frequencies much lower than the operating frequency, where the performance of the larger WEC is better.

In the top plot of Fig. 4.28, the ω_p is much lower than the ω_n of the three sizes of WEC considered. The normalised capture width for all sizes of WEC is very similar across all frequencies. Closer examination shows that the large WEC performs marginally better (at most 2%) at frequencies far from the ω_p.

In the second and subsequent plots in Fig. 4.28, the three different sized WECs have normalised capture widths that are similar at frequencies near ω_p, but different at frequencies much lower than ω_p. The larger WEC has better performance at these lower frequencies. However, on closer inspection, for a narrow band of frequencies about the ω_p, the largest WEC does not have the best performance. In the second plot the largest WEC only performs better at frequencies below 1.35 rad/s, in the third plot at frequencies below 1.3 rad/s, in the fourth plot at frequencies below 1.18 rad/s, and in the last plot at frequencies below 1.04 rad/s. At the frequencies where the largest WEC does not have the highest value of the normalised capture width, the difference is at

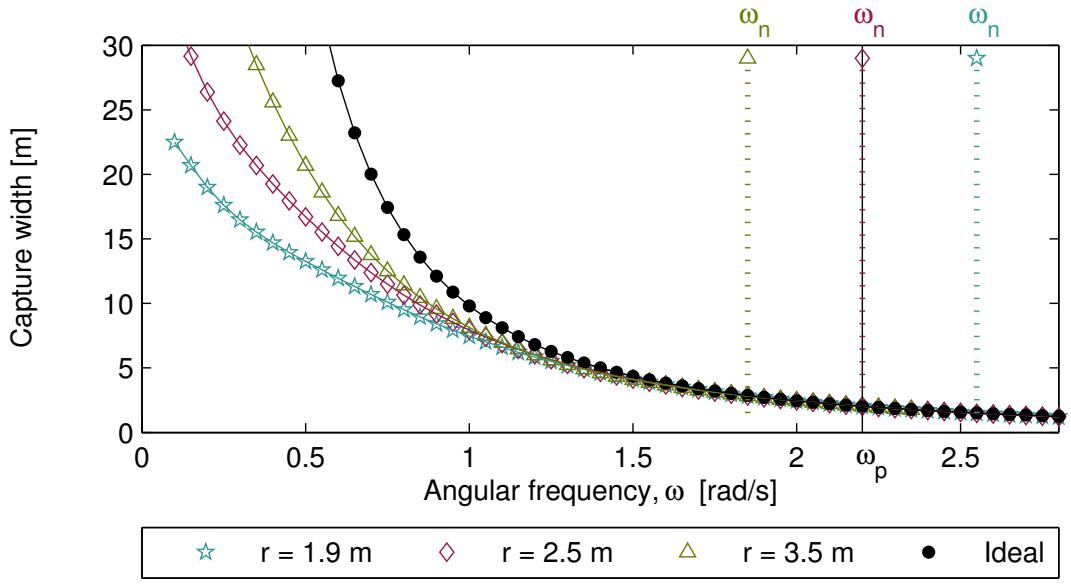

Figure 4.27: ***Capture width for three sizes of WEC:*** *Monochromatic capture width $C_W^s[\omega_j]$ under causal mass-damping-spring control for different sized WECs.*

most a couple of percentage points below those for the smaller WECs. At the lower frequencies where the larger WEC performs better, the difference is as much as 20%. In Fig. 4.27 it can be seen that improved performance at lower frequencies can translate into higher monochromatic capture width in the order of metres.

The conclusions that may be drawn from this are that for a WEC with mass-damping-spring control, smaller WECs have a highly tuned response, with very high performance at a narrow band of frequencies surrounding the chosen ω_p. In contrast, larger WECs have a broader band response. At the frequencies close to the ω_p, their performance is marginally less than that of a smaller device, while at frequencies much lower than the ω_p, their performance is significantly better than that of smaller devices. The top plot of Fig. 4.28 suggests that the performance of large WECs is also good at frequencies higher than the ω_p. However, it cannot be said with certainty that this applies to all choices of ω_p because of the absence of hydrodynamic parameters (and hence results) at higher frequencies in this dataset (Fig. 4.7). The difference in size between the WECs considered in this study is small, but the results give an indication of the effects of much larger differences in size. In narrow bandwidth sea states, it may be possible for small WECs to capture marginally more of the wave front than larger WECs. In broad bandwidth sea states, it may be possible for large WECs to capture substantially more of the wave front than smaller WECs.

It has long been known that a larger device would absorb more energy than a smaller device, because the displacements required for optimal control are smaller [58]. The new evidence of superior performance of large WECs in broad bandwidth seas is in addition to this effect: Fig. 4.28 shows that even in linear unrestrained conditions, it is possible for a larger WEC to capture more energy than a smaller WEC. This is not well known because previous work has focussed on the upper limit due to causal optimal control. This upper limit is independent of the size of a WEC [56]. Note however that the difference in performance between the three sizes of WEC is nevertheless small. In practice, the tendency of larger WECs to need fewer displacement restraints may make a greater contribution to their superior performance. This topic is discussed in more detail in § 6.4.

The points of note in Fig. 4.27 and Fig. 4.28 are that the performance of the mass-damping-spring scheme (4.9) for a given ω_p depends on the size of the device, and hence the ω_n. Larger WECs have better low frequency performance, even when the ω_p is closer to the ω_n of smaller WECs.

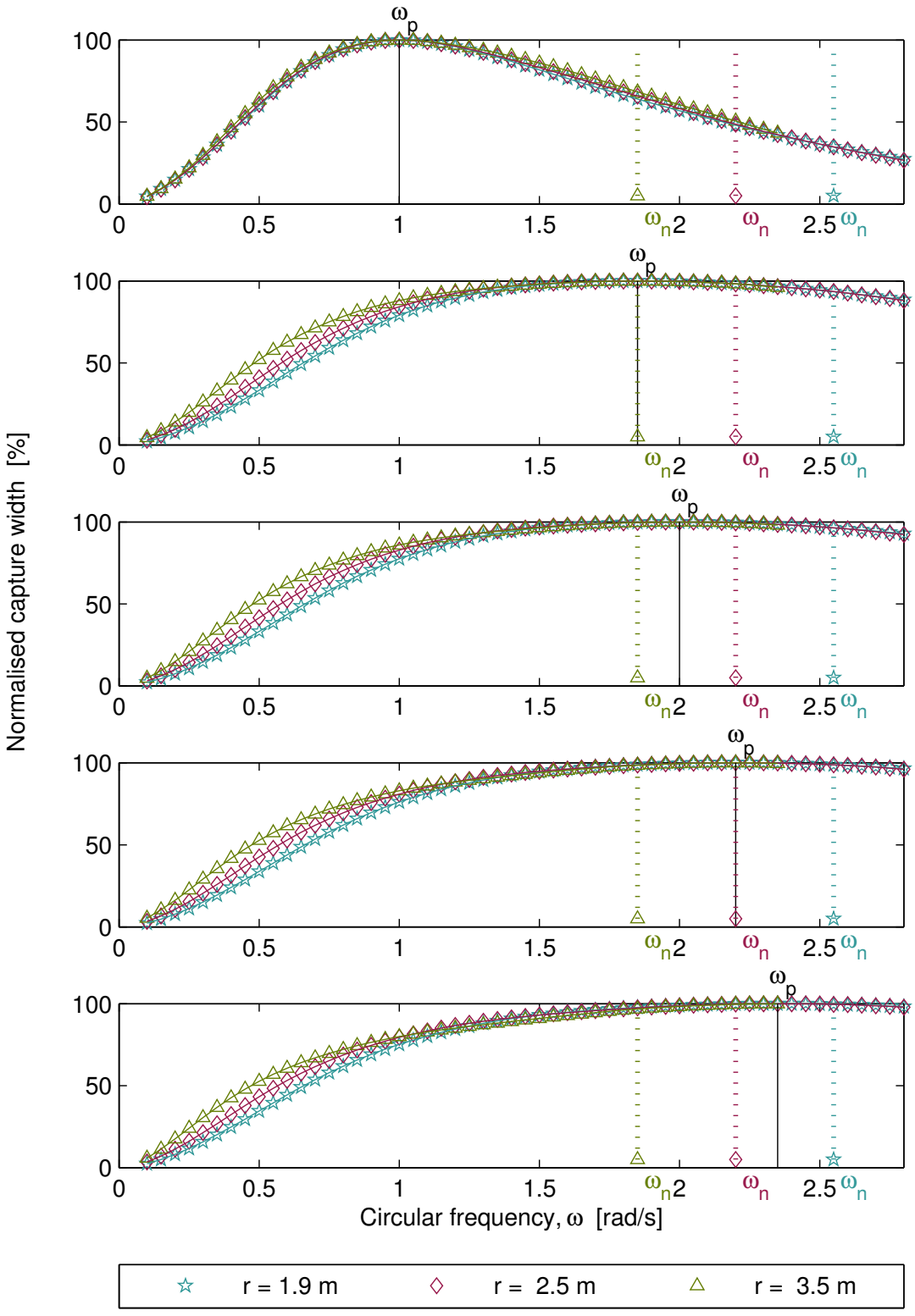

Figure 4.28: ***The effects of scaling - three PTO settings:*** *Normalised capture width under causal sub-optimal control for different sized WECs. The dotted lines indicate the natural frequencies, ω_n, and the solid line indicates the operating frequency ω_p.*

4.9.2 The effect of size on performance of a damping-spring scheme

In § 4.8.1 it was shown that a commonly used impedance matching strategy, involving only damping and spring PTO settings, did not give as broad a bandwidth as using mass, damping and spring PTO settings. Here causal control with damping and spring PTO settings (4.53) is considered for three different sizes of WEC (Fig. 4.29).

Whereas impedance matching using three PTO coefficients favours larger sized WECs, Fig. 4.29 indicates that using only damping and spring coefficients favours smaller WECs. In the top plot of Fig. 4.29, ω_p is much lower than the natural frequencies for all sizes of WEC, but is closest to ω_n of the largest WEC. Once again, at frequencies close to ω_p, all three sizes of WEC have similar performance. At frequencies lower than ω_p, the performance of the largest WEC is marginally better than the others. At frequencies higher than ω_p, the performance of the smallest is slightly better than the others.

The second plot shows a surprising result. The operating frequency is equal to the ω_n of the largest WEC. It would seem logical that a large WEC with a low ω_n would be better suited to seas with a low (peak) frequency than a smaller WEC with a higher ω_n. Yet the medium and small WECs have substantially better performance than the large WEC at frequencies below and above ω_p. Using this control strategy (and not accounting for energy lost due to non-linear behaviour or restraints), a smaller WEC will perform better than a large WEC in the design sea state of the large WEC. In the design sea state of the small WEC (last plot), the smaller WEC will perform substantially better than larger WECs.

This behaviour is an artefact of the chosen control strategy. It is not to be interpreted as an indication that WECs should be *undersized* for their design sea state. The mechanism behind this artefact can be seen by examining the PTO impedance due to impedance matching, and comparing this to the ideal value of the PTO impedance (the complex conjugate of the intrinsic impedance at each frequency).

Fig. 4.30 is for the small WEC ($r = 1.9$ m) and Fig. 4.31 is for the large WEC ($r = 3.5$ m). Both show the PTO impedance for $\omega_p = 2$ rad/s (corresponding to the third plot in Fig. 4.29). It can be seen that for the smaller WEC the imaginary part of the PTO impedance (second plot of Fig. 4.30) follows the ideal curve much closer than in the larger WEC (second plot of Fig. 4.31). In § 4.7.2 it was shown that the damping-spring scheme had poor performance when $\omega_p > \omega_n$.

The points of note in Figs. 4.29 - 4.31 are that the performance of the damping-spring scheme (4.42) for a given ω_p depends on the size of the device, and hence the ω_n. Smaller WECs have better performance, even when the ω_p is closer to the ω_n of larger WECs. The PTO reactance is much closer to the ideal value for the smaller WEC than for the larger WEC.

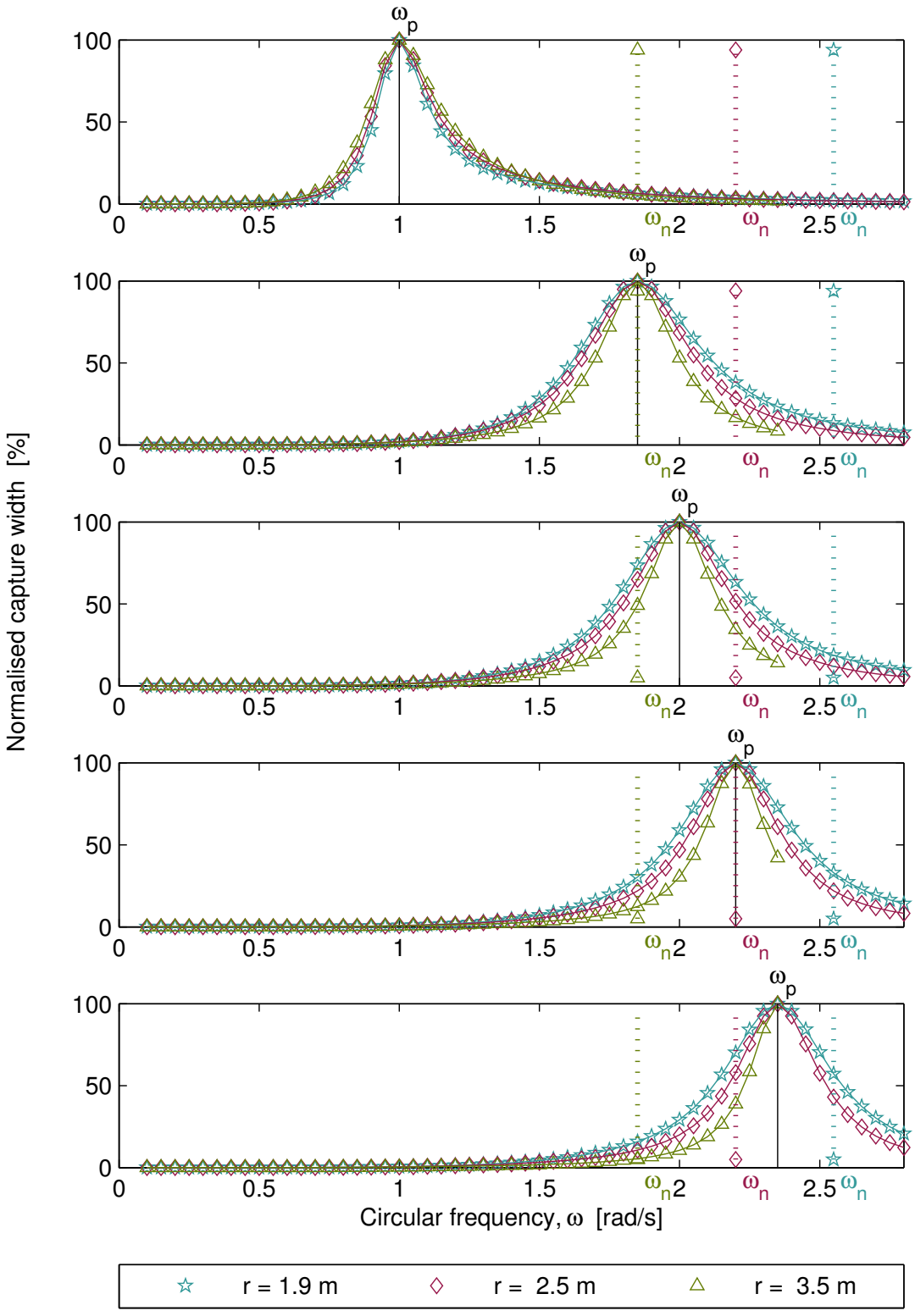

Figure 4.29: ***The effects of scaling for a damping-spring scheme:*** *Normalised capture width under causal sub-optimal control for different sized WECs. The dotted lines indicate the natural frequencies, ω_n, and the solid line indicates the operating frequency ω_p.*

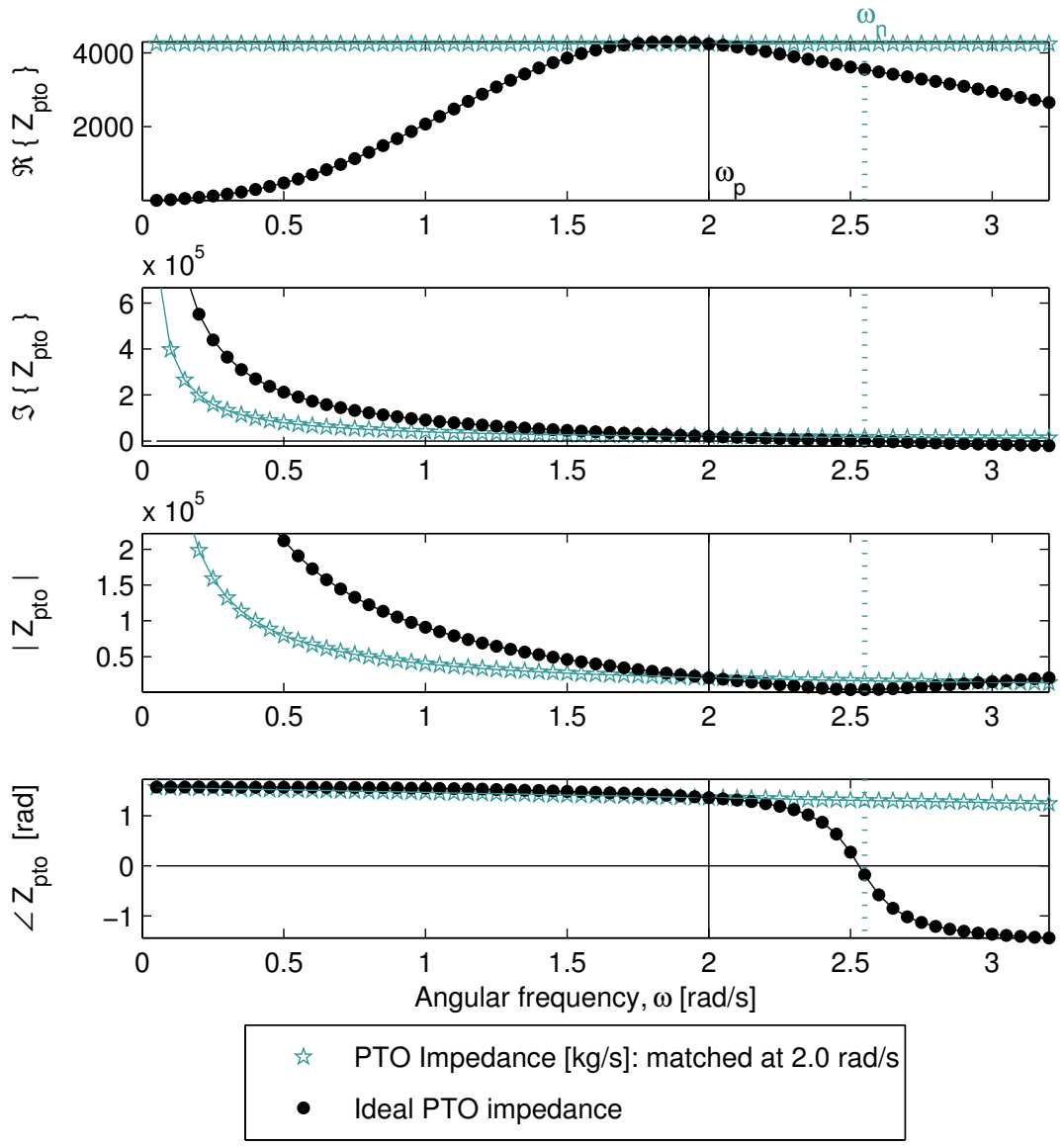

Figure 4.30: ***PTO impedance for a small WEC under a damping-spring scheme:*** *PTO impedance due to causal sub-optimal control (open markers) compared to ideal PTO impedance given by optimal acausal control (solid markers), for* $\omega_p = 2$ *rad/s. The small WEC, with* $r = 1.9$ *m, is considered.*

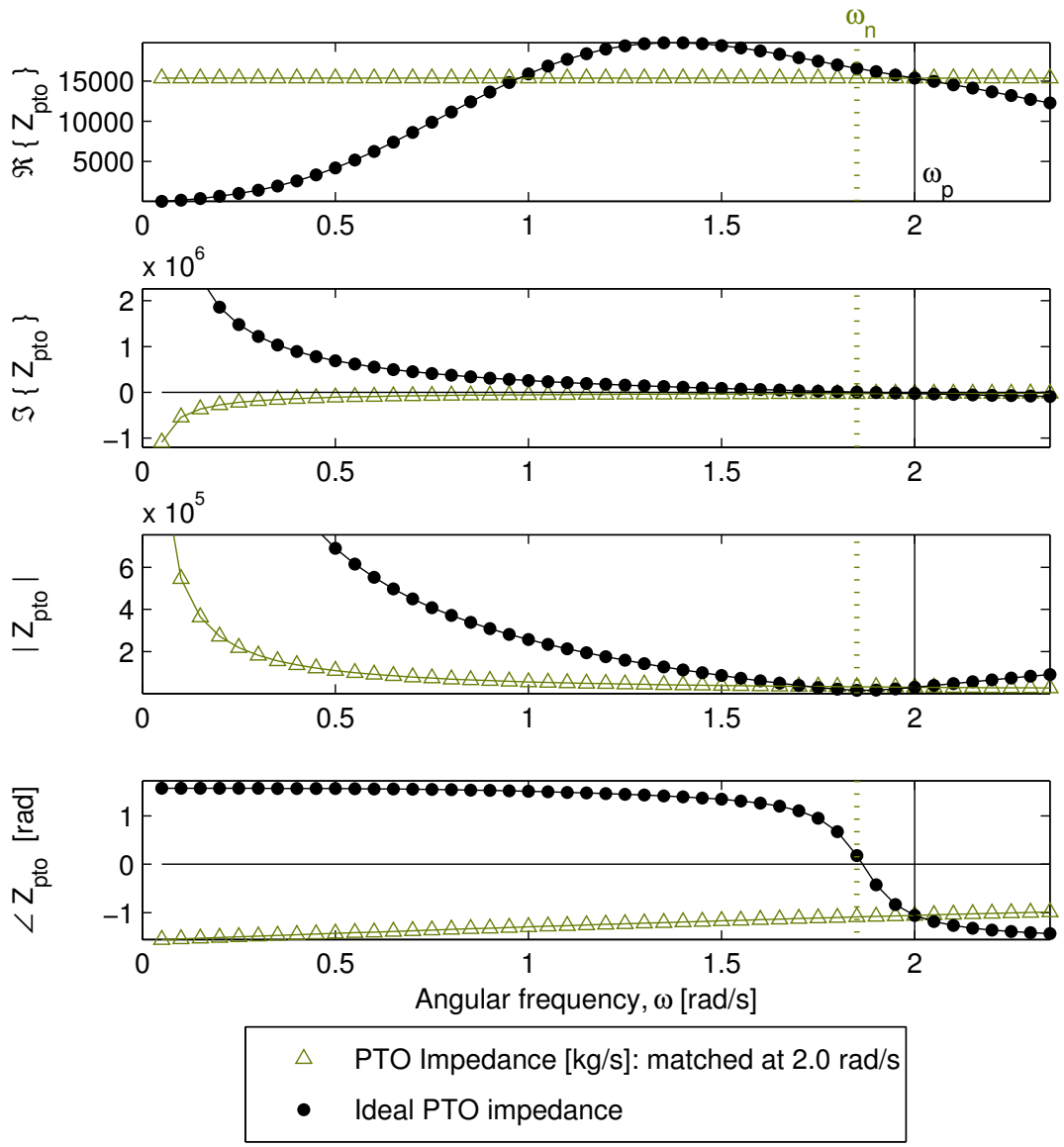

Figure 4.31: ***PTO impedance for a large WEC with a damping-spring scheme:*** *PTO impedance due to causal sub-optimal control (open markers) compared to ideal PTO impedance given by optimal acausal control (solid markers), for $\omega_p = 2$ rad/s. The large WEC, with $r = 3.5$ m, is considered. Note that the x-axis is different to that of Fig. 4.30 as this scales with the size of WEC.*

4.9.3 The effect of size on performance of a mass-damping scheme

In § 4.8.3 it was shown that an impedance matching strategy involving only mass and damping PTO settings is not as good as using all three (mass-damping-spring) PTO settings. Here, the mass and damping strategy is considered for three different sizes of WEC. Fig. 4.32 shows the normalised capture width for causal control with mass and damping PTO settings (4.43). As before, the natural frequency ω_n of each size of WEC is indicated by a dotted line, while the operating frequency ω_p is indicated by the solid line.

Fig. 4.32 indicates that the mass-damping scheme favours larger WECs. Once again, this behaviour is an artefact of the chosen control strategy. The mechanism behind this artefact can be seen by comparing the PTO impedance due to causal control to that due to acausal optimal control. As discussed already, Fig. 4.12 shows that for mass-damping reactive control, an ω_p higher than ω_n results in a PTO reactance (second plot) that follows the shape of the ideal curve (i.e. has a similar slope at ω_p) much better than when ω_p is at or below ω_n.

In Fig. 4.32 it can be seen that the most difference in performance is for very low values of ω_p, and that there is little difference in performance at higher values of ω_p. This is the opposite to the damping-spring scheme shown in Fig. 4.29, for which the biggest differences are at higher frequencies.

The points of note in Fig. 4.32 are that the mass-damping scheme (4.42) for a given ω_p depends on the size of the device, and hence the ω_n. For $\omega_p < \omega_n$ a larger device has better performance than a small device. The bandwidths of all sizes of WEC shown however are narrower at the low ω_p than for the damping-spring scheme.

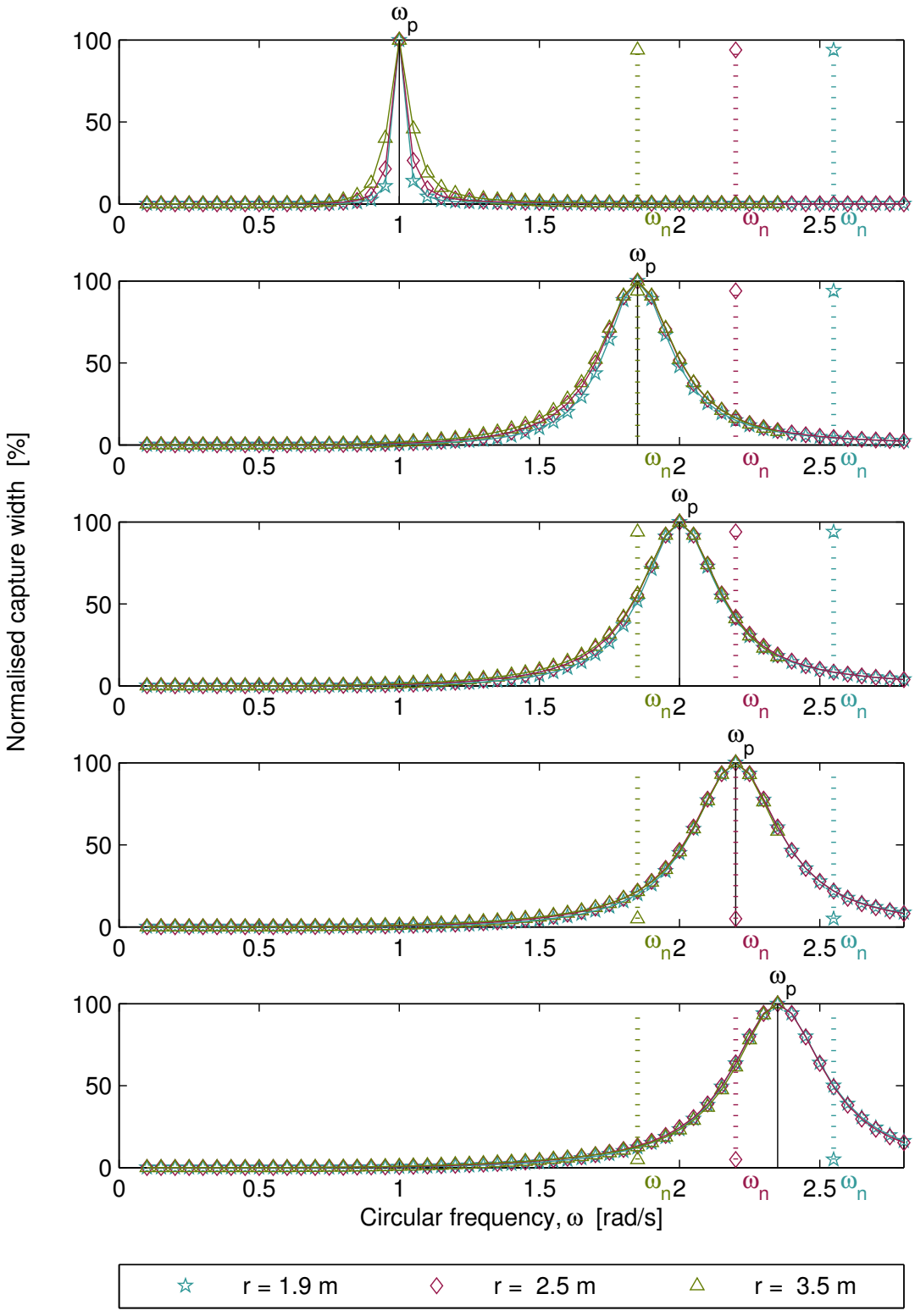

Figure 4.32: ***The effects of scaling for a mass-damping scheme:*** *Normalised capture width under causal sub-optimal control for different sized WECs. The dotted lines indicate the natural frequencies, ω_n, and the solid line indicates the operating frequency ω_p.*

4.9.4 The effect of size on performance of a damping only scheme

The previous sections considered control using reactive elements (mass and/or spring), which shall be termed reactive control. Here real control will be considered. As discussed in § 4.8.4, sub-optimal control using damping only is important to study, as its simplicity and low cost makes it suitable for full-scale prototypes.

Fig. 4.33 shows the normalised capture width for real control (4.49), used with three different sizes of WEC. As before, the natural frequency ω_n of each size of WEC is indicated by a dotted line, while the operating frequency ω_p is indicated by the solid line. It can be seen that real control gives good performance (comparable to the mass-damping, or the damping-spring strategies) when the operating frequency is close to the natural frequency of the WEC.

Some important insights can be gained from this fact. Firstly, real control should not be used when it is important to have efficient power absorption for values of ω_p that are very different from the WEC's natural frequency. The impact of this on the types of control suitable for small or large WECs is discussed in § 6.4. Secondly, real control would be an effective method if the natural frequency could be changed during operation. It is possible to adjust the natural frequency using geometry control (slow tuning) techniques. As described in § 2.3.1, these include making changes to water ballast, adjustable springs, or the axes of motion. These techniques are potentially cheaper than implementing reactive control, and are thus worth further study.

The main point of note in Fig. 4.33 is that the damping scheme (4.48) has very poor performance when the ω_p is not close to the ω_n. The peak in performance appears to be influenced more by ω_n than ω_p.

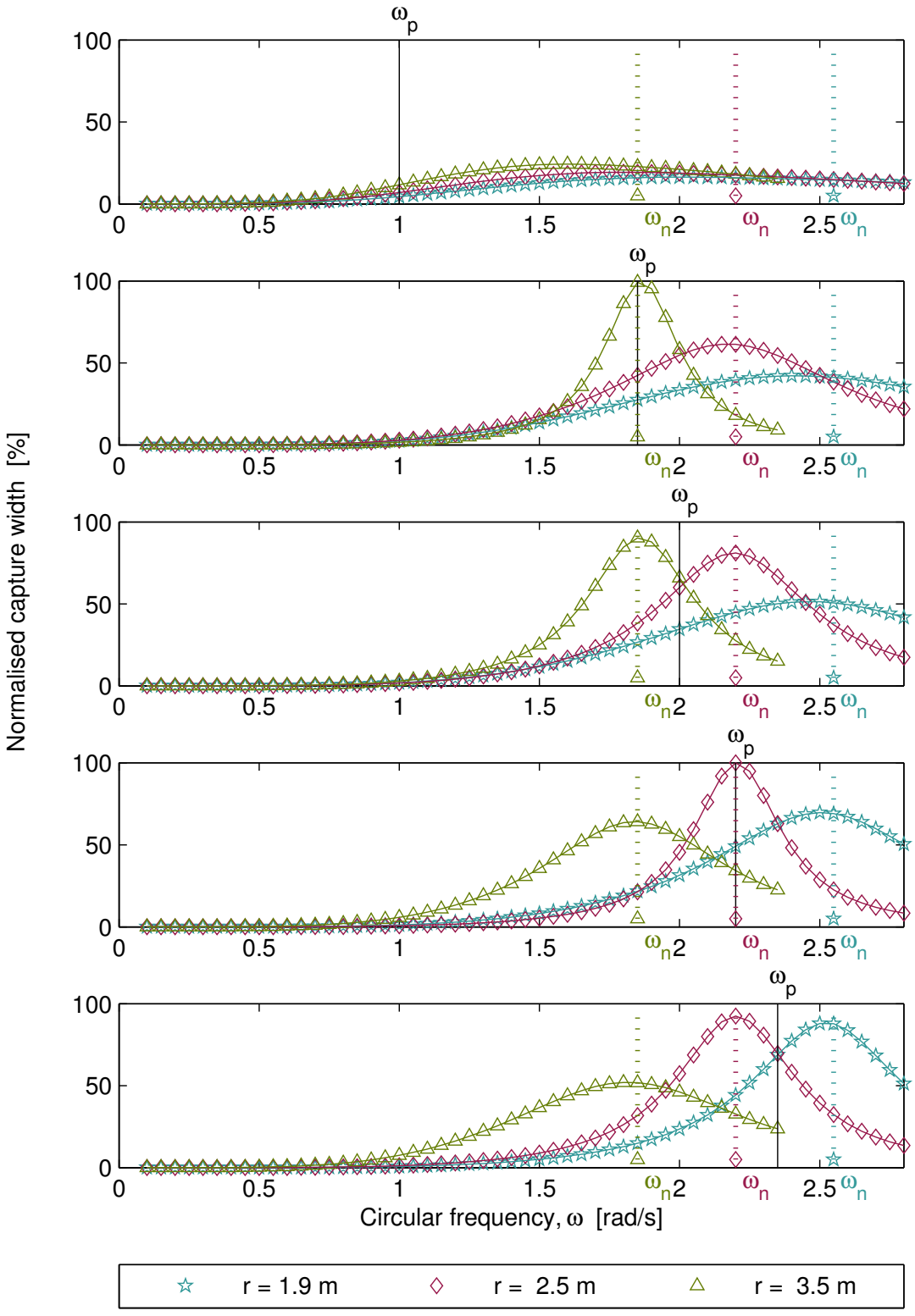

Figure 4.33: ***The effects of scaling for a damping scheme:*** *Normalised capture width under real causal sub-optimal control for different sized WECs. The dotted lines indicate the natural frequencies, ω_n, and the solid line indicates the operating frequency ω_p.*

4.9.5 Comparison of the effects of size on displacement

Fig.4.26 showed that the superior performance of the mass-damping-spring scheme came at the cost of higher displacements. Figs. 4.34 and 4.35 show the controlled displacement amplitude response operators for the small ($r = 1.9$ m) and large ($r = 3.5$ m) sizes of buoy respectively. Note that the x axis is different for these graphs because the original data is dimensionless, and when it dimensionalised by choosing a particular value of radius (as in Fig. 4.7), this effects both the x and y axes. Note also that in both figures, the y axis of the first plot has a different scale to that of the subsequent plots.

The important point shown by Figs. 4.34 and 4.35 is that a smaller buoy has a higher controlled displacement response amplitude operator. This means that for the same sea state, a smaller buoy will have higher displacements than a larger buoy. This is important when comparing point absorbers to large WECs. There will exist sea states for which the response of a large WEC will be low amplitude and weakly non-linear, and for which the response of a point absorber WEC will be either non-linear or will require displacement restraints (which often another source of non-linear behaviour in itself). Another way of interpreting this is to say that large WECs operate in the power maximising control regime without reaching displacement limits (see Table 2.5 on page 33) for a much greater proportion of the time than point absorbers.

While the mass-damping-spring scheme gives higher displacements than control schemes involving only one or two coefficients, these displacements are larger in the small buoy. This suggests that in very large WECs, there may be more sea states in which it would be possible to use the mass-damping-spring scheme and not exceed amplitude limits. The converse of this relates to optimal acausal control: for smaller geometries this would result in high displacements. This suggests that, even if accurate forecasts were available, in very small WECs it may not be possible to implement acausal control because this would result in excessively large displacements.

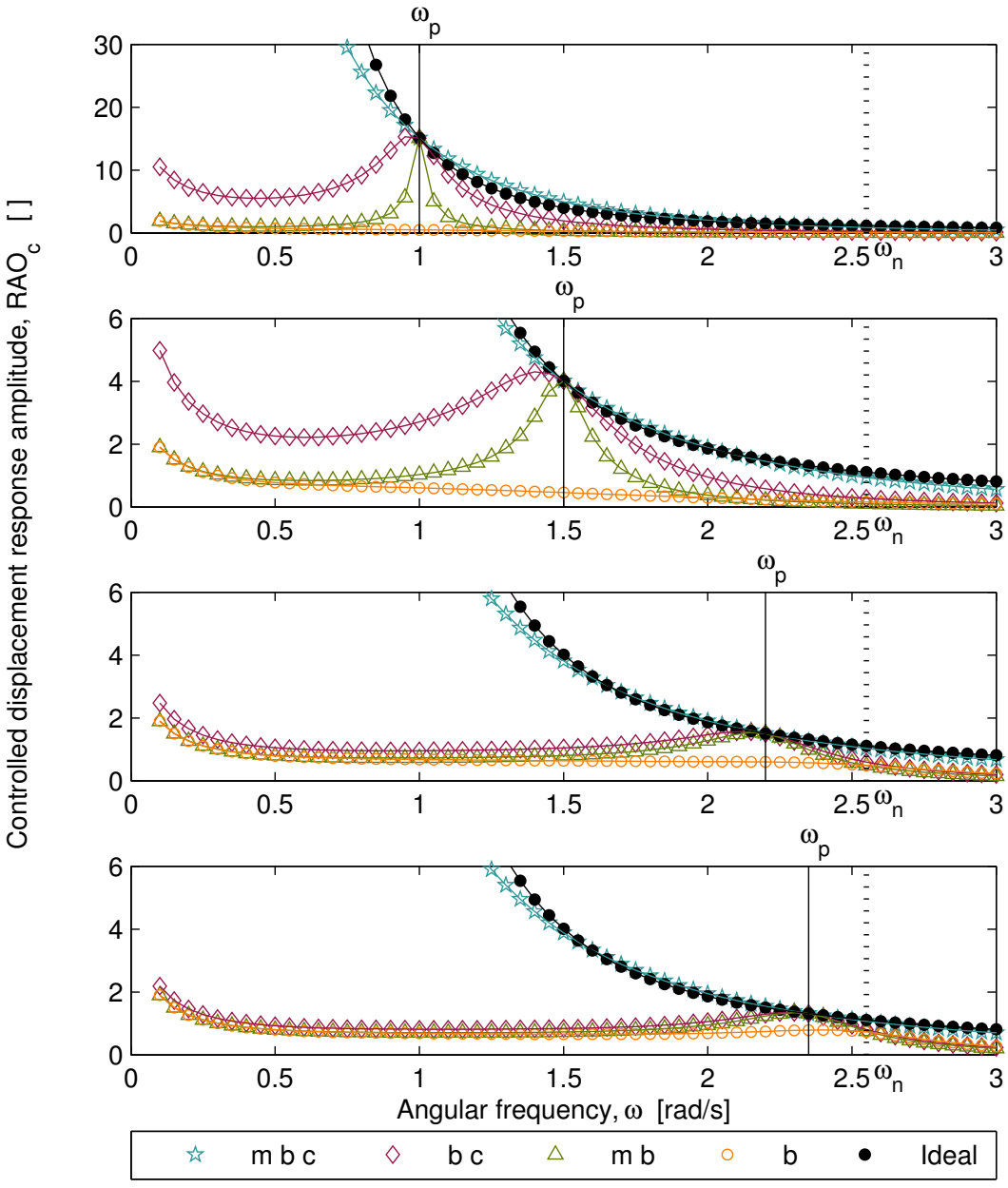

Figure 4.34: ***The effects of scaling on displacement for the small buoy:*** *Controlled displacement response amplitude operator for a heaving buoy of radius* $r = 3.5\,m$

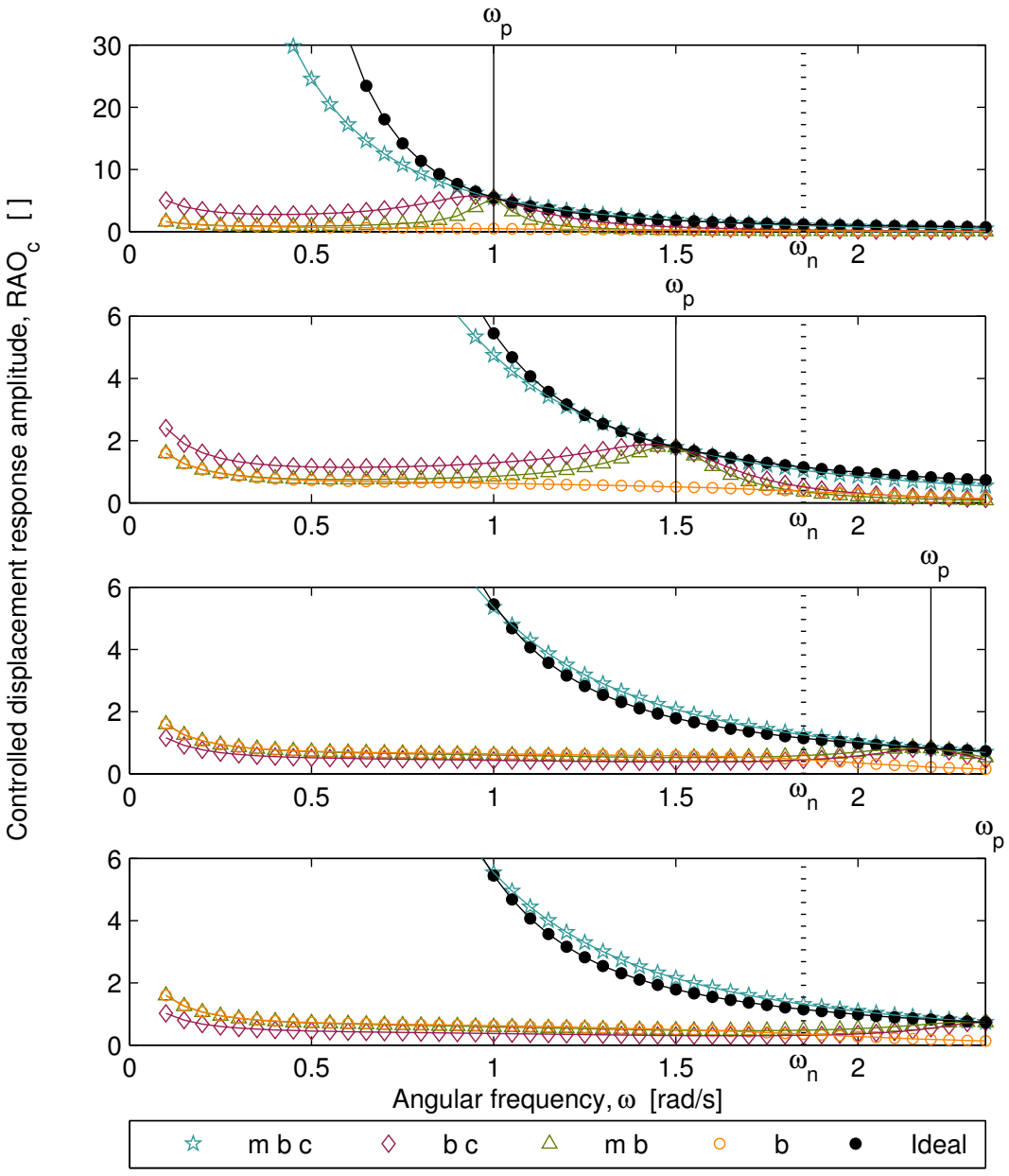

Figure 4.35: ***The effects of scaling on displacement for the large buoy:*** *Controlled displacement response amplitude operator for a heaving buoy of radius* $r = 3.5\,m$

4.9.6 The interaction of size and impedance matching techniques

The most important issue highlighted by this case study of three different sized WECs is that the shape of the monochromatic capture width function for reactive control depends the scale of a WEC. This is a significant result, as there are no published results showing how monochromatic capture width due to reactive control varies with WEC size. The monochromatic capture width due to acausal control is independent of WEC scale, and this is often interpreted as meaning that a reactively 'tuned' point absorber will capture the same amount of energy as a large WEC in polychromatic seas. Here it has been shown that the linear unrestrained performance for reactive control depends on the size of the WEC.

This can be understood by considering equations (4.51) and (4.52) on page 170. In the monochromatic capture width for optimal control (4.51) the hydrodynamic coefficients cancel, so it is independent of the size of the WEC. The monochromatic capture width for mass-damping-spring control (4.52) is a function of the hydrodynamic coefficients. Table 4.1 is key to understanding how size effects performance. The difference between the PTO impedances of optimal control and the reactive schemes is the amount by which B_p differs from $B[\omega_j]$ and by which M_p differs from $M[\omega_j]$.

When using the best reactive control strategy, the mass-damping-spring scheme with the best choice of reactive PTO coefficients (4.9), the case studies considered here indicate that a smaller WEC has a narrower bandwidth of performance than a larger WEC. The reason for the smaller WEC's slightly better performance at frequencies close to the ω_p can be seen from Fig. 4.7: the slope of the added mass and damping curves of the smallest WEC is less steep and so for a given band of frequencies surrounding the ω_p there is less of a difference between the hydrodynamic parameters ($B[\omega_j]$ and $M[\omega_j]$) and the 'tuned' hydrodynamic parameters (B_p and M_p). The reason for the larger WEC's significantly better performance at frequencies further away from the operating frequency is not as clear. It is possible that the relationship between the choice of ω_p and the frequencies at which there are extreme values of added mass and damping (Fig. 4.7) is important.

This indicates that these results are specific to the choice of ω_p with respect to the shape of the hydrodynamic coefficients and therefore more research is required to determine how the size of a WEC effects the other modes of motion. Furthermore, it would be useful to repeat this case study using hydrodynamic coefficients that approach their high-frequency asymptotic values. This would give results at higher frequencies which would show whether larger WECs have broader bandwidth performance for all values of ω_p.

The case studies presented here on real control indicated that performance at frequencies close to the chosen ω_p is much higher for sizes of WEC where the ω_n is close to the ω_p. This suggests that geometry control has potential for use with real control.

4.10 Chapter summary

The main purpose of this chapter was to show how causal sub-optimal control schemes differ from each other, and from ideal (acausal optimal) control. To begin with, the relationship between causality and optimality was studied. Optimal control is the result of applying the ideal condition (impedance matching) at every frequency. Acausality is a result of applying the ideal condition at more than one frequency, and thus optimal control of polychromatic motion is by necessity acausal. A control scheme tailored for steady-state sinusoidal behaviour would only need to implement the ideal condition at a single frequency. Such a scheme could be considered optimal because the ideal condition is met at all frequencies, which in this case is only one frequency. It will also be causal because the ideal condition is only applied at one frequency. Causal control schemes are restricted to using PTO settings that are not functions of frequency. A causal control scheme used for polychromatic behaviour is necessarily sub-optimal because constant PTO settings cannot be used to apply the ideal conditions at all frequencies. Two new classes of control were introduced: geometry control and acausal sub-optimal control.

This chapter included analysis of the interaction between the operating frequency ω_p, the size of the WEC and the impedance matching scheme. Points of note from this analysis were:

- Reactive control using three PTO settings (mass-damping-spring) gives a much wider bandwidth of absorption than reactive control using only two PTO settings (mass-damping, or damping-spring); the resulting capture width is close to that given by optimal control.
- Reactive control using three PTO settings gives a much wider bandwidth of controlled displacement response amplitude $R\breve{A}O_c(\omega)$ than reactive control using only two PTO settings. The resulting $R\breve{A}O_c(\omega)$ is very close to that given by optimal control $R\tilde{A}O_c(\omega)$. High values of $RAO_c(\omega)$ increase the likelihood of displacement restraints being required.
- For a mass-damping-spring scheme, it appears likely that the bandwidth of performance for a small WEC working in its design seas ($\omega_p = \omega_n$) will be narrower than that of a large WEC working in the small WEC's design seas ($\omega_p < \omega_n$).
- The mass-damping scheme gives a very narrow bandwidth performance when $\omega_p < \omega_n$.
- The damping-spring scheme gives a narrow bandwidth performance when $\omega_p > \omega_n$.
- Real control gives poor performance when the operating frequency is substantially different to the natural frequency.
- For real control, an ω_p close to ω_n will yield a capture width approximately centred on ω_n, with a lower peak but a broader bandwidth than using $\omega_p = \omega_n$. Thus for real control

in design seas (the spectrum peak equals the natural frequency) with a broad spectrum, choosing $\omega_p = \omega_n$ may not be the best option.

- The combination of geometry control and real control (PTO damping) has the potential to be cheaper than and almost as effective as reactive control.

Chapter 5

Sea-state and geometry interaction

5.1 Overview

Work presented in this thesis so far has pointed towards the interaction between the sea state and the device. In the present chapter, the theory on this interaction is formalised. The topic of device sea state interaction is approached from two directions: the frequency domain and the time domain. The frequency domain parameter capture width is used to measure the extent to which predictions could be useful (§ 5.3), while the time domain parameter premonition time is used to indicate how easy the required prediction might be (§ 5.4).

Chapter 4 used monochromatic capture width extensively as a performance indicator. In § 5.2 it is shown how it interacts with a new parameter which describes the spectral shape of the sea state. The equation relating monochromatic capture width to this new spectral shape parameter is derived. This equation gives a mathematically rigorous yet accessible and insightful description of the interaction between WEC geometry and sea state. It demonstrates why an operating frequency that corresponds to the wave spectrum peak frequency results in good performance. This relation can also be used to show that the spectral peak frequency is not always the choice of operating frequency that results in the most power capture. The equation can also be rearranged to give captured power as a function of monochromatic capture width and the sea state. Use of this relation to calculate power capture due to a specific sea state requires caution and rigour. Conditions for the validity of monochromatic capture width are given in § 5.2.2 and § 5.2.6, and common pitfalls of power calculations are described in § 6.2.5.

While Chapter 4 showed that optimal control required accurate predictions of future response, and ultimately future sea state, § 5.4 examines how far into the future these predictions are required, and how far into the future accurate predictions can be made from data collected on-site. Consideration of these time horizons shows how the sea state and the geometry of a WEC interact with control schemes that require future predictions. A newly introduced parameter, the premonition time, describes the shortfall between the required prediction horizon, and the prediction horizon possible using data collected on-site. This gives important indications as to the types of techniques suitable for making predictions, which shall be discussed further in § 6.3.

5.2 Capture width theory

When response is non-linear due to large displacements or non-linear PTO, then the appropriate performance indicator is the power captured for a particular spectrum or group of spectra. When the response is linear, the performance indicator capture width may be used. This section elaborates on the new theory presented in [122]. The capture width of a linear WEC is shown to depend on two properties: the spectral power fraction, a property introduced here which depends entirely on the sea state, and the monochromatic capture width, which is determined by the geometry of the WEC and the chosen power take off (PTO) coefficients. Each of these properties is examined in detail. Capture width is shown to be a measure of how well these two properties coincide.

The standard definition of capture width is the ratio of the power absorbed by the WEC to the power per metre wave front. The new theory presented here requires an expansion of the absorbed power and the wave energy transport using Plancherel's theorem. These expansions are discussed in § 5.2.2 - 5.2.4, and are put to use in § 5.2.5. The new theory suggests techniques for improved PTO control, and endorses the argument that geometry control deserves more attention. While capture width is a valuable design tool, its limitations must be recognised. Assumptions made in the formulation of capture width are listed in § 5.2.3.

5.2.1 Plancherel's theorem

In Chapter 4, various control strategies were compared by using the monochromatic capture width, calculated using discrete data, as the performance indicator. Therefore the theory developed here is for discrete data, and the type of Fourier transform used is the DFT (Table 2.6 on page 49). Plancherel's theorem for this configuration of the DFT is shown in Appendix B.1 to be (B.3): $\sum_{n=0}^{N-1} a[t_n]\, b[t_n] = \frac{1}{N} \sum_{j=0}^{N-1} A^*[\omega_j]\, B[\omega_j]$.

Plancherel's theorem is a generalised version of the better known Parseval's theorem, and can be used to describe the product of two time domain functions, integrated over time, as the product of their Fourier transforms, integrated over frequency. For discrete quantities, the product of two time domain functions, $a[t_n]\ b[t_n]$, summed over time, is related to the product of their DFTs, summed over frequency.

When transforming a sampled time series of finite length to the frequency domain, the DFT treats the time series as periodic with N. Thus the DFT version of Plancherel's theorem is defined for periodic functions.

5.2.2 Expansion of absorbed power

The instantaneous power absorbed by a WEC is the product of the PTO force and the velocity of the PTO mechanism relative to its point of reaction. The average power absorbed by a WEC,

P_A, over an interval of time containing N samples is the mean of this instantaneous power:

$$P_A = \frac{1}{N} \sum_{n=0}^{N-1} f_{pto}[t_n]\ u[t_n] \tag{5.1}$$

Assuming the PTO force and velocity are periodic with N, the DFT version of Plancherel's theorem (B.3) can be used to express the absorbed power as:

$$P_A = \sum_{j=0}^{N/2-1} P_A[\omega_j] = \frac{2}{N^2} \sum_{j=0}^{N/2-1} \Re\left\{F_{pto}[\omega_j]\ U^*[\omega_j]\right\} \tag{5.2}$$

The full derivation in Appendix B shows the origin of the $2/N^2$ coefficient. Multiplying a complex number by its complex conjugate gives the magnitude squared. So when the PTO force is a linear function of velocity (3.39), then (5.2) can be reduced to:

$$P_A = \frac{2}{N^2} \sum_{j=0}^{N/2-1} B_{pto}[\omega_j]\ \left|U[\omega_j]\right|^2 \tag{5.3}$$

It is useful to express absorbed power as a function of hydrodynamic coefficients and wave elevation. Combining (3.41) and (3.28), the velocity can be defined as:

$$U[\omega_j] = Z_{net}^{-1}[\omega_j]\ W[\omega_j]\ H[\omega_j] \tag{5.4}$$

Here Z_{net}^{-1} indicates either scalar reciprocal or matrix inverse. Notation consistent with matrix algebra is used for easy comparison with equations for multiple degrees of freedom, such as those in [71]. Substituting velocity (5.4) into the average absorbed power (5.3) gives:

$$P_A = \frac{2}{N^2} \sum_{j=0}^{N/2-1} B_{pto}[\omega_j]\ \left|Z_{net}^{-1}[\omega_j]\right|^2 \left|W[\omega_j]\right|^2 \left|H[\omega_j]\right|^2 \tag{5.5}$$

If the WEC is vertically symmetrical and moving in heave, then the diffraction coefficient can be eliminated. Substituting (3.36) into (5.5), absorbed power expands to:

$$P_A = \frac{8\rho g}{N^2} \sum_{j=0}^{N/2-1} \frac{B_{pto}[\omega_j]\ c_g(\omega_j, h)\ B[\omega_j]\ \left|H[\omega_j]\right|^2}{k(\omega_j, h)\ \left|Z_{net}[\omega_j]\right|^2} \tag{5.6}$$

The above equation is for a single degree of freedom. For a single degree of freedom, $Z_{net}[\omega_j]$ is not a matrix but a scalar, and as such the $Z_{net}^{-1}[\omega_j]$ notation is not used.

5.2.3 Conditions for the validity of expansions of absorbed power

The conditions to preserve the validity of the expansions of absorbed power are as follows:

(i) Equation (5.1) is defined for the general case where $u[t_n]$ is the velocity of the PTO mechanism

(ii) Equation (5.2) holds for velocity and PTO force that are periodic with the interval over which power is averaged

(iii) Equation (5.3) holds for PTO force that is a linear function of velocity

(iv) Equation (5.5) holds for velocity that is a linear function of wave elevation: (5.4)

(v) Equation (5.6) holds for vertical symmetry and one degree of freedom: heave

The hydrodynamic parameters, and hence velocity, are never truly linear functions of wave elevation. However, all experimental and numerical models assume that the relationship is linear, and indeed experimental work is often intentionally limited to small motions so that behaviour falls within a linear regime, as defined by those carrying out the experiment.

Note that no restrictions on causality have yet been put into place. No assumptions have been made about control schemes which have assigned values to the PTO settings. The most general definition of PTO impedance is used (3.40), which is why the PTO damping is expressed as $B_{pto}[\omega_j]$ rather than b_{pto}.

5.2.4 Expansion of wave energy transport

The power per metre wave front (also known as wave energy transport or power flux), as shown in Appendix B.3, can be expanded as:

$$P_{IW} = \sum_{j=0}^{N/2-1} P_{IW}[\omega_j] = \frac{2\rho g}{N^2} \sum_{j=0}^{N/2-1} c_g(\omega_j, h) \left|H[\omega_j]\right|^2 \tag{5.7}$$

Any expansion of wave energy transport is only valid for linear propagation of waves. Waves of small steepness are approximately linear in this respect. Any expansion of wave energy transport also implicitly presumes that the wave elevation $\eta[t_n]$ is caused by the passage of superimposed sinusoidal waves, all moving in the same direction. Furthermore, the above expansion (5.7), which uses the DFT version of Plancherel's theorem (B.3), is only valid for a time series of wave elevation that is periodic with N.

5.2.5 Standard definition of polychromatic capture width

Polychromatic capture width is defined as the ratio of the power absorbed (P_A) to the wave energy transport (P_{IW}):

$$C_W = \frac{P_A}{P_{IW}} \tag{5.8}$$

This is the width of the incident wave that contains the same amount of power as that absorbed. This definition implies that the spectrum of the incident wave is known, and that the waves are unidirectional. Despite this limitation, it is a useful performance indicator.

For small periodic waves, wave energy transport may be written as a linear function of wave elevation (5.7). Assuming that velocity is periodic and a linear function of wave elevation (conditions (ii)- (iv) in §5.2.3), absorbed power may also be written as a linear function of wave elevation (5.5). When all these conditions are satisfied, capture width (5.8) may be written as:

$$C_W = \frac{\sum_{j=0}^{N/2-1} B_{pto}[\omega_j] \left|Z_{net}^{-1}[\omega_j]\right|^2 \left|W[\omega_j]\right|^2 \left|H[\omega_j]\right|^2}{\sum_{l=0}^{N/2-1} \rho g c_g(\omega_l, h) \left|H(\omega_l)\right|^2} \tag{5.9}$$

Relative capture width

The theory that shall be presented in this chapter is also relevant to a widely used variation on the capture width, the relative capture width. Sometimes referred to as efficiency, this is the capture width normalised by the width of the WEC, w, with respect to the direction of wave propagation: $C_{Wr} = \frac{P_A}{\mathrm{w} P_{IW}}$. This performance indicator is used to compare WECs of different sizes. For the spherical geometry used in this research as an example, the width is the diameter: $\mathrm{w} = 2r$.

Capture width for monochromatic motion

In monochromatic experiments at the frequency ω_s, only one term in each sum is non-zero. The result is the monochromatic capture width:

$$C_W^s[\omega_s] = \frac{P_A[\omega_s]}{P_{IW}[\omega_s]} \tag{5.10}$$

Substitution for the expansions of absorbed power (5.5) and wave energy transport (5.7) gives:

$$C_W^s[\omega_s] = \frac{B_{pto}[\omega_s] \left|Z_{net}^{-1}[\omega_s]\right|^2 \left|W[\omega_s]\right|^2}{\rho g c_g[\omega_s, h]} \tag{5.11}$$

5.2.6 New extension to definition of polychromatic capture width

Following on from the assumption that both absorbed power and wave energy transport can be written as linear functions of wave elevation, absorbed power may be expressed as a linear function of wave energy transport. This is done by manipulating (5.5) so that it contains some terms that can be grouped as $P_{IW}[\omega_j]$, as seen in (5.7):

$$\begin{aligned} P_A &= \sum_{j=0}^{N/2-1} \frac{B_{pto}[\omega_j] \left|Z_{net}^{-1}[\omega_j]\right|^2 \left|W[\omega_j]\right|^2}{\rho g c_g(\omega_j, h)} P_{IW}[\omega_j] \\ &= \sum_{j=0}^{N/2-1} L[\omega_j]\, P_{IW}[\omega_j] \end{aligned} \tag{5.12}$$

where $L[\omega_j]$ is a linear operator. From (5.11) it can be seen that $L[\omega_j]$ is a function of frequency whose value is defined as the monochromatic capture width at that frequency, $C_W^s[\omega_j]$. Absorbed power may thus be written as:

$$P_A = \sum_{j=0}^{N/2-1} C_W^s[\omega_j]\, P_{IW}[\omega_j] \tag{5.13}$$

Substituting this into (5.8) gives:

$$C_W = \sum_{j=0}^{N/2-1} C_W^s[\omega_j] \frac{P_{IW}[\omega_j]}{P_{IW}} \tag{5.14}$$

Introducing a new term, the *spectral power fraction*:

$$P_f[\omega_j] = \frac{P_{IW}[\omega_j]}{P_{IW}} \tag{5.15}$$

allows the polychromatic capture width to be expressed as:

$$C_W = \sum_{j=0}^{N/2-1} C_W[\omega_j] = \sum_{j=0}^{N/2-1} C_W^s[\omega_j]\, P_f[\omega_j] \tag{5.16}$$

From this equation, it can be seen that capture width is a measure of the interaction between the monochromatic capture width (5.9), $C_W^s[\omega_j]$, which is a property of the device, and the spectral power fraction (5.15), $P_f[\omega_j]$, which is a property of the shape of the incident wave spectrum. The spectral power fraction is a new term introduced as an aid for clarity in this study.

5.2.7 Spectral property: power fraction

The spectral power fraction (5.15) is a function that gives the fraction of the total wave energy transport contained in each frequency component for a given wave spectrum. Its derivation assumed that the spectrum was defined for periodic seas, so it cannot be directly related to spectral measurements of real seas.

Substitution for wave energy transport (5.7) and group velocity (3.15) gives:

$$P_f[\omega_j] = \frac{\frac{D(\omega_j,h)}{\omega_j}\left|H[\omega_j]\right|^2}{\sum_{k=0}^{N/2-1}\frac{D(\omega_k,h)}{\omega_k}\left|H(\omega_k)\right|^2} \tag{5.17}$$

There are three important points to observe about this equation:

1. Spectral power fraction remains unchanged if the wave elevation spectrum is scaled, using the same scaling factor on each amplitude component. This means that power fraction characterises the spectral shape of the incident wave power spectrum.

2. Spectral power fraction is a function of water depth.

3. Spectral power fraction depends on the number of points in the DFT. This is because the magnitude of the elevation component $\left|H[\omega_j]\right|$ in the numerator, depends upon the width of the bin, whereas the wave energy transport in the denominator is the same, regardless of bin width. Nevertheless, the sum of the components of $P_f[\omega_j]$ over any given band of frequencies will always be the same, regardless of the bin width.

5.2.8 Device property: monochromatic capture width

In (5.16) it was shown that polychromatic capture width measured the interaction of a spectral property and a device property. This device property is a function giving the monochromatic capture width at each frequency:

$$C_W^s[\omega_j] = \frac{P_A[\omega_j]}{P_{IW}[\omega_j]} \tag{5.18}$$

This definition is a rearrangement of (5.13). Although it appears similar to (5.11), there is a subtle yet important difference. Equation (5.11) states that when only one sinusoid is present in the unidirectional wave, the capture width is $C_W^s[\omega_s]$. Equation (5.18) implies that the capture width due to a sinusoidal wave of frequency ω_s also equals the corresponding component of the device property that interacts with the spectral property to give the capture width in polychromatic conditions. The monochromatic capture width function $C_W^s[\omega_j]$ may be expanded as in (5.11) with $[\omega_j]$ for $[\omega_s]$.

Note that in (5.11) the monochromatic capture width does not contain wave amplitude terms. It does not depend on the wave spectrum; only on device characteristics. The polychromatic capture width (5.16) does however depend on characteristics of both the device and the wave spectrum. This important distinction between the monochromatic and polychromatic capture widths should not be forgotten. The distinction has been noted by some researchers, for example Delauré and Lewis [123], who described them as the steady state and spectral efficiencies. Work conducted for this degree of study showed for the first time [122] how these capture widths are related to one another.

5.2.9 The impact of PTO impedance on the capture width

From (5.11) it is seen that the monochromatic (and hence polychromatic) capture width depends on both the geometry and the control scheme. The geometry determines the values of the excitation coefficient W and the intrinsic impedance Z, while the control scheme determines the PTO impedance Z_{pto}. In Chapter 4 both the geometry (size) and the PTO scheme were shown to have an impact on the monochromatic capture width.

As any plot of capture width is specific to a particular choice of PTO impedance, care must be taken when producing or interpreting plots. Since capture width is defined in terms of PTO impedance, in order to evaluate it numerically and plot it, specific values must be assigned to the PTO impedance.

Capture width for causal control

One commonly used convention for indicating that capture width depends on the PTO impedance, is to plot several curves to show the effect of different PTO options. Fig. 4.19 is an example of this approach, displaying the monochromatic capture width calculated using (4.24) for the spherical buoy described in Table A.1. Each line indicated by a coloured open marker shows the monochromatic capture width due to impedance matching (4.33) at different values of operating frequency ω_p. Matching the impedance at one frequency is causal control, and the resulting monochromatic capture width is denoted $\breve{C}^s_W[\omega_j]$.

Capture width for optimal control

Another commonly used convention for plotting capture width is shown by the solid black markers in Fig. 4.19. This is the capture width for sinusoidal motion at frequency ω_s, when the PTO impedance has been chosen for optimal causal control (4.4), denoted $\tilde{C}^s_W[\omega_s]$. As indicated in Fig. 4.4, the choice of PTO coefficients that gives causal optimal control in monochromatic conditions, results in acausal optimal control for polychromatic conditions. Plotting various values of optimised $\tilde{C}^s_W[\omega_s]$ against frequency gives the upper limit associated with acausal optimal control $\tilde{C}^s_W[\omega_j]$. In monochromatic tests, the solid markers are realisable

without knowledge about the future. In polychromatic tests, they indicate an upper limit that is only attainable with the benefit of future knowledge [110].

Some authors, for instance [115], helpfully emphasise that this is an upper limit, using adjectives such as 'maximum'. The monochromatic capture width in [115] is a maximum not only because displacement restraints, as applied in [58], have not been considered, but also because the chosen PTO impedance assumes acausal optimal control. Many authors do not however indicate that this an upper limit when using PTO impedance optimised at each frequency. Therefore it is important when viewing a capture width plot to discern what value of PTO impedance was used.

Choice of control scheme when calculating capture width

The extension to the definition of capture width (5.16) given in this research is a measure of the interaction between the device (monochromatic capture width) and the sea state (power fraction). When performing this calculation, it is vital that the choice of PTO impedance is suitable. The upper limit of capture width (solid black markers in Fig. 4.19) should not be used to calculate polychromatic capture width. This is because optimising PTO at each frequency amounts to acausal optimal control, which cannot be implemented in real time. Estimating absorbed power (5.13) using monochromatic capture width calculated in this manner will give the power that would be absorbed if acausal control were somehow possible. Instead, monochromatic capture width calculated using a causal control scheme, such as those indicated by open coloured markers in Fig. 4.19, should be used. The PTO impedance used must be that applied in polychromatic waves. This will give the absorbed power due to linear motion in unidirectional waves. As discussed in §6.2.5, even this does not give a good indication of the absorbed power in real seas.

5.3 Application of capture width theory

5.3.1 Interaction between spectral and device properties

While the monochromatic capture width $C_W^s[\omega_j]$ has a different value at each frequency bin, the polychromatic capture width C_W is not a function of time or frequency, but has a single value. This is found by summing components at each frequency: $C_W = \sum_{j=0}^{N/2-1} C_W[\omega_j]$. Each frequency component is the monochromatic capture width multiplied by the power fraction (5.16): $C_W[\omega_j] = C_W^s[\omega_j]P_f[\omega_j]$. This multiplication can be visualised by plotting power fraction and monochromatic capture width on the same axes.

The upper plot in Fig. 5.1, shows the monochromatic capture width due to causal sub-optimal control (open diamonds), $\breve{C}_W^s[\omega_j]$, and monochromatic capture width due to acausal optimal control $\tilde{C}_W^s[\omega_j]$ (solid circles). This is the same heaving buoy as Fig. 4.19. It also shows the

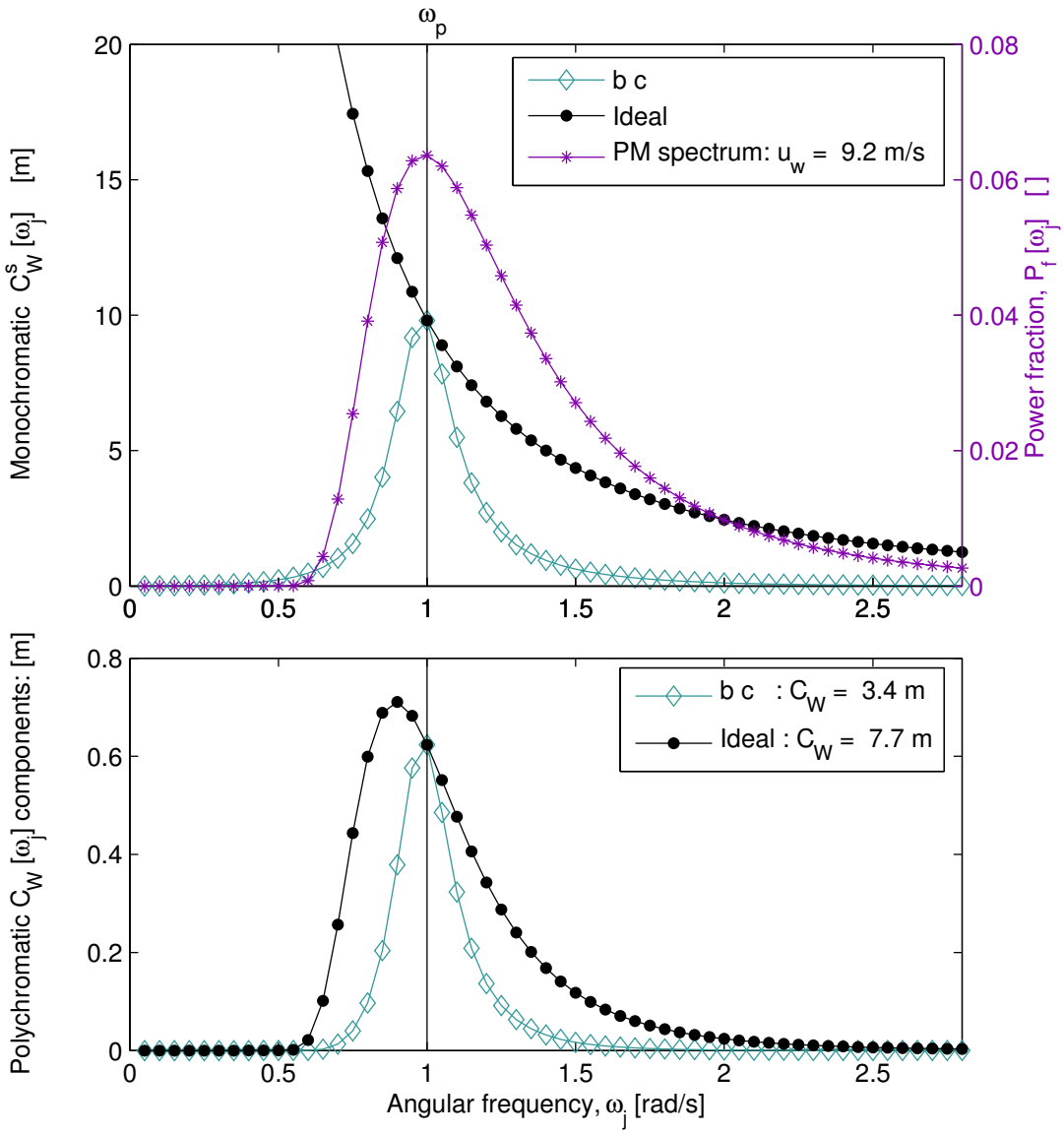

Figure 5.1: ***Polychromatic capture width for a damping-spring scheme:*** *monochromatic capture width for a 5 m diameter heaving WEC with a causal damping-spring scheme ($\breve{C}^s_W$ - b c), and for acausal optimal control ($\tilde{C}^s_W$ - ideal), plotted with power fraction for a PM spectrum (top). The components of polychromatic capture width are given for the causal and acausal schemes (bottom). The sum of these components gives the capture width: $C_W = \sum C_W[\omega_j]$ (legend in bottom plot).*

power fraction (asterisks) for a Pierson-Moskowitz (PM) spectrum [19]. The power fraction is for the PM spectrum due to a wind-speed of 9.2 m/s, which results in a peak in power fraction at 1 rad/s. The bin width used in 0.01 rad/s.

In the upper plot of Fig. 5.1, as well as the examples presented in Chapter 4, the monochromatic

capture width for the causal control scheme $\breve{C}_W^s$ equals that for acausal optimal control $\tilde{C}_W^s$ at ω_p. At all other frequencies, it is less than the upper limit:

$$\breve{C}_W^s \begin{cases} = \tilde{C}_W^s & \text{for all} \quad \omega_j = \omega_p \\ < \tilde{C}_W^s & \text{for all} \quad \omega_j \neq \omega_p \end{cases} \tag{5.19}$$

The amount by which $\breve{C}_W^s$ and $\tilde{C}_W^s$ differ is described by the normalised capture width introduced in § 4.6.2.

The products $\breve{C}_W[\omega_j] = \breve{C}_W^s[\omega_j]P_f[\omega_j]$ and $\tilde{C}_W[\omega_j] = \tilde{C}_W^s[\omega_j]P_f[\omega_j]$ can be seen in the lower plot. The legend in the lower plot gives the sum of these components $C_W = \sum C_W[\omega_j]$, which is the capture width as defined by (5.8).

There are two ways to view how the device and spectral parameters in the upper plot interact to give the components of capture width in the lower plot. The monochromatic capture width can be considered as a filter that operates on the power fraction, and weights the contributions of each spectral component to the capture width. Alternatively, the power fraction can be considered a band-pass function, or a tapered window, that determines which section of the $\breve{C}_W^s[\omega_j]$ contributes most to C_W. A large C_W requires that high values of monochromatic capture width coincide with high values of spectral power fraction. Indeed, the polychromatic capture width is effectively a measure of how well matched the monochromatic capture width and the spectral power fraction are.

5.3.2 Definition of polychromatic capture width in the presence of a monochromatic wave

Although the monochromatic $C_W^s[\omega_j]$ and polychromatic capture widths C_W share the same conceptual definition, they have different formulations, as seen in (5.16). They may be compared by considering the polychromatic capture width when the sea state is a monochromatic wave. The power fraction of a monochromatic wave is a delta function: $P_f = \delta[\omega_j - \omega_s]$, which means it has the following values:

$$\delta[\omega_j - \omega_s] = \begin{cases} 1 & \text{for} \quad \omega_j = \omega_s \\ 0 & \text{for all} \quad \omega_j \neq \omega_s \end{cases} \tag{5.20}$$

The product of this delta function and the monochromatic capture width, summed over all frequencies, gives the value of monochromatic capture width at ω_s:

$$C_W = \sum_{j=0}^{N/2-1} C_W^s[\omega_j]\ \delta[\omega_j - \omega_s] = C_W^s[\omega_s] \tag{5.21}$$

This equation is shown diagrammatically in Fig. 5.2. It shows the same data in Fig. 5.1, except

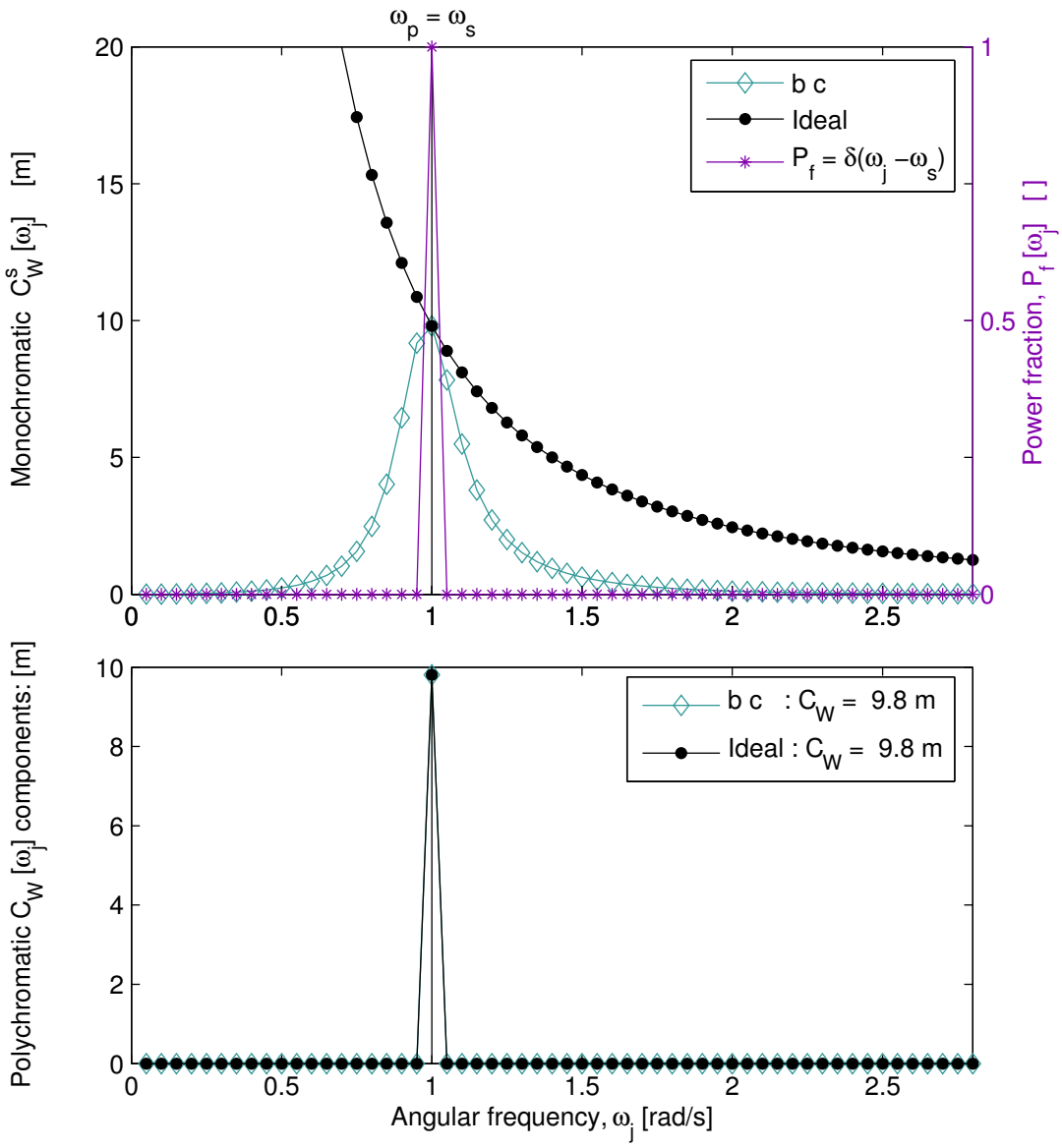

Figure 5.2: ***Polychromatic capture width for a monochromatic wave:*** *monochromatic capture width for a 5 m diameter heaving WEC with a causal damping-spring scheme ($\breve{C}_W^s$ - b c) and for optimal control ($\tilde{C}_W^s$ - ideal), plotted with power fraction for a monochromatic wave (top). The components of polychromatic capture width are given for the damping-spring and optimal schemes (bottom). The sum of these components is the capture width: $C_W = \sum C_W[\omega_j]$ (legend in bottom plot).*

that the spectral power fraction is that for a monochromatic wave (a delta function). There are several interesting points of note. The first is the value of the polychromatic capture width, shown in the legend in the lower plot. For both causal and acausal control, this happens to be the upper limit $C_W^s[\omega_s] = \frac{g}{\omega_s^2} = 9.8$ m, as the value used for gravity is $g = 9.8$ m/s^2.

This confirms that, for a monochromatic wave, the (total) capture width *is* the monochromatic capture width at that frequency.

The second point of note is that the polychromatic capture width C_W is the same for the optimal and damping-spring schemes. If a reactive impedance matching scheme is used with the operating frequency set to the frequency of the sinusoid, $\omega_p = \omega_s$, then the capture width is maximised for that frequency. This means that (5.21) gives the same results regardless of whether $\breve{C}_W^s[\omega_j]$ or $\tilde{C}_W^s[\omega_j]$ are used. It can be seen that the mass-damping and mass-damping-spring schemes discussed in Chapter 4 will also lead to optimal power production in monochromatic seas.

The third point of note is that the capture width $\breve{C}_W$ (legend in lower plot in Fig. 5.2) in a monochromatic sea is greater than that in the polychromatic sea (legend in lower plot in Fig. 5.1) shown here. This means that a given WEC could absorb more power in a monochromatic sea than in a polychromatic sea that contains exactly the same amount of power. This behaviour was noted by Salter and Lin [52], who showed for experimental measurements that monochromatic capture width plotted against period ($2\pi/\omega_s$) was higher than polychromatic capture width plotted against energy period for a spectrum with the same energy content as the monochromatic wave. Results presented in this thesis and in [122] *explain* the mechanism behind this phenomenon for the first time.

Not only is the capture width due to causal control less in polychromatic seas than in monochromatic seas, but the capture width due to optimal control $\tilde{C}_W$ is also less. The fact that the capture width due to optimal control should be less in spectral seas than in monochromatic seas is particularly surprising. It challenges the idea that for a heaving WEC, the upper limit of capture width that could be attained with perfect predictions is $\tilde{C}_W = \frac{g}{\omega^2} = \frac{\lambda}{2\pi}$. This upper limit is only ever valid in a theoretical sea containing only one sinusoidal component. When there are more components present, and there always are, the upper limit of capture width (legend in lower plot in Fig. 5.1) can be less than the capture width (legend in lower plot in Fig. 5.2) at the peak frequency of the spectrum, as is shown here. Further research is needed to confirm whether, there are spectra for which it is possible for the causal capture width, and the upper limit of capture width, to be higher than their respective counterparts given by monochromatic motion.

The effect of sea state bandwidth on the polychromatic capture width

The differences between Fig. 5.1 and Fig. 5.2 show that the bandwidth of the sea state has an effect on the capture width due to causal control. This has already been concluded from numerical simulation results [118]. The theory presented here confirms these results and explains their origin. It is worth keeping in mind that polychromatic capture width plotted against energy period, as in [52], is only valid for a particular shape of spectrum (spectral

power fraction). In general, a *peakier* spectrum will result in a higher polychromatic capture width than a broader spectrum, as more energy will lie at frequencies where there is better absorption.

5.3.3 The effect of sea state bandwidth on the extent to which forecasts can improve capture width

The differences between Fig. 5.1 and Fig. 5.2 also indicate that the bandwidth of the sea state has an effect on the upper limit of capture width due to optimal acausal control, and on the relationship between capture widths due to causal and acausal control. Two new parameters are introduced to describe this relationship: the forecast benefit parameter $(\tilde{C}_W - \breve{C}_W)/\breve{C}_W$, which is a measure of the extent to which forecasts can improve power capture, and $(\breve{C}_W)/\tilde{C}_W$, which is a measure of the performance of a causal scheme relative to the ideal scheme which requires forecasts. For a theoretical sinusoidal sea (Fig. 5.2), forecasts do not improve power capture. As the bandwidth of the spectral power fraction becomes wider, both the polychromatic capture width due to acausal optimal control, and the capture width due to causal sub-optimal control, become less than the $\tilde{C}_W = \frac{g}{\omega^2} = \frac{\lambda}{2\pi}$ limit. The capture width due to causal sub-optimal control drops faster, and so for wider bandwidth sea states the extent to which forecasts can improve power capture $(\tilde{C}_W - \breve{C}_W)/\breve{C}_W$ is higher. This is true for any WEC where the hydrodynamic coefficients vary over the band of frequencies for which the wave spectrum contains a significant amount of power. The high frequency asymptote of added damping is zero for all modes of motion [90], and as energy can only be captured when there is a non-zero added damping [105], it follows that in general WECs will have hydrodynamic parameters that vary over the band of frequencies defined by a sea state's spectral power fraction. Thus for all types of WEC, the power captured is inversely related to the bandwidth of the sea state.

Figs. 5.1 and 5.2 are for a damping-spring scheme. This was used as its performance is poor at frequencies distant from the operating frequency, and the differences between the causal and acausal optimal control schemes are thus clear. However, when measuring the extent to which forecasts can improve capture width, it is important to compare the capture width due to optimal control with that due to the mass-damping-spring scheme. The reason for this is that the high values of displacement due to optimal control are also seen in the mass-damping-spring scheme (Fig. 4.26). This is thus a fair comparison.

The effect of the control scheme on the polychromatic capture width

In Fig. 5.3 the difference between the various PTO schemes can be seen. For this combination of geometry (a 5 m diameter heaving spherical buoy) and sea state (a PM spectrum characterised by a wind speed of 9.2 m/s), the mass-damping-spring scheme gives a much higher capture width than the schemes involving only two PTO coefficients. In the lower plot of Fig. 5.3

Control scheme	$\check{C}_W$	$\tilde{C}_W$	$\check{C}_W/\tilde{C}_W$	$(\tilde{C}_W - \check{C}_W)/\check{C}_W$
mass-damping-spring	7.21 m	7.74 m	93 %	7.4%
damping-spring	3.41 m	7.74 m	44 %	130 %
mass-damping	1.07 m	7.74 m	14 %	620 %
damping	0.648 m	7.74 m	8.4 %	1100 %

Table 5.1: ***Capture width compared to that for optimal control:*** *The results from Fig. 5.3 are summarised. For the PM spectrum considered (with a spectral peak at 1 rad/s), optimal control can only improve on full reactive control by 7.4%.*

it can be seen that the superior performance of the three PTO coefficient scheme over those with two PTO coefficients is due to the bandwidth of $C_W[\omega_j]$, rather than the peak value. The schemes with only two PTO coefficients can be thought of as bandwidth limited reactive control schemes. They only have high efficiency absorption, as measured by normalised capture width, at a very narrow band of frequencies. They also only have a very narrow band for which there are high values of controlled displacement amplitude response, as shown in Fig. 4.26.

It is also interesting to note that the capture width for ideal control, which requires perfect predictions, is not much higher than that for the mass-damping-spring scheme. This was noted by Niato, [121] who compared 'variable and constant coefficient systems', which correspond to acausal optimal control and causal sub-optimal control using a damping-spring scheme.

The percentage by which a control scheme requiring predictions can improve on mass-damping-spring causal control, depends on the bandwidth of the sea state (see Fig. 5.2, which has the bandwidth of one bin), and, as shall be discussed next, the operating frequency (Fig. 5.5) and scale of the device (Fig. 5.9). For this combination of sea state, operating frequency, and geometry, upgrading from mass-damping-spring causal control to acausal optimal control yields only a modest increase of 7.4 % in capture width (see Table 5.1). Note that this figure does not take into account displacement restraints. The application of displacement restraints will reduce the benefits of predictions.

Fig. 5.3 shows that the capture width for real control is very low compared to the reactive schemes. The reason for this is that in this example the operating frequency is far from the natural frequency. As shown in Chapter 4, the performance of real control degrades as the separation between ω_p and ω_n increases. For $\omega_p = \omega_n$ the monochromatic capture width, and hence power capture, for real control and the two coefficient reactive control schemes are the same (Fig.4.25 on page 180).

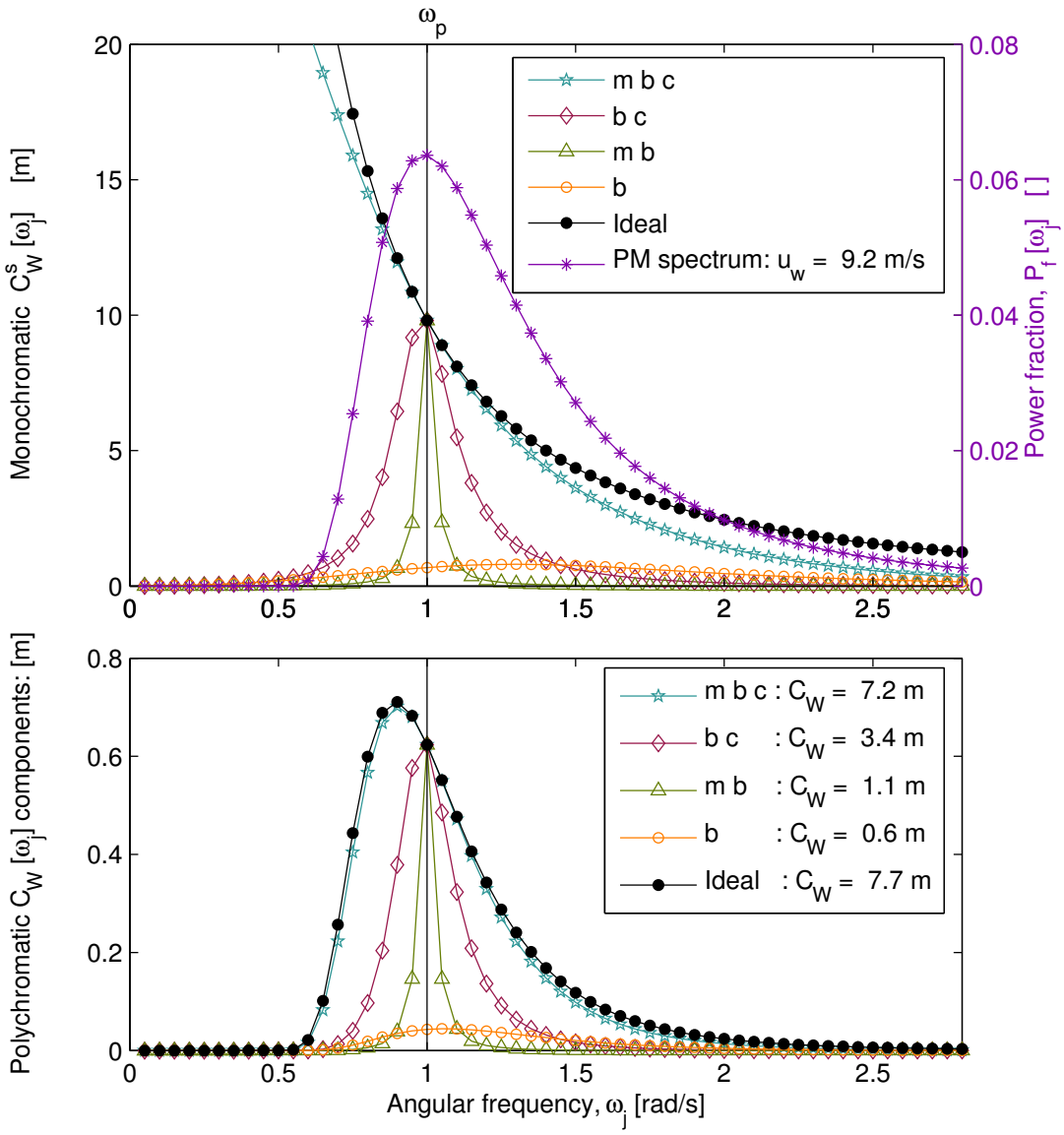

Figure 5.3: ***Polychromatic capture width for various PTO schemes:*** *monochromatic capture width for a* 5 *m diameter heaving WEC controlled with causal schemes (*$\check{C}^s_W$ - m b c, b c, m b, and b) and the optimal scheme ($\tilde{C}^s_W$ - ideal), plotted with spectral power fraction P_f for a PM spectrum (top). The sum of the components of the product of C^s_W and P_f is the capture width: $C_W = \sum C_W[\omega_j]$ (legend in bottom plot).

5.3.4 Aligning spectral and device properties using impedance matching

It seems intuitive that the monochromatic capture width should be optimised at the frequency for which the spectral power fraction is the highest [124]. Fig. 5.4 shows that in general, operating frequencies that are very far removed from the spectral power fraction peak do not

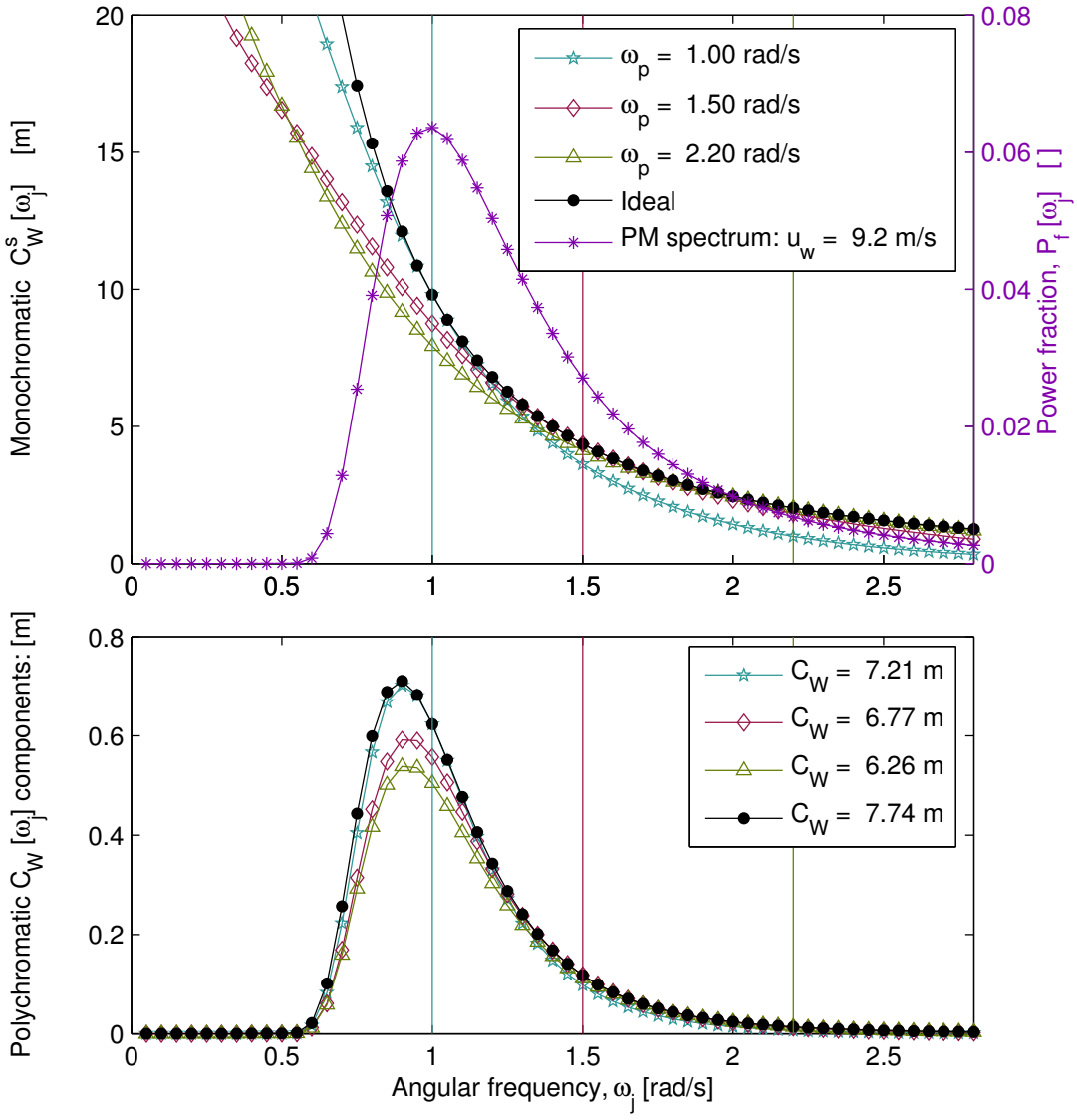

Figure 5.4: ***The effect of operating frequency on a mass-damping-spring scheme:*** *monochromatic capture width for mass-damping-spring schemes using different values of ω_p, applied to a 5 m diameter heaving buoy, and for optimal acausal control (ideal), plotted with spectral power fraction P_f for a PM spectrum (top). The sum of the components of the product of C_W^s and P_f is the capture width: $C_W = \sum C_W[\omega_j]$ (legend in bottom plot).*

give good performance. However, Fig. 5.5 shows that the spectral power fraction peak does not necessarily guarantee the best capture width. In this case, an operating frequency slightly higher than the spectral peak gives the best performance.

It is not a general rule that an operating frequency slightly higher than the spectral peak is preferable. The best choice of operating frequency depends upon the interaction between the

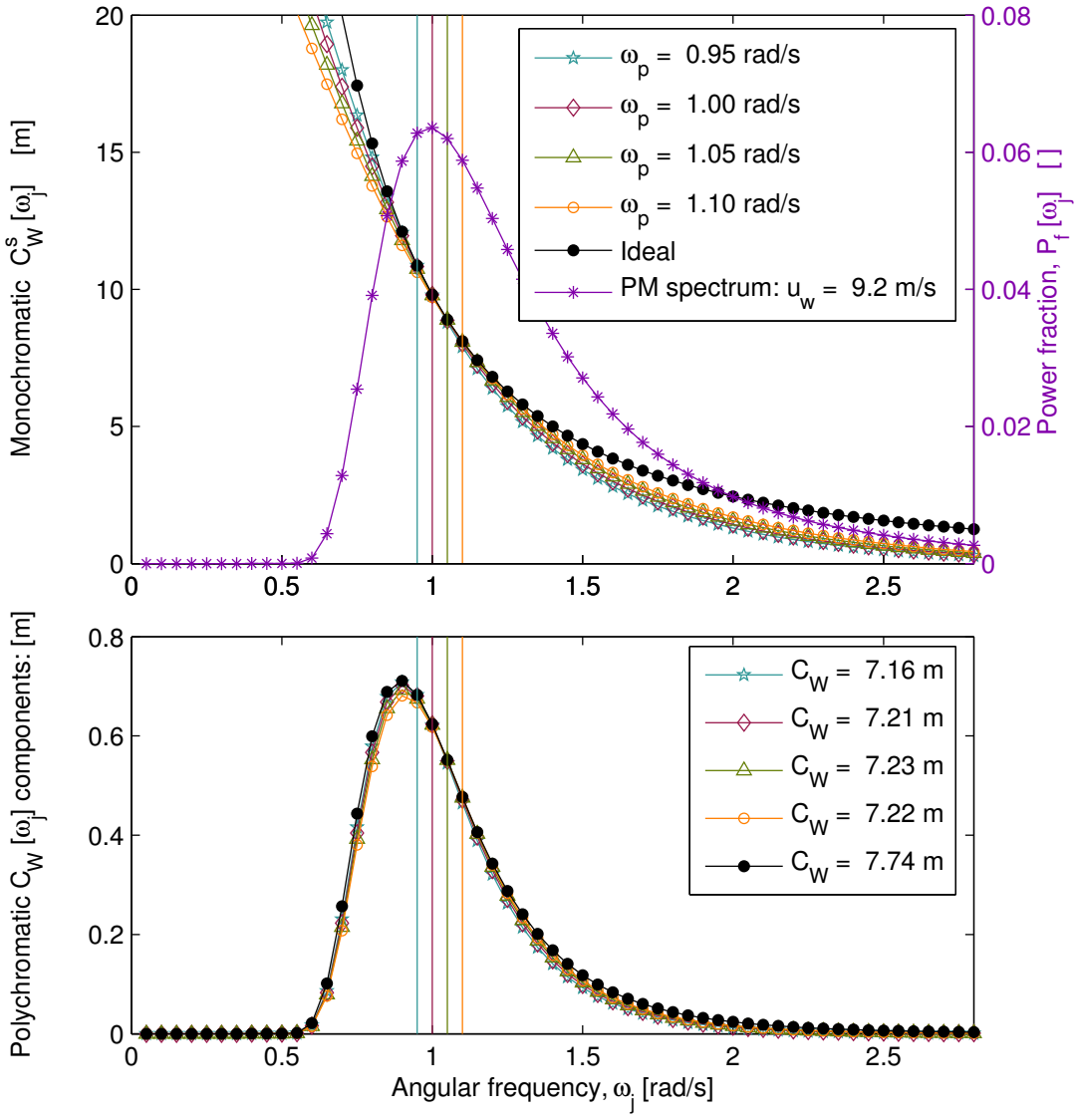

Figure 5.5: ***Optimal operating frequency for mass-damping-spring schemes:*** *monochromatic capture width for mass-damping-spring schemes using different values of ω_p, applied to a 5 m diameter heaving buoy, and for optimal acausal control (ideal), plotted with spectral power fraction P_f for a PM spectrum (top). The sum of the components of the product of C_W^s and P_f is the capture width: $C_W = \sum C_W[\omega_j]$ (legend in bottom plot).*

spectral power fraction and the monochromatic capture width. For the mass-damping scheme, an operating frequency slightly higher than the spectral peak gives the best performance (Fig. 5.6). However, this is not the case for the damping-spring scheme (Fig. 5.7). Here the spectral peak appears to be the best choice.

For all three reactive control schemes in combination with the PM spectrum shown, the spectral

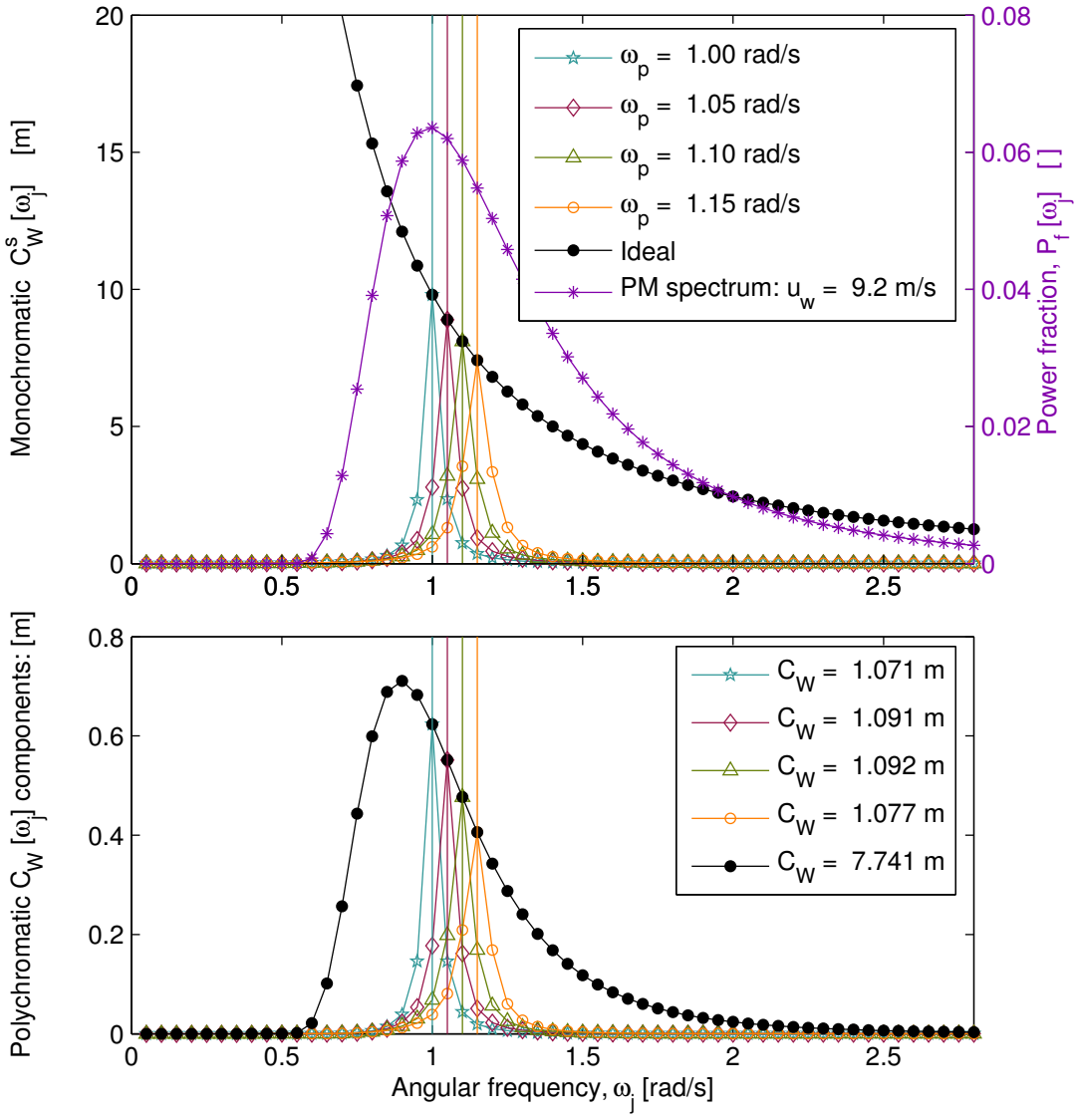

Figure 5.6: ***Optimal operating frequency for mass-damping schemes:*** *monochromatic capture width for mass-damping schemes using different values of ω_p, applied to a 5 m diameter heaving buoy, and for optimal acausal control (ideal), plotted with spectral power fraction P_f for a PM spectrum (top). The sum of the components of the product of C_W^s and P_f is the capture width: $C_W = \sum C_W[\omega_j]$ (legend in bottom plot).*

peak is a safe choice of operating frequency. In cases where there is a better choice of operating frequency, it is very close to the spectral peak, and it results in an improvement in capture width of under 1 % (Table 5.2 on page 222). For real control this is not the case (Fig. 5.8). Noting that the combination of the PM spectrum and geometry used leads to a natural frequency much higher than the spectral peak, the optimal choice of ω_p lies inbetween the ω_n and the spectral

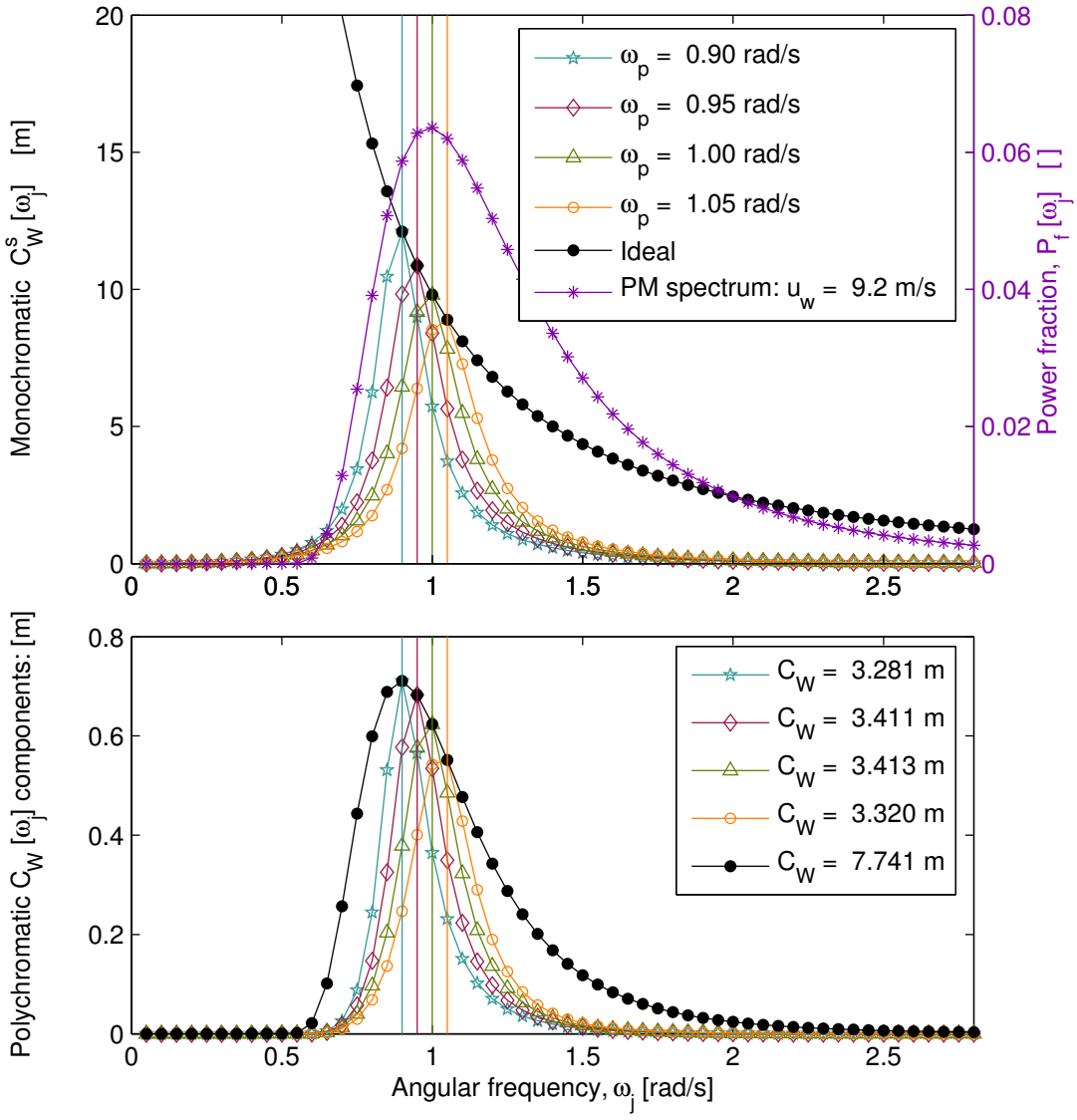

Figure 5.7: ***Optimal operating frequency for damping-spring schemes:*** *monochromatic capture width for damping-spring schemes using different values of ω_p, applied to a 5 m diameter heaving buoy, and for optimal acausal control (ideal), plotted with spectral power fraction P_f for a PM spectrum (top). The sum of the components of the product of C_W^s and P_f is the capture width: $C_W = \sum C_W[\omega_j]$ (legend in bottom plot).*

peak. The choice of an ω_p higher than the spectral peak results in an increase in performance of 6.5 % (Table 5.2). While this is not a substantial improvement, it is significant enough to be of interest to industrial developers whose devices are restricted to real control. Furthermore, this potential for improvement will depend on hydrodynamic design, and on the relationship between the ω_n and spectral peak.

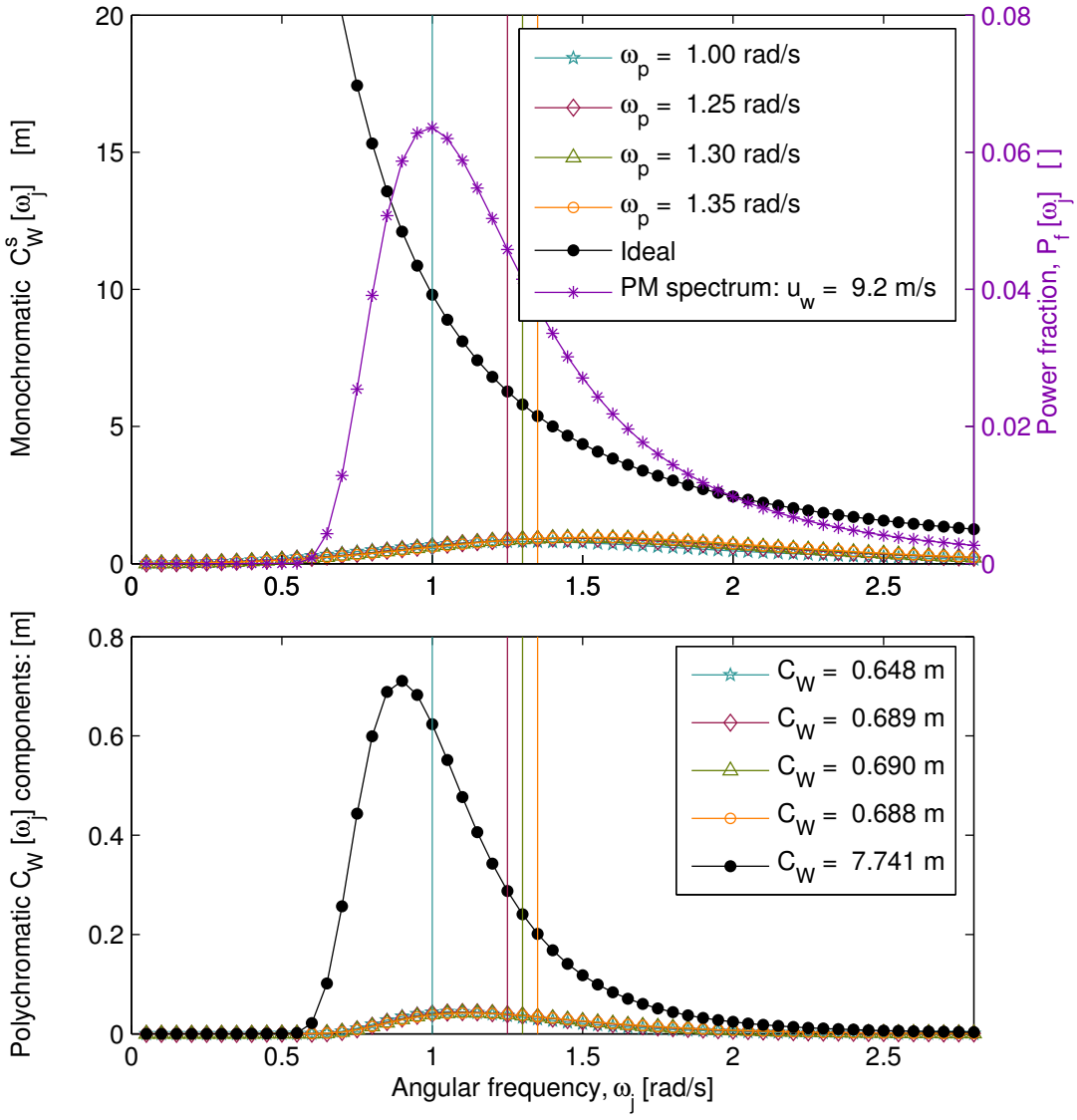

Figure 5.8: ***Optimal operating frequency for damping schemes:*** *monochromatic capture width for damping schemes using different values of ω_p, applied to a 5 m diameter heaving buoy, and for optimal acausal control (ideal), plotted with spectral power fraction P_f for a PM spectrum (top). The sum of the components of the product of C_W^s and P_f is the capture width: $C_W = \sum C_W[\omega_j]$ (legend in bottom plot).*

5.3.5 Choice of operating frequency

Table 5.2 shows that for real control, and the combination of geometry and sea state considered, capture width can be improved by the choice of operating frequency, ω_p. Calculating the optimal choice of ω_p using the theory of polychromatic capture width presented here can give improved performance compared to using the spectral peak. Table 5.2 also shows that for

Control scheme	$\breve{C}_W$ **at spectral peak**	$\breve{C}_W$ **at optimal** ω_p	$\%$ **increase**
mass-damping-spring	7.21 m	7.23 m	0.3 %
damping-spring	3.41 m	3.14 m	0.0 %
mass-damping	1.07 m	1.09 m	0.9 %
damping	0.65 m	0.69 m	6.5 %

Table 5.2: ***Performance increases due to optimal operating frequency:*** *For the PM spectrum considered (with a spectral peak at 1 rad/s), the percentage increase due to using the optimal operating frequency rather than the peak frequency, is the difference between the values of $\breve{C}_W$ given using the optimal ω_p and the spectral peak respectively, divided by the value of $\breve{C}_W$ at the spectral peak.*

reactive control, there is not much scope for large increases in performance by optimising the ω_p. Note that this only holds for this particular sea state. For spectral power fractions with broader bandwidths or different symmetry characteristics, this may not be the case. For a spectrum that does not have a single peak, it is clear that choosing the frequency location of the highest peak is not guaranteed to give the best performance. Thus even for reactive control, it may be useful to calculate the optimal ω_p using the polychromatic capture width. For a given sea state, the polychromatic capture width can be calculated for different values of ω_p. A plot of capture width against ω_p would identify the optimal choice of ω_p.

5.3.6 The limitations of PTO control using impedance matching

There are limitations associated with causal sub-optimal control. The limits to the polychromatic capture width that can be attained with causal sub-optimal control are:

1. The upper limit of the monochromatic capture width (acausal optimal control) $\tilde{C}^s_W[\omega_j]$ is determined by directionality and modes of motion.

2. In polychromatic seas the monochromatic capture width $\breve{C}^s_W[\omega_j]$ only reaches this upper limit at one frequency (5.19). At any other frequency, the difference between the monochromatic capture widths achieved with causal control, and aspired to with acausal control, depends on the intrinsic impedance.

3. The polychromatic capture width for causal control may be limited by the stroke, which is a displacement amplitude limitation. [58].

4. The polychromatic capture width for causal control may be limited by the rating of the PTO equipment and any restraints on reactive power necessary due to losses in the PTO cycle.

5. Causal sub-optimal control is only possible when the PTO equipment is capable of producing a force that is a linear function of its velocity.

The upper limit shown in Fig. 4.19 is that defined by Evans [56]. In the case of heave, this upper limit is a function of frequency: $\tilde{C}_W^s[\omega_j] = g/\omega_j^2$ (§ 4.6.2). It is determined by directionality and modes of motion only, and does not depend on the size, shape or orientation of the absorber.

However, the monochromatic capture width which is achievable using causal control $\breve{C}_W^s[\omega_j]$ does depend on the intrinsic impedance. It is affected by the size, shape and orientation of the absorber. Fig. 4.27 on page 184 shows monochromatic capture width (4.24) for three different sizes of the same heaving buoy, with impedance matched at the same frequency, using a mass-damping-spring scheme (4.33). For the larger buoy, the monochromatic capture width is closer to the upper limit over a broader band of frequencies than is the case for the smaller buoys.

Limits of the displacement and power restraints effect the polychromatic capture width rather than the monochromatic capture width because they depend on the sea state. Nevertheless, it is possible to apply such upper limits to the monochromatic capture width as long as the behaviour of the PTO remains linear. For instance, Pizer [58] applied displacement restraints at each frequency. As monochromatic waves were assumed, and the control was optimised at each frequency, the restraints were applied to the $\tilde{C}_W^s[\omega_j]$ given by causal optimal control (§ 4.5.1). One consequence of the need for restraints is that it may not be possible to use the most productive control scheme. For instance, rather than using the impedance matching scheme with three PTO coefficients, it may be necessary to use a scheme with only one or two PTO coefficients. Another consequence of restraints is that the behaviour of the PTO may become non-linear. Point five above acknowledge that causal sub-optimal control requires a PTO force that is a linear function of its velocity. Non-linear PTO behaviour may arise from power or displacement restraints, but may even be present when these restraints are not in place.

5.3.7 The effect of geometry on polychromatic capture width

Fig. 4.27 showed that at frequencies far from the operating frequency, the monochromatic capture width due to causal control is better for larger geometries. Fig. 5.9 is a repeat of this plot but for an operating frequency of 1 rad/s. A calculation of capture width as in Fig. 5.5 has not been undertaken as the hydrodynamic data used in this study does not cover high enough frequencies. As can be seen in Fig. 5.9, the frequency axis scales with radius, and high frequency values are not available for larger sized buoys. The spectral power fraction of a PM spectrum is asymmetrical, with a peak skewed towards lower frequencies and a tail that extends to higher frequencies where the data is incomplete. A fair comparison can only be made using data where the hydrodynamic coefficients approach their asymptotic infinite frequency values.

It is however possible to speculate on the impact WEC geometry could have on the capture width. The monochromatic capture width due to causal control of different sized WECs (Fig. 5.9) is similar in appearance to that for different values of operating frequency, shown in

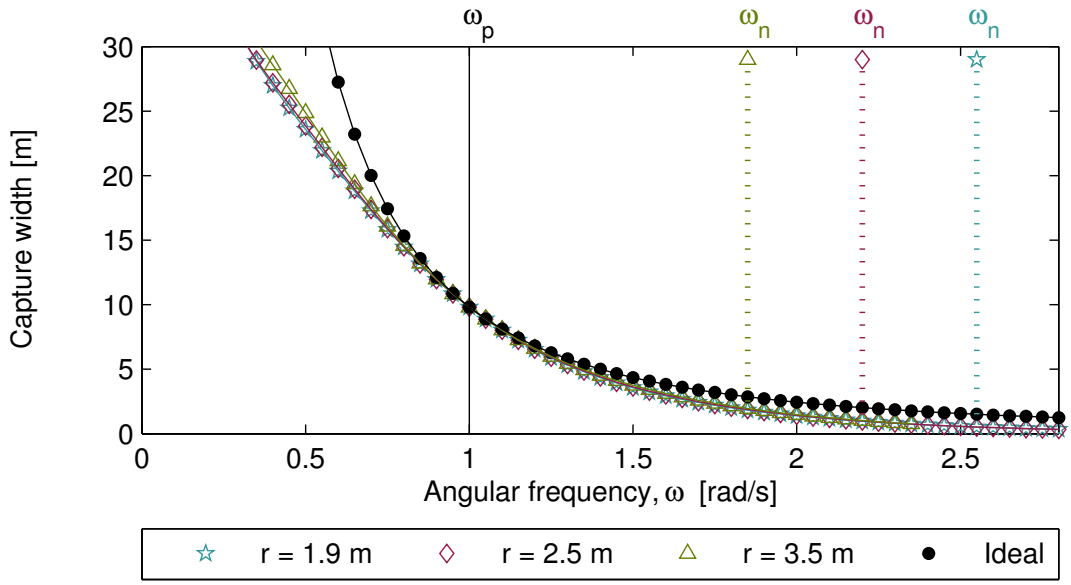

Figure 5.9: ***Monochromatic capture width for reactive controlled WECs of different sizes:*** *monochromatic capture width for a mass-damping-spring scheme using different values of radius, r.*

the upper plot of Fig. 5.5. It can be seen that the difference in polychromatic capture width for the different sized geometries is likely to be very small, as is the case for Fig. 5.5. Differences will be more pronounced for broader spectra.

Fig. 5.10 shows the monochromatic capture width for the same three sizes of buoy, using real control. There is more of a difference between the different sized WECs, particularly near the operating frequency. From this graph it looks likely that the polychromatic capture width associated with a PM spectrum with a peak at 1 rad/s will be higher for the larger geometry. This indicates that the size of the body (the position of the natural frequency) is more important for real control than for (full, mass-damping-spring) reactive control.

Matching spectral and device properties with geometry

In § 5.3.6 the limitations of PTO control were listed. Optimising (polychromatic) capture width via the PTO impedance is only one of the available tools. Another available tool is the geometry of the WEC. In this context, a change in geometry refers to anything that alters the intrinsic impedance or excitation coefficient. Geometry control used along with PTO (causal sub-optimal) control has the potential to be more effective than impedance matching alone.

The geometry can be considered at the design stage and during operation. At the design stage, it is important to choose a geometry for which implementable control, such as impedance matching at one frequency, results in a good (monochromatic) capture width relative to the

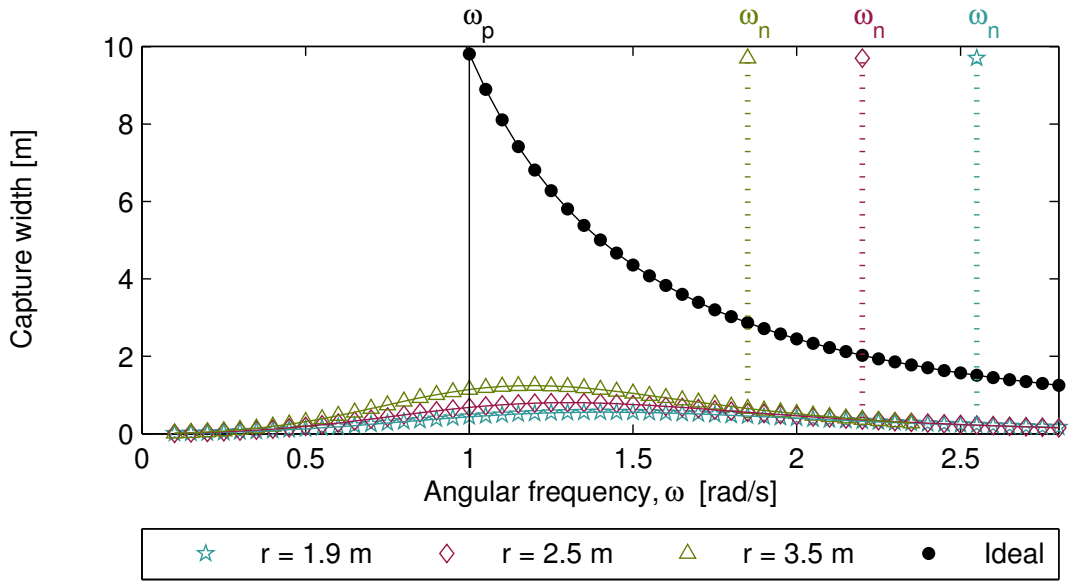

Figure 5.10: ***Monochromatic capture width for real controlled WECs of different sizes:*** *monochromatic capture width for a damping control scheme using different values of radius, r.*

expected sea states. Design approaches that consider the trade-off between displacement restraints and capacity factor, or ensure broad response, or where the choice of natural frequency is influenced by the spectral peak of a design sea state, fall into this category.

If during operation, the physical properties are altered to improve the match of the monochromatic capture width with the sea state, then this is geometry control. There are two mechanisms for this. Either the directionality or modes of motion can be used to change the upper limit of monochromatic capture width, or the intrinsic impedance can be changed so that it is easier to match using a given control strategy.

One of the ways in which geometry control works is by moving the natural frequency, ω_n, closer to the operating frequency, ω_p. In Chapter 4 it was shown that all types of impedance matching, especially real control, worked better when the ω_n and the ω_p were closer. The value of ω_p has an optimal value for a given sea state, and moving from this optimal ω_p towards the ω_n will reduce the power captured (see for example Fig. 5.5). Allowing some adjustment of the ω_n gives the control system an additional *degree of freedom* (in the metaphorical sense).

The various methods of implementing geometry control (§ 2.3.1) are well known [32] and are receiving attention from device developers (§ 2.3.4). The Archimedes Waveswing incorporates air springs [43]. The Pelamis controls its angle of motion with respect to the water surface by changing the ratio of PTO forces in two orthogonal degrees of freedom [48]. The Wavedragon adjusts air levels in reservoirs, which affects the wetted surface and acts as an air spring [46].

5.3.8 The relationship between design and geometry control

Both design and geometry control involve making decisions that effect the device dynamics (intrinsic impedance) or the coupling with the sea (excitation coefficient). However, in design the decisions are made before construction, whereas in geometry control the decisions are made during operation.

The design of a WEC could include mechanisms to allow geometry control. If the provision for geometry control is not built in to the design, then once the device is constructed, it is not possible to control the WEC's hydrodynamic and dynamic characteristics. This does not mean that once a WEC without geometry control has been designed and built, that these coefficients do not change. Although there is no control over them, they could change in some circumstances. For example, in a bottom-mounted, overtopping device or OWC, the wetted volume will change with tidal levels. In an asymmetrical device that is not able to orientate itself, the coupling with the waves depends on wave direction, because the exciting force is a function of wave direction.

Thus design does not necessarily involve choosing and fixing the hydrodynamic and dynamic device characteristics. Instead, it determines the operational range of hydrodynamic and dynamic characteristics due to resource variability and geometry control. There is great freedom in choosing this range of characteristics. Once the device has been built, geometry control can be used to tweak these characteristics, within the range predetermined by the design.

5.3.9 New contributions to capture width theory

Similarities to previous work

Some of the ideas presented in § 5.2 can be seen in different forms in the literature. Several authors have illustrated that it is preferable for the performance to coincide with the wave spectrum, by plotting the performance (monochromatic capture width) and a spectral parameter on the same graph. For instance, Falnes plotted the performance together with the spectrum [55], while Thomas plotted the performance together with the spectrum normalised by the peak spectral component [24] (see also earlier work by Weber and Thomas [125]).

The components of capture width, $C_W[\omega_j]$, seen in the lower plot of diagrams such as Fig. 5.8 are called the power absorption density by Thomas, and have been calculated and plotted by Thomas and Gallagher [126], and Weber and Thomas [127]. To calculate the power absorption density, the equation for capture width (5.16): $C_W = \sum_{j=0}^{N/2-1} C_W^s[\omega_j]\ P_f[\omega_j]$ is required. While it is clear that an equation of this nature was in use as early as 1993 [126], the formula was first published in 2008 [24]. Equation (3.52) in [24] is of a similar form to (5.16) presented

in this thesis. Using the same notation as in this thesis, Thomas's equation is:

$$\breve{C}_W = Max\left\{\frac{1}{P_{IW}}\int_{f_1}^{f_2} P_{IW}(f)\breve{C}_W^s(f)df\right\} \tag{5.22}$$

There is an integral rather than a sum because a continuous range of frequencies is considered. It can be seen that the spectral power fraction term introduced in this thesis is expressed as two terms in (5.22): the component of incident power within the integral, $P_{IW}(f)$, and the total incident power, P_{IW}, which appears outside of the integral. Plots of what appears be the power absorption density appeared as early as 1982, in a conference paper reporting on the Kværner multiresonant OWC [128].

New contribution

While some aspects of the theory presented in this section have been used by other authors, for the first time a thorough consistent description of capture width theory is given. The decomposition of the power absorption density $C_W[\omega_j]$ into parameters describing the device and sea state (monochromatic capture width and spectral power fraction) gives a clear description of why and how capture width is a measure of the interaction between the WEC (geometry and PTO) and the sea state. The concept of capture width is well established in wave energy literature, so it is useful to differentiate between capture width in monochromatic and polychromatic conditions. The relationship between monochromatic and polychromatic capture widths is confirmed by theoretical consideration of monochromatic behaviour (5.21). The derivation in § 5.2 is mathematically rigorous and can be traced back to first principles using Plancherel's decompositon.

As monochromatic and polychromatic capture widths are so well established, it is conceptually appealing to have a single sea state parameter linking these concepts. While the spectrum normalised by the peak spectral component has the same shape as the spectrum, the spectral power fraction has a different shape: in (5.17) it can be seen it differs from the spectrum by a factor of $1/\omega$. When plotting the WEC performance and a representation of the sea state on the same axes, it is more meaningful to choose the spectral power fraction than the spectrum (or normalised spectrum): the product of the spectral power fraction and WEC performance gives an indication of the proportion of power absorbed at each frequency.

The representation of spectral power fraction $P_f[\omega_j]$ and performance $C_W^s[\omega_j]$ in one plot, and power absorption density $C_W[\omega_j]$ in a second linked plot is seen here for the first time. This representation clearly demonstrates the new capture width formulation (5.16). These plots have been used to demonstrate that the optimal choice of operating frequency is not the spectral peak (Fig. 5.8), and to explain why the capture width $\breve{C}_W$ in irregular seas (PM spectrum) is lower than in a sinusoidal sea of corresponding period (Figs. 5.1 - 5.2). This representation was also

used to identify that even the theoretical upper limit of capture width $\tilde{C}_W$ is lower in a PM spectrum than in a corresponding sinusoidal sea, which was not previously known. As these plots can also be used to show the theoretical upper limit of power absorption density $\tilde{C}_W[\omega_j]$, they also give a visual indication of the forecast benefit parameter $(\tilde{C}_W - \breve{C}_W)/\breve{C}_W$.

5.4 Premonition time

In the previous section, a study of the measure of the interaction between a WEC and the sea state (the polychromatic capture width) showed that (for the geometries and sea states considered) there was a modest improvement in energy capture by using control that required the use of predictions. In this section, the required prediction horizons, and the locally available prediction horizons are studied. For this, it is necessary to consider the control problem in the time domain, and to understand the relationships between time and frequency domain descriptions of hydrodynamic parameters.

5.4.1 Mathematical expression of the need for future knowledge

The need for predictions becomes clear when the forces due to optimal acausal control are considered in the time domain. In Chapter 4 the PTO force for ideal optimal control was defined as (4.18):

$$\tilde{f}_{pto}(t) = -(m + m_\infty)a(t) + \int_0^\infty k(\tau)u(t+\tau)d\tau - cx(t) \tag{5.23}$$

Adding the optimal PTO force (4.18) to the equation of motion (3.48) gives the equation of motion that would result under optimal control:

$$\begin{aligned} \tilde{f}_e(t) &= (m + m_\infty)a(t) + \int_0^t k(\tau)u(t-\tau)d\tau + cx(t) + \tilde{f}_{pto}(t) \\ &= \int_0^t k(\tau)u(t-\tau)d\tau + \int_0^\infty k(\tau)u(t+\tau)d\tau \end{aligned} \tag{5.24}$$

The terms involving spring and mass cancel. What remains behind is the integral from (3.48), which represents the effects of past motion on instantaneous radiation force, and the integral from (4.18), which represents the effects of future motion on the ideal control force. The first integral is associated with system memory. In drawing a parallel to this concept, the second

integral can be thought of as the *premonition integral*:

$$\int_0^\infty k(\tau)u(t+\tau)\,d\tau \tag{5.25}$$

Another way of expressing this is $k(t) * u(-t)$; the memory kernel is convolved with the time reversed velocity. Although the limits of (5.25) are from 0 to ∞, the upper limit is a finite time dictated by the duration of the memory kernel, Δt. At $t > \Delta t$ the memory kernel, and thus the premonition integral, is zero.

The kernel duration is the required prediction horizon; beyond this foresight is not required. It is also useful to have a time horizon beyond which it is not possible to predict behaviour using only locally gathered information. As shall be explained, this horizon is the coherence time of the velocity τ_c. The remainder of this chapter is about the interaction of these two time horizons. The time by which the required prediction horizon exceeds the prediction horizon possible with locally gathered information has been named the *premonition time*, τ_{future} [88].

5.4.2 Prediction horizons defined by duration and coherence

In order to find the required prediction horizon from the memory kernel and the locally available prediction horizon from the velocity, the concepts of duration and coherence time are essential. Related to these is the frequency domain concept of bandwidth. Bandwidth Δf, duration Δt, and coherence τ_c are described below.

Bandwidth

Bandwidth is the range of frequencies over which a signal contains a significant amount of energy. In general it is defined by the difference between bounding frequencies: $\Delta f = f_2 - f_1$. In the present problem, the bandwidths of the frequency dependent radiation impedance $K(\omega)$ and the velocity $U(\omega)$ are of interest.

Duration

The expansion - compression principle [60] or scaling law [61] is a property of the Fourier transform (§ 2.4.3). An expansion of the time domain signal over time leads to a compression of the frequency domain expression over frequency (both in amplitude and phase), and vice versa. The duration of a time domain signal that decays to zero is inversely related to the bandwidth of its Fourier transform: $\Delta t \propto 1/\Delta f$. The constant of proportionality is also known as the time-bandwidth product, and it is greater than or equal to a certain minimum value, the size of which depends on the values of the time and frequency functions at zero [61].

Coherence time

For a signal with infinite duration, the reciprocal of the bandwidth gives another interesting time domain property: the coherence time. This is a concept borrowed from the field of optics, where light waves, such as those from lasers, can be close to sinusoidal over large distances. The coherence time can be thought of as the time over which a signal can be approximated by its sinusoidal extrapolation. It is defined as the time for which the autocorrelation of the time domain signal [129] is above a given threshold. Given the correct choice of thresholds, the bandwidth and coherence time are the reciprocal of one another: $\tau_c \approx 1/\Delta f$.

For sea waves, which typically have bandwidths too broad to be classified as pseudo-sinusoidal, the coherence time is relatively short. In the present problem, it is the coherence time of the WEC velocity that is of interest. Section 5.4.4 discusses how the bandwidth of the sea state affects the coherence time of the velocity.

Locally available data

Coherence time is the time for which predictions can be made to a given accuracy, using only past values of the signal. Thus it describes the prediction horizon for locally collected data. Here locally collected means that the data to be predicted and the data used for prediction are past and future values of the same time series. It is possible to use signals other than past values of the signal being predicted. For these to be useful, they must be collected from a position upstream of wave propagation. This means that the wave will pass the data collection point before it reaches the WEC. The directionality and non-linearity of wave propagation will inevitably place limits on the increased prediction horizon possible using remotely collected data (§ 5.5.2). More research is needed to ascertain whether the prediction horizon for remotely collected data (in real seas) is sufficient to improve on the performance of full (mass-damping-spring) reactive control.

Choice of formula for duration, coherence time, and bandwidth

There are several definitions of bandwidth [130], each with different definitions of the bounding frequencies. In electrical engineering, the most widely used definition of bandwidth is the half power, or 3dB, bandwidth [131]. Here the bounding frequencies are those at which the signal has half the power it has at the peak frequency. These frequencies are where the magnitude of the Fourier transform drops below a threshold, given by $1/\sqrt{2}$ of the maximum value of the Fourier transform.

Like bandwidth, there are many ways to measure duration. The definition of duration corresponding to the half power bandwidth is the half power equivalent rectangular duration: a rectangle with height equal to the signal's peak, and width equal to the duration, has an area that is half the area under the square of the signal. Duration can also be defined in terms of

the signal's autocorrelation [132]. In all cases there are pairs of definitions for bandwidth and duration, and likewise for bandwidth and coherence time. What matters most is that consistent definitions are used.

When the duration is used for the upper limit of the premonition integral, it is assumed that $\int_{\Delta t}^{\infty} k(\tau)u(t+\tau)\ d\tau \approx 0$. It is therefore preferable to choose a definition of Δt, and consequently Δf and τ_c, where $\int_0^{\Delta t} k(\tau)u(t+\tau)\ d\tau \approx \int_0^{\infty} k(\tau)u(t+\tau)\ d\tau$ is a good approximation. Values of coherence and duration are not calculated here, but it is nevertheless useful to have in mind how these prediction horizons would be calculated.

5.4.3 The interaction of duration and coherence

The premonition time is now examined qualitatively. The premonition time is defined as the time for which the required prediction horizon (duration of the memory kernel) exceeds the locally available prediction horizon (coherence of the velocity):

$$\tau_{future} = \max\{\Delta t - \tau_c, 0\} \tag{5.26}$$

First, two extreme theoretical cases are examined (Fig. 5.11): the case where the velocity is sinusoidal (infinite coherence) and the case where the velocity is white noise (no coherence). Next, two cases that could realistically occur are considered (Fig. 5.12): the case where the coherence of the velocity is so long that all the information required for optimal control can be readily deduced by sinusoidal extrapolation, and the case where the coherence is not long enough to provide the required information.

In all diagrams, the velocity plot shows the future value of the velocity signal as a solid line, and the sinusoidal extrapolation as a dotted line. The coherence can then be visualised as the length of time for which the velocity signal and its sinusoidal extrapolation have similar values. The signals shown in Fig 5.11- 5.12 are for demonstration purposes only, and do not represent specific geometry or sea states.

Infinite coherence

First the case of a WEC operating in a sinusoidal sea is considered. This is not to suggest that this is behaviour to be expected in a WEC; rather this is an examination of the consequences of this theoretical case. For a linear model, a sinusoidal wave elevation will result in a sinusoidal velocity. The bandwidth of a single sinusoid is zero, so the coherence is infinite. It is well known that for experiments in sinusoidal conditions, the optimal control conditions can be achieved without requiring any future knowledge (for instance [111]). The PTO force could be written as:

$$\tilde{f}_{pto}(t) = -[m + M_s]a(t) + B_s u(t) - cx(t) \tag{5.27}$$

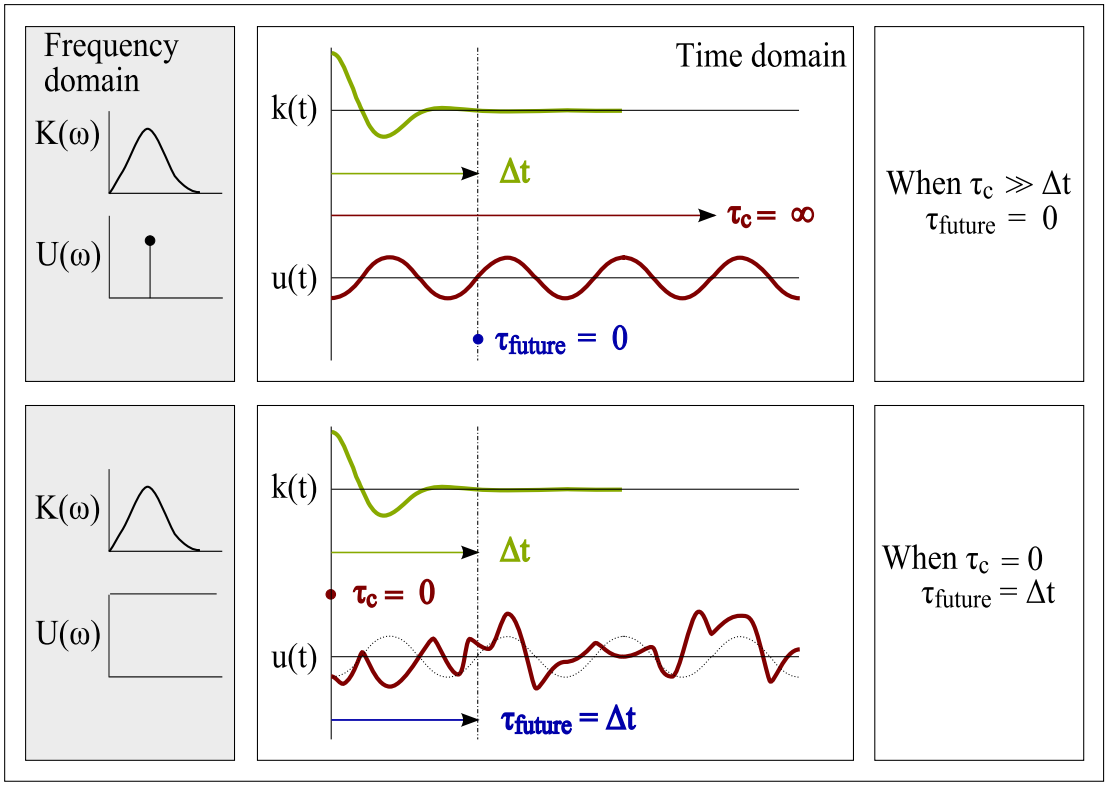

Figure 5.11: ***Duration of memory compared to coherence of velocity for theoretical extreme cases:*** *of infinite coherence (top) and zero coherence (bottom). Shaded box shows Fourier transform magnitudes corresponding to each time plot. The dotted line on the velocity plot shows a sinusoidal extrapolation.*

where the subscript zero indicates a single value, rather than a function of time, that depends on the frequency of the sinusoid, ω_s. The multiplication of a time domain function with a constant is mathematically equivalent to convolving the function with a delta function scaled by the constant: $B_s u(t) = B_s \delta(t) * u(t)$. Equation (5.27) can be compared to the general equation for PTO force, (5.23), by considering an alternative arrangement of the corresponding equation in the frequency domain (4.16) that resulted in two convolutions, one with acceleration and the other with velocity. For sinusoidal motion, the convolution kernels, which are functions of time, may be replaced with scaled delta functions. This is possible because all the information about the future motion that would be windowed by the kernel functions is contained in the values of instantaneous motion (acceleration and velocity). The top plot in Fig. 5.11 shows that whatever the duration of the memory kernel, the function of velocity within that duration can be calculated by sinusoidal extrapolation. When the available information is infinite, the premonition time, τ_{future}, is zero.

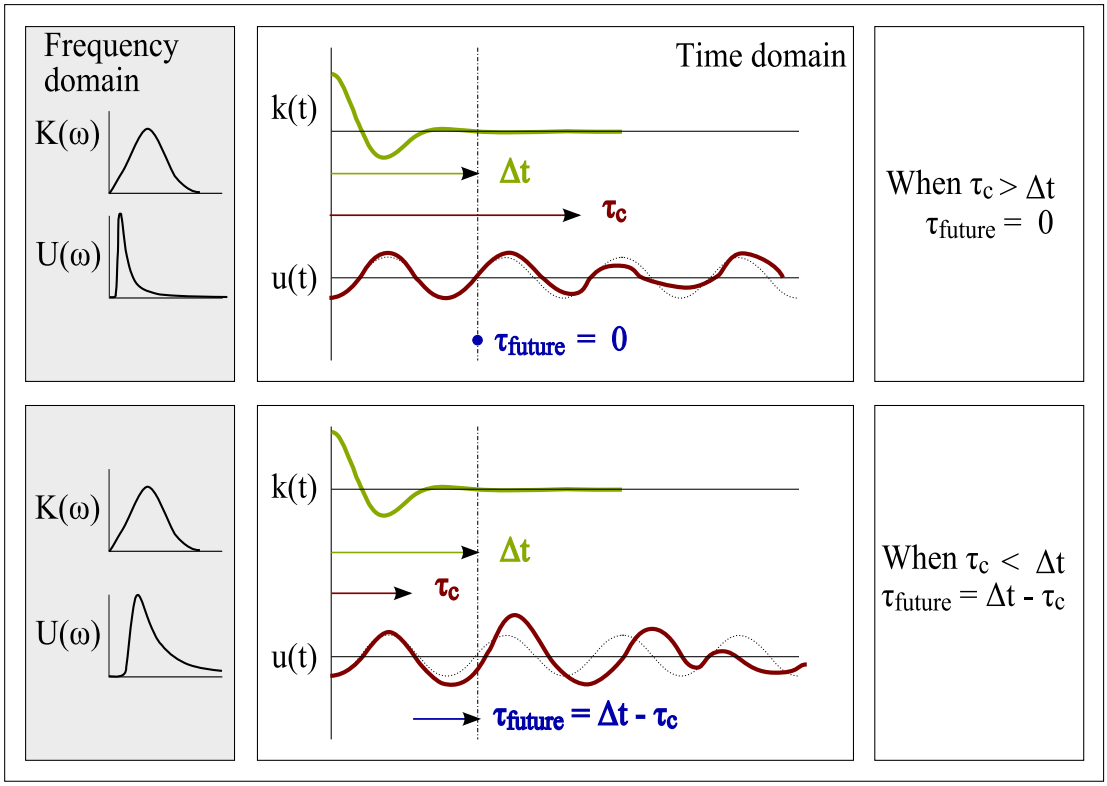

Figure 5.12: ***Duration of memory compared to coherence of velocity for possible cases:*** *of coherence being longer than the duration (top) and coherence being shorter than the duration (bottom). Shaded box shows Fourier transform magnitudes corresponding to each time plot. The dotted line on the velocity plot shows a sinusoidal extrapolation.*

No coherence

The extreme opposite of sinusoidal motion is velocity consisting entirely of white noise. Once again, this is not a realistic sea state, but an examination of the consequences of this theoretical case. The bandwidth of white noise is infinite; the coherence is therefore zero.

For optimal control, the required knowledge is the memory duration, Δt. Within the window of this duration, it is not possible to predict the velocity using sinusoidal extrapolation. The bottom plot in Fig. 5.11 shows that when the velocity has no coherence, future knowledge for the full duration of the memory kernel is required to find the optimal control force. When the available information is zero, the premonition time, τ_{future}, is the duration of the required information, Δt. The dotted line shows a sinusoidal extrapolation. A sinusoidal extrapolation in this case is problematic as it is not clear how the frequency is chosen. However, it does not matter. The extrapolation for any chosen frequency will have zero correlation with a noisy signal at all time shifts.

Long coherence

The sea states expected in the real world will lead to velocity that falls between the extreme theoretical cases of a sinusoid and white noise. In the upper diagram of Fig. 5.12, it can be seen that if the coherence of the velocity is longer than the duration of the memory kernel, then no future knowledge is required. When the available information is more than the required information, the premonition time, τ_{future}, is zero.

Short coherence

When the locally available prediction horizon is less than the required prediction horizon, the premonition time, τ_{future}, is the shortfall between them, $\Delta t - \tau_c$. This is shown in the bottom plot of Fig. 5.12. Given access to accurate information about the motion at a time $\Delta t - \tau_c$ into the future, the coherence of the velocity could be used to calculate the remaining future velocity required for convolution with the memory kernel.

5.4.4 Factors that influence the memory duration

The effect of radiation damping on memory duration

The frequency dependent radiation impedance $K(\omega)$ is dominated by the radiation damping $B(\omega)$, and the added mass and radiation damping are linked by the Kramers-Kronig relations. Thus it would be expected that the bandwidths of $K(\omega)$ and $B(\omega)$ are related. For a given geometry [102] and size, the bandwidth of $K(\omega)$ was found to equal the bandwidth of $B(\omega)$. Scaling up (considering larger sized buoys) results in a smaller bandwidth of $B(\omega)$ and $K(\omega)$, and thus a longer memory duration, Δt.

The effect of radiation damping on velocity coherence

For linear PTO, velocity can be expressed as $U(\omega) = W(\omega)H(\omega)/Z_{net}(\omega)$. The magnitude of the $W(\omega)/Z_{net}(\omega)$ term is the transfer function between velocity and wave elevation. Here it is referred to as the controlled velocity response amplitude operator, and is denoted R_c. The shape of R_c is important as it operates on the shape of the wave elevation magnitude. The bandwidth of the velocity depends on the bandwidth of the wave elevation, and on how R_c modifies the shape of $H(\omega)$. Fig. 5.13 compares the R_c for acausal control with that for various causal control schemes, at different values of operating frequency, ω_p.

For bandwidth restricted reactive control (mass-damping and damping-spring) a choice of ω_p close to the spectral peak results in a passband filter, the bandwidth of which depends on the relationship between ω_p and ω_n. As a result, the bandwidth of velocity is narrower than the bandwidth of wave elevation.

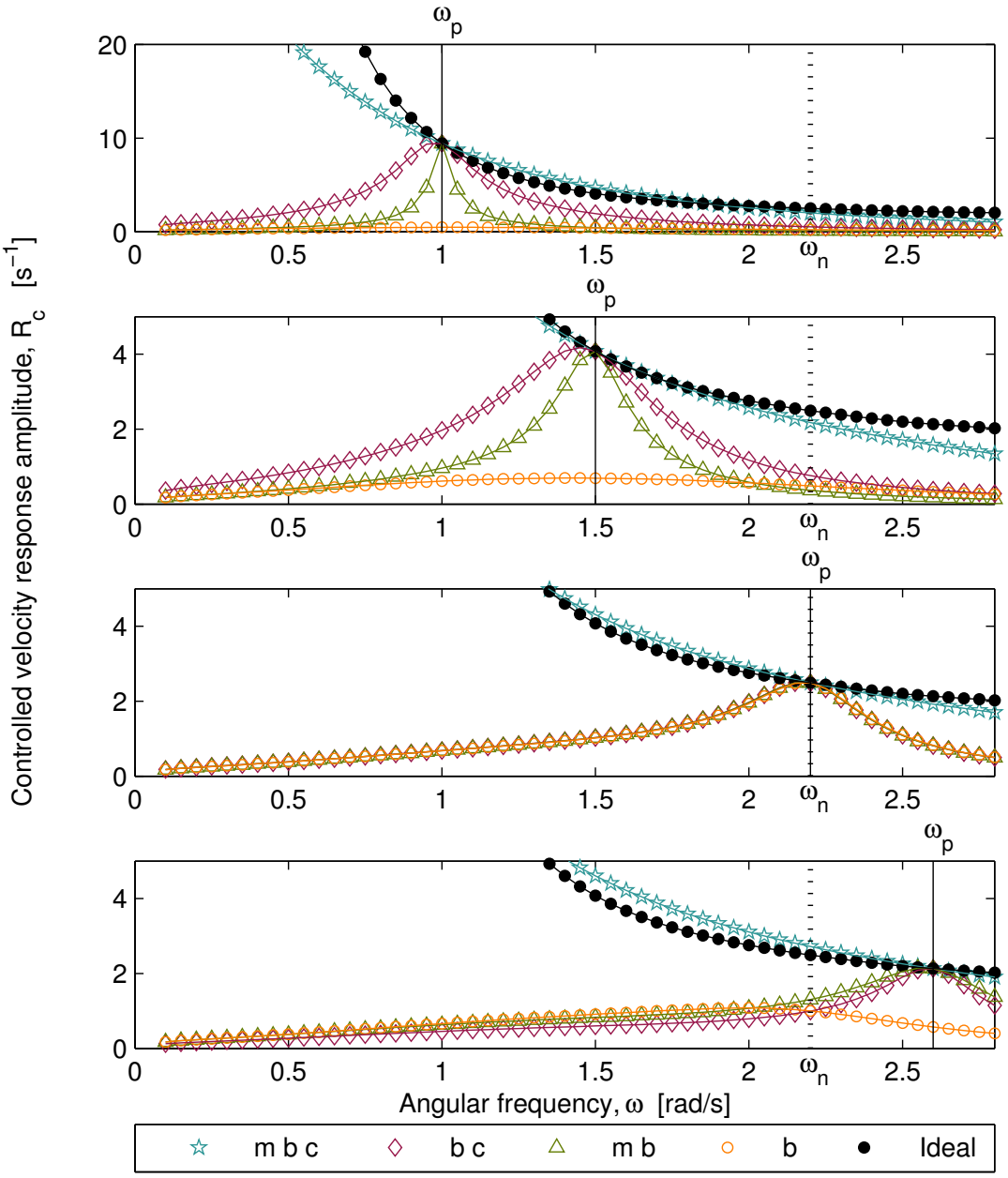

Figure 5.13: ***Controlled velocity response amplitude:*** *For acausal optimal control (solid black markers) and causal sub-optimal control (open coloured markers), the magnitude of velocity with respect to magnitude of wave elevation, R_c.*

For mass-damping-spring reactive control and for acausal optimal control, the R_c is a filter that passes all frequencies of wave elevation, but gives higher weighting to lower frequencies. For a PM spectrum, which has a peak skewed towards low frequencies, and a tail extending to high frequencies, the velocity will have the same, or a slightly narrower bandwidth than that of the

wave elevation. For a different shaped spectrum, or for a different size of WEC, it is possible for the velocity to have a slightly broader bandwidth than the wave elevation.

The effect of sea state on velocity coherence

In general, the coherence of the velocity $u(t)$ is very similar to the coherence of the sea state $\eta(t)$. Depending on the interaction between the wave elevation $H(\omega)$ and the controlled velocity response amplitude operator, R_c, the coherence of the velocity may be slightly longer or shorter than the coherence of the sea state.

5.5 The relationship between capture width and premonition time

This chapter has considered the extent to which predictions can improve power capture. In § 5.2, the interaction between the device (monochromatic capture width) and the sea state (spectral power fraction) was measured using the polychromatic capture width. The ratio between the capture width for full reactive control and that for acausal control showed the extent to which predictions could improve performance. In § 5.4, the interaction between the device (memory duration, and controlled velocity response amplitude operator) and the sea state (wave elevation coherence / bandwidth) was measured using the premonition time. It is informative to compare the results arising from these different viewpoints

5.5.1 The capture width and premonition time for monochromatic behaviour

Fig. 5.2 and the top row of Fig. 5.11 both consider the case of a WEC of arbitrary size moving under sinusoidal excitation. The figure of capture width (Fig. 5.2) compares optimal control to reactive control with the operating frequency chosen as the frequency of oscillation, $\omega_p = \omega_s$. It can be seen that the capture width for optimal control $\tilde{C}_W$ is identical to that for causal control $\breve{C}_W$, giving $\breve{C}_W/\tilde{C}_W = 100\%$. The availability of preditions would not result in any improvement in power capture; in this case predictions are not useful. This is true for any type of reactive control scheme with $\omega_p = \omega_s$. It should be noted that the function giving the components of capture width, $C_W[\omega_j]$, has a bandwidth equal to one frequency bin.

While capture width indicates how useful predictions are, premonition time indicates the ease with which predictions can be made. The longer the premonition time, the further away data must be collected to have a chance of meeting the required prediction horizon. The top row of Fig. 5.11 shows that the premonition time for sinusoidal excitation is zero. No remote data is required in order to achieve optimal control. Optimal control can be achieved by sinusoidal extrapolation of past values of velocity. This amounts to no predictions being required at all,

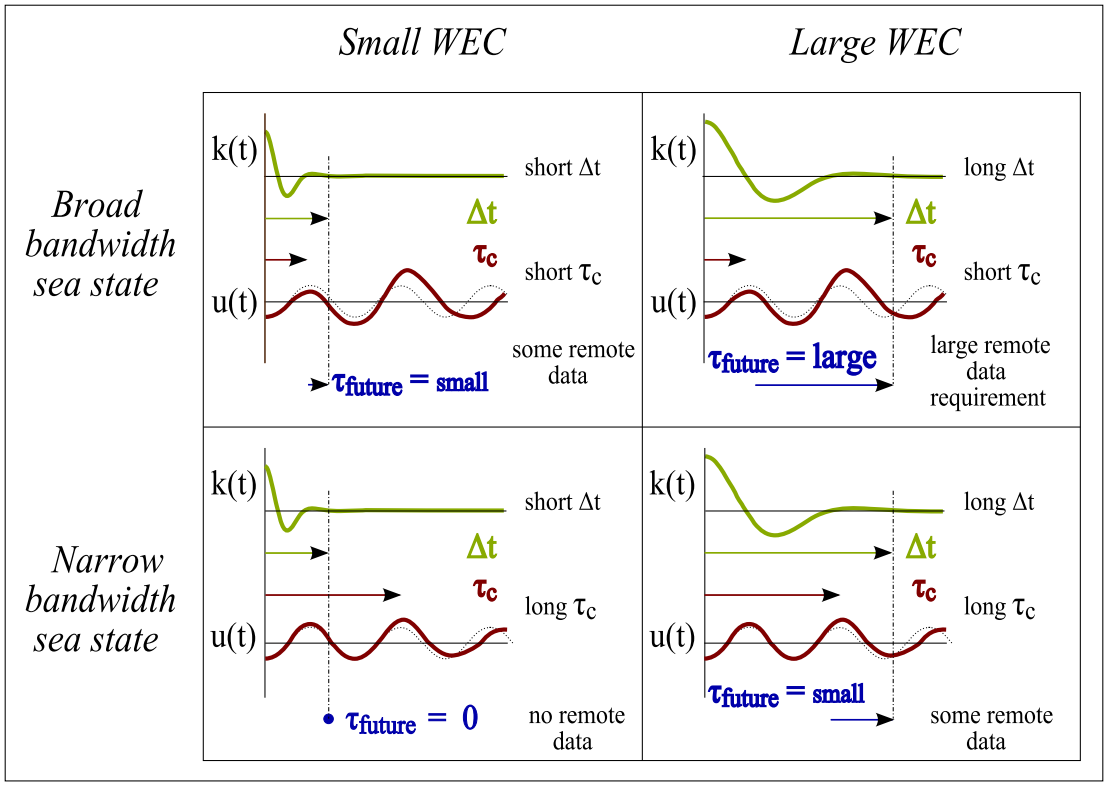

Figure 5.14: ***The effect of WEC size and sea state bandwidth on the feasibility of predictions:*** *these results apply to all types of WEC.*

because the optimal control force can be expressed (5.27) as a function that has no reference to future values.

5.5.2 The usefulness and feasibility of predictions for improving control

In order to assess the usefulness and feasibility of the predictions that are required for optimal control, the effect of the size of the WEC and the bandwidth of the sea state shall now be considered. Fig. 5.14 shows the memory duration Δt, velocity coherence τ_c, and resulting premonition time τ_{future}, for large and small WECs and for broad and narrow sea states. The plots shown are for demonstration purposes, rather than a specific geometry or sea state. As the same scaling laws apply to all the modes of motion, Fig. 5.14 applies to all types of WEC.

A large WEC has a narrower bandwidth radiation damping coefficient than a smaller WEC. Therefore a smaller WEC has a shorter duration memory kernel (first column), and a larger WEC has a longer duration memory kernel (second column). A broad bandwidth sea state results in a broader bandwidth velocity than a narrower bandwidth sea state. Therefore a broader bandwidth sea state results in a shorter velocity coherence time (first row), and a narrower bandwidth sea state results in a longer velocity coherence time (second row). The

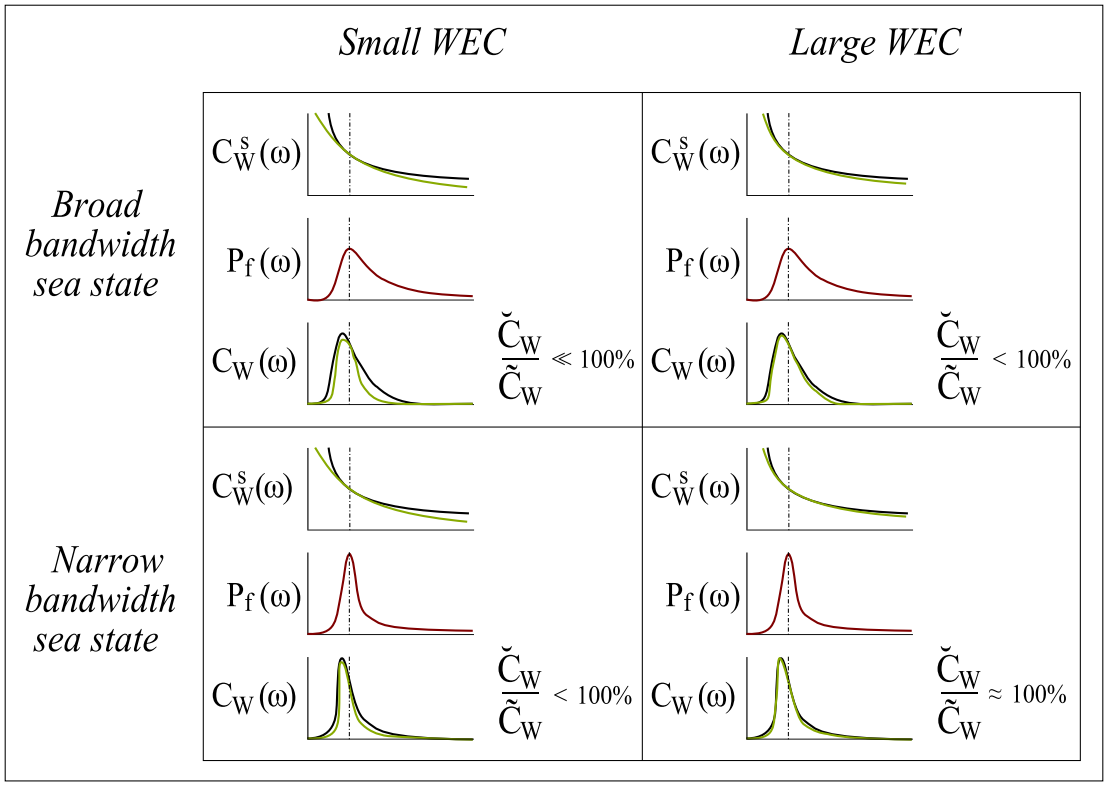

Figure 5.15: ***The effect of WEC size and sea state bandwidth on the usefulness of predictions:*** *these results are specific to a heaving cylindrical buoy and an ω_p lower than the ω_n.*

only case where a premonition time of zero is likely is the combination of a narrow bandwidth sea state and a small WEC (bottom left). Conversely, the combination of a broad bandwidth sea and a large WEC results in the longest premonition time (top right). The larger the WEC, the further afield data must be collected to have a chance of achieving the required prediction horizon in the presence of broad bandwidth seas. However, the more remote the data collection, the more uncertainty about the accuracy of the predictions [133].

The same combinations of WEC size and sea state bandwidth are now considered for polychromatic capture width in Fig. 5.15. The effect of these combinations on the ratio of the capture width using causal mass-damping-spring control, to the capture width for optimal control, $\breve{C}_W/\tilde{C}_W$, is shown. Results from § 4.9 are used, and further research is required to identify whether these results apply to all geometries and choices of ω_p. Fig. 5.15 is specific to a spherical buoy with PTO in heave and an ω_p lower than the ω_n. It is possible that these results may represent the general case, but this can only be shown by a broader study. Fig. 5.9 (see also Fig. 4.28 on page 186) indicates how the size of a heaving cylindrical WEC impacts the monochromatic capture width. A large WEC results in a wider band of frequencies over which the normalised capture width is close to 100% ($\breve{C}_{Wn} = \breve{C}_W^s/\tilde{C}_W^s \approx 100\%$). A broad

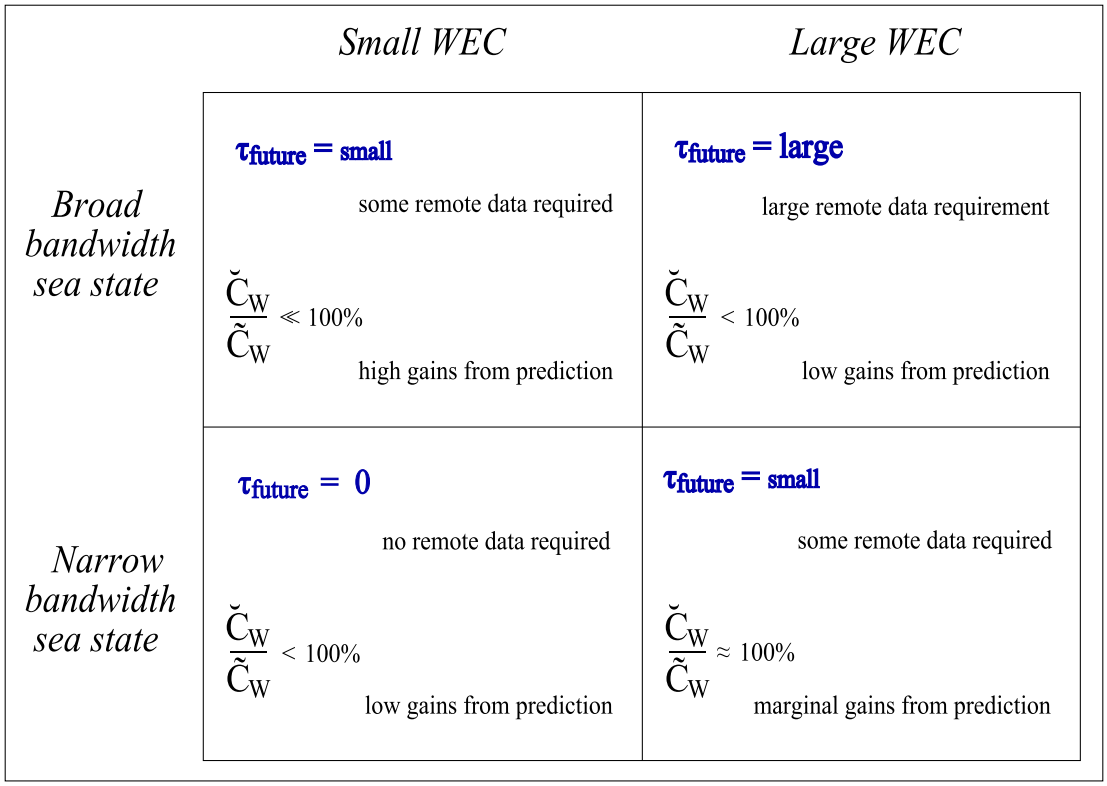

Figure 5.16: ***The effect of WEC size and sea state bandwidth on the feasibility and usefulness of predictions:*** *these results are specific to a heaving cylindrical buoy and an ω_p lower than the ω_n.*

bandwidth of wave elevation results in a broad bandwidth of spectral power fraction (first row), while a narrow bandwidth of wave elevation results in a narrow bandwidth of power fraction (second row).

Assuming linear operation and not accounting for displacement restraints, the improvement in power capture due to optimal control (requiring predictions) is the least for the combination of a large WEC in a narrow bandwidth sea state (bottom right) and the highest for the combination of a small WEC operating in a broad bandwidth sea state (top left). This suggests that small WECs operating in broad bandwidth seas could benefit from using optimal control. Note however that the requirement for displacement restraints is inversely proportional to size. Furthermore, (5.16) only applies to linear operation. The values values of C_w^s would be lower if displacement restraints were implemented, in which case $\breve{C}_W/\tilde{C}_W$ would not be as high as indicated. So although decreasing WEC size results in increased $\breve{C}_W/\tilde{C}_W$, it also decreases the accuracy of the term $\breve{C}_W/\tilde{C}_W$ as indicated here. The displacement restraints required for small WECs apply to all modes of motion so this conclusion holds for all WECs.

Fig. 5.16 summarises the usefulness and ease of acquisition of predictions according to size

of WEC and bandwidth of sea state. Once again, linear motion is assumed and displacement constraints have not been considered. It can be seen that in general predictions do not result in large improvements in the capture width of large WECs. Although it appears that the use of forecasts may give improvements in capture width for small WECs, the requirement for displacement limits will mean that it is not physically possible to implement optimal control. Fig. 5.16 also shows that for larger WECs the premonition time is longer, and hence the acquisition of the data required for predictions is more challenging.

5.6 Chapter summary

This chapter studied the usefulness and feasibility of using forecasts for optimal control. New parameters were introduced: the forecast benefit parameter, $(\tilde{C}_W - \breve{C}_W)/\breve{C}_W$; the performance of a causal scheme relative to the ideal scheme $\breve{C}_W/\tilde{C}_W$; and the premonition time $\tau_{premonition}$.

The main points of interest and new concepts discussed in this chapter included:

- The relationship between the monochromatic and polychromatic capture widths was defined mathematically. The polychromatic capture width is a measure of how well the WEC geometry and control scheme (via the monochromatic capture width) interact with the sea state (via the newly introduced parameter, the spectral power fraction).
- The capture width for a sinusoidal wave of frequency ω_s is the same for optimal control as for any type of reactive causal control with $\omega_p = \omega_s$. The use of predictions does not improve capture width. The value of the capture width is $\tilde{C}_W = \lambda_s/2\pi = g/\omega_s^2$, the well known upper limit.
- The capture width for a PM spectrum was considered. The capture width due to optimal control was less than the upper limit for the frequency at the spectral peak $\tilde{C}_W < \lambda_p/2\pi$. The capture width due to mass-damping-spring control was less than for optimal control, $\breve{C}_W < \tilde{C}_W$, suggesting that predictions could be used to improve capture width. For the geometry and sea state considered, these improvements were near 7 %.
- For the geometry and sea state considered, mass-damping-spring reactive control gave a substantially higher capture width than other types of reactive control.
- As the displacement for mass-damping-spring control is large and may result in displacement restraints, mass-damping and damping-spring control can be considered as bandwidth restricted reactive control.
- It was shown that the spectral peak is not necessarily the optimal operating frequency, especially for real control. For the geometry and sea state considered, the optimal operating frequency for real control led to an increase in capture width of almost 7 %.

- The concepts of memory duration, coherence time and premonition time were introduced. Their relationship was defined mathematically and illustrated with diagrams.
- Larger values of $\breve{C}_W/\tilde{C}_W$ indicate that predictions are less useful; smaller values of $\breve{C}_W/\tilde{C}_W$ indicate that predictions are more useful.
- Forecasts will not be beneficial for small WECs because most of their operation will require displacement restraints or involve non-linear response, so optimal control will not be possible. This result applies to all types of WEC.
- Case studies of a heaving buoy indicated that forecasts would be marginally useful for larger WECs. Further studies are required to assess whether this applies to all types of WEC.
- For large WECs, in the sea states where forecasts are most useful (broad bandwidths), the data required for these forecasts is more difficult to attain. This result follows from the scaling law for hydrodynamic parameters so applies to all WECs.

Chapter 6
Discussion and interpretation

6.1 Overview

There are several strands of storyline that run through this thesis. As these common themes were not the main topics of any of the chapters, they were not dealt with in depth. This chapter now ties up all these loose ends and discusses their relevance. There is a particular focus on how the material presented in this thesis builds on existing research and how it compares to viewpoints presented in the literature.

The strongest common theme throughout this thesis is the difference between monochromatic and polychromatic modelling and experimentation. This theme appears in Chapter 2, which discusses the difference between the frequency response (Fig. 2.12), and parameters that are relevant only to monochromatic experiments (Fig. 2.13); in Chapter 3, which introduces the wet and dry oscillator models; Chapter 4, which classifies causal and optimal control; and Chapter 5, which provides the proof that for monochromatic motion, causal and optimal control are equivalent. Section 6.2 discusses these ideas in the context of the literature. Common modelling practices and approaches are discussed, and these are used to interpret the literature correctly. The time domain dry oscillator model is commonly presented as a model for the motion of a WEC. Several authors have warned against this, but communication has been hindered because the wet and dry oscillator models are conceptually very similar when presented in the frequency domain. Other authors, in criticising the use of the dry oscillator model, have given the impression that frequency domain modelling is not suitable for polychromatic response. This section clarifies which types of frequency domain models are suitable for polychromatic motion, and which are not. Application of models suitable only for sinusoidal response to spectral seas could lead to overestimations of power capture.

Another important topic is the extent to which predictions can improve control. This work began in Chapter 4 with the comparative study of the monochromatic capture widths of control methods that worked without, or required, predictions. Chapter 5 extended this work by quantifying the extent to which predictions can improve primary power capture, and discussing data requirements for these predictions. In § 6.3 the use of predictions is discussed in more depth. The types of data that can be obtained by measurement on-board a WEC are discussed, as are the opportunities for using advanced prediction techniques, such as neural networks or Kalman filters, to turn this measured data into the information required for improved control. The usefulness of predictions for improving PTO control is discussed in general.

The usefulness and feasibility of improving power capture using forecasts is highly dependent on the size of the WEC. This leads on to an ongoing debate in wave energy literature, and indeed among developers of commercial devices, about the ideal size for an economic WEC. Small WECs are called point absorbers, while devices with dimensions of the same order of magnitude as typical wavelengths are known as attenuators and terminators. The classical theory states that the upper limit of capture width due to acausal optimal control is not determined by a WEC's physical size. However when considering causal sub-optimal control, the monochromatic capture width is influenced by a WEC's physical size. Chapter 5 indicated that large WECs would have higher polychromatic capture widths, but future research is required to determine whether this advantage is significant. It is important to interpret the results of Chapters 4 and 5 in the context of the interaction between the sea state and the requirement for displacement or power restraints. The discussion in § 6.4 is a useful addition to the debate about the optimal size of a WEC.

6.2 A clarification of frequency domain modelling practices

This section clarifies the techniques involved in modelling WECs. In particular, the practices and terminology that are ambiguous or which lack rigour are described. This is both to improve the interpretation of the literature, and to encourage communication that is less ambiguous. Specific papers are discussed to show how a fresh perspective can change the interpretation; the reinterpretation of one piece of work in particular has important implications for the direction of research on the control of WECs. This section arranged as a series of statements about potential ambiguities or pitfalls associated with frequency domain modelling of WECs. As work by specific authors is discussed, it is inevitable that this section will appear to be critical of other's work. The benefits of this frank discourse are seen in § 6.2.9, which lists recommendations to remedy all the potential problems described in this section.

The wet and dry oscillator models introduced in Chapter 3 are useful for discussing and contrasting how different authors model WECs. The first point of note is that the dry oscillator model is widely used as the equation of motion of a WEC. As shown in Chapter 3, this is not strictly correct, as an equation of motion should apply to all types of motion, and a dry oscillator model applies only to sinusoidal motion.

6.2.1 The wet and dry oscillator models appear similar in the frequency domain

All of the early theory of optimal power capture for a WEC assumed sinusoidal motion [56, 105, 106]. It is thus not surprising that first attempts at defining an equation of motion also assumed sinusoidal motion, and used a dry oscillator model [106, 114]. Authors such as Clément [30] commented that this was misleading as there was no explicit indication within the equation that the motion was limited to being sinusoidal. Newman (see equation (194) in [36]) commented

that the time domain equation of the dry oscillator could be used to superimpose components at each frequency, but did not represent general time domain motion. Despite protestations by Newman [36], Falnes [91] and Clément [30] that a WEC was a system with memory and that optimal control led to an acausal system, many recent papers can still be found [134–142] that describe the motion of a WEC in terms of the dry oscillator model. Correct interpretation of the models in these papers is important. A dry oscillator model only describes the dynamics for sinusoidal motion, and is thus not a general equation of motion. Use of such a model with a control technique that results in anything other than a sinusoidal control force, such as in [136, 138, 141, 142], is not strictly correct, as the model no longer describes the system dynamics. Likewise, the use of such a model in irregular (polychromatic) waves with values of hydrodynamic coefficients that are averaged over the frequency range of interest, as in [135], is incorrect.

Here correctness is qualitative, rather than quantitative. For WECs that are small compared to the characteristic wavelength, also known as point absorbers, a dry oscillator model may give results that simulate behaviour in polychromatic waves to an acceptable degree of accuracy. For instance, Folley and Whittaker [141] reported that the dry oscillator model predicted results that were "*typically less than 10%*" out from experimentally measured values. The non-linear models presented in [103] are interesting: equations are given for both a wet oscillator, and a dry oscillator using the value of radiation damping at the average frequency. The paper concluded that the results from a dry mass-spring-damper model fitted reasonably well to the measured data. While a dry oscillator model may be used to estimate response to reasonable accuracy, it nevertheless does not adequately describe the quality of the response and the true nature of the underlying dynamic process.

One reason why critics of the dry oscillator have had difficulty in explaining the limitations of this model, is that the wet and dry oscillator models appear similar when written in the frequency domain. In the frequency domain, neither model explicitly shows that radiation has memory and that optimal control is acausal. Furthermore, the same mathematical notation and associated terminology are used for both the wet and dry oscillator models. For instance, in the dry oscillator model, $B(\omega)$ is used to indicate a constant, denoted B_s in this work, which equals the radiation damping at the frequency of sinusoidal oscillation, ω_s. As B_s depends on the frequency of oscillation, the terminology "*a function of frequency*" is used to describe it. For the wet oscillator model, the notation $B(\omega)$ is used to indicate that the radiation damping has different values at each frequency, and as such could be described as *a function of frequency*. Thus it can be seen that it is very difficult to describe the difference between the frequency domain descriptions of the wet and dry oscillator models. A reader's interpretation of *a function of frequency* and the notation $B(\omega)$ inevitably depends on whether they interpret a frequency domain model of a WEC as a wet or dry oscillator.

Critics of the dry oscillator model have been hindered in communicating their message by the

notation and terminology used to describe both the wet and dry oscillator models. It was for this reason that the distinct concepts of wet and dry oscillators were introduced in Chapter 3. It is easier to show how they are different by examining their time domain equations. In the case of the wet oscillator model, the frequency domain radiation damping, $B(\omega)$, which is a function of frequency, becomes the memory kernel. This impulse response is a function of time, and describes how past motion influences the present radiation behaviour. In the case of the dry oscillator model, the radiation damping, B_s, which is a function of sinusoidal frequency ω_s, is a constant in the frequency domain and remains a constant in the time domain. There is no indication in the dry oscillator time domain equation that past motion has any influence on present radiation behaviour.

6.2.2 The dry oscillator model is not the frequency domain model of a WEC

The common notation and terminology describing the frequency domain versions of the wet and dry oscillator models, and the continued use of the dry oscillator model, are responsible for another inconsistency in the literature. Occasionally the dry oscillator model is described as the frequency domain model of a WEC, while the wet oscillator model is described as the time domain model of a WEC, as shall now be shown.

First it is necessary to make these distinctions clear. Both the wet and dry oscillator models can be written as time or frequency domain equations. The time domain equation of a wet oscillator is indeed the correct equation of motion for a linearised WEC. The frequency domain expression of a wet oscillator is also a valid model of a linearised WEC, whose solution gives the steady-state response. This is *the frequency domain model* of a WEC. As discussed in § 3.8, the dry oscillator model only correctly models steady-state sinusoidal response. This can be found from either the time or frequency domain equations. Just as a time domain model is valid for all values of time, a frequency domain model is valid over all values of frequency. A dry oscillator model of a WEC is suitable *only* for sinusoidal motion. It is not the frequency domain model of a WEC, because it cannot be used to describe motion that contains more than one frequency.

While the association of the dry oscillator model with the frequency domain may have had its origins in the similarity of the frequency domain descriptions of the wet and dry oscillators, at present this misconception continues because eminent authors have written texts that may be interpreted as advocating this point of view [90, 95, 110]. To dispel this misconception, it is not sufficient to state that the wet and dry oscillators are distinct models and that each can be represented in the time or frequency domains; it is necessary to identify these texts, and to demonstrate that they are describing a dry oscillator, *rather than* the frequency domain model.

The paper that most clearly shows the association of the dry oscillator model with the frequency domain is [95] by Greenhow and White. This paper aims to show that the dry oscillator is

not appropriate for modelling the non-sinusoidal motion resulting from the non-linear control technique used: latching. Perhaps to make the paper more accessible to those using the dry oscillator model, the authors wait until the end of the paper to state that they consider this to be "*an incorrect hydrodynamic model*". However, when the model is introduced, the time domain equation of the dry oscillator is given, and it is referred to as "*the frequency domain equation*". It is written in such a way that it could be mistaken for a frequency domain equation, namely the constants M_s and B_s are written in the form that was conventional at the time, $M_a(\omega)$ and $b(\omega)$, and none of the variables are explicitly written as functions of time. The only indications of time domain terms is the overdot notation, which is used to denote time domain functions that are the first and second time derivatives of the displacement, $\dot{x}$ and $\ddot{x}$. However, this convention is not followed universally by wave energy engineers, some of whom use the overdot notation for frequency domain variables.

Despite being called a frequency domain equation, this *incorrect hydrodynamic model* presented in [95] is given as a time domain equation. This is clear from the development and substitution of the equations that follow, and from the fact that the equation is used as a time domain equation to solve for displacement at each time step in the simulations presented later in the paper. The time domain version of the wet oscillator is described as the time domain equation of a WEC, and this is set against the "*the frequency domain equation*", which is in fact the time domain equation of the dry oscillator.

This paper presents various arguments as to why the time domain equation is suitable for polychromatic modelling, while the "*the frequency domain equation*" is not. Some of these arguments are true for frequency domain modelling in general: it is not suitable for modelling non-linear behaviour, time varying control, or transient responses. As discussed in § 3.8, the time domain dry oscillator is likewise not suitable for modelling these behaviours, but for different reasons: non-linearities, time variance and transients result in motion that is not sinusoidal. Latching control results in a time varying damping coefficient, and transients every time the damping is changed. Thus neither the frequency domain wet oscillator nor the time domain dry oscillator are suitable models, while the time domain wet oscillator can accommodate this behaviour. Several other criticisms are true only for the dry oscillator model: it does not model radiation memory; it is only valid for steady-state conditions. *Steady-state* is another ambiguous term. It is used by some to indicate post-transient response to monochromatic forcing, and by others to indicate post-transient response to polychromatic forcing. The reason why the contentious equation in [95] is an incorrect hydrodynamic model is not because it is a frequency domain model, but because it is a time domain representation of a dry oscillator valid only for sinusoidal motion.

It is important to recognise that the main message of [95] is to promote the correct wet oscillator model and to show that the dry oscillator is not a valid hydrodynamic model. The principal message is correct and important, but naming the dry oscillator model the frequency

domain model gives the strong impression that frequency domain modelling is not suitable for representing the behaviour of a WEC in polychromatic conditions.

Another paper that appears to question the validity of frequency domain modelling for polychromatic conditions is the seminal paper by Cummins [90]. This paper holds enormous authority in the wave energy community because it formulated the time domain equation of the wet oscillator still widely used. Before Cummins' paper, the hydrodynamic responses of ships were routinely expressed in terms of the added mass and damping at a particular frequency. This approach dates back to Stokes' [99] measurement of added mass using a pendulum, which of course oscillated at a single frequency. As discussed in § 3.7, authors such as Odar and Hamilton [101] have noted that the formulation using constant values of added mass and damping did not model the memory effects observed in polychromatic behaviour. When Cummins discussed the advantages of his new formulation over the model previously used [90], he used terminology that suggested that the model being replaced was the frequency domain version of the time domain model being presented. If it is not recognised that he is in fact describing the inadequacies of the dry oscillator model, this paper could be interpreted as a statement of the inadequacies of the frequency domain version of the wet oscillator model. This paper could be misread as claiming that the frequency domain wet oscillator model is not valid for polychromatic motion.

The association of the dry oscillator model with the frequency domain has resulted in a lack of clarity about the validity of frequency domain modelling of polychromatic behaviour in WECs. There are other reasons why frequency domain modelling may be perceived as suitable only for sinusoidal behaviour. These are the acausality of optimal control, and experimental uncertainty. These are now dealt with in turn.

6.2.3 Some frequency domain models are only valid for sinusoidal motion

As already described, the dry oscillator model is valid only for sinusoidal motion. It is thus possible to have a model represented in the frequency domain that is valid only for sinusoidal motion. This is not a limitation of presenting a model in the frequency domain, but a limitation of the model itself. The acausality of optimal control results in another model for which the frequency domain equation is valid only for sinusoidal motion. Chapter 4 described why optimal control was acausal in polychromatic conditions and causal in monochromatic conditions. Starting with a wet oscillator model, which is valid for polychromatic motion, and adding the optimal control force, results in a deceptive equation. It is valid for polychromatic motion only if future motion is known, in which case the equation is described as acausal. Acausality can be understood as not being possible using real-time system information.

Note however that for sinusoidal motion, optimal control is possible in real time, i.e. causal. As described in Chapter 3 there are plenty of frequency domain models that include controlled

PTO forces that are valid for polychromatic motion. These PTO schemes are however not optimal. The examples given in Chapter 3 are described as sub-optimal because performance is optimised at one frequency only. The frequency domain equations of the sub-optimal and optimal control strategies can be compared by substituting the respective values of PTO impedance into the frequency domain characteristic equation (3.41). As the resulting equations are in the frequency domain, it is not immediately clear that optimal control is not possible in real time, while the sub-optimal control schemes are.

The reason this is not clear is that the information about the acausality of radiation and the anticausality of the optimal control force is lost when converting from time to frequency domain. In § 3.6 it was noted that converting from the frequency to the time domain gave an acausal radiation convolution term (3.47). Additional information about the nature of the radiation kernel is required to show that the radiation convolution is in fact causal (3.48). The anticausality of the optimal control force follows directly from the causality of radiation (4.17).

For most practical modelling purposes, control that is possible in real time, causal control, is a requirement. Given this assumption, a wet or dry oscillator model with an optimal control force is valid for sinusoidal motion only, while a wet oscillator model with a sub-optimal control force is valid for polychromatic motion.

There is an interesting relationship between optimal control of sinusoidal motion and sub-optimal control of polychromatic motion. As shown in Fig. 4.4 the time domain equations are of similar form. In both cases, the PTO force is made up of a term directly proportional to velocity, and one or two terms that are proportional to displacement or acceleration. Fig. 4.4 shows PTO forces including terms proportional to displacement, velocity and acceleration. It can be seen that these equations have a different form from the time domain equation for optimal acausal control, which contains a term that is a convolution, as seen in Fig. 4.5.

This viewpoint is useful when interpreting another key paper in wave energy literature: Niato and Nakamura's derivation of the optimal control force [110]. There are some statements on the first page that could be interpreted as claiming that frequency domain modelling is suitable only for sinusoidal motion. However, another possible interpretation is that when using the mass-spring-damping PTO force shown in Fig. 4.4, optimal control is only possible when motion is sinusoidal.

In summary, one possible source of ambiguity is that optimal control of polychromatic motion, which is acausal, and optimal control of monochromatic motion, which is causal, result in similar equations where the difference is clear in the time domain formulation, but not in the frequency domain formulation. Another possible source of ambiguity is that optimal control of monochromatic motion, and sub-optimal control of polychromatic motion, which are both causal, result in similar time domain implementations.

6.2.4 The distinction between monochromatic and polychromatic conditions is important

The issue of acausality is the reason why it is vitally important to distinguish clearly between experiments conducted in monochromatic and polychromatic conditions. The time domain implementation of sub-optimal control in polychromatic conditions is identical to the implementation of optimal control in monochromatic conditions. Results of sinusoidal experiments are commonly plotted against frequency, as are the results for polychromatic experiments. Response due to optimal causal control of sinusoidal motion and optimal acausal control of polychromatic motion look identical when plotted in the frequency domain. If sinusoidal experiments are optimised at each frequency, then plotting the results against frequency represents performance due to acausal optimal control.

Estimations of power production should not use performance optimised at each frequency

Furthermore, calculating absorbed power using PTO impedance that has been optimised at each frequency will give an over-estimation. The absorbed power calculated in this manner is in fact the upper limit of power that would have been absorbed if acausal optimal control (knowledge of future state) were possible.

Measures of performance that have been optimised at each frequency amount to acausal control. As mentioned in § 6.2.5, using such performance indicators to estimate absorbed power will give the upper limit that could be achieved with perfect predictions of future waves, rather than a realistic indication of power production.

It is important to remember that the potential ambiguities described here have not always been widely known. Sometimes some detective work is required to determine whether experiments were conducted in monochromatic or polychromatic conditions. In Skyner's influential internal report [71], it is not stated whether values of efficiency calculated for monochromatic waves were used to estimate absorbed power in known (South Uist [64]) wave spectra. This is indeed the case, as can be seen from careful examination of Fig. 7.4, and from the statement on page 86 that the resulting control would be acausal. However, it is easy to overlook these clues. The section on the estimates of absorbed power from the South Uist spectra gives no indication that these levels of power capture rely on future knowledge.

Optimal control of monochromatic behaviour does not require future knowledge

The lack of a clear distinction between acausal and causal control can lead to misinterpretation, as exemplified in Nebel's thesis [104]. The introduction of *Part I* describes how complex conjugate control is optimal control for polychromatic seas and requires future knowledge (pages 7 – 8). The experimental method is then described (page 9) in a way that gives the impression that acausal optimal control is being simulated by using knowledge of future waves.

The remainder of *Part I* gives experimental results for complex conjugate control. There is no indication as to whether monochromatic or polychromatic waves were used. If *Part I* is extracted from the thesis and read in entirety, the reader is left with a very strong impression that the experiments were carried out for polychromatic waves. However, the first sentence of *Part II* leaves no doubt that monochromatic waves had been used. When using monochromatic waves, optimal control is no longer acausal: advance knowledge of future wave elevation is not required. Information about the frequency of the monochromatic wave is required, but this is a fundamentally less difficult problem. Only careful reading of Nebel's thesis in entirety shows that he did *not* use future knowledge to perform complex conjugate control in polychromatic experiments. This is not well known in the wave energy community [20, 32].

This blurred distinction between causal and acausal control has led to a crucial ambiguity in published results that will inevitably have influenced thinking to some degree. There is a risk that the claim of experimental verification of acausal optimal control, using advance knowledge of polychromatic waves, will have influenced the research direction of others. Experimentalists may have been discouraged from performing this experiment in the belief that it has already been done, while theoreticians may have given greater emphasis to some popular topics, such as wave prediction and acausal control, than would otherwise have been the case. This demonstrates how a deeper understanding of the issues of causality, along with a willingness to reinterpret past work can help to inform and direct contemporary research.

6.2.5 Calculations of annual power are rough estimations

As has been discussed in § 6.2.4, a lack of rigour in the use of results collected under sinusoidal conditions can lead to figures for annual power estimation that depend upon the availability of future knowledge [71, 104]. It is interesting to consider by how much power capture has been overestimated. In Fig. 5.3 it was seen for the best sub-optimal control, a mass-damping-spring scheme, that this overestimation was relatively small. Table 5.1 shows this was 7% for the example given. It is shown later that the method of annual power estimation has inherent assumptions and simplifications which may result in overestimations even larger than this. Within the context of these significant error bars, the error due to assuming acausal optimal control for a mass-damper-spring scheme is small.

What is important here is that the underlying concepts have not been clearly understood. The calculation of an upper limit is fine as long as it is clearly stated that it is an upper limit. Rigour in annual power estimation is important, because there are also instances that can lead to significant overestimations of power capture. For instance, if instead of the mass-damping-spring scheme, a bandwidth restricted scheme was used, such as the popular damping-spring scheme, then the over-estimations of power would be very much greater. Table 5.1 showed this was 130% for the example given. In [71] the full complement of mass,

damping and spring was not used in each mode of motion, so it is likely that the overestimation in absorbed power was large.

All the other assumptions and sources of error present when estimating annual power capture are also important to consider, so these will now be discussed. The method is based on the concept of generalised spectra.

Generalised spectra

As described in § 2.5.2, a set of generalised spectra describe the typical annual distribution of sea states in a given location. Measured spectra gathered at regular intervals over the course of a year are grouped into subsets according to characteristics such as the number of spectral peaks, the positions and heights of these peaks and bandwidth. The spectra in each subset are averaged to produce a generalised spectrum which represents that subset. The size of the subset indicates the annual occurrence of a given generalised spectrum. Time series of typical sea states can later be synthesised using randomly generated phase. An example of a group of generalised spectra is the South Uist 399 data set [64]. The measured data may come from one year, in which case that year is assumed to be typical.

The measured spectra are generated using measured wave records of surface elevation. Each sampled wave record (usually half an hour to two hours in length) is first processed to remove errors. Spectral noise reduction techniques are then implemented, such as multiplication with a tapered window function. The wave record is transformed using the DFT. The measured spectra consist of the magnitude of the DFT, or the spectral density. The phase is discarded.

Validity of annual power estimation

Equation (5.13), or variants thereof, are often used [71, 123] to estimate annual power capture for a set of generalised spectra. There are several reasons why this is only an approximation to the power that would be absorbed at the site described by the generalised spectra:

- This equation is only valid for conditions (ii)-(iv) outlined in §5.2.2, yet measured seas are never periodic with the measurement record, and sea states are often big enough to induce large displacements, which would invalidate the linearity assumptions or exceed displacement limits.
- Monochromatic capture width is defined for a unidirectional sea state, whereas wave propagation in the sea is multi-directional.
- Sea states vary year by year.
- Generalised spectra are not the actual measured spectra.

- The measured spectra are not the frequency domain equivalents of the measured wave records; noise reduction techniques such as windowing (§ 2.4.4) have removed the equivalence of the time and frequency domains.
- Forces due to tides and waves created by neighbouring bodies are not considered.
- PTO impedance is often optimised at a frequency, ω_p, calculated taking the whole spectrum into account; an option not available in real-time operation.
- The calculation assumes 100% availability from the plant, which is not realistic, even in mature technology. Plant failure is more probable during periods of high energy sea states, and maintanence cannot take place until the heavy seas have subsided. Unplanned down-time will tend to coincide with periods of potentially high energy production.

A further potential problem is the linearity of the monochromatic capture width. The monochromatic capture width is often derived experimentally, either directly, or by using experimentally measured hydrodynamic coefficients [71]. The monochromatic capture width can only be used in (5.13) if it is measured using waves (§ 5.2.4) and motions (§ 5.2.2) that are linear. When this the case, then monochromatic capture width is independent of wave elevation, as shown in (§ 5.11). When there is experimental evidence that the monochromatic capture width is affected by the magnitude of the wave elevation, as in [96], then this is a sign of non-linearity. Unless linearity checks have taken place, it cannot be certain that an experimentally derived value of monochromatic capture width is valid for use in (5.13).

When the correct (linear) values of the monochromatic capture width are used, the absorbed power in a high energy sea state will be overestimated. This is because the velocity of the WEC's PTO system will be more non-linear than it was when calculating the monochromatic capture width. Measuring the values of (non-linear) monochromatic capture width using waves with magnitudes comparable to those in the high energy sea state will give an indication of the scale of the overestimation of absorbed power.

6.2.6 The distinction between non-linearity and systemic errors is important

It has been shown that the complexity of the distinctions between acausal and causal control, and monochromatic and polychromatic conditions, have contributed to uncertainty about whether the frequency domain is suitable for polychromatic modelling. Interpretations of experimental results is another possible reason for lack of clarity about the limits of frequency domain modelling. In this case, it is important to distinguish between artefacts of frequency domain modelling, and the behaviour of a non-linear system.

If the frequency domain is indeed suitable for polychromatic modelling, then superposition of monochromatic results should match up with polychromatic results. If there is a poor match

between polychromatic results and the superposition of monochromatic results, then there are a number of possible reasons.

- The motion may have been non-linear; perhaps the linear limit chosen was too high; perhaps no limit was enforced as theory indicated the motion would fall within the linear regime, while in practice the linear regime was smaller than expected, due to component limitations.
- If the model's linear regime was small and a broad spectrum was required, it would have been difficult to choose wave amplitudes such that the largest induced motions remained linear, while the smallest induced motions were within sensor sensitivity and tank repeatability.
- The sampling time or number of samples were poorly chosen and so $T_{DFT} \neq T$ (§ 2.5.8).
- Systemic errors may have been present, such as tank reflections, poor calibration, poor repeatability, poor sensor sensitivity, or phase shifts due to electronic filters.

If superposition does not hold, this indicates that either there are non-linearities in the system, or systemic errors, or both. It is important to differentiate between these. When there are non-linearities in the system, frequency components of a particular experiment will not be the same as the frequency response, as discussed in § 2.5.4. Methods based on frequency response should not be used. When systemic errors are present, the frequency response can be found but the errors must first be removed. It is often not easy to distinguish systemic errors from non-linearities as the experimental requirements to avoid poor choice of DFT record, systemic errors and inadequate linear limits are not well documented. Their presence is often a matter of experimental house-style. Testing for linearity, particularly in mixed seas, is not standardised; neither is identification of systemic errors; neither is the use of a periodic waves: at some facilities it is standard practice, while at others a non-harmonic spectrum would be standard practice if the research priority were for waves to be statistically closer to real seas.

Frequency domain modelling using the DFT only applies to patterns of waves that repeat with the DFT record. It is quite correct to state that these methods are not valid in real sea waves. However DFT methods can be used to approximate the behaviour in wave tanks with polychromatic waves that repeat over the DFT record. In the case where these waves are synthesised using an IDFT (Fig. 2.11D), then they will repeat with the DFT record, and can be used for frequency domain experiments. If they are synthesised using a technique that does not result in repetition over a given interval, such as the white noise filter (Fig. 2.11G) then the frequency domain technique will not be as accurate.

6.2.7 Frequency domain modelling is valid for a sub-set of behaviour

The various models that are suitable only for sinusoidal motion have been discussed. Both frequency domain and time domain representations of these models apply only to sinusoidal motion. There are however some types of behaviour that can be adequately described by a time domain equation, but not a frequency domain equation. The restrictions of frequency domain modelling are now listed.

Restriction to linear systems

The behaviour of WECs is not generally linear so the frequency domain equation can only be used to model the sub-set of behaviour for which non-linearities are negligible: the linear operating regime. An important boundary of this regime is the restriction to small amplitude motions and wave elevations.

For linear waves, the wave amplitude should be low with respect to wavelength. The hydrodynamic coefficients: exciting force, added mass and added damping; can be calculated using linear potential flow theory, which treats the waves as linear and the wetted area of the body as constant. The assumption of constant wetted surface becomes increasingly inaccurate as the displacement relative to the water surface increases. Buoyancy spring is often linearised by assuming constant waterline area, an assumption that also becomes increasingly challenged for larger relative motion.

For large relative motions, in addition to the time variant/inaccurate coefficients, highly non-linear forces not included in the linear model appear and may dominate the behaviour. These forces could include the effects of:

- Non-linear spring such as mooring,
- Losses due to viscous drag, bearings and PTO,
- Wave slamming, overtopping, and re-emerging,
- Restraints on displacement, forces or power capture as these reach economic or practical design limits,
- Non-linear PTO strategies,
- Parasitic resonant responses in other degrees of freedom.

The non-linear effects described above are neglected from linear models. Non-linear terms can be added to a time domain equation, but not to the frequency domain model.

Restriction to post-transient response

When modelling a system, the solution of the frequency domain equation gives the post-transient response only. The post-transient response is a function of the forcing frequency. The transient response is not a function of the forcing frequency, but of the initial conditions. For this reason, the frequency domain is also not applicable to modelling a time varying, piecewise linear, function such as the PTO force due to latching control. The time domain can in general be used to represent a piecewise linear system, but this is only useful when the transients last for a short time compared to the window of time considered.

Possible restrictions to periodic excitation

Using the DFT for analysing linear systems is only accurate for periodic excitation (§ 2.5.8). A periodic signal has an equivalent representation in the frequency domain via the DFT. The DFT can not accurately represent the frequency content of an aperiodic signal, such as a real sea state, because of the problem of leakage. Spectral noise-reduction techniques that reduce leakage destroy the equivalence between the time and frequency domains.

6.2.8 Frequency domain modelling is useful

Although the frequency domain is not valid for describing most types of behaviour that are normal in a WEC, it is commonly used because people find it useful. It is complementary to potential flow theory, and rigorous experimental validation in the field of ship research has given credibility to the approach. It is widely known and, when used rigorously, facilitates interdisciplinary communication.

The frequency domain is a useful way of abstracting oscillatory motion. It is a valuable design technique for showing how the amplitude response responds to types of control scheme, values of operating frequency, sizes of WEC, and variations in geometry that will have an effect on the hydrodynamic coefficients. The frequency domain is better suited than the time domain for showing that the polychromatic capture width is a measure of how well the geometric and PTO properties match a given sea state.

An important reason why linear modelling is a worthy pursuit is that optimising power capture is more useful in smaller seas. Both power production and non-linear behaviour increase with wave amplitudes. In larger waves, linear modelling may not be valid, but power losses due to non-linearities will correspond to a requirement for displacement restraints. If a WEC is designed so that above rated power the motion is highly non-linear, this will not impact energy production, but will beneficially ease loads. When operating at rated power, linear control is not required. The set-point of power is known and conventional proportional-integral-derivative control may be used.

As behaviour becomes non-linear, power production becomes less than that estimated by linear models. Power restraints are often required for the large motions that result in non-linear damping losses. In this case the difference between the non-linear response and the linear response predicted by a frequency domain model are not important. Linear modelling provides an upper limit of power capture that would be possible without losses due to non-linearities, and displacement and power restraints.

If the frequency domain is used to model behaviour outside the strict limits of validity outlined in § 6.2.7, it is important to anticipate how the results will be affected. In many cases, errors introduced by using a linear model for a non-linear process are outweighed by the convenience of using the frequency domain. An example is design optimisation of a WEC. The frequency domain is a computationally efficient way of testing combinations of a large number of design parameters [123]. It can be used to narrow the search space for more accurate but time consuming tests such as experimental work, or design optimisation using non-linear time domain simulations.

6.2.9 A summary of recommendations for frequency domain modelling of WECs

The dry oscillator model is easy to formulate and quick to implement and is therefore a popular modelling technique. When using this model, it is important to clearly state the assumption of steady state sinusoidal motion. If this model is used in circumstances that invalidate this assumption, such as non-linear PTO, then this should be clearly stated and justified.

The wet and dry oscillator models appear similar when considering the frequency domain equations. In a discussion of the differences between these modelling approaches, it is useful to compare the time domain equations, as in [95]. It is important that the time domain equation for the dry oscillator is not described as a frequency domain equation, as this incorrect and can obscure the true reason for the differences between these models. When it is necessary to use a frequency domain model, terminology such as B_s or $B(\omega_s)$ can be used in the place of $B(\omega)$ to describe a parameter is a constant in a particular model.

It is useful to be able to clearly differentiate between the wet and dry oscillator models. An alternative description is that these are models with and without radiation memory. The terms *wet and dry oscillators* are preferred as they are frank about the limitations of a model without radiation memory, and the implications of this modelling simplification are clear even to those not familiar with the concept of memory in a causal system.

The distinction between monochromatic and polychromatic behaviour can have a crucial effect on the meaning of results. When interpreting literature, it is important not to assume one or the other but to find specific references to this, which may be require the document to be read in entirety. When writing about simulations or experimental work, a clear statement about whether

the results refer to monochromatic and polychromatic behaviour would improve clarity. PTO impedance optimised at each frequency is equivalent to acausal optimal control, and should not be used for estimation of annual energy capture. Instead, the PTO coefficients should be chosen so that they are optimised at one frequency. Even the use of causal control methods will lead to an overestimation of annual energy capture, so it is important to consider such performance indicators in the context of all the simplifying assumptions made in a linear unrestrained model.

When collecting experimental data for use with a frequency domain model, it is important to ensure that the behaviour is post-transient, periodic, and only weakly non-linear. Systemic errors should be identified and mitigated so that they do not obscure non-linear response. Clear documentation of experimental practices, along with an open comparative discussion of methods, will enable a better understanding of literature about experimental work, will allow experiments to be repeated, and will eventually lead to a standardisation of experimental methods by consensus.

6.3 The usefulness of advanced prediction methods

6.3.1 Parameters that can be used as control data

In § 3.4.2 the forces on a floating body were described according to where these forces react. It is particularly important to list the forces that occur between the body and the fluid (Fig. 3.9 centre), because a measurement of the fluid-body force could be used as data for a control system. The excitation would indeed be useful control data, but it is not possible to isolate this from the fluid-body force unless the forces due to radiation, buoyancy and losses can be calculated. While it is easy to calculate these forces for linear behaviour, the understanding of these forces in the context of non-linear behaviour is less well researched, and is highly device specific.

Measurements of the fluid-body pressure on the AWS [103] were found to have lower than expected correlation with power generated. It is not clear whether the measured fluid-body force was taken to be the wave exciting force, or the sum of all fluid forces. If the measured fluid-body force was interpreted as the wave exciting force then this is the source of the poor correlation. The correct approach is to subtract all fluid forces other than the excitation force from the measured fluid-body force. The radiation force can be calculated using measured velocity. If this approach was taken, then there is another source of error to consider. In this particular study, a dry oscillator model was used in conjunction with the value of radiation damping at the average frequency. Therefore calculations of the radiation force, and hence the wave exciting force, would contain some errors. Other possible explanations for the poor correlation are non-linear damping losses that are not of the mathematical form expected, or errors in data collected by localised pressure sensors that was then extrapolated and integrated to estimated the fluid-body force. Although the evidence in [103] indicates that fluid-body

pressure is not a useful measurement for use with control, if the possible errors listed above are identified and eliminated, then there is still potential for fluid-body force to be useful control data.

The absorbing wave paddles used in the Edinburgh Designs experimental wave tanks [69] can be compared to WECs. When they are not generating waves, they act as active absorbers. When they are generating waves, they continue to absorb waves, which ensures reflected waves are not added to the generated waves. They use a control method similar to damping-spring reactive control of WECs. In addition to this they also use force feedback. A piczo force sensor is used to take a measurement that closely approximates the fluid force felt over the entire paddle. A feedback controller is designed to minimise the difference between the measured fluid-body force and the desired fluid-body force. When no waves are being generated by the paddles, the desired fluid-body force is zero. It is not yet fully understood how the measured fluid-body force affects the control dynamics. It would be interesting to compare the time domain wave paddle drive forces due to non-linear feedback control, with the linear forces calculated for mass-damping-spring causal control, and for theoretical acausal optimal control.

Furthermore, it would be useful to determine whether this control technique could be scaled up for use with large WECs, and whether it has any advantages over existing techniques. When modelling this type of control, it is important to note that the fluid-body force has components due to excitation, radiation and if applicable, buoyancy and fluid losses, as shown in Fig. 3.9 (centre). Furthermore, the PTO force resulting from feedback control will be highly non-linear, and thus a non-linear time-domain model taking into account radiation memory should be used, which is not the case in [142].

If the PTO is between an oscillating body and the sea-bed, then sensors giving the fluid-body force are not required because the excitation can be found by measuring the force between the body and the point of reaction (the f_{pto}). Note that when the PTO is between two oscillating bodies, the WEC will not remain motionless even if the relative motion of the two oscillating bodies is zero, so the fluid-body force will contain components due to radiation, losses, and if relevant, buoyancy spring.

There is an acausal relationship between the elevation of the incident wave and the exciting force. As discussed in § 3.7.2 on page 106, the elevation of the incident wave cannot be measured directly because the diffracted and radiated waves are superimposed, and in the case of a floating wave energy converter, the air-water interface no longer exists. Wave elevation measured from several nearby locations that are each upstream with respect to the direction of wave propagation, could be used to infer the surface elevation a given point. This technique is being investigated by Belmont's group [133]. It has been shown that non-linear propagation and directionality limit the accuracy of this technique, while the spectral content (via the group velocity of the spectral components) limits the prediction horizon.

6.3.2 Types of advanced prediction methods

The information required by acausal PTO control, or indeed for storage management, is advance knowledge of the velocity of the PTO mechanism. This could be calculated if the excitation force or wave elevation were known sufficiently far into the future. Methods for providing predictions for this type of control that have been considered in the literature are Kalman filters [143] and neural networks [16].

Kalman filters can be used for sinusoidal extrapolation. They use a running average of the frequency to slowly modify previous values of the estimated frequency. The rate of this modification can be made sensitive to prediction error, so that the method adapts quickly to different sea states.

The term *neural networks* describes the structure of an algorithm that is built up of a number of simple functions (neurons) connected with weighting factors. These *weights* (coefficients within the algorithm) can be chosen to store experiential knowledge and so that it can be applied to similar problems. Neural networks can be thought of as black boxes that relate inputs to outputs. Inside the black box is an algorithm that has been derived using a form of non-linear regression. This algorithm is derived by *training* the network: this involves repeated exposure to example data in order to optimise network weights, and occasionally also the *architecture* (number and arrangement of neurons).

Neural networks are suitable for identifying a statistical relationship between the inputs and outputs and applying this relationship to unseen inputs. They are also suitable for identifying an underlying non-linear deterministic process where the input data has been corrupted with noise [144]. In short, they are good at the types of tasks performed by a well-informed human brain. Examples include the identification of cancerous cells, classifying spectral data [145], facial recognition [146], recognising the sound of a 'bad' engine noise [147], process control [148, 149], or extrapolating a time series [150]. It is equally important to recognise that a neural network cannot perform a task that would be impossible for a human brain: thus they do not work when there is no relationship between the inputs and output. Furthermore, neural networks do not give an optimal solution when there is a deterministic relationship between the inputs and outputs; they are not a substitute for identifying the correct deterministic model.

6.3.3 The use of neural networks for improving WEC control

Neural networks have been used to forecast significant wave height [151, 152] for 3 to 24 hours ahead. Previous values of significant wave height were used as inputs. In [151] results were compared with an ARMA (auto-regression moving average) model. In neither of these studies was there a test of whether the neural network performed better than adding a random number (with the statistically correct variance) to the present value. This type of test is important because, as noted by Agrawal and Deo [151], there is an "*Absence of any correlation pattern*

in between neighbouring values, which are separated by longer duration". Neither of these studies compared performance to that of the most well-known rival technique: wind-wave hind-cast models [153]. There is therefore no objective way of assessing whether neural networks outperform rival techniques for forecasting significant wave height.

Three possible uses of neural networks for improving WEC control were considered during the course of this PhD study: system identification, the use of an identified system to optimise control, and the prediction of near future waves. All three methods have been judged as having no useful potential, as shall now be described.

The use of neural networks for system identification

As described in § 1.2, earlier work conducted for this PhD study [11] investigated the use of a neural network to perform system identification on a WEC, installed and operational in its permanent site. Neural networks are not good function approximators when a deterministic function exists. The physical process that underlies the behaviour of a WEC is a deterministic process. Unknowns in the system, such as sensor noise and variation in component properties, can be dealt with using low pass filters and feedback respectively. Non-linear behaviour can be included in dynamic models, and although the computational time is high, it is possible to model, with very high accuracy, the deterministic response of a WEC to a given exciting force [13, 14].

Although the physical process behind the behaviour of a WEC is deterministic, the relationship between the available inputs and the required outputs is not. There are two reasons for this. The most fundamental is that the deterministic relationship between the optimal control force and the exciting force is anticausal: future values of excitation must be known in order to calculate the optimal control force. In any sea-state that is not a sinusoid, past values of excitation do not contain the information required to make these predictions. A further problem is that that deterministic relationship between wave elevation and exciting force is acausal: future values of incident wave elevation must be known in order to calculate the wave excitation force. Lastly, it is difficult to directly measure the incident wave elevation, or the excitation force § 6.3.1. These are all barriers to building a real-time deterministic model of a WEC. These same difficulties apply to using a neural network to build a black box dynamic model. There is nothing about this problem that suggests that a neural network could perform better than a deterministic dynamic model at predicting near future response of a WEC.

Optimising control using an identified system

In [11] the purpose of performing system identification on a WEC was to provide a test-bed for optimising the control parameters. Various combinations of parameters could be tested, and the ones that resulted in the most desirable behaviour were chosen. This paper suggested that a

neural network could be used to derive a heuristic relationship between the system inputs and the control parameters. In Fig. 4.5 on page 139, it is seen that the control force required to absorb the entire spectrum of the incident wave is acausal. To apply the force shown in Fig. 4.5 using the PTO configuration shown in Fig. 4.4 (on page 135), the PTO settings in Fig. 4.4 would need to change continually with time. At any time, the optimal choice of PTO settings requires information about future waves. To successfully relate the optimal PTO settings to present inputs essentially requires wave prediction.

6.3.4 Advanced methods for short-term wave prediction

In [16] neural networks were considered for short-term wave prediction. The value being predicted was the time until an extreme event: a minimum or maximum in excitation force. This study did not compare results with a prediction consisting of a random number (with the statistically correct variance) added to the present value, so it is not possible to conclude whether the results were better than random. Results were compared with sinusoidal extrapolation. Two datasets were considered: noisy sinusoidal data of various frequencies, and PM spectra of various peak frequencies and random phase, used with an excitation coefficient for a simple geometry to find the excitation force time series. This study pre-dated the work on premonition time, so there was no distinction between the prediction accuracy of events that were within or beyond the coherence time. For the sinusoidal dataset, the extreme events occurred within the coherence time, whereas for the PM dataset, the extreme events occurred both within and beyond the coherence time. Note also that the bandwidth of a PM spectrum depends on its peak frequency, so spectra of various coherence times were used.

The results of this study [16] were that for the noisy sinusoidal dataset, sinusoidal extrapolation outperformed neural networks, whereas for the PM spectrum, neural networks outperformed sinusoidal extrapolation. These results were as expected. What is interesting is that for a given dataset, the difference in accuracy between each method (neural networks or sinusoidal extrapolation) was small, whereas the difference in accuracy between the datasets was very large. The difference between the datasets can be described by the bandwidth: the noisy sinusoidal data had a very narrow bandwidth while the PM spectra dataset has comparatively wider bandwidths. The work in [16] suggests that the signal bandwidth (and hence the coherence time) has a much bigger impact on prediction accuracy than the type of prediction method.

Wave prediction within the coherence time

In § 5.4 it was shown that the bandwidth of a sea state is inversely related to its coherence time. Coherence time can be thought of as the time for which a sinusoidal extrapolation approximates the near future wave to a known level of accuracy. Thus any method employing sinusoidal

extrapolation would work better in a narrow bandwidth sea than in a broad bandwidth sea. As the shape of the function within the coherence time is likely to be close to sinusoidal, then any type of sinusoidal extrapolation will be superior to an extrapolation method using heuristic parameters gathered from past data. Therefore, for prediction horizons that are short compared to the coherence time, sinusoidal extrapolations will be better than auto-regression [154] or neural networks [16]. Kalman filtering [143] is particularly well suited to adaptively finding a frequency for sinusoidal extrapolation.

The problem of forecasting the timing of an extreme event is equivalent to making a series of predictions at each time step. For a short time into the future, there will be a narrow band of values of exciting force that are probable. With each time step into the future, this band will grow wider. The best a neural network can do is guess a random number close to the mean of the band bounded by error margins. Given that this is the most likely behaviour of a neural network used in this context, it seems that it would be more useful to understand the distribution of the possible predictions. A sensitivity analysis could then be performed, which would allow PTO settings that give the most desirable distribution of behaviour, to be chosen.

Wave prediction beyond the coherence time

Beyond the coherence time, there is no correlation between the input and output, and the band of probable values of exciting force for a given history of exciting force approaches the overall distribution of probable values of exciting force. In this case, the best a neural network can do is guess a random number close to the mean value. Once again, it would be more useful to perform a sensitivity analysis using the known distribution of exciting force.

Methods that estimate future knowledge from local data [16, 143, 154] are in a different category to methods that estimate future knowledge from remotely collected data [110, 133, 155]. Local and remote data prediction are described as fixed point and fixed time by Belmont, who specialises in fixed time wave prediction methods. Data collected remotely is described as *up-stream* or *up-wave* data by some authors to indicate that the wave is modelled as travelling in a straight line between the sensor and the WEC. Using remotely collected data, the limitation of coherence length is circumvented by having information about the waves before they arrive. If wave propagation is linear, Fourier analysis can be used to reconstruct the measured wave, later in time, at a down-stream location. The extra time granted by this method depends on the distance between the WEC and the upstream sensor, the velocity of each wave component, the bandwidth, linearity, and directionality of the sea state. This method is being studied by Belmont's group [133] and the technology is not yet developed enough for commercial use. Further research is required to determine whether this technique will be suitable for the requirements of optimal control. There is a trade-off between prediction horizon and accuracy: the further away the data collection location, the longer the prediction horizon, but the greater

the uncertainty. Accuracy is also effected by highly directional seas and by non-linear wave propagation.

6.3.5 The control challenge for industrial WEC developers

Fig. 5.16 shows what combination of WEC and sea state would make predictions possible and useful. For large WECs in broad bandwidth seas, a long prediction horizon is required, but the use of predictions would not improve power capture much compared to mass-damping-spring control. For a small WEC in broad bandwidth seas, a short prediction horizon is required, and the use of predictions could lead to a significant improvement in power capture compared to mass-damping-spring control. Unfortunately, mass-damping-spring is difficult to implement because of displacement restraints, and this is especially a problem for the combination of a small WEC in broad bandwidth seas.

Chapter 4 showed that mass-damping-spring control resulted in large values of displacement response; combined with a broad bandwidth sea state, this would result in large amplitude displacements. These displacements may not be physically possible, as they might exceed the stroke of the motion, or they may result in motion which invalidates the linearity assumptions upon which the theory of capture width is based, i.e. result in high values of non-linear damping losses. In addition, high displacements or power flows may exceed the chosen design limits of the power conversion chain. The PTO schemes using fewer than three coefficients can be viewed as the application of *soft limits*; hard limits involve a non-linear PTO force, whereas for soft limits the PTO force remains linear. They can also be treated as bandwidth restricted reactive control.

With the current state of technology, the PTO losses due to reactive control are too high to allow mass-damping-spring control. Pelamis uses limited reactive control, applying both hard and soft limits [49]. The most recent prototype of the AWS uses only damping control but will consider reactive control once technology improvements make this viable [47]. Thus the immediate challenge for developers is not the development of prediction technology to upgrade the performance of the mass-damping-spring scheme to that of ideal control, but rather to improve on real control or bandwidth restricted reactive control. Capture width due to real control can be greatly improved by geometry control measures that move the natural frequency closer to the operating frequency. Bandwidth restricted reactive control, examples of which are the mass-damping and damping-spring schemes shown in Fig. 5.3, can be improved by reducing the need for displacement or power restraints. This includes designing the WEC to allow greater amplitudes of displacement, reducing the losses in reactive PTO mechanisms, increasing the rating of the primary conversion system, or improving management of intermediate storage. Bandwidth restricted reactive control may also benefit from some form of geometry control.

6.4 The ideal size of a WEC

There is a wide variation in the size of WECs under commercial development, from the 180 m long 4 m diameter P2 Pelamis machine [4] to Ocean Power Technologies' 1.5 m diameter PowerBuoy™ [156]. The purpose of this section is not to argue that a particular size of WEC is better than any other, but instead to highlight how many areas are effected by the choice of WEC size.

This section first discusses the historical origins of the debate about the ideal size of a WEC, and then shows why this debate is important in the context of a technology moving to the commercial development stage. In previous chapters it was shown that the size of a WEC has an impact on primary energy capture. This is explored in more depth, taking into account displacement and power limits, and the choice of design sea state. It is not only the primary energy capture that has an impact on the cost of energy. The effect of the size of a WEC on the other factors that effect cost of energy is considered.

6.4.1 The historical context of the size debate

The debate about whether a small or large WEC will lead to the most economic production of electricity from waves has existed since Salter suggested wave energy was a candidate for large scale energy production in 1973. The history of the academic development and political context is described in [5, 21, 157]. Salter's lobbying efforts led to public funding of several investigations into the feasibility of generating a significant proportion of Britain's electricity demand from wave energy. The early feasibility studies ran concurrently with development of specific devices. The devices designed were all very large structures. The goal of installing gigawatt scale plant seemed to suggest comparison to large thermal plant of a similar rating; at the time there were no gigawatt rated wind farms for comparison. In Europe and Asia, where research on wave energy was not motivated by the political agenda of installing Gigawatt scale wave farms in the near future, the focus was on smaller devices. Several early test facilities were built, including an OWC in Japan in 1983, and the Tapchan and OWC in Norway in 1985 [157]. These were all shore-line devices. The early installation of prototype devices in Norway and Japan shows that they valued operational experience. The common ground between shore-line devices and point absorbers is that both are relatively easy to test and install with limited capital cost and using available technology.

While early research on point absorbers may have been influenced by the desire for a device that could be built with limited funds and technical innovation, theoretical studies suggested that the best ratios of cost to energy were given by smaller devices. These studies considered operation at one frequency only, and did not thoroughly take into account displacement restraints. In polychromatic seas, optimal control at every frequency results in acausal control. The theory shows that the upper limit of monochromatic capture width does not depend on the size of the

device, but on its modes of motion. The relative capture width is the capture-width normalised by the frontal width of the device with respect to the direction of wave propagation. The relative capture width due to acausal optimal control, without taking into account the inevitable displacement limits and non-linear behaviour, is large for small WECs and small for large WECs. High relative capture width, along with high capacity factors, have been used as arguments [158] for why small WECs have better power capture to weight ratios than larger WECS.

6.4.2 The importance of the ideal size of a WEC to the wave energy industry

There are now several WECs of varying sizes under commercial development [23]. It is likely that the debate about the ideal size of a WEC will be resolved by market forces and competition in the near future. The impact of the size of a WEC on the cost of energy production nevertheless remains a vital question. There are issues surrounding the perceived risk and returns expected by those funding commercial development. Several smaller devices may be perceived as less risky than one large device. As seen with the decommissioning of the AWS pilot plant in 2004 and the attempted installation of Applied Research and Technology's Osprey in 1995, the early lack of operational experience was indeed risky. The cost of capital for funding present development will be influenced by the depth of understanding of how scaled up devices will perform relative to smaller prototypes.

It is interesting to look at appropriate examples from other energy sectors. The cost of energy from wind turbines has dropped steadily. Besides technical improvements, operational experience, and economies of scale, the interaction between the resource and the turbines benefits from scaling up. Not only is energy capture for a given wind speed proportional to the square of the turbine diameter, but it is also proportional to the cube of the wind speed, which increases with height from the ground.

The cost of energy from waves is presently not competitive, and most commercial funding of development is based on the assumption that costs will fall with installed capacity. Cost reductions due to scaling up of devices or installation in more energetic seas may be assumed but is not well understood. As shall presently be discussed, the interaction between the wave energy resource and a WEC suggests that wave energy will not benefit as much as wind energy from scaling-up. More certainty about the relationship between the size of a WEC and the cost of energy will make investment capital less expensive and be a useful consideration for the strategic plans of industrial developers. It will also give an indication of economically recoverable resource, which would be a valuable input for the energy scenarios used to inform national energy policies.

These considerations were the drivers behind the study in § 4.9 on the impact of scaling on the capture width due to causal sub-optimal control, and the study in § 5.5.2 on the impact

of scaling on the requirement for future knowledge. These studies were not presented in the context of the debate of the effect of scaling on cost of energy, and it is necessary to include a more rounded discussion here. This discussion includes the effects of primary energy capture, capacity factor, design sea states, and the relationship between the natural frequency and the operating frequency. The influence of each of these on large and small WECs is now discussed.

6.4.3 Primary energy capture

Much of the discussion about small and large WECs in Chapter 4 focussed on primary energy capture. It was assumed that motions were small enough for the behaviour to be linear and unrestrained, and for the control regime to be maximisation of energy capture. This means that no hard or soft limits were applied, and one of the four causal sub-optimal control schemes was used.

Monochromatic capture width due to acausal optimal control

In the early days of wave energy, it was assumed that the power capture of small and large WECs was identical. The reason for this is that the capture width at any one particular frequency was considered: the monochromatic capture width. The monochromatic capture width due to acausal optimal control (assuming linearity and neglecting displacement restraints) does not depend on WEC size.

Relative monochromatic capture width due to acausal optimal control

When considering the capture width per unit frontal width of the device, the relative capture width is used. The smaller the WEC, the larger the relative capture width. High values of relative capture width suggest high values of power capture to volume ratio. Displacement constraints effect smaller WECs more than larger WECs, so the high values of relative capture width over-emphasise the potential of small WECs. Note also that this standard definition of relative capture width is in fact the relative monochromatic capture width due to acausal optimal control.

Monochromatic capture width due to causal sub-optimal control

It is important to consider control that can be applied in real time for polychromatic seas: causal sub-optimal control. In § 4.9 the monochromatic capture widths for large and small WECs were compared. There it was shown that the monochromatic capture width for large WECs had broader bandwidths than for small WECs. Although the range of sizes in this study was not very large, the trend shown in § 4.9 can be extrapolated to include the extreme cases of point absorbers and attenuators, since the values of the hydrodynamic coefficients follow

a well-known scaling law (Appendix A). Likewise, although the case study was for heave motion, the scaling rules apply for all modes of motion.

Polychromatic capture width due to causal sub-optimal control

In § 5.3 it was shown that it is important to consider how the monochromatic capture width interacts with the sea state, in the form of the spectral power fraction. It would be instructive to apply the methods presented in § 5.3 to WECs on extreme ends of the size scale to see how much influence size had on the polychromatic capture width. The bandwidth of the sea-state will be an important factor here. In broad bandwidth seas, a broad bandwidth performance, in the form of monochromatic capture width, is more beneficial than in narrow bandwidth sea states. It is expected that in broad spectrum seas, large WECs will have greater polychromatic capture widths than small WECs, whereas in narrow spectrum seas their capture widths will be similar.

Relative monochromatic capture width due to causal sub-optimal control

When considering the ratio of power capture to weight, the relative polychromatic capture width, which is the polychromatic capture width per unit frontal width of the device, is more important than the relative monochromatic capture width. It would be interesting to compare the relative polychromatic capture width for large and small WECs over different sea states, particularly those with combinations of bandwidth and peak frequency that can be expected during operation. For a fair comparison between small and large WECs, displacement limits need to be considered. Displacement limits in polychromatic conditions must take into account the spectrum: spectral power fraction is not sufficient as it describes the shape rather than the magnitude of the sea state.

6.4.4 Capacity factor

Capacity factor describes the average annual energy capture as a percentage of the energy that would have been captured if operating at rated power over the entire period. It gives a rough indication of how often the operating regime is seeking to maximise power, and how often it is working to a power set-point (see Table 2.5 on page 33). Small WECs generally have high capacity factors: this is an integral part of their design philosophy [158]. A greater proportion of time is spent at full stroke, resisting design loads, and generating rated power. Consequently a small proportion of time is spent in the maximising or soft limits regimes, and a large proportion of time is spent in the hard limits and power set-point regimes. The reverse is true for large WECs. For a given wave climate, capacity factor is inversely proportional to scale.

Hard and soft limits generally result in displacement restraints , although they may also be limits on reactive power flow or limits due to insufficient available storage capacity. Power set-points

are generally power restraints. Existing literature does consider power [71] and displacement [58, 97] restraints. Once again, existing theory focusses on the monochromatic case. It would be useful to extend this theory to the polychromatic case for specific sea states. As hard limits and power set-points result in non-linear behaviour, a time domain approach will be required.

6.4.5 Design sea states

Any discussion of large and small WECs must take into also account the interaction with the sea state. Here the design sea state is defined as the spectrum which has a peak at the natural frequency of the WEC, and has bandwidth and magnitude characteristics typical for sea states with that spectral peak. Small WECs have design sea states with high peak frequencies, while large WECs have design sea states with low peak frequencies. General properties of these design sea states can be observed by examining the spectral power fractions of Pierson-Moskowitz (PM) spectra with high or low peak frequencies. PM spectra with low peak frequencies have narrow bandwidth spectral power fractions, while those with high peak frequencies have broad spectral power fractions.

There are two reasons for this, and both apply to PM spectra as well as more realistic sea states. The first is that power is inversely proportional to frequency, and the second is that the spectra of high energy sea-states have low peak frequencies and narrow bandwidths. The power in any component of wave elevation is proportional to the magnitude squared and to the period. As the power in a spectral component is inversely proportional to the frequency of the component, low frequency components transport high amounts of power. Sea states with low frequency peak spectra also tend to have higher magnitude spectral components. The PM spectra embody the theory that for a fully developed sea the spectrum is related to the speed of the wind that created the waves. The PM spectra was developed using the actual spectra of fully developed seas [19]. High wind speeds result in wave elevation spectra that are high in magnitude and low in frequency. Low wind speeds result in wave elevation spectra that are low in magnitude and high in frequency.

6.4.6 Power restraints

When considering the difference between the capacity factors of small and large WECs in § 6.4.4, it was seen that large WECs spend a greater proportion of time in the power maximising regime. Efficient performance during primary energy capture is therefore more important in a large WEC than in a small WEC. Power restraints occurs when the power capture reaches the rated power of the WEC. As discussed, sea states with lower peak frequencies have higher magnitudes, and transport more power.

For small WECs, there will be power restraints for most sea states, apart from those with very small power levels. These will tend to have high peak frequencies. The natural period

of a small WEC is also high, so during the power maximisation control regime, it is likely that the operating frequency will be close to the natural frequency. This is good because the performance is better for values of operating frequency close to the natural frequency, particularly for real control. However, as small WECs have larger displacements, it is likely that displacement limits will be required (or applied naturally) when operating in the design sea state.

For large WECs, there will be power restraints in high energy sea states, which will tend to have low peak frequencies. Large WECs also have low values of natural frequency. It is possible that the design sea state for a large WEC could contain enough power to require restraints of some sort. In this case a WEC would not be operating in the maximising control regime when working in its design sea state. This may be a disadvantage as performance is better for operating frequencies close to the natural frequency. However, as seen in Chapter 4, large WECs have broader bandwidth performances than small WECs. In a broad bandwidth sea state, a large WEC would still capture more power than a small WEC when both are operating in the small WEC's design sea state.

6.4.7 Cost of energy

The impact of size on the amount of annual power capture has been discussed. The implications for small and large WECs are now summarised. A small WEC may have a slightly narrower bandwidth of acausal unrestrained performance compared to a large WEC. More significant however is that smaller WECs have a lower threshold for displacement limits and thus are not able to capture all the power as indicated by capture width theory. Small WECs tend to operate at their maximum power rating for longer periods of time, so have larger capacity factors than large WECs. When operating under the power maximisation regime, they may require displacement limits, but generally the operating frequency will be close to the natural frequency. Large WECs require fewer displacement limits and may give broader bandwidth causal unrestrained response. It is likely that they will operate at rated power (power limitation regime) for their design sea states, and that under the power maximisation regime, the operating frequency will be higher than the natural frequency.

Besides the annual power capture, the other important contributions to the cost of energy are the cost of the plant (WEC) and the balance of plant costs, which are all the other costs of the project apart from the plant costs, such as moorings, cables, installation and maintenance [159]. The devices may only be a small proportion of the capital costs. As there are many fixed overheads per device, the balance of plant costs for a wave farm with a few large WECs may be less than that for a wave farm with many small WECs.

The conventional wisdom (based on unrestrained relative monochromatic capture width) is that that the capital costs of smaller WECs will be cheaper per unit of delivered energy than

larger WECs. However, there are as yet no studies that show the effect of displacement and power limits on the ratio of capital cost to delivered energy for small and large WECs. When optimising the size of WEC, the payback time [160] is a more useful optimisation parameter than annual power capture and leads to a different optimum design [160, 161]. It would be interesting to extend this method to a time domain simulation that included displacement and power constraints.

6.5 Chapter summary

This chapter addressed various important topics that were identified and explored during the course of this thesis. Frequency domain modelling of WECs was shown to be suitable for finding the post-transient polychromatic response, provided the system is linear, and, when the DFT is used, provided the excitation is periodic with the DFT record. Various exceptions and ambiguities were identified. The dry oscillator model described in Chapter 3 is commonly used, but is suitable only for modelling monochromatic behaviour of a WEC. In the literature, the frequency domain equation, and occasionally the time domain equation, of a dry oscillator were associated with the frequency domain model of a WEC. This gave the impression that all frequency domain models of WECs, rather than just the dry oscillator model, were restricted to sinusoidal motion. The inclusion of a control force in the governing equation compounds the ambiguity. When performing impedance matching, the frequency at which the impedance is matched, the operating frequency ω_p, must be chosen. Experiments and simulations can be carried out at individual frequencies and then superimposed, provided the same value of ω_p is used at each frequency bin, ω_j. If the PTO impedance is optimised at each frequency, $\omega_p = \omega_j$, then this amounts to causal control when using monochromatic waves, and acausal control (requiring future knowledge) when using polychromatic waves. Assuming that causality is a requirement, an equation with an optimal control force is only valid for sinusoidal motion.

Prediction data and prediction methods were discussed. It was highlighted that the force measured between the fluid and the body is the sum of several forces. To find the exciting force from the measured fluid-body force is it necessary to first subtract the other forces. The opportunities for advanced control techniques were discussed. Within the coherence length of the velocity, the Kalman filter has good potential as a sinusoidal extrapolator. At times beyond the coherence length, sinusoidal extrapolation techniques will become less accurate. While techniques such as neural networks may perform marginally better than sinusoidal extrapolation, their performance will also degrade with the prediction horizon. Data collected upstream of the direction of wave propagation potentially contains more information than locally collected data. It is not yet known whether this technique could provide predictions of the required accuracy. This indicated that given the current immaturity of wave energy technology, the development of prediction systems for upgrading from causal

mass-damping-spring control is not a priority. Mass-damping-spring control itself is not currently feasible, and provides marginally less power capture than optimal control requiring predictions. The challenge for industry is rather to shift the performance due to real control, or bandwidth limited reactive control, in the direction of mass-damping-spring control. Predictions using remotely collected data may however be useful for storage management, which could lead to significant improvements in delivered power.

A better understanding of the effect of the size of a WEC on its cost of energy would be beneficial for investor confidence, and would be useful information for industrial planning and energy policy. All the factors that influence the cost of energy must be considered. When comparing large and small WECs, the cost of energy of wave farms composed of either small or large WECs, and producing comparable annual energy, must be considered. Wave farms composed of large WECs will have higher installed capacities, lower capacity factors, higher capital costs for the WECs and lower balance of plant costs. The sub-optimal linear control schemes described in Chapter 4 are only important when the aim of the control system is to maximise primary energy capture. In the maximising regime, small WECs will be operating in their design seas, where the operating frequency is close to the natural frequency, while large WECs will be operating in lower energy sea states than their design seas, where the operating frequency is higher than the natural frequency.

Chapter 7

Conclusions and further work

7.1 Chapter overview

This chapter presents the principal conclusions (§ 7.2) of the research presented here. Some of the new theory which has been presented formalises well understood principles, while other new ideas present completely new perspectives for viewing the problem of controlling wave energy converters (WECs). These new perspectives, particularly the normalised capture width and the premonition time, have presented more questions than answers. They point to many intriguing lines of research. This chapter concludes with recommendations for industrial development (§ 7.3) and for further academic research (§ 7.4).

7.2 Summary of findings

The most important thing to emerge from this research is that the use of forecasts will lead to zero or marginal improvement in PTO control of WECs. In cases where there is potential for marginal benefits, the data required for these forecasts will be difficult to acquire: locally collected data is not adequate, while remotely collected data also has physical limits to its usefulness, and requires technologies for collection and processing that are not yet available.

Equally important are the new perspectives on the control problem that did not previously exist. It is now clear that important information about the nature of the control problem is lost when considering only sinusoidal behaviour. Using mass, damping and spring coefficients is not, as previously thought, equivalent to using damping and spring coefficients. Monochromatic and polychromatic capture widths are mathematically distinct for behaviour that is not sinusoidal. Applying these techniques to a simple example of a heaving buoy with linear unrestrained motion led to some surprising results: larger WECs can capture more energy in broad bandwidth sea states than small WECs; the spectral peak is not necessarily the best choice of operating frequency, especially for real control; capture width due to causal sub-optimal control decreases with the bandwidth of the spectrum. Particularly surprising is that the capture width due to acausal optimal control decreases with the bandwidth of the spectrum. These new perspectives can be applied to the design of WECs, or to improve control in a given sea state.

7.2.1 Thesis response

The thesis postulated in § 1.3 was that it should be possible to establish the extent to which forecasts could improve power capture. In Chapter 5 it was shown that it is indeed possible to establish the additional primary energy capture, assuming linear unrestrained motion, due to a control scheme that requires forecasts. The extent of this improvement is given by the forecast benefit parameter, which relates the capture widths of causal sub-optimal, and acausal optimal control, $(\tilde{C}_W - \breve{C}_W)/\breve{C}_W$. The value of the forecast benefit parameter was shown to depend on the sea state, the size of WEC, the choice of operating frequency and the PTO coefficients chosen to implement sub-optimal control. This ratio will also depend on the modes of motion; in this work only heave was discussed; the linearity of behaviour, and restraints on displacements or power.

7.2.2 Contributions to knowledge

During the process of investigating the research question, many useful findings or new perspectives on the control or design of WECs were introduced. Key contributions to the body of knowledge are now described.

Classification of WECs by power flow

A new classification system for WEC concepts was introduced. It consistently classifies all types of devices, is useful for classifying control methods, defines a WEC's governing equation, and encourages a fair comparison between direct-drive and buffered-drive concepts.

Classification of control methods for WECs

A new control classification system, which distinguishes between concepts previously treated as equivalent, was introduced. The distinctions between geometry control, PTO control and power regulation complement the WEC concept classification system. The concepts of *acausal optimal* control, *causal sub-optimal* control and *causal optimal* control were defined in a systematic way. These definitions are more rigorous than their use in existing literature. This systematic classification also identified a previously unknown type of control, *acausal sub-optimal* control. It was shown that this is a suitable description for control using forecasts that cover a shorter duration than the prediction horizon required for optimal control.

Capture width theory

The formula for capture width (5.16) was arranged to emphasise that it is a function of the WEC performance (the monochromatic capture width) and the sea state (the spectral power fraction): $C_W = \sum_{j=0}^{N/2-1} C_W^s(\omega_j)\ P_f(\omega_j)$. It was shown that the capture width in a sinusoidal sea is higher than that for a Pierson Moskowitz spectrum of corresponding energy period.

PTO impedance configuration for reactive control

It is widely known that in monochromatic conditions there is no difference between a PTO scheme that employs a mass, spring and damper, or one that employs a mass and damper, or spring and damper. Here it was shown that PTO impedance configuration is important in polychromatic conditions. The mass-damping-spring scheme has a much broader bandwidth of performance and displacement response.

The effect of scaling on performance for reactive control

It was previously thought that displacement restraints were the only reason why large WECs could capture more power than smaller WECs. Here it was shown that even in sea-states where displacement restraints are not required, large WECs will capture more energy than small WECs. This is because for mass-spring-damping reactive control they have a broader bandwidth of performance (monochromatic capture width).

Real control

It was shown how the performance bandwidth of real control depends on both the operating frequency and the natural frequency. An operating frequency that equals the natural frequency gives the narrowest bandwidth of performance. Operating frequencies either above or below the natural frequency give broader bandwidths of performance, but also lower peak values. So when considering how the size of a WEC influences the bandwidth of performance, the operating frequency, and hence sea-state, is important.

Wet and dry oscillator models

The wet and dry oscillators were introduced to distinguish between two methodologies present in the literature. The descriptions *wet* and *dry* emphasise that they differ in how they model the effects of the surrounding fluid. Both the wet and dry oscillators can be expressed in the time or frequency domain.

The validity of frequency domain modelling

An important source of ambiguity in the literature was identified. Several papers appeared to claim that frequency domain modelling is only valid for motion at a single frequency. It was shown that the correct interpretations are that the dry oscillator model is only valid for sinusoidal motion, and that causal damping-spring control is only optimal for sinusoidal motion. Once the incorrect interpretation of these papers was refuted, it was then possible to make a credible assertion that frequency domain modelling is valid for modelling post-transient polychromatic linear response of WECs.

The special case of sinusoidal behaviour

New theory showed that for the special case of sinusoidal behaviour, the following are equivalent: the wet and dry oscillator models; optimal and sub-optimal control; and the monochromatic and polychromatic capture widths.

Reinterpretation of key literature

The distinction between monochromatic and polychromatic behaviour highlighted the misinterpretation of a crucial experimental result. It was previously thought that there was experimental evidence of almost complete power capture of irregular waves using advance knowledge of waves as 'forecasts'. It is now clear that simpler monochromatic experiments were performed and that advance knowledge was not used in the manner previously thought.

The extent to which forecasts improve power capture

For any given sea-state, the forecast benefit parameter $(\tilde{C}_W - \breve{C}_W)/\breve{C}_W$ gives a measure of the extent to which optimal control is an improvement over a given sub-optimal control scheme. As the mass-damping-spring scheme described gives the best performance, this is what should be compared to optimal control. The increase in performance can then be attributed solely to the use of future knowledge. For the example considered it was shown that the mass-damping-spring scheme performed almost as well as optimal control.

Premonition time

Another new piece of theory relates the prediction horizon required for optimal control, the *memory duration* Δt, to the prediction horizon that is achievable for a given sea-state, the *coherence time* of the velocity τ_c. *Premonition time* was defined here as the shortfall between the coherence time and the memory duration: $\tau_{future} = \max\{\Delta t - \tau_c, 0\}$. It gives a measure of how difficult it is to access the information required for optimal control.

The effect of WEC size on the potential for improving performance with forecasts

It was shown that as a WEC increases in size, the extent to which forecasts can improve power capture in linear unrestrained conditions decreases. So for large WECs the benefits of using forecasts with PTO control are marginal. As a WEC decreases in size, the need for displacement restraints, and the non-linearity of response, are greater. So for small WECs the benefits of using forecasts with PTO control are marginal or zero.

The effect of sea state on the potential for improving performance with forecasts

The sea-state also influences the extent to which forecasts could improve linear unrestrained power capture. For sea-states that result in the largest potential for improved power capture using forecasts (broad bandwidth spectra), the premonition time is long: this means it is difficult to attain accurate forecasts to cover the required prediction horizon. Conversely, for the sea-states in which accurate forecasts are easier, meaning there is a short premonition time (narrow bandwidth spectra), the potential benefits of these forecasts are smaller.

The potential for improving performance with forecasts

For a premonition time above zero, locally gathered data are not sufficient for making the required forecasts. As there is no correlation between past values and the required future values, advanced techniques such as Kalman filters or neural networks will not be useful. While it may be possible to use Fourier analysis on remotely gathered data, spectral content and the distance of the remote sensors place limits on accuracy and the prediction horizon. Thus the new knowledge is that using forecasts to improve PTO control is unlikely to result in significant increases in power capture, regardless of whether the data feeding the predictions are gathered locally or remotely, and regardless of the sophistication of the forecasting technique. However, short and medium term wave forecasts may be useful for improving the power regulation of WECs.

The potential for improving performance without forecasts

Several methods that did not require forecasts were shown to have potential for improving performance. These include geometry control, the choice of operating frequency, and the configuration of PTO impedance.

7.3 Recommendations for industrial research and development

Operational research

Research into the effects of various factors on the cost of energy could be carried out by monitoring wave farms. With one group of units treated as the control case, and all other groups differing from the control case in one aspect only, life-cycle costs and revenues can be compared. If the differences being monitored are small this should not concern the owners of the machines. Interesting aspects to monitor are changes to the power conversion chain that affect capacity factor. An indication of the effects of scaling up on energy capture will improve strategic planning. Comparative research on control schemes can be carried out most effectively if the control algorithm can be upgraded remotely.

Power conversion chain

There may be alternative arrangements of power conversion chain that lead to improved performance or robustness of plant. When comparing direct drive and buffered PTO systems, it is important to consider the entire power conversion chain required to produce comparable quality delivered power.

Relative sizing of the PTO mechanism, storage capacity, and power regulation plant

The relative sizes of the PTO mechanism, storage, and power regulation plant will determine the plant capacity factor. The most cost effective capacity factor will depend on the size and variability of the resource (water depth and geographical location), and on whether there are political or economic penalties for power fluctuations. Storage serves two functions: smoothing of intermittent power, and providing power for reactive control. The amount of storage on individual machines required for power smoothing will drop with the number of units in a wave farm. If reactive control can be applied using electricity from neighbouring machines then the storage capacity per machine will drop with the number of units in the wave farm. If reactive control can only be applied using on-board storage, then the storage capacity per machine required for reactive control will remain the same regardless of the size of the wave farm.

Hard and soft limits

The choice between hard and soft limits will involve a trade-off between power capture and mechanical wear. Mechanical wear could lead to downtime (reduced annual energy capture) and expensive unscheduled maintenance. The risks of mechanical wear will only be understood with operational experience. The manner in which restraints are applied will thus also affect the cost of energy.

Storage management

Storage management on individual machines could be co-ordinated to improve power quality from a wave farm. The contribution made by each individual machine to the net power generation could be set according to the amount of spare storage capacity. Such a scheme could be integrated with an element of forewarning from neighbouring units. Data from up-wave units could be used to determine the desired spare storage capacity of down-wave units, or even the level of net power generation from the wave farm.

Recommendations for real control

Real control is not a good choice when the operating frequency is distant from the natural frequency. For spectra centred around the natural frequency, the best choice of operating

frequency is probably not the natural frequency, but a frequency slightly higher or lower. This suggests that the ability to change the natural frequency using geometry control would be beneficial for use with real control.

Geometry control

Geometry control will improve the performance of real or reactive control. Geometry control combined with real PTO control could rival reactive PTO control. It has the potential to be more cost effective, as high reactive power flow requires either higher ratings for the PTO mechanism and storage, or constraints to limit power capture. Plant required to implement geometry control need not necessarily be expensive. If there is PTO in orthogonal degrees of freedom, this can be used to control the angle of motion. Ballast tanks and positioning equipment that would be useful for geometry control may already exist to perform other important tasks.

Choice of reactive PTO coefficients

Although the mass-damping-spring scheme is much better than either of the single reactance term schemes, it also leads to high magnitudes of PTO impedance at frequencies remote from the operating frequency. In broad bandwidth seas this would lead to unacceptably high reactive PTO forces. Soft limits could be applied by a non-optimal choice of operating frequency (de-tuning), or by choosing one of the single reactive term schemes.

Using predictions to improve performance

Storage management using forewarnings from up-wave units shows potential for reducing the mechanical wear and limiting reductions in power capture due to hard limits. The study presented in Chapter 5, suggests that the benefits of PTO control requiring forecasts are marginal and that there are physical limits to acquiring the required forecasts. It would be interesting to repeat this study for realistic device geometries and sea states.

7.4 Recommendations for further academic research

Extension of results to different geometries and sea states

The results presented here are for a narrow range of sizes of one shape of buoy, operating in one mode of motion, excited by a one particular sea state. A repeat of this analysis using hydrodynamic coefficients that extended to frequencies where they approached their asymptotic values would make the results more conclusive. Repetition of results using different sea states, geometries and modes of motion would ensure they are not artefacts of the hydrodynamic parameters, and would allow sensitivity analyses (such as in [160]) to be conducted on these parameters.

Representing displacement and power limits in the frequency domain

The results presented here are for unrestrained motion. For a fair comparison of small and large WECs, it is more meaningful to consider amplitude and power restraints. Existing work [58] on imposing restraints on the capture width applied only to monochromatic behaviour. To extend these results to polychromatic conditions, the interaction with waves must also be taken into account. It is easy to apply non-linear restraints during a time simulation. A method for applying linear restraints would be useful as it would allow the use of frequency domain capture width theory.

The number of coefficients in the PTO force

The reason for the success of the mass-damping-spring scheme described here is that with two reactive PTO coefficients, the imaginary part of the PTO impedance has a good fit with the imaginary part of the complex conjugate of intrinsic impedance. However, with only one real coefficient, the PTO damping is not a good fit with the real part of the complex conjugate of intrinsic impedance. It is worth exploring whether performance could be improved using additional real coefficients, for instance the second and fourth derivatives of velocity.

Choice of operating frequency

The best choice of operating frequency is not necessarily the spectral peak. Research on optimising the choice of operating frequency would be beneficial to all WECs with linear motion in small sea states. Challenges to this research are the inclusion of linear power and displacement restraints, and access to the spectra of the undisturbed incident wave.

Benefits of future knowledge

It would be interesting to experimentally verify the central finding of this thesis: that for small WECs forecasts would give no benefits; while for large WECs the benefits would be marginal and the data requirements large and possibly unattainable. The experiment described in [20] would be a useful starting point. To operate in the time domain, an iterative technique is required to calculate future values of velocity from future values of wave elevation (which are known when highly repeatable facilities are used). The benchmark would be the mass-spring-damper scheme described here. Such experiments could be used to measure premonition time, and to perform a sensitivity analysis on forecast accuracy. The conclusion of marginal benefit would be supported if theory was developed to conclusively show the link between premonition time and the forecast benefit parameter.

Using feedback for control

The successful use of the fluid-body force as feedback for absorbing wave paddles suggests that this technique may be useful for WECs. The resulting PTO force is non-linear with respect to velocity, so a time domain model is required. It would be interesting to test experimentally, or show by comparing equations, the relative performance of control using feedback, impedance matching at one frequency, and impedance matching at all frequencies.

The effect of geometry on performance

It would be informative to compare monochromatic capture width and premonition time for a series of cylindrical buoys of different aspect ratio [162] but identical volume. A study comparing two such buoys by Pizer [51] indicated that the tall buoy had a broader bandwidth heave damping coefficient than the flat buoy. Comparison of normalised capture widths for cylindrical buoys of the same radius but different drafts could be used to model the effects of water ballast for geometry control.

The ideal intrinsic impedance for a given sea state

Further studies are required to investigate the effects of size, aspect ratio, and geometry control on the natural frequency, and on the shape of the intrinsic impedance as a function of frequency. The ideal intrinsic impedance for a given sea state would result in low values of forecast benefit parameter. Defining the theoretical ideal intrinsic impedance for a given sea state would be useful for adapting the design of a given WEC to its size (scale) and to the resource at a specific site, as well as identifying suitable types of geometry control.

An expression of the capture width in time domain

Polychromatic capture width is defined in the frequency domain. A time domain version, derived with Plancherel's theorem, might be beneficial. Modelling of displacement restraints would be more meaningful in the time domain. This could be a useful tool for studying optimal control of a non-linear or time varying system.

Bandwidth limited control

The mass-damping-spring scheme presented here gives the best performance, but high displacement response. The mass-damping and damping-spring schemes can be treated as bandwidth limited reactive control for use as a soft-limit. It should be possible to have forms of sub-optimal reactive control that use both spring and mass coefficients, that lie somewhere between the good performance and large displacement response of the mass-damping-spring scheme described, and the narrow bandwidth performance and small displacement response of the mass-damping and damping-spring schemes.

References

[1] http://www.carbontrust.co.uk/technology/technologyaccelerator/mea.htm.

[2] http://www.berr.gov.uk/energy/environment/etf/marine/page19419.html.

[3] http://www.ofgem.gov.uk/Sustainability/Environment/RenewablObl/Pages/RenewablObl.aspx.

[4] http://www.pelamiswave.com/.

[5] A. H. Clément, P. McCullen, A. F. de O. Falcão, A. Fiorentino, F. Gardner, K. Hammarlund, G. Lemonis, T. Lewis, K. Nielsen, S. Petroncini, M.-T. Pontes, P. Schild, B.-O. Sjöström, H. C. Sørensen, and T. Thorpe, "Wave energy in Europe: current status and perspectives," *Renewable and Sustainable Energy Reviews*, vol. 6, pp. 405–431, 2002.

[6] S. Barstow, G. Mørk, D. Mollison, and J. Cruz, "The wave energy resource," in *Ocean Wave Energy* (J. Cruz, ed.), pp. 93–132, Springer, 2008.

[7] R. P. M. Parker, G. P. Harrison, and J. P. Chick, "Energy and carbon audit of an offshore wave energy converter," *Proc. Inst. of Mech. Eng., Part A: J. of Power and Energy*, vol. 221, no. 8, pp. 1119–1130, 2007.

[8] R. Gross, M. Leach, and A. Bauen, "Progress in renewable energy," *Environmental International*, vol. 29, no. 1, pp. 105–122, 2003.

[9] S. J. Couch, A. R. Wallace, and I. G. Bryden, "Overview of the SUPERGEN marine energy research consortium," in *International conference on clean electrical power*, (Capri, Italy), 2007.

[10] A. P. McCabe, A. Bradshaw, and M. B. Widden, "A time-domain model of a floating body using transforms," in *6th European Wave and Tidal Energy Conference*, (Glasgow), 2005.

[11] A. A. E. Price, T. Mundon, A. F. Murray, and A. R. Wallace, "A test-bed for advanced control of wave energy converters," in *6th European Wave and Tidal Energy Conference*, (Glasgow), 2005.

[12] D. Soloway and P. J. Haley, "Neural generalized predictive control," in *Proc of the 1996 IEEE International Symposium on Intelligent Control*, (Patras), pp. 277–281, 1996.

[13] C. Retzler, D. Pizer, R. M. Henderson, J. Ahlqvist, F. L. Cowieson, and M. G. Shaw, "Pelamis: Advances in the numerical and experimental modelling programme," in *5th European Wave and Tidal Energy Conference*, (Cork), 2003.

[14] R. Henderson, "Case study: Pelamis," in *Ocean Wave Energy* (J. Cruz, ed.), pp. 169–188, Springer, 2008.

[15] L. Tarassenko, *A guide to neural computing applications*. Arnold publishers, 1998.

[16] A. A. E. Price and A. R. Wallace, "Non-linear methods for next-wave estimation," in *7th European Wave and Tidal Energy Conference*, (Porto), 2007.

[17] A. Babarit and A. H. Clément, "Optimal latching control of a wave energy device in regular and irregular waves," *Applied Ocean Research*, vol. 28, pp. 77–91, 2006.

[18] A. H. Clément, A. Babarit, and G. Duclos, "Système Electrique Autonome de Récupération de l'Energie des Vagues." Patent number: 04 10 927, Paris, October 2004.

[19] W. J. Pierson and L. Moskowitz, "A proposed spectral form for fully developed wind seas based on the similarity theory of S. A. Kitaigorodskii," *J. Geophys. Res.*, vol. 69, no. 24, pp. 5181–5190, 1964.

[20] S. H. Salter, "Wavenet full report." European Community: ERK5-CT-1999-20001, March 2003. `http://wave-energy.net/Library/WaveNet Full Report(11.1).pdf`.

[21] S. H. Salter, "Looking back," in *Ocean Wave Energy* (J. Cruz, ed.), pp. 7–38, Springer, 2008.

[22] M. T. Pontes, A. H. Clément, A. F. de O. Falcão, A. Fiorentino, P. di Archimede, L. M. C. Gato, P. Justino, and A. J. N. A. Sarmento, "Wavenet full report." European Community: ERK5-CT-1999-20001, March 2003. `http://www.wave-energy.net/Library/WaveNet Section B - Generic Technologies(11.1).pdf`.

[23] T. W. Thorpe, "The wave energy program in the UK and the European Wave Energy Network," in *4th European Wave Energy Conference*, (Denmark), 2000.

[24] G. Thomas, "The theory behind the conversion of ocean wave energy: A review," in *Ocean Wave Energy* (J. Cruz, ed.), pp. 41–91, Springer, 2008.

[25] Y. Masuda, "Experimental full scale result of wave power machine KAIMEI in 1978," in *1st Symposium on wave energy utilization*, (Göteburg), pp. 349–363, 1979.

[26] C. Grove-Palmer, "Development of wave energy in the uk," in *1st Symposium on wave energy utilization*, (Göteburg), pp. 190–203, 1979.

[27] G. Boyle, *Renewable Energy: Power for a Sustainable Future*. Oxford University Press, 1996.

[28] G. Hagerman, "Wave energy resource and economic assessment for the state of hawaii," tech. rep., Department of Business, Economic Development and Tourism, State of Hawaii, 2002. http://hawaii.gov/dbedt/info/energy/renewable/wave.

[29] M. J. French, *Conceptual design for engineers*. London: Design Council, 1975.

[30] A. H. Clément, "Wavenet full report." European Community: ERK5-CT-1999-20001, March 2003. http://www.wave-energy.net/Library/WaveNet Full Report(11.1).pdf.

[31] R. Boud, "Status and research and development priorities - wave and marine currents energy annex I report," International Energy Agency, Ocean Energy Systems DTI report FES-R-132, Future Energy Solutions - AEA Technology, 2003. http://www.iea-oceans.org/_fich/6/IEA-OES_Wave_and_Tidal_report.pdf.

[32] S. H. Salter, J. R. M. Taylor, and N. J. Caldwell, "Power conversion mechanisms for wave energy," *Proceedings of the Institution of Mechanical Engineers, Part M: Journal of Engineering for the Maritime Environment*, vol. 216, pp. 1–27, January 2002.

[33] M. J. French, "A generalized view of resonant energy transfer," *J Mech Eng Sci*, vol. 21, pp. 299–300, 1979.

[34] K. Nielsen, "Development of recommended practices for testing and evaluating ocean energy systems." International Energy Agency, Ocean Energy Systems, 2003. http://www.iea-oceans.org/_fich/6/IEA-OES_Annex_II_2003_(2406).pdf.

[35] J. Khan, G. Bhuyan, and A. Moshref, "An assessment of variable characteristics of the Pacific northwest region's wave and tidal current power resources, and their interaction with electricity demand & implications for large scale development scenarios for the region - Phase 1," BPA Technology Innovation project 17458-21-00 (Rep 3), Powertech labs, 2007. http://www.powertechlabs.com/temp/200972248698/BPAoceans_phase1_Full.pdf.

[36] J. N. Newman, *Marine Hydrodynamics*. The MIT Press, 1977.

[37] C. C. Mei, *The applied dynamics of ocean surface waves*, vol. 1 of *Advanced Series on Ocean Engineering*. Wiley-Interscience, 1983.

[38] R. Harris, L. Johanning, and J. Wolfram, "Mooring systems for wave energy converters: A review of design issues and choices," in *3rd International Conference on Marine Renewable Energy, MAREC*, (Blyth, UK), 2004. http://www.oreg.ca/docs/MooringSystems.pdf.

[39] L. Johanning, G. Smith, and J. Wolfram, "Mooring design approach for wave energy converters," *Proceedings of the Institution of Mechanical Engineers, Part M: Journal of Engineering for the Maritime Environment*, vol. 220, pp. 159–174, 2004.

[40] J. Fitzgerald and L. Bergdahl, "Including moorings in the assessment of a generic offshore wave energy converters: A frequency domain approach," *Marine Structures*, vol. 21, pp. 23–46, 2008.

[41] E. Spooner and M. A. Mueller, "Comparative study of linear generators and hydraulic systems for wave energy conversion." ETSU V/06/00189/REP, 2001. `http://www.tridentenergy.co.uk/pdf/DTI Report.pdf`.

[42] `http://www.waveenergy.no/WorkingPrinciple.htm`.

[43] H. Polinder, M. E. C. Damen, and F. Gardner, "Linear PM generator system for wave energy conversion in the AWS," *IEEE transaction on Energy Conversion*, vol. 19, no. 3, pp. 583–589, 2004.

[44] B. M. Count, "The theoretical analysis of wave power devices with non-linear mechanical conditioning," tech. rep., CEGB Marchwood, 1978. R/M/N1008.

[45] A. E. Kiprakis and A. R. Wallace, "Power control and conditioning for wave energy converters," in *6th European Wave and Tidal Energy Conference*, (Glasgow), 2005.

[46] J. Tedd, J. P. Kofoed, M. Jasinski, A. Morris, E. Friis-Madsen, R. Wisniewski, and J. D. Bendtsen, "Advanced control techniques for WEC Wave Dragon," in *7th European Wave and Tidal Energy Conference*, (Porto), 2007.

[47] J. Fitzgerald. Private communication, 3 March 2008. AWS, By email.

[48] R. Yemm, "Full-scale wecs: Pelamis," in *Ocean Wave Energy* (J. Cruz, ed.), pp. 304–321, Springer, 2008.

[49] R. Henderson, "Design, simulation, and testing of a novel hydraulic power take-off system for the Pelamis wave energy converter," *Renewable Energy*, vol. 31, no. 2, pp. 271–283, 2006.

[50] D. Pizer, C. Retzler, R. M. Henderson, F. L. Cowieson, M. G. Shaw, B. Dickens, and R. Hart, "Pelamis WEC - Recent advances in the numerical and experimental modelling programme," in *6th European Wave and Tidal Energy Conference*, (Glasgow), 2005.

[51] D. Pizer, "Numerical modelling of wave energy absorbers," tech. rep., Edinburgh Wave Power Project, 1994. `http://www.see.ed.ac.uk/~ies/Wave_power_group_reports/`.

[52] S. H. Salter and C. P. Lin, "Wide tank efficiency measurements on a model of the sloped IPS buoy," in *Proc of the 3rd European Wave Energy Conference*, (Patras), pp. 200–206, 1998.

[53] E. R. Jefferys and T. Whittaker, "Latching control of an oscillating water column device with air compressibility," in *Hydrodynamics of Ocean Wave-Energy Utilization* (D. Evans and A. F. de O. Falcão, eds.), pp. 281–291, Lisbon: Springer Verlag, 1985.

[54] G. S. Payne, J. R. M. Taylor, T. Bruce, and P. Parkin, "Assessment of boundary-element method for modelling a free-floating sloped wave energy device. Part 1: Numerical modelling," *Ocean Engineering*, vol. 35, no. 3–4, pp. 333–341, 2008.

[55] J. Falnes, *Ocean Waves and Oscillating Systems*. Cambridge University Press, 2002.

[56] D. V. Evans, "A theory for wave-power absorption by oscillating bodies," *J. Fluid Mech.*, vol. 77, no. 1, pp. 1–25, 1976.

[57] T. H. Havelock, "Waves due to a floating sphere making periodic heaving oscillations," *Proc R. Soc.*, vol. 231, no. 1184, pp. 1–7, 1955.

[58] D. Pizer, "Maximum wave-power absorption of point absorbers under motion constraints," *Applied Ocean Research*, vol. 15, no. 4, pp. 227–234, 1993.

[59] A. Henry. Private communication, 2008.

[60] S. W. Smith, *The Scientist and Engineer's Guide to Digital Signal Processing*. California Technical Pub, 1998.

[61] C. D. McGillem and G. R. Cooper, *Continuous and discrete signals and system analysis*. CBS College Publishing, 1984.

[62] R.F.Hoskins, *Delta functions: an introduction to generalised functions*. Chichester: Horwood Pub, 1999.

[63] S. A. Hughes, *Physical models and Laboratory techniques in Coastal Engineering*, ch. 8. Advanced Series on Ocean Engineering - Vol 7, World Scientific Publishing Company, 1993.

[64] J. A. Crabbe, "Synthesis of a directional wave climate," in *Power from Sea Waves* (B. Count, ed.), pp. 41–74, London, UK: Academic Press, 1980.

[65] K. Hasselman, T. P. Barnett, E. Bouws, H. Carlson, D. E. Cartwright, K. Enke, J. A. Ewing, H. Gienapp, D. E. Hasselmann, P. Kruseman, A. Meerburg, P. Muller, D. J. Olbers, K. Richter, W. Sell, and H. Walden, "Measurements of wind-wave growth and swell decay during the joint north sea wave project (JONSWAP)," *Deutschen Hydrografischen Zeitschrift*, vol. Supplement A(8), no. 12, 1973.

[66] C. L. Bretschneider, "Wave variability and wave spectra for wind-generated gravity waves," Tech Memo 118, CERC, USA, 1959.

[67] M. D. Miles and E. R. Funke, "A comparison of methods for synthesis of directional seas," *Journal of Offshore and Arctic Engineering*, vol. 111, no. 1, pp. 43–48, 1989.

[68] S. A. Hughes, *Physical models and Laboratory techniques in Coastal Engineering*, ch. 7. Advanced Series on Ocean Engineering - Vol 7, World Scientific Publishing Company, 1993.

[69] `http://www.edesign.co.uk/`.

[70] D. Nunes, "Random wave generation by linear digital filtering of gaussian white noise," in *2nd Congress of I.M.A.E.M.*, (Trieste, Italy), 1981.

[71] D. J. Skyner, "Solo duck linear analysis," tech. rep., Edinburgh Wave Power Project, 1987. `http://www.see.ed.ac.uk/~ies/Wave_power_group_reports/`.

[72] S. A. Hughes, *Physical models and Laboratory techniques in Coastal Engineering*, ch. 3. Advanced Series on Ocean Engineering - Vol 7, World Scientific Publishing Company, 1993.

[73] `http://www.wamit.com/`.

[74] M. Darras, "List of sea-state parameters," in *IAHR Seminar on wave generation and analysis in basins*, (Lausanne), 1987.

[75] Y. Goda, *Random seas and design of maritime structures*, vol. 15 of *Advanced Series on Ocean Engineering*. World Scientific, 2000.

[76] R. G. Dean and R. A. Dalrymple, *Water wave mechanics for engineers and scientists*, vol. 2 of *Advanced Series on Ocean Engineering*. World Scientific, 1991.

[77] J. N. Newman, "The interaction of stationary vessels with regular waves," in *Proc 11th Symp Naval Hydrod*, (London), pp. 491–501, 1976.

[78] M. W. Dingemans, *Water wave propagation over uneven bottoms*, vol. 13 of *Advanced Series on Ocean Engineering*. World Scientific, 1997.

[79] G. G. Stokes, "On the theory of oscillatory waves," *Trans Camb Philos Soc*, vol. 8, pp. 441–455, 1847. Reprinted in Stokes, G.G. (1880). Mathematical and Physical Papers, Volume 1, Cambridge University press, pp197–229 `http://www.archive.org/stream/mathphyspapers01stokrich#page/n213/mode/2up`.

[80] F. Ursell, "The long-wave paradox in the theory of gravity waves," *Proc Camb Philos Soc*, vol. 49, pp. 685–694, 1953.

[81] http://en.wikipedia.org/wiki/Dispersion_(water_waves).

[82] J. B. Shiach, C. G. Mingham, D. M. Ingram, and T. Bruce, "The applicability of the shallow water equations for modelling violent wave overtopping," *Coastal Engineering*, vol. 51, no. 1, pp. 1–15, 2004.

[83] J. A. Battjes and H. W. Groenenddijk, "Wave height distributions on shallow foreshores," *Coastal Engineering*, vol. 40, no. 3, pp. 161–182, 2000.

[84] M. Longuet-Higgins, "On the statistical distributions of heights of sea waves," *Journal of Marine Research*, vol. 11, pp. 245–266, 1952.

[85] S. H. Salter, D. C. Jeffrey, and J. R. M. Taylor, "Study of mechanisms for extracting power from sea waves," tech. rep.

[86] S. A. Hughes, *Physical models and Laboratory techniques in Coastal Engineering*. Advanced Series on Ocean Engineering - Vol 7, World Scientific Publishing Company, 1993.

[87] K. Ogata, *System Dynamics*. Prentice-Hall, 1978.

[88] A. A. E. Price, D. I. M. Forehand, and A. R. Wallace, "Time-span of future information necessary for theoretical acausal optimal control of wave energy converters," in *Accepted invited paper for the European Control Conference*, (Budapest), 2009.

[89] J. S. da Costa, A. Sarmento, F. Gardner, P. Beirão, and A. Brit-Melo, "Time domain model of the Archimedes Wave Swing wave energy converter," in *6th European Wave and Tidal Energy Conference*, (Glasgow), 2006.

[90] W. E. Cummins, "The impulse response function and ship motions," *Schiffstechnik*, vol. 47, no. 9, pp. 101–109, 1962.

[91] J. Falnes, "On non-causal impulse response functions related to propagating water waves," *Applied Ocean Research*, vol. 17, no. 6, pp. 379–389, 1995.

[92] J. V. Wehausen, "The motion of floating bodies," *Annual review of fluid mechanics*, vol. 3, pp. 237–268, 1971.

[93] E. R. Jefferys, "Device characterisation," in *Power from Sea Waves* (B. Count, ed.), pp. 413–438, London, UK: Academic Press, 1980.

[94] R. Taghipour, T. Perez, and T. Moan, "Hybrid frequency-time domain models for dynamic response analysis of marine structures," *Ocean Engineering*, vol. 35, pp. 685–705, 2008.

[95] M. Greenhow and S. P. White, "Optimal heave motion of some axisymmetric wave energy devices in sinusoidal waves," *Applied Ocean Research*, vol. 19, no. 3–4, pp. 141–159, 1997.

[96] M. F. P. Lopes, J. Hals, R. P. F. Gomes, T. Moan, L. M. C. Gato, and A. F. de O. Falcão, "Experimental and numerical investigation of non-predictive phase control strategies for a point-absorbing wave energy converter," *Submitted to Applied Ocean Research*, 2008.

[97] J. Falnes, "A review of wave-energy extraction," *Marine Structures*, vol. 20, no. 4, pp. 185–201, 2007.

[98] S. Niato and M. Minoura, "Research on element wavemakers and wave field generated by their combination," in *Proceedings of the Fourth International Offshore and Polar Engineering Conference*, vol. 3, (Osaka, Japan), pp. 3–16, 1994.

[99] G. G. Stokes, "On the effects of the internal friction on the motion of a pendulum," *Trans Camb Philos Soc*, vol. 9, no. II, pp. 8–106, 1851. `http://www.marcdatabase.com/~lemur/lemur.com/library-of-antiquarian-technology/horology/stokes1850.pdf`.

[100] A. B. Basset, *A treatise on hydrodynamics: with numerous examples*, vol. II. Deighton, Bell and Co., 1888. `http://www.archive.org/details/atreatiseonhydr01bassgoog`.

[101] F. Odar and W. S. Hamilton, "Forces on a sphere accelerating in a viscous fluid," *Journal of Fluid Mechanics*, vol. 18, no. 2, pp. 302–314, 1964.

[102] Z. Yu and J. Falnes, "State-space modelling of a vertical cylinder in heave," *Applied Ocean Research*, vol. 17, no. 5, pp. 265–275, 1995.

[103] M. G. S. Prado, F. Neumann, M. E. Damen, and F. Gardner, "AWSresults of pilot plant testing 2004," in *6th European Wave and Tidal Energy Conference*, (Glasgow), 2006.

[104] P. Nebel, *Synthesis of Optimal Control of a Wave Energy Converter*. PhD thesis, The University of Edinburgh, 1994.

[105] J. Falnes and K. Budal, "Wave power conversion by point absorption," *Norw Maritime Res*, vol. 6, no. 4, pp. 2–11, 1978.

[106] C. C. Mei, "Power extraction from water waves," *Journal of Ship Research*, vol. 20, no. 2, pp. 63–66, 1976.

[107] W. N. Caron, *Antenna impedance matching*. American radio relay league, 1989.

[108] I. R. Sinclair, *Dictionary of Electronics*. Collins, 1988.

[109] K. Budal and J. Falnes, "Optimum operation of improved wave-power converter," *Marine Science Communications*, vol. 3, no. 2, pp. 133–150, 1977.

[110] S. Niato and S. Nakamura, "Wave energy absorption in irregular waves by feedforward control system," in *Hydrodynamics of Ocean Wave-Energy Utilization* (D. Evans and A. F. de O. Falcão, eds.), pp. 269–280, Lisbon: Springer Verlag, 1985.

[111] P. Nebel, "Maximizing the efficiency of wave-energy plant using complex-conjugate control," *Proc. of Institute of Mech. Eng.*, vol. 206, no. 4, pp. 225–236, 1992.

[112] D. V. Evans, "Some analytic results for two and three dimensional wave-energy absorbers," in *Power from Sea Waves* (B. Count, ed.), pp. 213–249, London, UK: Academic Press, 1980.

[113] J. M. B. P. Cruz and S. H. Salter, "Numerical and experimental modelling of a modified version the Edinburgh duck wave energy device," *Proc. Inst. of Mech. Eng., Part M: J. of Engineering for the Maritime Environment*, vol. 220, no. 3, pp. 129–147, 2006.

[114] D. V. Evans, D. C. Jeffrey, S. H. Salter, and J. R. M. Taylor, "Submerged cylinder wave energy device: theory and experiment," *Applied Ocean Research*, vol. 1, no. 1, pp. 3–12, 1979.

[115] D. V. Evans, "Maximum wave-power absorption under motion constraints," *Applied Ocean Research*, vol. 3, no. 4, pp. 200–203, 1981.

[116] M. Karolewski, "Tracer 1.71," 2003. `http://www.geocities.com/karolewski/soft.htm`.

[117] D. I. M. Forehand. Private communication, 5 March 2009.

[118] J. B. Saulnier, P. Ricci, M. T. Pontes, and A. F. de O. Falcão, "Spectral bandwidth and WEC performance assessment," in *7th European Wave and Tidal Energy Conference*, (Porto), 2007.

[119] J. Cândido and P. A. P. Justino, "Frequency-domain and stochastic model for an articulated wave power device," in *7th European Wave and Tidal Energy Conference*, (Porto), 2007.

[120] D. V. Evans and C. M. Linton, "Hydrodynamics of wave-energy devices." Joule 1, Device Fundamentals Hydrodynamics, 1993. unpublished.

[121] S. Niato, "Wave generation and absorption in wave basins: theory and application," *International Journal of Offshore and Polar Engineering*, vol. 16, no. 2, pp. 81–89, 2006.

[122] A. A. E. Price, C. J. Dent, and A. R. Wallace, "On the capture width of wave energy converters," *Submitted to Applied Ocean Research*, 2009.

[123] Y. M. C. Delauré and A. Lewis, "3D hydrodynamic modelling of fixed oscillating water column wave power plant by a boundary element methods," *Ocean Engineering*, vol. 30, no. 3, pp. 309–330, 2003.

[124] J. Brooke, *Wave energy conversion*. Elsevier, 2003.

[125] J. Weber and G. Thomas, "An investigation into the importance of the air chamber design of an Oscillating Water Column wave energy device," in *Proc 11th Int Offshore Polar Eng Conf*, (Stravanger, Norway), pp. 581–588, 2001.

[126] G. Thomas and B. Ó. Gallachóir, "An assessment of design parameters for the Bristol Cylinder," in *Proc 1st Eur Wave Energy Symp*, (Edinburgh, Scotland), pp. 139–144, 1993.

[127] J. Weber and G. Thomas, "Optimisation of the hydrodynamic-aerodynamic coupling for an Oscillating Water Column wave energy device," in *Proc 4th Eur Wave Energy Conf*, (Aarlborg,Denmark), pp. 581–588, 2000.

[128] N. Ambli, K. Bønke, O. Malmo, and A. Reitan, "The Kværner multiresonant OWC," in *Wave Energy Utilisation – Proc. of 2nd Int. Symp. on Wave Energy Utilisation*, (Trondheim, Norway), pp. 275–295, 1982.

[129] L. Mandel and E. Wolf, *Optical coherence and quantum optics*. Cambridge University Press, 1995.

[130] S. Kikkawa, "On unification of equivalent bandwidths of a random process," *IEEE signal processing letters*, vol. 11, no. 8, pp. 670–673, 2004.

[131] M. E. V. Valkenburg, *Network analysis*. Prentice-Hall, 1974.

[132] D. G. Lampard, "Definition of 'bandwidth' and 'time duration' of signals which are connected by identity," *IRE Trans. Circuit Theory*, vol. CT, no. 3, pp. 286–288, 1956.

[133] M. R. Belmont, J. Horwood, R. Thurley, and J. Baker, "Filters for linear sea-wave prediction," *Ocean Engineering*, vol. 33, no. 17-18, pp. 2332–2351, 2006.

[134] U. A. Korde, "Efficient primary energy conversion in irregular waves," *Ocean Engineering*, vol. 25, pp. 79–91, 2003.

[135] M. Vantorre, R. Banasiak, and R. Verhoeven, "Modelling of hydraulic performance and wave energy extraction by a point absorber in heave," *Applied Ocean Research*, vol. 26, no. 1-2, pp. 61–72, 2004.

[136] A. P. McCabe, A. Bradshaw, J. A. C. Meadowcroft, and G. Aggidis, "Developments in the design of the PS Frog Mk 5 wave energy converter," *Renewable Energy*, vol. 31, no. 2, pp. 141–151, 2006.

[137] A. A. Temeev, V. P. Belokopytov, and S. A. Temeev, "An integrated system of the floating wave energy converter and electrolytic hydrogen producer," *Renewable Energy*, vol. 31, pp. 225–239, 2006.

[138] K. Rhinefrank, E. B. Agamloh, A. von Jouanne, A. K. Wallace, J. Prudell, K. Kimble, J. Aills, E. Schmidt, P. Chan, B. Sweeny, and A. Schacher, "Novel ocean energy permanent magnet linear generator buoy," *Renewable Energy*, vol. 31, pp. 1279–1298, 2006.

[139] R. Godoy-Diana and S. P. R. Czitrom, "On the tuning of a wave-energy driven oscillating-water-column seawater pump to polychromatic waves," *Ocean Engineering*, vol. 34, pp. 2374–2384, 2007.

[140] P. Filianoti and S. M. Camporeale, "A linearized model for estimating the performance of submerged resonant wave energy converters," *Renewable Energy*, vol. 33, pp. 631–641, 2008.

[141] M. Folley and T. Whittaker, "The cost of water from an autonomous wave-powered desalination plant," *Renewable Energy*, vol. 34, pp. 75–81, 2009.

[142] J. Spinneken and C. Swan, "Second-order wave maker theory using force-feedback control. part 1. a new theory for regular wave generation," *Ocean Engineering*, vol. 36, no. 8, pp. 539–548, 2009.

[143] K. Budal, J. Falnes, L. C. Iversen, P. M. Lillebekken, G. Oltedal, T. Hals, T. Onshus, and A. S. Høy, "The Norwegian wave–power buoy project," in *Wave Energy Utilisation – Proc. of 2nd Int. Symp. on Wave Energy Utilisation*, (Trondheim, Norway), pp. 323–344, 1982.

[144] A. Yazdizadeh and K. Khorasani, "Adaptive time delay neural network structures for nonlinear system identification," *Neurocomputing*, vol. 47, pp. 207–240, 2002.

[145] J. Pardey, S. Roberts, L. Tarassenko, and J. Stradling, "A new approach to the analysis of the human sleep/wakefulness continuum," *J Sleep Res*, vol. 5, no. 4, pp. 201–210, 1996.

[146] J. M. Vincent, "Face finding in images," in *Applications of Neural networks* (A. F. Murray, ed.), pp. 35–58, Kluwer academic publishers, 1995.

[147] S. Ogaji and R. Singh, "Advanced engine diagnostics using artificial neural networks," *Applied Soft Computing*, vol. 3, no. 3, pp. 259–271, 2003.

[148] S. Millar and R. J. Williams, "Temporal difference learning: a chemical process control application," in *Applications of Neural networks* (A. F. Murray, ed.), pp. 287–298, Kluwer academic publishers, 1995.

[149] M. Willis, G. Montague, and C. Peel, "On the application of neural networks to process control," in *Applications of Neural networks* (A. F. Murray, ed.), pp. 191–216, Kluwer academic publishers, 1995.

[150] M. Ghiassi, H. Saidane, and D. Zimbra, "A dynamic artificial neural network model for forecasting time series events," *International Journal of Forecasting*, vol. 21, pp. 341–362, 2005.

[151] J. Agrawal and M. Deo, "On-line wave predictions," *Marine Structures*, vol. 15, pp. 57–74, 2002.

[152] O. Makarynskyy, A. Pires-Silva, D. Makarynska, and C. Ventura-Soares, "Artificial neural networks in wave predictions at the west coast of portugal," *Computers and Geosciences*, vol. 31, no. 4, pp. 415–424, 2005.

[153] P. Lui, D. Schwab, and R. Jensen, "Has wind-wave modelling reached its limit?," *Ocean Engineering*, vol. 29, no. 1, pp. 81–98, 2005.

[154] J. L. Forsberg, "On-line identification and prediction of waves," in *Hydrodynamics of Ocean Wave-Energy Utilization* (D. Evans and A. F. de O. Falcão, eds.), pp. 185–193, Lisbon: Springer Verlag, 1985.

[155] J. Tedd and P. Frigaard, "Short term wave forecasting, using digital filters, for improved control of wave energy converters," in *17th ISOPE conference proceedings*, (Lisbon), 2007.

[156] `http://www.oceanpowertechnologies.com/`.

[157] T. W. Thorpe, "A review of wave energy," tech. rep., ETSU-R-72, 1992.

[158] J. Falnes, "Small is beautiful: How to make wave energy economic," in *European wave energy symposium*, (Edinburgh), pp. 367–372, 1993.

[159] R. Taylor, "Wave energy: the influence of maintenance/repair requirements," in *2nd Int Symp on Wave and Tidal Energy*, (Cambridge), pp. 99–104, 1981.

[160] J. Weber and G. Thomas, "Some aspects of the design optimisation of an OWC with regard to multiple sea states and combined object functions," in *5th European Wave and Tidal Energy Conference*, (Cork), pp. 141–148, 2003.

[161] A. F. de O. Falcão, "Maximum energy production and maximum profit as alternative criteria for wave power equipment optimization," in *5th European Wave and Tidal Energy Conference*, (Cork), pp. 149–156, 2003.

[162] R. W. Yeung, "Added mass and damping of a vertical cylinder in finite-depth waters," *Applied Ocean Research*, vol. 3, no. 3, pp. 119–133, 1981.

All websites correct on 22 July 2009

Appendix A

Dataset

The non-dimensionalised radiation coefficients used in this research were first presented by Havelock [57]. Several authors [58, 115] have since used these results, and have calculated the excitation coefficient from the radiation coefficient (3.36). The research in this thesis follows this precedent.

Havelock presented added mass and damping for a spherical buoy, non-dimensionalised with respect to the radius, a. The values were plotted against $\sigma^2 a/g$, where σ is the circular frequency and $g = 9.81$ m/s is acceleration due to gravity. Non-dimentionalised added mass was denoted k and was converted to added mass by multiplying by $2/3\pi\rho a^3$. Non-dimensionalised radiation damping was denoted $2h$, and was converted to radiation damping by multiplying by $2/3\pi\rho a^3\omega$. See pg 300 of [36] for details. This denormalisation gives parameters consistent with the real DFT. As the complex DFT was used in this work, the magnitudes of the added mass and damping were divided by two before being used here.

Most of the analysis presented was for a 5 m diameter buoy. The values of mass and buoyancy spring for this size buoy are given in Table A.1 below.

Physical parameter	**Symbol**	**Value**
radius	r	2.5 m
density	ρ	1000 kg/m^3
mass	$m = \frac{2}{3}\pi r^3\rho$	32725 kg
spring	$c = \pi r^2\rho g$	192423 kg/m^3

Table A.1: ***Physical characteristics of the*** 5 ***m buoy.***

Appendix B
Derivations

B.1 Plancherel's theorem depends on the form of the transform

Commonly used non-unitary form of the DFT

For the most common form of the DFT [61]:

$$X[\omega_j] = \sum_{n=0}^{N-1} x[t_n]\, e^{-i2\pi jn/N} \tag{B.1}$$

and its inverse transform:

$$x[t_n] = \frac{1}{N} \sum_{j=0}^{N-1} X[\omega_j]\, e^{\,i2\pi jn/N} \tag{B.2}$$

Plancherel's equation for any two real signals, $a[t_n]$ and $b[t_n]$, is:

$$\sum_{n=0}^{N-1} a[t_n]\, b[t_n] = \frac{1}{N} \sum_{j=0}^{N-1} A^*[\omega_j]\, B[\omega_j] \tag{B.3}$$

Multiplication is commutative so $\sum_{n=0}^{N-1} a[t_n]\, b[t_n] = \frac{1}{N} \sum_{j=0}^{N-1} A[\omega_j]\, B^*[\omega_j]$ also holds.

Regardless of the form of Fourier transform, the derivation of Plancherel's theorem, following the method for deriving Parseval's theorem in [61], follows the same process. This is now demonstrated for the most commonly used form of DFT. Plancherel's theorem is found by substituting the inverse transform (B.2) for the second term of the product:

$$\sum_{n=0}^{N-1} a[t_n]\, b[t_n] = \sum_{n=0}^{N-1} a[t_n]\, \frac{1}{N} \sum_{j=0}^{N-1} B[\omega_j]\, e^{\,i2\pi jn/N} \tag{B.4}$$

then rearranging the order of summation (or integration, for transforms of continuous signals):

$$\sum_{n=0}^{N-1} a[t_n]\, b[t_n] = \frac{1}{N} \sum_{j=0}^{N-1} B[\omega_j] \sum_{n=0}^{N-1} a[t_n]\, e^{\,i2\pi jn/N} \tag{B.5}$$

and substituting the relevant form of Fourier transform ((B.1) in this case) for the final term:

$$\sum_{n=0}^{N-1} a[t_n]\, b[t_n] = \frac{1}{N} \sum_{j=0}^{N-1} B[\omega_j]\, A[-\omega_j] \tag{B.6}$$

When the time domain is real, as is the case here, taking the complex conjugate of the frequency domain is the same as reversing the frequency axis. The DFT form of this relation is:

$$A[-\omega_j] = A^*[\omega_j] \tag{B.7}$$

Making this change to (B.6) yields (B.3). This derivation may be applied to other forms of the DFT, including a less common form of the non-unitary DFT (B.8) used by Smith [60] and the unitary form to the DFT (B.10), which is not in common use in engineering.

Less commonly used non-unitary form of DFT

There are other conventions for describing the DFT and its inverse. The $1/N$ factor may appear in the DFT rather than its inverse transform [60]:

$$\begin{aligned} X[\omega_j] &= \frac{1}{N}\sum_{n=0}^{N-1} x[t_n]e^{-i2\pi jn/N} \\ x[t_n] &= \sum_{j=0}^{N-1} X[\omega_j]e^{\,i2\pi jn/N} \end{aligned} \tag{B.8}$$

in which case, Plancherel's equation for real functions is defined as:

$$\sum_{n=0}^{N-1} a[t_n]\; b[t_n] = N\sum_{j=0}^{N-1} A^*[\omega_j]\; B[\omega_j] \tag{B.9}$$

Unitary form of DFT

In the symmetrical (unitary) form, the $1/N$ factor is spread equally between the DFT and its inverse transform :

$$\begin{aligned} X[\omega_j] &= \frac{1}{\sqrt{N}}\sum_{n=0}^{N-1} x[t_n]e^{-i2\pi jn/N} \\ x[t_n] &= \frac{1}{\sqrt{N}}\sum_{j=0}^{N-1} X[\omega_j]e^{\,i2\pi jn/N} \end{aligned} \tag{B.10}$$

in which case, Plancherel's equation for real functions is defined as:

$$\sum_{n=0}^{N-1} a[t_n]\; b[t_n] = \sum_{j=0}^{N-1} A^*[\omega_j]\; B[\omega_j] \tag{B.11}$$

Plancherel's theorem is used to express the power absorbed by a linear WEC as a function of the DFT of the (PTO mechanism's) velocity. The coefficient of the power decomposition depends

on which form of DFT is assumed. However, the same is true when the wave energy transport is expressed as a function of wave elevation. As capture width is the ratio of absorbed power to incident power (wave energy transport), the coefficients that arise from different forms of the DFT, i.e. (B.1) or (B.10), cancel in (5.9). Likewise, any coefficients resulting from a different form of Fourier transform, such as the discrete time Fourier transform [71] or the continuous Fourier transform (for example [114]), cancel when calculating the ratio of absorbed to incident power.

Commonly used non-unitary form of the Fourier transform

For the most common form of the continuous Fourier transform [61] and its inverse transform:

$$\begin{aligned} X(\omega) &= \int_{-\infty}^{+\infty} x(t) e^{-i\omega t} dt \\ x(t) &= \frac{1}{2\pi} \int_{-\infty}^{+\infty} X(\omega) e^{i\omega t} d\omega \end{aligned} \tag{B.12}$$

For any two real signals, $a(t)$ and $b(t)$, Plancherel's theorem is found by substituting the inverse transform for the second term of the product:

$$\int_{-\infty}^{\infty} a(t)\, b(t) dt = \int_{-\infty}^{+\infty} a(t)\, \frac{1}{2\pi} \int_{-\infty}^{+\infty} B(\omega) e^{i\omega t} d\omega dt \tag{B.13}$$

Rearranging and substituting the relevant form of Fourier transform

$$\int_{-\infty}^{\infty} a(t)\, b(t) dt = \frac{1}{2\pi} \int_{-\infty}^{+\infty} \int_{-\infty}^{+\infty} a(t)\, e^{i\omega t} dt B(\omega) d\omega = \frac{1}{2\pi} \int_{-\infty}^{+\infty} A^*(\omega) B(\omega) d\omega \tag{B.14}$$

B.2 Derivation of absorbed power for the DFT

Average absorbed power is usually expressed as a function of the complex amplitude, or the continuous Fourier transform, of (the PTO system's) velocity [24, 55]. In an experimental system where velocity is measured or calculated at discrete points in both the time and frequency domains, the transformation between domains is the DFT. It is thus useful to express averaged absorbed power in terms of the DFT of velocity.

The average absorbed power over an interval of time containing N samples is the mean of the instantaneous power at each sample:

$$P_A = \frac{1}{N} \sum_{n=0}^{N-1} f_{pto}[t_n] u[t_n] \tag{B.15}$$

As both force and velocity are real, either may be written as its complex conjugate. When force (3.39) and velocity are periodic over the interval N, the DFT version of Plancherel's theorem [B.3] can be used to express the absorbed power as:

$$P_A = \frac{1}{N^2} \sum_{j=0}^{N-1} F_{pto}[\omega_j] U^*[\omega_j] \tag{B.16}$$

Assuming that N is an even number, which is always the case for the Fast Fourier transform implementation of the DFT, this sum can thus be split into two sums with limits up to and from $N/2$:

$$P_A = \frac{1}{N^2} \left(\sum_{j=0}^{N/2-1} F_{pto}[\omega_j] U^*[\omega_j] \; + \sum_{j=N/2}^{N-1} F_{pto}[\omega_j] U^*[\omega_j] \right) \tag{B.17}$$

This is useful because the DFT is periodic with frequency. The information in the bins $N/2$ to $N-1$ is exactly the same as that in the bins from $-(N/2-1)$ to 0. The limits on the second sum can be changed to reflect this:

$$P_A = \frac{1}{N^2} \left(\sum_{j=0}^{N/2-1} F_{pto}[\omega_j] U^*[\omega_j] \; + \sum_{j=-(N/2-1)}^{0} F_{pto}[\omega_j] U^*[\omega_j] \right) \tag{B.18}$$

Reversing the frequency limits on the second sum gives it the same limits as the first sum:

$$P_A = \frac{1}{N^2} \left(\sum_{j=0}^{N/2-1} F_{pto}[\omega_j] U^*[\omega_j] \; + \sum_{j=0}^{N/2-1} F_{pto}[-\omega_j] U^*[-\omega_j] \right) \tag{B.19}$$

Applying (B.7)to the terms in the second sum gives:

$$P_A = \frac{1}{N^2} \left(\sum_{j=0}^{N/2-1} F_{pto}[\omega_j] U^*[\omega_j] + \sum_{j=0}^{N/2-1} F^*_{pto}[\omega_j] U[\omega_j] \right) \tag{B.20}$$

The second sum is now the complex conjugate of the first sum. Any function added to its complex conjugate gives twice the real part of that function:

$$P_A = \frac{2}{N^2} \sum_{j=0}^{N/2-1} \Re \left\{ F_{pto}[\omega_j] U^*[\omega_j] \right\} \tag{B.21}$$

B.3 Derivation of wave energy transport for the DFT

This working follows Falnes's derivation of the wave energy transport in pages 47,71 and 77 of [55]. Falnes uses the continuous Fourier transform. Here a discretised periodic wave elevation is assumed, and the DFT is used.

Using linear wave theory, a directional sea can be divided into a number of unidirectional seas. The equation is written for a unidirectional wave. Only waves travelling in the forward direction are considered, as waves travelling in the opposite direction can be treated separately (see equation (4.122) in ([55]). The intensity is the energy passing a vertical plane perpendicular to the direction of wave propagation per unit time and per unit area. For surface water waves the intensity is the averaged product of pressure and fluid particle velocity in the direction of wave propagation, v_x, where x indicates the direction of propagation. This reduces to the averaged product of the dynamic pressure, p and the fluid particle velocity (see equation (3.14) in ([55]):

$$I = p\bar{v}_x \tag{B.22}$$

As so much experimental and simulation work involves discrete values, a discrete version of this is required. To use the DFT, it must also be periodic with the averaging period:

$$I = \frac{1}{N}\sum_{n=0}^{N-1} p[t_n]v_x[t_n] \tag{B.23}$$

According to the definition of the DFT used in this thesis (See Table 2.6) Parseval's theorem can be used to write this as a sum of the DFTs of pressure and velocity:

$$I = \frac{1}{N^2}\sum_{j=0}^{N-1} P[\omega_j]V_x^*[\omega_j] \tag{B.24}$$

Following the same arguments as § B.2 above, this can be simplified. Splitting the equation into two sums with limits up to and from $N/2$:

$$I = \frac{1}{N^2}\left(\sum_{j=0}^{N/2-1} P[\omega_j]V_x^*[\omega_j] + \sum_{j=N/2}^{N-1} P[\omega_j]V_x^*[\omega_j]\right) \tag{B.25}$$

As the information in the bins $N/2$ to $N-1$ is identical to that in the bins from $-(N/2-1)$ to 0, the limits on the second sum can be changed:

$$I = \frac{1}{N^2}\left(\sum_{j=0}^{N/2-1} P[\omega_j]V_x^*[\omega_j] + \sum_{j=-(N/2-1)}^{0} P[\omega_j]V_x^*[\omega_j]\right) \tag{B.26}$$

Reversing the frequency limits on the second sum gives it the same limits as the first sum:

$$I = \frac{1}{N^2}\left(\sum_{m=0}^{N/2-1} P[\omega_j]V_x^*[\omega_j] + \sum_{j=0}^{N/2-1} P[-\omega_j]V_x^*[-\omega_j]\right) \tag{B.27}$$

When the time domain is real, as is the case here, taking the complex conjugate of the frequency domain is the same as reversing the frequency axis:

$$I = \frac{1}{N^2}\left(\sum_{j=0}^{N/2-1} P[\omega_j]V_x^*[\omega_j] + \sum_{j=0}^{N/2-1} P[\omega_j])^*V_x[\omega_j]\right) \tag{B.28}$$

The second sum is now the complex conjugate of the first sum. Any function added to its complex conjugate gives twice the real part of that function:

$$I = \frac{2}{N^2}\sum_{j=0}^{N/2-1} \Re\left\{P[\omega_j]V_x^*[\omega_j]\right\} \tag{B.29}$$

Equations (4.93) and (4.94) in [55] express the pressure and velocity as functions of wave elevation. The equations are written in terms of complex amplitudes. Here they are written in DFT form,which implicate assumes that the waves are periodic with N:

$$P[\omega_j] = \rho g H[\omega_j] e(kz) \tag{B.30}$$

$$V_x[\omega_j] = H[\omega_j]\frac{gke(kz)}{\omega_j} \tag{B.31}$$

$$\tag{B.32}$$

Note that $e(kz)$ and the wavenumber k are still a continuous function of the wavenumber and depth. The continuous terms are later removed by integration over depth. Substituting (B.32) into intensity (B.29) gives:

$$I = \frac{2}{N^2}\sum_{j=0}^{N/2-1} |H[\omega_j]|^2 \frac{\rho g^2 k e^2(kz)}{\omega_j} \tag{B.33}$$

The wave elevation $H[\omega_j]$ is the only complex quantity here. The wave elevation multiplied by its complex conjugate is the square of its magnitude. This, along with all other terms are real.

The intensity varies with vertical distance from the water surface, z. The wave energy transport, P_{IW} is the intensity integrated over z. It is the total power passing a vertical plane, one metre

wide and perpendicular to wave transport.

$$\begin{aligned} P_{IW} &= \int_{-h}^{0} I dz \\ &= \int_{-h}^{0} \frac{2}{N^2} \sum_{j=0}^{N/2-1} |H[\omega_j]|^2 \frac{\rho g^2 k}{\omega_j} e^2(kz) dz \\ &= \frac{2}{N^2} \sum_{j=0}^{N/2-1} \frac{\rho g^2}{\omega_j} |H[\omega_j]|^2 2k \int_{-h}^{0} e^2(kz) dz \end{aligned} \tag{B.34}$$

As the depth function is defined as: $D(kh) = 2k \int_{-h}^{0} e^2(kz)dz$ (equation (4.112) in [55]), this can be written as:

$$P_{IW} = \frac{2}{N^2} \sum_{j=0}^{N/2-1} \frac{\rho g^2}{\omega_j} |H[\omega_j]|^2 D(kh) \tag{B.35}$$

Writing this as:

$$P_{IW} = \frac{8}{N^2} \sum_{j=0}^{N/2-1} \frac{\rho g^2}{4\omega_j} |H[\omega_j]|^2 D(kh) \tag{B.36}$$

allows it to be easily compared to the commonly seen phasor notation (equation (ref) in this thesis and equation (4.136) in [55]), which is:

$$P_{IW} = \frac{\rho g^2}{4\omega} \left|\hat{H}(\omega)\right|^2 D(kh)$$

Note that (B.35) has a rather messy combination of discrete and continuous variables. A common assumption is to assume operation in deep water, in which case the depth function is one, and the wave energy transport can be written as a function of discrete variables only:

$$P_{IW} = \frac{2}{N^2} \sum_{j=0}^{N/2-1} \frac{\rho g^2}{\omega_j} |H[\omega_j]|^2 \tag{B.37}$$

Appendix C
Published papers

The following papers are bound into the back of this thesis:

- A test-bed for advanced control of wave energy converters [11].
- Non-linear methods for next-wave estimation [16].
- Time-span of future information necessary for theoretical acausal optimal control of wave energy converters [88].
- On the capture width of wave energy converters [122].

The first two are published conference papers; the third is a conference paper accepted for publication, and the fourth is a journal paper submitted for publication.

The published conference papers do not cover work reported in this thesis. The two papers submitted for publication [88, 122] cover work that is also reported in Chapter 5. Specifically, § 5.2 is based on theory presented in [122], § 5.3 includes some theory presented in [122] but is largely new material, § 5.4 is based on theory presented in [88] but includes some new material, and § 5.5 is new material that is built on the principles laid out in the two papers. Both papers were written with co-authors other than the supervisor of this PhD project. It is important to acknowledge the contributions of these co-authors as Chapter 5 is largely based on the material in these papers. The contributions made by the co-authors of these papers are examined in terms of ownership of the research question and the research answers.

The paper on capture width was developed in close collaboration with the second author. Both myself and Chris Dent have ownership of the intellectual contribution to the research answer. Chris Dent provided focus and corrected mistakes in the early stage of the collaboration, and this enabled me to proceed with the investigation. I acknowledge that without his involvement, this paper would not exist in its current form. Nevertheless, the research question was my own, I made vital contributions to the research answer, and I was the main author. As such this work has been included in this thesis. The conference paper on premonition time was written for inclusion in this thesis. I have ownership of both the research question and answer. However, the second author, David Forehand, ensured that the mathematics was rigorous and elegant. It was necessary to include the work presented in both these papers in this thesis, as § 5.3 and § 5.5, which make key contributions to the research question, depend on the theory contained within these papers.